

# Contributions to the study of oil based binding media with ToF-SIMS

An investigation of the influence of pre-treatment, ageing and pigment presence on  
the ionisation of oil paint fatty acids

Dissertation presented by  
**Tom VANDE MOORTEEL**

for obtaining the Master's degree in  
**Physical Engineering**

Supervisor(s)  
**Arnaud DELCORTE, Jana SANYOVA**

Reader(s)  
**Arnaud DELCORTE, Jana SANYOVA , Francisco MEDEROS**

Academic year 2015-2016



# Contents

<b>1</b>	<b>Introduction</b>	<b>4</b>
1.1	Context and objectives . . . . .	4
1.2	Methodology . . . . .	6
1.3	Science and art, the place of ToF-SIMS in cultural heritage studies . . . . .	10
1.4	ToF-SIMS: history, working principles and experimental conditions . . . . .	12
<b>2</b>	<b>Linseed oil: drying and ageing</b>	<b>20</b>
2.1	Introduction . . . . .	20
2.2	Linseed oil . . . . .	21
2.3	Drying of oil . . . . .	21
2.3.1	Auto-oxidation process . . . . .	23
2.3.2	Destructive reactions: formation of aldehydes or dicarboxylic esters . . . . .	24
2.3.3	Destructive reactions: hydrolysis . . . . .	24
2.3.4	Illustration . . . . .	24
2.4	Study of fresh and aged linseed oil with ToF-SIMS . . . . .	26
2.4.1	Samples . . . . .	26
2.4.2	Observed positive ions . . . . .	28
2.4.3	Observed negative ions . . . . .	28
2.4.4	Discussion of the results for dried and aged non boiled and boiled linseed oil (sample series A and B) . . . . .	29
2.4.5	Discussion of the results for linseed oil pre-treated with lead driers (samples C and D) . . . . .	43
2.4.6	Conclusion . . . . .	48
<b>3</b>	<b>Pigments</b>	<b>49</b>
3.1	Introduction . . . . .	49
3.2	Samples . . . . .	49
3.3	XPS study of lead based pigments . . . . .	50
3.4	Study of lead-based pigments with ToF-SIMS . . . . .	55
3.4.1	Observed positive ions . . . . .	55
3.4.2	Observed negative ions . . . . .	60
3.4.3	Discussion of the results . . . . .	60
3.5	Study of lead isotope abundance ratios in lead based pigments . . . . .	66
3.5.1	ToF-SIMS study of isotope abundancy ratios in lead based pigments . . . . .	67
3.6	Study of azurite with ToF-SIMS . . . . .	71
3.6.1	Observed positive ions . . . . .	71
3.6.2	Observed negative ions . . . . .	72
<b>4</b>	<b>Study of oil-pigment mixtures</b>	<b>73</b>
4.1	Introduction . . . . .	73
4.2	Study of linseed oil-flake white mixtures in ToF-SIMS . . . . .	73
4.2.1	Observed positive ions . . . . .	74
4.2.2	Observed negative ions . . . . .	74
4.3	Study of linseed oil-lead carbonate mixtures in ToF-SIMS . . . . .	74
4.3.1	Observed positive ions . . . . .	75
4.3.2	Observed negative ions . . . . .	75
4.4	Study of linseed oil-lead chloride mixtures in ToF-SIMS . . . . .	75

4.4.1	Observed positive ions . . . . .	75
4.4.2	Observed negative ions . . . . .	76
4.5	Study of linseed oil-minium mixtures in ToF-SIMS . . . . .	76
4.5.1	Observed positive ions . . . . .	76
4.5.2	Observed negative ions . . . . .	76
4.6	Discussion of results of ToF-SIMS measurements of mixtures of linseed oil and lead-based pigments . . . . .	77
4.6.1	Pigment related ions . . . . .	77
4.6.2	Fatty acids: oil binder related ions . . . . .	77
4.6.3	Lead Soaps . . . . .	82
4.7	Depth Profiling and Imaging . . . . .	82
4.8	Study of linseed oil-azurite mixtures in ToF-SIMS . . . . .	87
4.8.1	Observed positive ions . . . . .	88
4.8.2	Observed negative ions . . . . .	88
4.9	Discussion of results of ToF-SIMS of a mixture of linseed oil and azurite . . . . .	88
4.9.1	Fatty acids: oil binder related ions . . . . .	88
4.10	Conclusions . . . . .	92
<b>5</b>	<b>Study of linseed oil-turpentine mixtures</b>	<b>94</b>
5.1	Introduction . . . . .	94
5.2	Chemical composition . . . . .	94
5.3	Study of oil-turpentine mixture with ToF-SIMS . . . . .	95
5.3.1	Observed positive ions . . . . .	95
5.3.2	Observed negative ions . . . . .	95
5.4	Observations . . . . .	96
<b>6</b>	<b>Conclusion</b>	<b>97</b>
6.1	Future Prospects . . . . .	98
<b>A</b>	<b>Results of ToF-SIMS measurements of Linseed oil</b>	<b>104</b>
A.1	Discussion of observations . . . . .	104
A.1.1	Aliphatic chain fragments of the type $C_2H_3(CH_2)_xCOO^-$ . . . . .	104
A.1.2	Decanoic acid . . . . .	104
A.1.3	Monoglycerides with palmitic or stearic acid . . . . .	104
A.1.4	Monoglyceride with linoleic acid . . . . .	105
A.1.5	Monoglyceride with azelaic acid . . . . .	105
A.1.6	Diglycerides with palmitic and stearic acids . . . . .	105
A.1.7	Diglycerides with palmitic or stearic acid and oleic acid . . . . .	105
A.1.8	Diglyceride with palmitic and linoleic acid . . . . .	105
A.1.9	Diglyceride with stearic and linolenic or linoleic acid . . . . .	106
A.1.10	Diglycerides with palmitic or stearic acid and suberic, azelaic or sebacic acid	106
A.1.11	Diglyceride with linolenic acid . . . . .	106
A.2	Results of ToF-SIMS measurements . . . . .	106
<b>B</b>	<b>Results of ToF-SIMS measurements of Linseed oil pre-treated with lead driers</b>	<b>121</b>
<b>C</b>	<b>Results of ToF-SIMS measurements of Linseed oil with Flake White</b>	<b>136</b>
<b>D</b>	<b>Results of ToF-SIMS measurements of Linseed oil with Lead Carbonate</b>	<b>150</b>
<b>E</b>	<b>Results of ToF-SIMS measurements of Linseed oil with Lead Chloride</b>	<b>165</b>
<b>F</b>	<b>Results of ToF-SIMS measurements of Linseed oil with Minium</b>	<b>179</b>

<b>G Results of ToF-SIMS measurements of Linseed oil with Azurite</b>	<b>193</b>
<b>H Results of ToF-SIMS measurements of Lead containing Pigments</b>	<b>206</b>
<b>Bibliography</b>	<b>213</b>

# Chapter 1

## Introduction

### 1.1 Context and objectives

Works of art are an essential part of a society's cultural heritage and their long-term conservation is an important and demanding task. A respectful conservation-restoration requires a very good knowledge of the art work and its history. One hopes to be able to trace back the original appearance of the painting, as intended by the artist. This is not straightforward: not only the ageing changes the colours and consistence of a painting, also the conservation history does (because of humidity, heat and sunlight, cleaning and unvarnishing agents or even much more drastic events such as a fire or a flood). Furthermore, later additions, restorations and retouches can render the look of a painting very different from its original appearance. Several scientific analysis techniques are applied to help in this task and to complement the information retrieved from historical sources.

The information on paint material history can be studied through two main sources, a contemporary written source or by scientific analyzes of microsamples taken from aged paint. For this last, many analytical methods are used, and the present work concentrates on the application of Time of Flight-Secondary Ion Mass Spectrometry (ToF-SIMS), which is especially promising in this field thanks to its sensitivity, its high spatial resolution and its ability for the identification of both organic and inorganic compounds. It is this last characteristic that makes the technique particularly apt for the study of oil paints, as they combine an oleaginous, organic part with pigments, which are often inorganic. Oil painting has been the dominant painting technique in occidental art from the 15th century on. Developing a better understanding of its characteristics and ageing behaviour is therefore vital for conservators around the world. Several SIMS studies of oil paint and its ageing process have been done, one of its spearheads being the Dutch MOLART project (1995-2002).[1]

The fundamental processes are now better understood (see Chapters 2 and 4) but a lot of questions remain. One particularly difficult point is the interaction between the oil and the pigments and how this interaction influences the capability of fatty acids to be ionised under the SIMS conditions. This ionisation can also be influenced by the ageing process. It happens that spectra of real painting cross-sections, for example those taken from the Van Eyck's Ghent Altarpiece during its ongoing restoration (see [2]) show only very low signal for the fatty acids, although other methods such as Fourier Transform Infrared Spectroscopy (FT-IR) and Gas Chromatography/Mass Spectrometry (GC/MS) clearly proved that the painting is oil-based. This work is a modest attempt to try to fill a part of this lacuna. We will systematically study oil samples, pure and mixed with pigments, and compare their ToF-SIMS spectra for different stadia of ageing. In particular, we will take a closer look at a group of marking peaks, watch their evolution and compare them between several samples. We decided to focus on the interaction

between lead pigments and linseed oil, as this interaction is known to be particularly strong. Lead pigments are abundantly present in historical paintings, mostly as white. Lead white was until the 20th century the most used white pigment, when it was largely replaced by titanium white. The objective will be first of all to watch the effects of different stadia of ageing on the marker peaks, as well as how this process is influenced by pre-treatment (*in casu* heating with the presence of oxygen with or without lead containing driers) or by the presence of (lead containing) pigments. We will compare our findings with previous studies. Secondly, we want to see whether ToF-SIMS enables us to distinguish between different pre-treatments and different pigments, in the hope that we can trace back the origin of a sample, based on the result of its ageing process. Mainly, we look whether our experiments can show us a reason why the fatty acids in the real samples give such low signal.

Finding a comprehensive chemical theory explaining every part of the ageing process is a work that largely exceeds the scope of a master thesis. We hope nevertheless that this work will give some valuable information on the ageing process of oil paints and the influence of (lead-based) pigments, that it can help to confirm or question previous observations and that it might be of use for future studies on this fascinating subject.

This work has been realised under the supervision of Prof. Arnaud Delcorte at the Bio and Soft Matter (BSMA) centre of the Institute of Condensed Matter and Nanosciences of the Université catholique de Louvain (UCL), in partnership with Jana Sanyova of the Belgian Royal Institute for Cultural Heritage (Koninklijk Instituut voor het Kunstpatrimonium - Institut Royal du Patrimoine Artistique, KIK-IRPA). This study finds its roots in the research project *The Ghent Altarpiece in the Laboratory 60 Years after Paul Coremans: The Contribution of New Analytical Techniques*, carried out under the coordination of the co-promotor of this work, Jana Sanyova from the KIK-IRPA Laboratories Dpt. and founded by the Belgian Science Policy Office (BELSPO).[3] This project was leading simultaneously with the ongoing restoration-conservation of the *Ghent Altarpiece* by the Van Eyck brothers, a project in which KIK-IRPA plays a leading role.[2][4]

The Belgian Royal Institute for Cultural Heritage was founded in 1948 and brings together art historians, scientists and conservators to offer advice and assistance to public and private collections in Belgium and is active in various specific projects. One of these projects is the restoration of the polyptych *The Adoration of the Mystic Lamb* (1432, also known as the *Ghent Altarpiece*, see Figures 1.1 and 1.2). This work was begun by Hubert Van Eyck (ca. 1390-1426) and finished by his brother Jan (ca. 1390-1441) as a commission for the Ghent patrician Joost (or Jodocus) Vijd for his chapel in the Saint John the Baptist church (Ghent). The church became later the Saint Bavo cathedral and, after an eventful history, the altarpiece is nowadays displayed there. It is considered as one of the absolute masterpieces of Early Netherlandish painting and one of Belgium's most fine works of art. The goal of the restoration project, started in 2012 and scheduled to end in 2017, is to render the painting its original appearance. Research has discovered that under several layers of varnish, there were also paint layers that covered the original work of the artists. It has been decided that they should be removed, a work that is very difficult and time-consuming. Afterwards, retouches will be applied on the original layers, together with a new varnish. The supporting panels must be checked and also the wooden frames will be freed from the layers that have been painted over the original polychrome decoration. The work is carried out by an international team of experts, sponsored by the Flemish Region, the Flemish Community and the Fund InBev-Baillet Latour. As mentioned, the scientific research on the paint samples of Van Eyck's altarpiece is realised by the KIK-IRPA's laboratory. This research is carried out in collaboration with the BSMA of the Université catholique de Louvain and it is in this context that this master thesis was executed.



Figure 1.1: *The Adoration of the Mystic Lamb* opened (*Ghent Altarpiece*), 1432, Hubert (ca. 1390-1426) and Jan Van Eyck (ca. 1390-1441), oil on oak panel, Saint Bavo cathedral, Ghent

## 1.2 Methodology

In order to study the influence of pigments and ageing on the ionisation of oil paint fatty acids, we will first examine the pigments and the linseed oil apart. We will look two types of linseed oil, the second of which has undergone pre-treatment:

- Fresh linseed oil, refined, (product number 5840 650) from Maimeri, Mediglia, Italy (IRPA code PR-00-02)
- Heated linseed oil, linseed oil bought from the Droguerie Le Lion (Brussels) was heated for two hours on a low heat
- a mixture in equal parts of the first sample (fresh linseed oil) and Venice Turpentine-Refined Linseed oil mix (equal parts), workshop INP, december 2005

The oil samples were dried for about 10 days in an oven at a temperature around 35 celsius. The samples must be dry to be measured with ToF-SIMS. For the study of the pigments we will first examine a series of lead-based pigments (for more information, see Chapter 3):

- hydrocerussite ( $Pb(OH)_2PbCO_3$ )
- lead carbonate ( $PbCO_3$ )
- *blanc de saturne*, *blanc de plomb traditionnel*, formule Paul Arsic, Ent. Vermeer (IRPA code MC-0G-03/1972)
- flake white (with etiquette S. W&N 17-9-48) (IRPA code MC-0G-03/1983)
- *blanc d'argent mou*, Blocqx (Blocqx et Fils, Terwagne) (IRPA code MC-0G-03/2872)

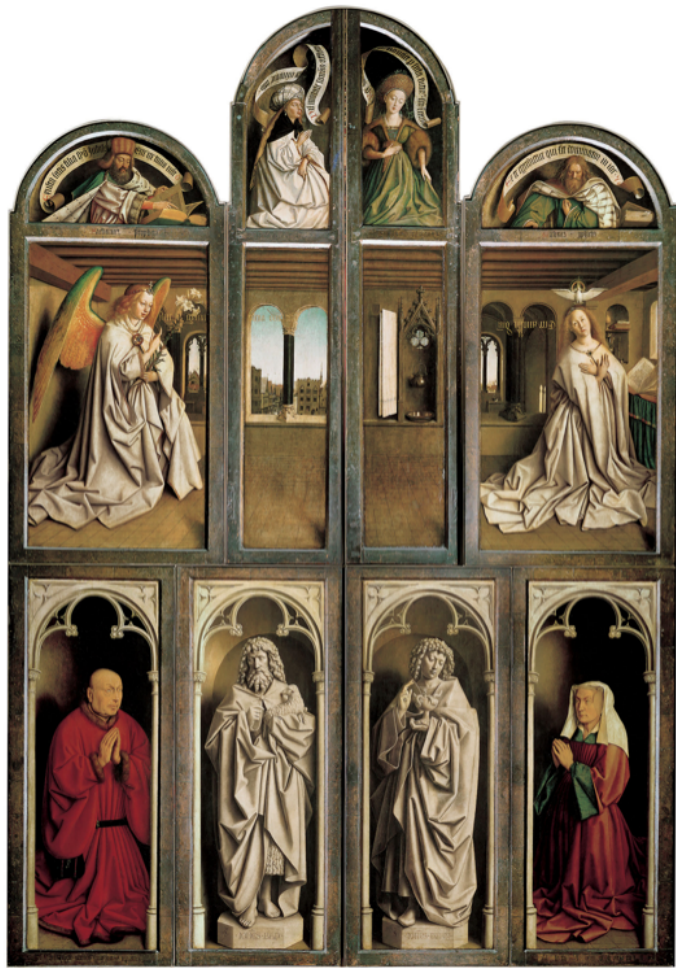


Figure 1.2: *The Adoration of the Mystic Lamb* closed

- minium (a red-orange lead pigment)
- lead chloride ( $PbCl_2$ )

All samples were provided by the laboratory of KIK-IRPA.

The blue pigment azurite (with etiquette 'Japan Forbes', IRPA code MC-0G-02/2115) will be taken as comparison, as it does not contain lead. These oil and pigment samples were studied with ToF-SIMS, for which the experimental conditions are given in Section 1.4. In order to get a more quantitative image of their composition, we will examine the named lead-based pigments with X-ray Photoelectron Spectroscopy (XPS). A small section will be devoted to the examination of the lead isotope ratios, a technique that has been used to identify the origin of the lead used in pigments.

For the second part of this work, four different types of oleaginous binder were each mixed with 8 pigments in order to imitate oil paints. The binders are:

- Fresh linseed oil, refined, (see *supra*)
- Heated linseed oil, (see *supra*)
- Stand Oil-Linseed Oil, in equal parts from Kremer Pigmente, KIK-IRPA laboratorium 13/04/2006 (IRPA code PR-00-02)
- a mixture in equal parts of the first sample (fresh linseed oil) and Venice Turpentine-Refined Linseed oil mix (equal parts), workshop INP, december 2005 (see *supra*)
- a mixture in equal parts of the second sample (heated linseed oil) and the same Venice Turpentine-Refined Linseed oil mix

The pigments are:

- Minium (a red-orange lead pigment)
- Azurite (the same sample as *supra*)
- Verdigris copper acetate from MERLIK L.K. (IRPA code MC-0F-03/2055)
- Purple madder lake (*Lacque de Garance, pourpre*) from Blocqx (J. Blocqx et Fils, Terwagne) (IRPA code Lac RT3)
- Flake White (the same sample as *supra*)
- Lead Carbonate (the same sample as *supra*)
- Lead Chloride (the same sample as *supra*)
- Lead-Tin-Yellow 02 ( $Pb_2Sn_4$ ) (type I) (IRPA code MC-0F-01/2009)

All samples were provided by the laboratory of the KIK-IRPA.

The oil and the pigment were ground together for about one minute and then applied in strips next to each other, without touching, on a glass support (glass plates of approximately 8 cm by 2.5 cm). For each of the binders, two glass plates were needed, one for the first four pigments, together with a stroke of pure binder, and a second for the last four pigments. Three of such series of  $4 \times 2$  glass plates were made and a fourth using cardboard strips as support. Figure 1.3 shows an example of a glass series.



Figure 1.3: One complete series of glass plates. Four such series were made (three on glass plates and one on cardboard). Eight of the ten plates are visible with the aluminium foil covering one half.

The cardboard series and one of the glass series are kept as a back up in a dark and cool environment at the KIK-IRPA. The second series of glass plates was dried by exposure to direct sunlight and the third was artificially aged in a SUNTEST CPS+ at the laboratory of KIK-IRPA. This device is frequently used for artificial ageing. It has one 1500 W air cooled xenon lamp with an irradiance of  $650 \text{ W m}^{-2}$  and an illuminance of 175 000 lux. A UV-filter was used (with suppression of wavelengths shorter than 380 nm). Due to some machine defects, the temperature and the relative humidity are difficult to control, but it is estimated that the temperature is between 50 and 60 °C with low relative humidity. This series was left in the SUNSET CPS+ machine for 35 days. During that time however, several glass plates became loose and, moved by the air flow of the ventilation in the ageing chamber, recovered each other. ToF-SIMS tests were made on this series, but they showed that the samples were too contaminated to be of use. For that reason, the series that had been in open air and direct sunlight for 35 days was put in the artificial ageing chamber for a complimentary 22 days. One half of each of the glass plates was covered with aluminium foil, in order to reduce its exposition to the light (UV) light and to slow down the photo-degradation process (see Figure 1.3). In that way the two ends of each plate could be compared.

After 22 days, the series was removed and stored in a protective box in a dry and cool place. Due to time constraints, only a part of the samples was measured. We decided therefore to focus on lead based pigments and their influence on the ageing process and the capability of ionisation of fatty acids and relative compounds.

ToF-SIMS measurements were done for following samples which were applied on the glass slide, dried in the sunlight and then aged in the SUNTEST CPS+. One half of each slide was exposed to ultraviolet light and one half was covered with aluminium foil and therefore not

exposed to UV:

- fresh and pre-heated linseed oil
- mixtures of fresh and pre-heated linseed oil with flake white
- mixtures of fresh and pre-heated linseed oil with lead carbonate
- mixtures of fresh and heated linseed oil with lead chloride
- mixtures of fresh and pre-heated linseed oil with minium
- mixtures of fresh and pre-heated linseed oil with azurite
- mixture of fresh linseed and pre-heated linseed oil with a Venice turpentine-linseed oil mixture

A number of important peaks was chosen, largely based on previous works (for example [5], [6] or [7]) and compared for the different samples. We hope to see how the ageing process changes the behaviour of the samples under the condition of SIMS measurement and how this is influenced by the presence of lead and copper pigments. Furthermore, we hope to find a way to distinguish between a pre-treated (heated) oil sample and a fresh oil sample. In order to answer some of the questions that were raised by the observations, a further investigation was done by measuring a depth profile of two samples.

### 1.3 Science and art, the place of ToF-SIMS in cultural heritage studies

During the last century, science has taken an ever greater place in the cultural heritage landscape and has become a tool of paramount importance in the struggle to better understand and better conserve works of art. They are vital to retrace their original appearance, determine the techniques used and to verify the authenticity.[8]

Most of the analysis techniques that have been developed through the years have been applied on paintings, textiles, ceramics or metal objects. However, the analysis of art works poses one important restriction on the techniques used, and that is that the samples can never be replaced and that therefore consuming or even damaging the sample should only be allowed in a very restricted number of specific situations. The allowed techniques are therefore divided in three categories. First of all, non-invasive techniques do not require the taking from a sample. Secondly, non-destructive techniques do need a sample to be taken, but the sample is not damaged and re-analysing is possible. Lastly, micro-destructive techniques render the analysed sample useless for further examinations.[8]

Very diverse techniques are used for the analysis of paintings. Ultraviolet and infra-red photography can help to indicate places that have been repainted. X-ray radiography and infra-red reflectography can visualise underpaintings and the support of a painting. Scanning Electron Microscopy (SEM) is used to study the surface of paintings. X-ray fluorescence (XRF) is also a non destructive technique that can be used for elemental identification. Spatial resolutions of some tenths of micrometers are possible and with the so-called  $\mu$ -XRF technique elemental mapping is possible. Often this is used in combination with XRD (X-ray diffraction), but this requires a microsample to be taken. In PIXE (Particle induced X-ray Emission) bombardment with an ion beam creates electromagnetic radiations in the x-ray end of the spectrum. It delivers elemental information and does not require a vacuum, which means that its use is less demanding.[8][9]

The elemental information delivered by the previous techniques is often not sufficient and molecular information is required, most certainly for organic pigments. A combination of XRF and XRD or the  $\mu$ -Raman spectroscopy technique gives such information as does Gas Chromatography/Mass-Spectrometry (GC/MS). The major disadvantage of those techniques is that positional information is lost (unless one uses techniques as imaging Raman spectroscopy and imaging UV/VIS spectroscopy).[8][5]

Of particular interest for the study of paintings is the analysis of cross-section samples. These samples are embedded in an acrylic resin and polished until the stratigraphy of all layers is visible (see for example Figure 1.5). They therefore permit to study the different layers the artist has applied on the support. Various analytical spectroscopic methods can be applied for the studying of these cross-sections: scanning electron microscope (SEM) in combination with energy dispersive X-ray analysis (EDX),  $\mu$ -Raman spectroscopy or infrared microscopy. The results, although preserving spatial information (with a resolution of about 1  $\mu\text{m}$ ), give only elemental compositions. Two important techniques, containing both elemental and positional information, arise: FT-IR and SIMS. The most complete information on a sample is obtained by combining the three techniques: SEM, FT-IR and SIMS.[5]

Fourier Transform Infra-red Spectroscopy (FT-IR) can reveal specific chemical groups (such as carbonates) and their distribution, with a spatial resolution limited to about 7  $\mu\text{m}$ . FT-IR can measure inorganic and organic components, but in a mixture of the two, the former has a tendency to dominate the spectrum, rendering the organic compounds invisible. The technique also requires the surface to be perfectly flat and some pigments are difficultly visible.[5]

A particularly promising technique is Secondary Ion Mass Spectrometry or SIMS in which a sample is bombarded with an ion beam and the emitted secondary ions are studied. Those ions are mostly molecular fragments, and the technique therefore gives the sought-after molecular information. With a substance corresponds a certain 'fingerprint' spectrum, which allows for its identification. Another major advantage of the technique is that it is sensitive to both organic and inorganic compounds, which is quite exceptional. This makes it an interesting technique to study mixtures of oil (organic compounds) and (inorganic) pigments. Furthermore, SIMS shows a remarkable lateral resolution, up to 1  $\mu\text{m}$ . This makes it possible to keep positional information. Lastly, it is a very sensitive technique and is able to measure components that are only present in a concentration in the ppm or ppb range. [10][8] The disadvantage is that SIMS is a micro-destructive technique. However, the damage only takes place on a very small area and therefore most samples can be re-used although that is not always straightforward. An additional disadvantage is that SIMS has to be carried out in a ultra high vacuum (about  $1 \times 10^{-9}$  mbar in our case), which means that samples must be vacuum compatible. Furthermore, SIMS results are particularly sensitive to unevenness of the sample and to chemical contaminations: the peaks of poly-dimethylsiloxane (PDMS) are a sign of contamination and can dominate a whole spectrum. Finally, as will be discussed in the next paragraph, ionisation probability is very dependent on the species and the matrix, rendering the SIMS technique only semi-quantitative.[10][5]

An example of the application of these techniques on a cross-section from the blue robe of the Virgin Mary in the painting *The Descent from the Cross* (ca. 1435) from the Flemish artist Rogier van der Weyden (1399-1464) (see Figure 1.4) is shown in Figures 1.5 to 1.8. In Figure 1.5, seven layers are visible. Layer 1 is a thick white layer, corresponding to the chalk ground. Layer 2 is very thin and brownish and is probably the underpainting. After a thin light-brown layer (layer 3), three layers of paint are visible. Layer 4 is a light blue underpaint containin azurite and small red particles in a white matrix. The second paint layer, layer 5, is dark blue with ultramarine particles. The upper paint layer is a clear blue layer also containing ultramarine



Figure 1.4: *The Descent from the Cross*, 1435, Rogier van der Weyden (1399-1464), oil on oak panel, Museo del Prado, Madrid

particles in a white matrix. Layer 7 corresponds to the varnish layer.[11] The figures show how the different techniques visualise different layers of the painting and help with their identification.

## 1.4 ToF-SIMS: history, working principles and experimental conditions

Secondary Ion Mass Spectrometry (SIMS) is a surface analysis technique based on the collecting of ions that have been ejected from that surface by a focused beam of primary ions. The set-up of a SIMS experiment is shown in Figure 1.9. The first applications date back from the 1940s, but the static SIMS technique was developed in the 1980s in the laboratories of the university of Münster under the supervision of Alfred Benninghoven. Those early experiments were conducted with inert gas ions, mostly  $Ar^+$  but also  $Xe^+$ , as primary ions. They steadily proved that there was a direct relation between the chemical structure of the surface of the samples studied and the SIMS results. Later on, liquid metal atomic ions ( $Ga^+$ ,  $In^+$ ) were used as primary ions. Those Liquid Ion Metal Guns (LMIGs) allowed for much better focussing and therefore a better spatial resolution. In the same period, the old quadrupole based analysers were replaced by Time of Flight (ToF) analysers. After confidence had grown through the successful application of the method on complex materials, ToF-SIMS was used for the first time on biological samples in the 1990s. The results, although promising, also showed the weak spots of atomic metallic ions as ion source: low sensitivity and small yield for high mass molecules. Molecular Dynamics simulations show that the emission of such large molecules, having multiple contact points to the surface, is only possible when there is a cooperative uplifting with different atoms striking on

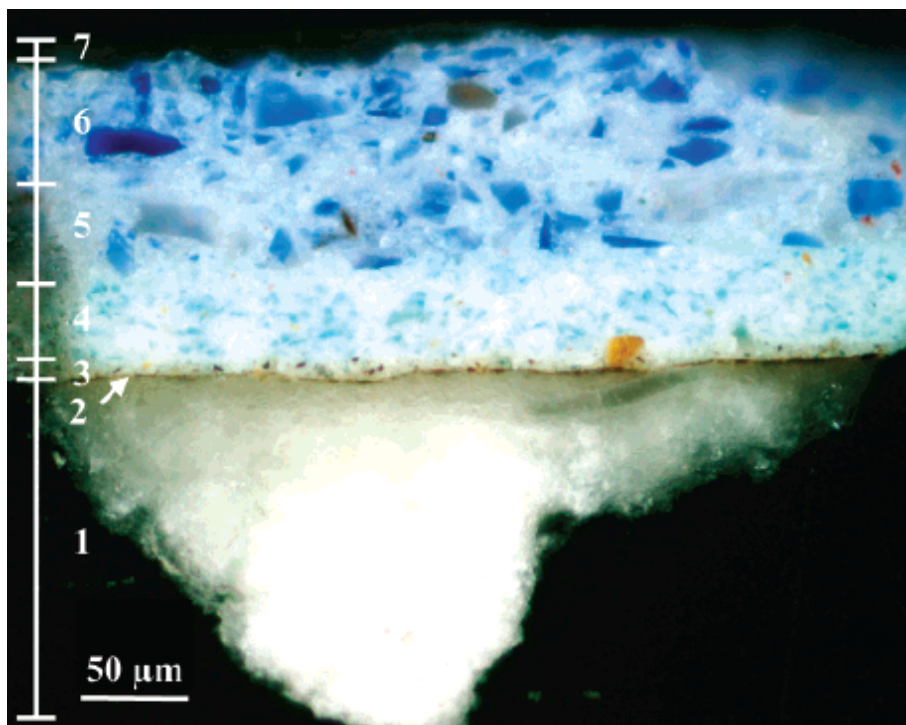


Figure 1.5: Light microscopic image of a paint cross-section van der Weyden; seven layers in this paint cross-section can be distinguished. Image and caption taken from [11].

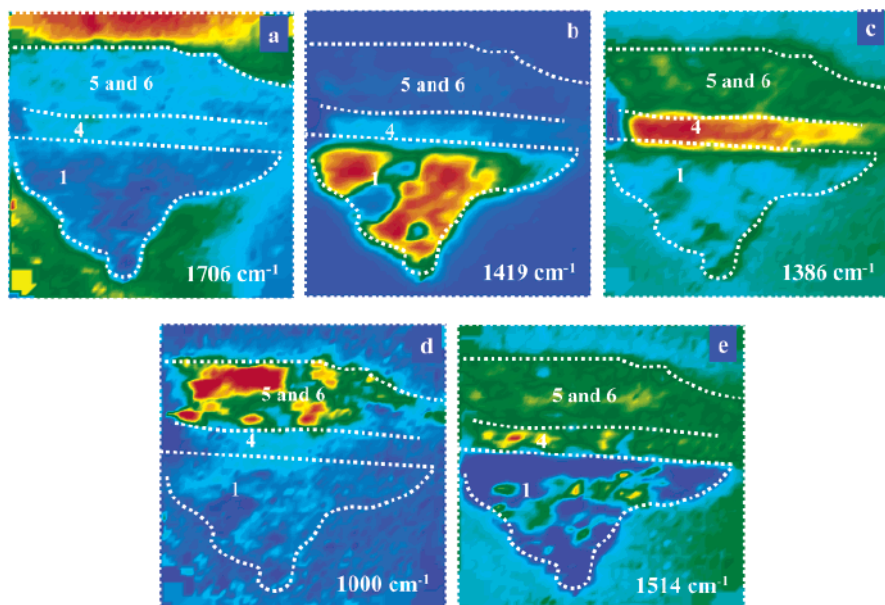


Figure 1.6: Reflection FT-IR images; false color images with red representing a high absorption. FT-IR image (a) at 1706 cm<sup>-1</sup> represents the embedding medium, (b) at 1419 cm<sup>-1</sup> and (c) at 1386 cm<sup>-1</sup> show the presence of carbonates. The FT-IR image (d) at 1000 cm<sup>-1</sup> images silicon-oxygen vibration and (e) at 1514 cm<sup>-1</sup> the asymmetric vibration of lead carboxylate. The layers (1, 4, 5 and 6) which can be discerned are indicated in the images. Image and caption taken from [11].

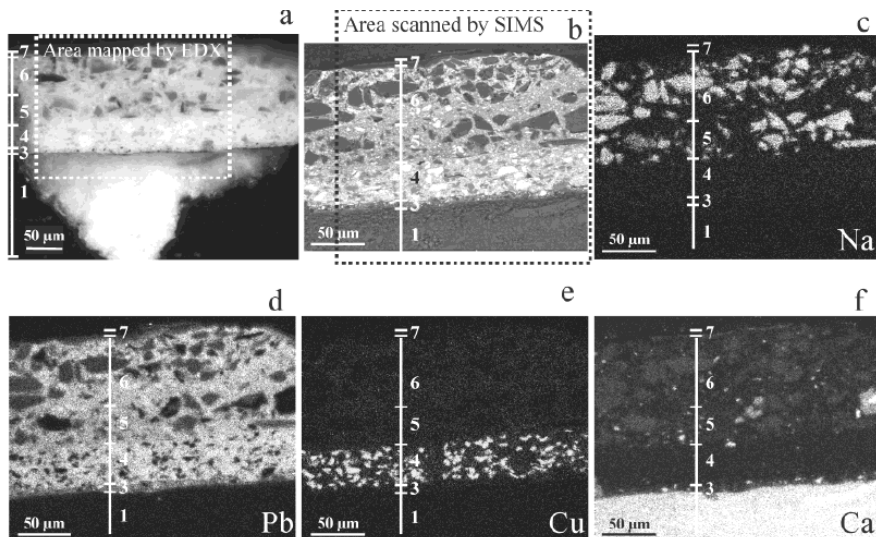


Figure 1.7: (a) Light microscopic image of paint cross-section van der Weyden with a square indicating the measured area for the backscattered X-ray maps; (b) backscattered electron (BSE) image of paint cross-section van der Weyden with a square outlining the scanned SIMS area; (c-f) X-ray maps of sodium (c), lead (d), copper (e) and calcium (f). Image and caption taken from [11].

different parts of the molecule.[12] The probability of such a process is low for atomic primary ions, but grows when clusters are used, in particular consisting of heavy atoms such as gold or bismuth.  $Au_x^+$  with  $x$  ranging from one to 7, in particular  $Au_3^+$ , and  $Bi_3^+$  and  $Bi_5^+$  were found to be effective. These years saw also the rise of the use of multivariate computational methods to analyse complex spectra with many significant peaks. Later on, the idea of using polyatomic ion beams ( $SF_5$  and even  $C_{60}$ ) gained traction. The damage done by the bombardment is much less with such species. Their energy is divided over all the atoms of the polyatomic cluster (leading to a much lower energy per atom), which leads to a higher secondary ion yield and a lower penetration. Metallic atomic or cluster ion beams penetrate deeply, causing chemical degradation, which means that after a certain sputtering time, the information becomes useless. For the polyatomic cluster ion beams, however, the rate of this chemical degradation follows broadly the rate of the removal of material and therefore those beams can be maintained for much longer. These properties opened the way for depth profiling and 3D chemical imaging. In 2009, a new study showed the potential of the use of a giant argon cluster ( $Ar_x$  with  $x$  ranging from 500 to 10 000) as profiling beam, while maintaining an LMIG as analysing beam, due to the high yield of high mass molecules it delivers. In our studies, we will use a metallic cluster ion,  $Bi_3^+$ . Very briefly, we will measure a depth profile of a sample, using  $Ar_{3000}$  for sputtering and  $Bi_3^+$  for the analysis beam.[13]

As outlined above, SIMS exists in two different modes: static and dynamic. In the static regime (SSIMS), positive and negative spectra are measured from a spot on the surface. This regime also allows for imaging: the primary ion beam scans the surface and spectra are taken at difference points. This is demonstrated in Figure 1.10. The dynamic SIMS mode makes bulk analysis and depth profiling possible: a layer is analysed as in the static mode, but afterwards it is removed with a profiling beam such that the underlying layer becomes accessible.

Upon striking the surface, the primary ions lose their energy through collisions, that induce a collision cascade. Some of these collisions can lead to an atom or a cluster of atoms to be ejected. The majority of these particles originate from the first layers of the sample. They are mostly

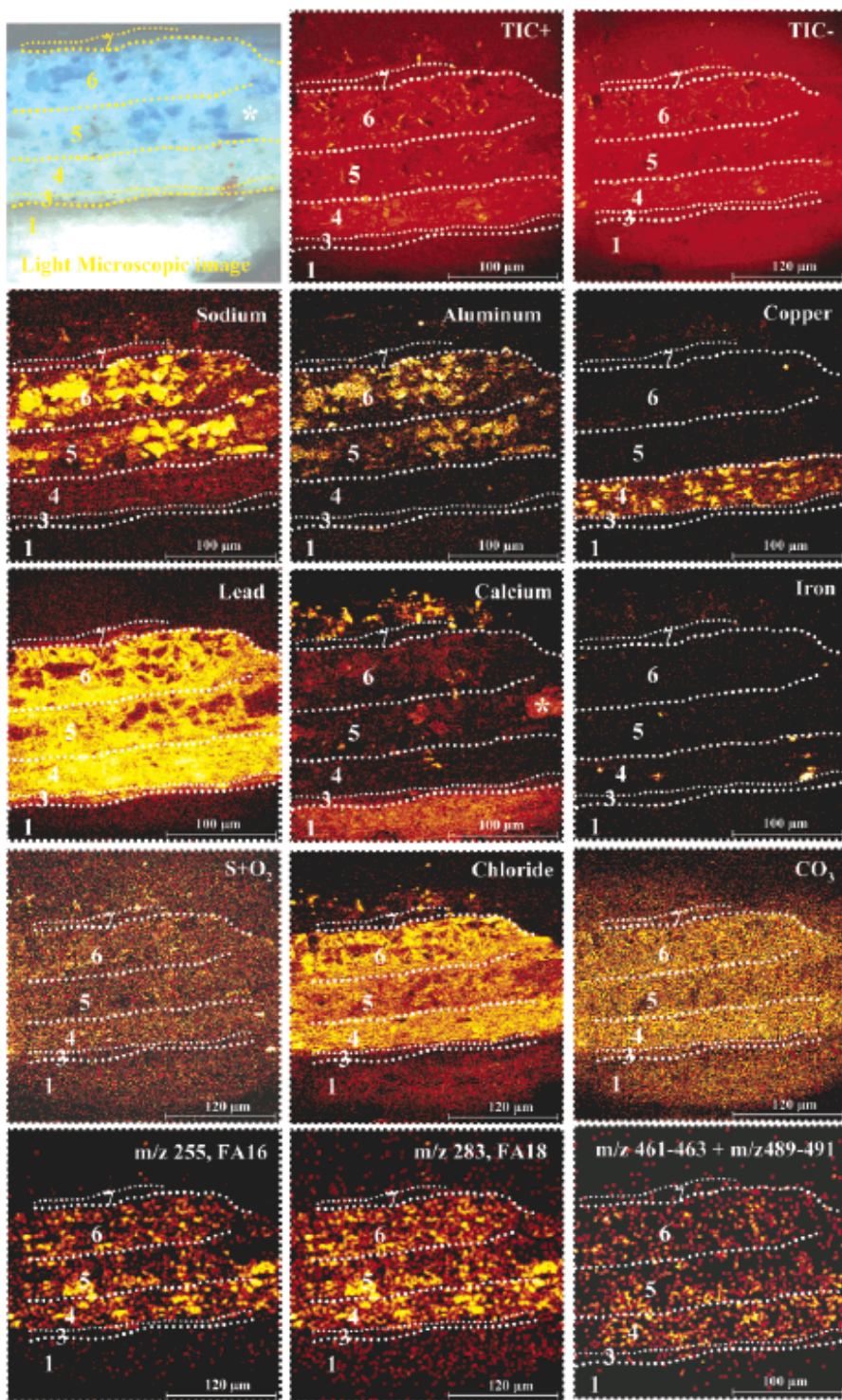


Figure 1.8: SIMS images showing the spatial distribution of the total ions ( $TIC^+$  and  $TIC^-$ ), elements (sodium, aluminium, copper, lead, calcium, iron, sulfur and chloride), and organic fragments ( $CO_3$ , palmitic acid ( $m/z$  255), stearic acid ( $m/z$  283) and a sum image of palmitic and stearic acid lead soap ( $m/z$  461-463, 489-491)) detected in the SIMS spectra of the paint cross section van der Weyden in positive ( $250\ \mu\text{m} \times 250\ \mu\text{m}$ ) and negative mode ( $300\ \mu\text{m} \times 300\ \mu\text{m}$ ). The layers (1, 3-7) detectable with SIMS are indicated in the images, yellow represents high intensity and black low yields. Image and caption taken from [11].

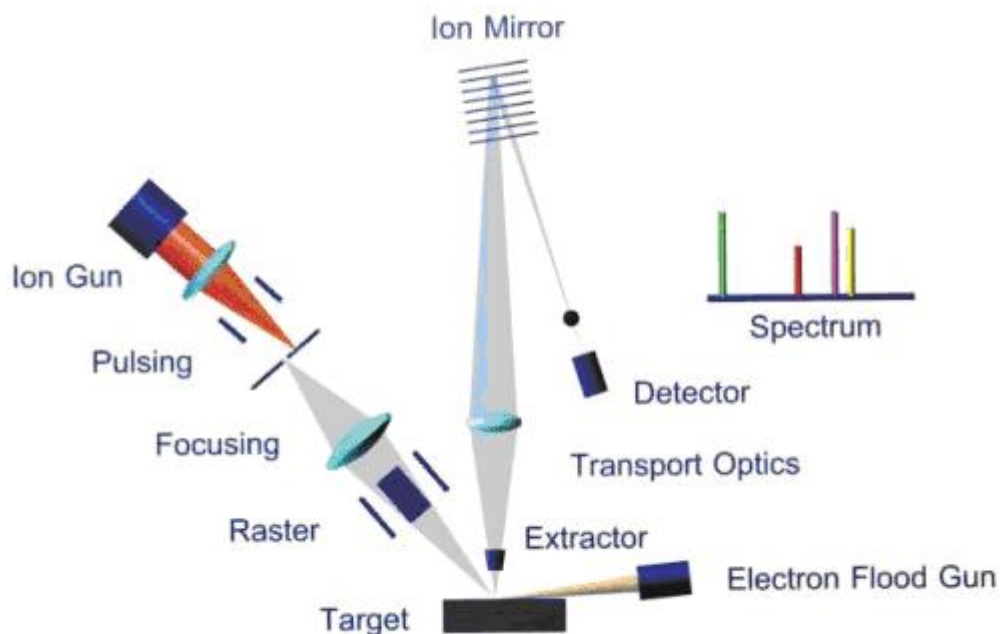


Figure 1.9: An overview of the experimental set-up of a SIMS experiment (from <https://www.aif.ncsu.edu/equipment/time-of-flight-secondary-ion-mass-spectrometry/>, courtesy of IONTOF GmbH)

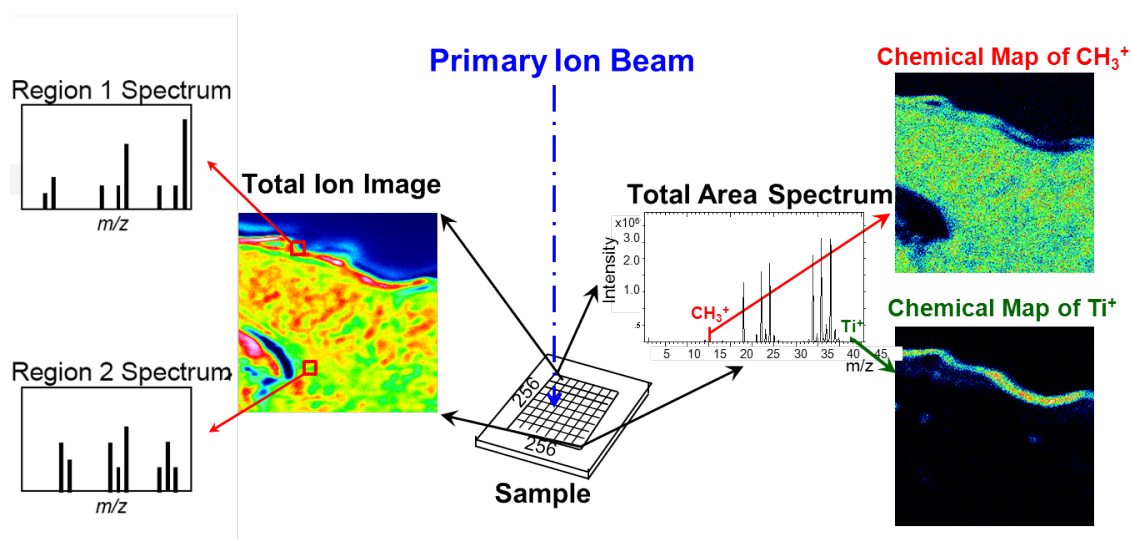


Figure 1.10: Illustration of the static SIMS regimes and its possibilities for imaging (from <https://www.aif.ncsu.edu/equipment/time-of-flight-secondary-ion-mass-spectrometry/>)

neutral, but some are ionised. Ionisation happens almost simultaneously with the emission and is therefore very much influenced by the matrix of the surrounding species. The equation governing SIMS describes the secondary flux of a species  $m$  ([13]):

$$I_m = I_p y_m \alpha^+ \theta_m \eta$$

with  $I_p$  being the flux of primary ions,  $y_m$  the sputter yield,  $\alpha^+$  the ionisation probability for positive ions,  $\theta_m$  the fractional concentration of the species  $m$  in the surface layer and  $\eta$  the transmission of the analysing system.[13] For atomic ions and very small clusters is the sputter yield (the number of  $m$ , both ionic and neutral, species ejected per impact of a primary ion) energy dependent, showing a maximum for a specific energy. When the energy is too low, sputtering will obviously occur less. At too high energies, however, the primary ion penetrates too deep in the material and collisions do not take place as close to the surface as necessary to allow species to leave the surface. The sputtering yield depends also on the angle of incidence (showing a maximum for  $60^\circ$  to  $80^\circ$  measured from the surface normal) and on the mass of the primary particles, with a higher yield for higher mass ions. The ionisation probability heavily depends on the species, with differences between elements of several orders of magnitude. It is particularly interesting to see how the ionisation probability is much higher (up to 1000 times) for the metal oxide than for the pure metal as the strong electronegativity of the oxygen atom enhances the ionisation. This probability is also greatly influenced by the matrix.[13][10] SIMS is therefore not a quantitative technique: the yield of a particular ion relative to another, does not immediately imply that that species is more present in the (surface of the) sample. However, with careful comparison and the use of standards, some conclusions on concentrations can be drawn. SIMS is therefore called a semi-quantitative technique.

The sputtering can change the chemical structure of the sample studied, rendering it useless. However, the key point of SIMS is to use very low primary ion doses to make sure that during one experiment less than 1% of the surface atoms receives an impact. The maximum ion dose (about  $10^{13} \text{ cm}^2$ ), called the static limit, is such that the probability of one spot receiving more than one primary ion is practically non-existent. Molecular Dynamics simulations show that atomic primary ions have the tendency to generate this damage much deeper in the material than polyatomic clusters that only affect the first layers. It is therefore useful to introduce a parameter quantifying this damage. This parameter is the so-called damage cross-section  $\sigma$ . It relates the declining secondary flux of a, chemically meaningful, i.e. not affected by damage, species  $m$  with the flux of primary ions ([13]):

$$I_m = I_{m0} \exp(-\sigma I_p)$$

The damage cross-section  $\sigma$  increases with the energy and mass of the primary ion beam and with increasing angle of incidence (away from the surface normal). As already mentioned previously, in polyatomic primary ions the removal of material will keep pace with the damage done, which allows for analysis beyond the static limit.[13][14]

The secondary particles are emitted with a whole range of different kinetic energies. This energy distribution is defined in the first place by the binding species in the surface, by the number of bonds that need to be broken and on how much energy can be stored in the emitted species (for example by vibration or rotation) To a lesser extent the distribution is also influenced by the energy of the primary ions and their angle of incidence. The range tends to be broad for metallic atoms as primary species and more narrow for cluster ions.[13]

After emission, the secondary particles are conducted to a mass spectrometer for analysis. Currently, the most used analyser is a so-called Time of Flight (ToF) mass spectrometer, a device that distinguishes between the different mass to charge ratio ( $m/z$ ) of the species, based

on their time of flight. The primary ion gun is pulsed in the nanosecond order and therefore the secondary ions arrive in trains at the detector. They have passed through a constant accelerating potential  $V_{acc}$  and have thus acquired an energy  $qV_{acc}$ . The detectors are arranged thus that the initial velocities and energies can be neglected. The corresponding velocity of the ion with mass  $m$  is therefore:

$$E_k(m) = \frac{1}{2}mv^2(m) \Rightarrow v(m) = \sqrt{\frac{2qV_{acc}}{m}}$$

The corresponding time of flight for a detector with length  $L$  is:

$$v(m) = \frac{L}{t(m)} \Rightarrow t(m) = \frac{L\sqrt{m}}{\sqrt{2qV_{acc}}} = \frac{L}{\sqrt{2V_{acc}}} \sqrt{\frac{m}{q}}$$

With all other parameters known, the time  $t$  is measured in order to find the mass to charge ratio  $m/z$  ( $\frac{m}{q}$  in the formula above). In order to find the mass resolution, we differentiate the equation above:

$$\Delta t(m) = \Delta m \left( \frac{\partial t}{\partial m} \right)_{E,L} + \Delta E \left( \frac{\partial t}{\partial E} \right)_{m,L} + \Delta L \left( \frac{\partial t}{\partial L} \right)_{m,E}$$

and we find:

$$\frac{\Delta m}{m} = 2 \frac{\Delta t}{t} + \frac{\Delta E}{E} - 2 \frac{\Delta L}{L}$$

ToF mass spectrometers will deflect high energy ions in order to increase the path length. In that way one tries to enhance the mass resolution by making sure that  $\frac{\Delta E}{E} \approx 2 \frac{\Delta L}{L}$ . The mass resolution is then given by:

$$\left( \frac{\Delta m}{m} \right)^{-1} \approx \left( 2 \frac{\Delta t}{t} \right)^{-1}$$

In this configuration, it is mostly the pulsation of the primary ion beam that limits the resolution.[15]

When an insulator is bombarded with a positive primary ion beam, positive charges will pile up on the surface, increasing the kinetic energy of the emitted positive ions above the acceptance of the analyser. There exist several possible solutions to this problem: a conducting grid can be placed in close contact with the sample or the sample can be deposited on a thin film of silver. The most used technique however, is to remove the surface charges through sputtering, either through bombardment with a neutral atom beam or with an electron flood gun. The flood gun technique, using low energy electrons, seems to work well, certainly for the positive spectrum. For the negative spectrum, however, 10 times more electrons are needed, as the surface potential must be negative in order to release negative ions from the surface, and sample degradation becomes a danger to take into account. In this case, finding the good balance can be a strenuous task.

The experimental conditions and settings that were used for this work are summed up in Table 1.1. We used an IONTOF V instrument, produced by the company ION-TOF GmbH in Münster, Germany and installed in 2010. A picture of a similar system is shown in Figure 1.11

---

<sup>1</sup>The cycle time is the time for one pulse of data collection

<sup>2</sup>Depending on the sample. Rough surfaces such as some of the pigments, in the form of powders, need a smaller analysis area

Primary ion gun	LMIG $Bi_3^{+++}$
Primary beam energy	60 keV
Cycle time <sup>1</sup>	200 $\mu$ s
Primary ion current	0.3 pA
Angle of incidence	45°
Flood gun energy	20 eV
Total acquisition time	1 minute
Analysed area	varies between 500 $\mu$ m $\times$ 500 $\mu$ m, 250 $\mu$ m $\times$ 250 $\mu$ m and 100 $\mu$ m $\times$ 100 $\mu$ m <sup>2</sup>

Table 1.1: Experimental conditions and settings for the ToF-SIMS measurements



Figure 1.11: An IONTOF V system, similar to the one used for this work (from [www.iontof.com](http://www.iontof.com))

## Chapter 2

# Linseed oil: drying and ageing

### 2.1 Introduction

Linseed oil, having good drying properties, was in the past very often used as paint medium, making oil paints fluid, transparent and glossy. It is available in several varieties such as for example cold pressed, sun thickened, pre-polymerized without oxygen, boiled with oxygen or ‘leaded oil’ (which means heated with oxygen and with a lead containing pigment to increase fastness of its drying).

Authors in the X<sup>th</sup> and XI<sup>th</sup> century (like Theophilus Presbyter) mention the facility of painting with an oil medium, but complain that the slow drying renders the technique too laborious and time-consuming.[16] Nevertheless, a myth designating Jan Van Eyck (ca. 1390-1441) as the inventor of oil painting was spread by the publication of Giorgio Vasari’s book (1550) *Le Vite de’ più eccellenti pittori, scultori e architettori* (Lives of the Most Excellent Painters, Sculptors and Architects) in 1550.[17] Modern analysis of artworks has revealed many examples of oil technique in artworks created before Jan van Eyck. However, despite many controversial discussions that refuted this assertion, this myth seems to be still alive.

In the XIX<sup>th</sup> century, when it was finally accepted that Van Eyck did not invent oil paint, the debate shifted to another technique which discovery was attributed to him. This new technique, the so called “varnish technique”, allowed the artist to achieve an enamel-like surface using thin glazes of colour based on oil medium, in which a resinous ingredient is added. Because of the high viscosity and dark colour of hard resin and oil medium, some writers at the beginning of XX<sup>th</sup> century suggested that the principal improvement of Van Eyck was the addition of an essential oil as diluent to make his medium more fluid, limpid and siccative.

But later in the XX<sup>th</sup> century, a new approach focussed on the use of emulsion as medium, including an aqueous medium (protein or polysaccharide) and oil. These components were either mixed or superposed, as layering of tempera and oil paints. The emulsion hypothesis was problematic, because the use of tempera technique was already abandoned less than a century after its first use.

The modern era of conservation science, after the Second World War, brought a new insight in the question of Van Eyck’s medium. In 1950-51, the Central Laboratory (the predecessor of the current KIK-IRPA) started the first in-depth technical analysis of the *Ghent Altarpiece* under the direction of Paul Coremans, founder of the institute. This project was a milestone in the history of the scientific study of paint. Micro-chemical tests revealed Van Eyck’s medium was primarily drying oil, with the addition of a variable quantity of another additive, named “X”. (ref. Agneau Mystic au laboratoire). Although, with the help of modern instrumental analysis, like FT-IR or GC-MS the researchers identified the medium as linseed oil with the

possible addition of diterpenoid resins or as linseed oil alone, the question is still open, not only for the Van Eyck's *Ghent Altarpiece*, but also for other early Netherlandish painters, whose technique shows many similarities with that of the Van Eyck brothers.

Oil painting has the advantage that the slow drying process, in contrast to egg *tempera* or other water based paints, allows the painter to rework and to add details to an extent that was not imaginable before. Furthermore, as mixture in oil can make pigments transparent, it made it possible for the artist to apply the colour in thin layers, called *glazes*, a technique with which a remarkably good imitation of different materials, from velvets over jewels and noble metals to marble, a characteristic on which depended much of the fame of Netherlandish painters, in particular Van Eyck (see for example Figure 2.1).[17][18] The fame of the new method quickly spread to Italy where artists like the Sicilian Antonello da Messina (ca. 1430-1479) played an important role in its propagation. [17] During the next five centuries, oil paint would remain almost every painter's technique of preference.

## 2.2 Linseed oil

Linseed oil was the medium of predilection of most Netherlandish oil painters. This non-volatile drying oil is retrieved from the seeds of the flax plant (*Linum usitatissimum*), a plant originally from the Caucasus and later cultivated in Egypt and Assyria. It finally spread to the North, where its fibres were used to produce linen cloth. The extraction of the oil from the seeds is traditionally done by pressing them after they have been dried and lightly grilled.[19] The best quality oil is obtained when the seeds are pressed cold, as the formation of coloured by-products is prevented.[20] It is considered as one of the best painting mediums thanks to its resistance and its drying properties (in which it is superior to all other oils used for painting). A disadvantage is however that it has a slight natural colour, but the oil can be clarified by exposure to sunlight. Drying in a dark environment, the oil can turn yellowish, but this can also be prevented by allowing contact with sunlight.[19]

Although modern authors do not recommend it ([20]), it seems that the old masters often used to boil the oil before use, either by contact with an open fire or with boiling water. This leads to a better viscosity, a more lively sheen and superior drying properties. To further enhance its drying properties, the oil was often boiled together with metallic salts. Those added driers were mostly lead based, such as litharge ( $PbO$ ) or white lead ( $2PbCO_3Pb(OH)_2$ ), or manganese based, such as manganese oxide ( $MnO$ ) or manganese dioxide ( $MnO_2$ ).<sup>1</sup>[19] According to Xavier de Langlais ([19]), Van Eyck did not use such driers, in contrast to later painters such as da Messina.

## 2.3 Drying of oil

Oil is a fat and is therefore a triglyceride (or triacylglycerol) formed from the combination of glycerol ( $C_3H_8O_3$ ) with three fatty acids (see Figure 2.2). Drying oil also contains small amounts of sterols and vitamins.[6] Glycerol is a polyol (an alcohol with multiple hydroxyl ( $-OH$ ) groups) and fatty acids are so-called carboxylic acids, which means that they have a carboxyl group ( $-COOH$ ). When alcohols and organic acids are combined, an ester is formed with water ( $H_2O$ ) as by-product, as shown in Figure 2.2. The triglycerides in linseed oil contain different types of fatty acids, the major ones being the triply unsaturated linolenic, doubly

---

<sup>1</sup>The term 'boiled oil' is often used for these oils that have been boiled together with lead or manganese oxides. [19] To prevent confusion in this text we shall only use the term 'boiled oil' as such if no other elements were present during the boiling process.



Figure 2.1: Detail of *Virgin and Child with Canon van der Paele* (1434-1436), Jan Van Eyck (ca. 1390-1441), oil on wood, Groeningemuseum, Bruges

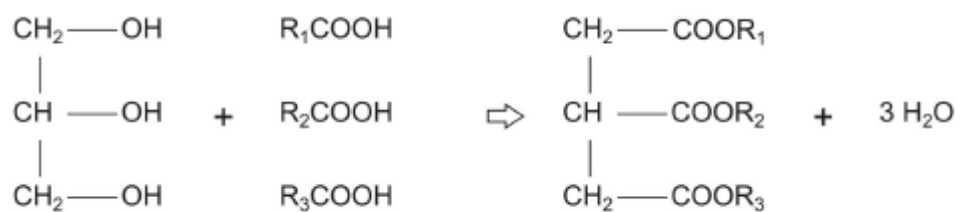


Figure 2.2: Formation of triglyceride by esterification of glycerol (to the left) and three fatty acids. Figure taken from [15]

$C_{16}H_{32}O_2$	palmitic acid	6-7%
$C_{18}H_{30}O_2$	linolenic acid	48-60 %
$C_{18}H_{32}O_2$	linoleic acid	14-19%
$C_{18}H_{34}O_2$	oleic acid	14-24%
$C_{18}H_{36}O_2$	stearic acid	3-6 %

Table 2.1: Principle fatty acids and their relative presence in fresh linseed oil, based on Gas Chromatography measures (taken from [21] via [15])

linolenic-linolenic-linolenic	24%	linolenic-oleic-stearic	7%
linolenic-linolenic-linoleic	14%	linolenic-stearic-stearic	1%
linolenic-linolenic-oleic	15%	linoleic-linoleic-linoleic	1%
linolenic-linolenic-stearic	12%	linoleic-linoleic-oleic	2%
linolenic-linoleic-linoleic	3%	linoleic-oleic-oleic	1%
linolenic-linoleic-oleic	5%	linoleic-oleic-stearic	3%
linolenic-linoleic-stearic	5%	oleic-oleic-oleic	1%
linolenic-oleic-oleic	5%	oleic-oleic-stearic	2%

Table 2.2: Relative presence of different triglycerides in fresh linseed oil (taken from [22] via [15])

unsaturated linoleic and mono-unsaturated oleic acids and the saturated palmitic and stearic acids (see Table 2.1). The way these fatty acids are combined in triglycerides is shown in Table 2.2.

In the context of oils, we call 'drying' the process of the formation of an impermeable, elastic and solid-like film, which corresponds microscopically to the forming of a tangled and cross-linked polymeric network. The drying properties of oil are due to the presence of double bonds in the unsaturated acids of the triglyceride molecules and their interaction with oxygen from the environment allows for the formation of said polymeric network.<sup>2</sup>[23] [20] [24] The exact nature of this process is complicated and still not fully understood. In the following we give an overview of three important processes in the drying of oil. At the beginning of the ageing process, the auto-oxidation and hydrolysis processes dominate, later on the structure of the aged oil is primarily defined by the hydrolysis process.[24]

### 2.3.1 Auto-oxidation process

The first step in the drying process is an auto-oxidation reaction with oxygen from the air. First of all, a carbon loses its associated hydrogen and forms a radical (see Figure 2.3). Such radical reactions are light initiated and metal catalysed.[6] This reaction is energetically the most advantageous when the carbon atom is situated between a double bond on the one side and a single bond followed by another double bond on the other side.[15] The linolenic and linoleic acids present such carbon configurations. The fact that linseed oil is particularly rich in linolenic acid (see Table 2.1) explains its superior drying properties compared to other oils.[23] This free radical will now react with the oxygen present in the air, which leads to the formation of a peroxide (see Figure 2.4). The peroxide radical can attract a hydrogen atom of another chain, making this the active chain. [15] The active peroxide radical can also interact with the double bond of a chain. In this way the two chains are combined and the active centre moves from the peroxide radical to the carbon atom (see Figure 2.5). Once more, carbons atoms situated between a double bond on the one side and a single bond followed by a double bond on the other, as they exist in linolenic and linoleic acids, are energetically favoured.[15] Through the new active centre, the process can continue and a cross-linked network appears. The peroxide

<sup>2</sup>To have drying properties, oils must have a high content of unsaturated fatty acids (>50 %. Olive oil contains mostly monounsaturated oleic acid and has therefore drying properties much inferior to those of linseed oil.)[6]

bond  $O - O$  is not very strong, however, and therefore breaks easily. The free alkoxy radical can now react with a double bond in the same way as described above, once more combining two chains (through an ester group) and leaving a new active centre for further ramification (see Figure 2.6).

### 2.3.2 Destructive reactions: formation of aldehydes or dicarboxylic esters

Instead of merging with another chain and forming a cross-linked network, the alkoxy radical discussed above can also split up. Two results are possible, depending on which side of the ketone group the splitting occurs: a free aldehyde can be formed while an alkyl radical remains bound to the glycerol backbone (see Figure 2.7) or a free alkyl radical is formed with a dicarboxylic ester (see Figure 2.8).[15] The length of the formed chains therefore depends on the place where the auto-oxidation took place. This is mostly near the middle of the chain. For this reason the formed chains will most often consist of 8, 9 or 10 carbon molecules. The corresponding dicarboxylic acids are suberic acid ( $C_8H_{14}O_4$ ), azelaic acid ( $C_9H_{16}O_4$ ) and sebacic acid ( $C_{10}H_{18}O_4$ ).[15]

### 2.3.3 Destructive reactions: hydrolysis

Under the influence of temperature, the contact with water can hydrolyse the triglyceride esters with the liberating of a fatty acid (see Figure 2.9). This is the reversed process from the forming of triglyceride from glycerol and fatty acids. Through this process unbound fatty acids are also present in dried oil. Furthermore, dicarboxylic acids, formed according to the process described above, can also be present as well as acid-rich network oligomers. [15][5]

### 2.3.4 Illustration

The process described above is illustrated in an interesting way in the 2011 article of Bonaduce and his colleagues ([6]). Samples of linseed oil that have undergone different pre-treatments were exposed to a constant temperature of  $80^\circ\text{C}$  and an air flow while their mass is constantly measured. The results are shown in Figure 2.10. We see for the Z oil that there is a certain induction time (a few hundred minutes). This is due to the presence of antioxidants such as carotenoids and sterols in the oil that gradually disappear after having reacted with the oxygen. Thereafter, the oil increases in mass (with a maximum of 10% mass gain). This is due to the reaction of the oxygen with the double bonds of the unsaturated fatty acids, as described above. After reaching a maximum, the mass start to decrease, an effect explained by destructive reactions that form smaller and volatile compounds.[6]

Looking at the oils that have undergone a thermal treatment before (samples ZH150 and ZH300 in Figure 2.10), we see that there is no induction time before and that the mass increase begins almost right away. This suggests that the antioxidants are removed during the pretreatment. Secondly, we see that the oxygen uptake of the preheated oil is less than that of the Z oil. This is due to the fact that these samples have already oxidised and have formed cross-links during the preheating. This leaves less unsaturated chains to oxidise. This effect is even more pronounced for the ZH300 sample treated at  $300^\circ\text{C}$  than for the ZH150 sample, treated at  $150^\circ\text{C}$ . Thirdly, we observe that the mass decrease is slower than in the Z oil sample. This could be explained by the fact that the small and more volatile fragments produced during the destructive reactions are trapped in the polymeric network and cannot escape as easily as in the Z sample.[6]

AH2, the sample that has been heated in the presence with litharge (a typical drier, as mentioned above) shows a pattern like the ZH300 sample. The induction time is even less which implies that, compared to a simple heat treatment, the consumption of antioxidants has increased through to the addition of litharge. The oxygen absorption is at the same level as that of sample ZH300.



Figure 2.3: Resonance forms after the loss of a hydrogen atom: first step of the auto-oxidation process. Figure taken from [15]

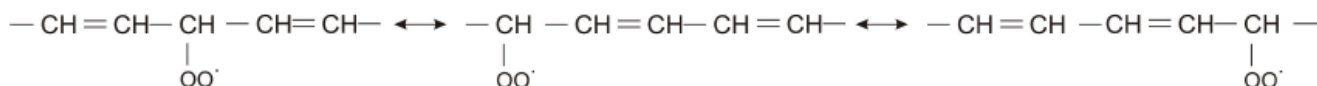


Figure 2.4: Formation of a peroxide radical after reaction with oxygen: second step of the auto-oxidation process. Figure taken from [15]

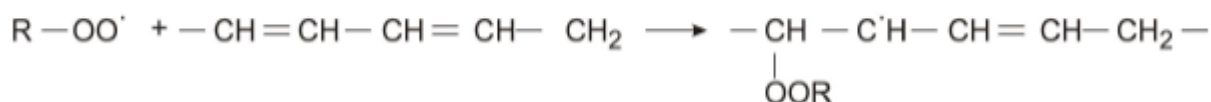


Figure 2.5: Merger of two chains through the peroxide radical: third step of the auto-oxidation process. Figure taken from [15]

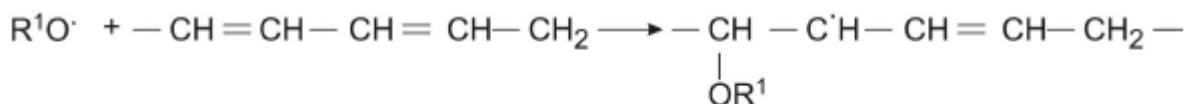


Figure 2.6: Splitting of the peroxide bond and merger of two chains through the alkoxy radical: optional fourth step of the auto-oxidation process. Figure taken from [15]

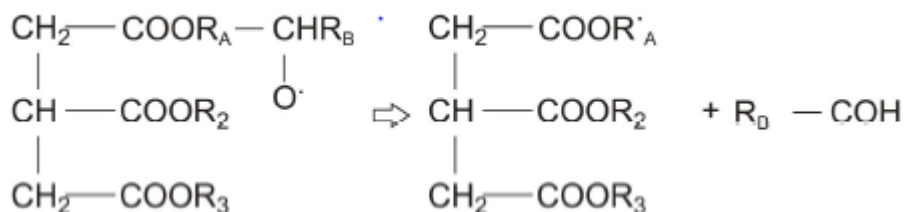


Figure 2.7: Formation of a free aldehyde and a alkyl radical linked to the glycerol backbone: first possibility for destructive reaction. Figure taken from [15]

Although the two samples differ in composition (AH2 is more oxidised but less cross-linked than ZH300 [6]), this apparently results to a similar amount of double bonds present.

## 2.4 Study of fresh and aged linseed oil with ToF-SIMS

### 2.4.1 Samples

The following samples were analysed with the ToF-SIMS technique. They represent different types of pretreatment that artists used for linseed oil.

- Sample A1: Fresh linseed oil, refined, (product number 5840 650) from Maimeri, Mediglia, Italy; taken from the stocks of KIK-IRPA.
- Sample A2: Fresh linseed oil, refined (same origin as Sample A1), undergone simulated ageing treatment. However this sample was covered with aluminium foil during the treatment.
- Sample A3: Fresh linseed oil, refined (same origin as Samples A1 and A2), undergone simulated ageing treatment.
- Sample B1: Boiled linseed oil, boiled for two hours on a low heat from Le Lion; taken from the stocks of KIK-IRPA.
- Sample B2: Boiled linseed oil (same origin as Sample B1), undergone simulated ageing treatment. However this sample was covered with aluminium foil during the treatment.
- Sample B3: Boiled linseed oil (same origin as Samples B1 and B2), undergone simulated ageing treatment.
- Sample C: Exact composition unknown, named 'oil with lead'. Probably linseed oil with lead based driers added; taken from the stocks of KIK-IRPA. The sample has previously undergone simulated ageing treatment the exact conditions of which are unclear.
- Sample D: Linseed oil, boiled with litharge, from Vermeer; taken from the stocks of KIK-IRPA. The sample has previously undergone simulated ageing treatment the exact conditions of which are unclear.

Samples A1 and B1 were dried in the laboratory during four weeks in an oven at approximately 30 °C. In order to check the meaningfulness of the results, different measurements were always taken on different places of the sample and this for each sample and for each ion mode (positive or negative). For samples A1 and B1, three different measurements were taken at different places on the sample in both ion modes (positive and negative, leaving six different measurements at six different places). Those measurements shall be referred to as P\_Sample A1\_1 (P\_Sample B1\_1) to P\_Sample A1\_3 (P\_Sample B1\_3) for the measurements of the positive ions and as N\_Sample A1\_1 (N\_Sample B1\_1) to N\_Sample A1\_3 (N\_Sample B1\_3) for the negative ions. For all the other samples (A2, A3, B2, B3, C and D) six measurements were taken in each ion mode. Analogously, those will be referred to as, for example, P\_Sample B3\_1 to P\_Sample B3\_6.

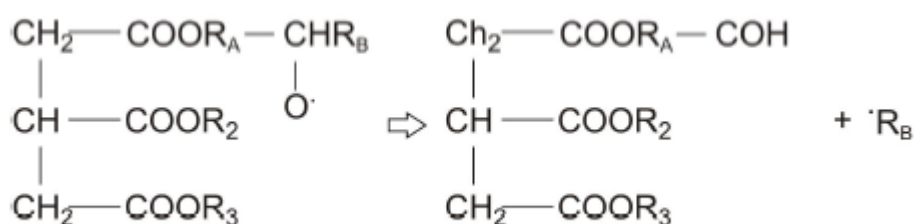


Figure 2.8: Formation of a free alkyl radical and a dicarboxylic ester (a dicarboxylic acid bound on the glycerol backbone): second possibility for destructive reaction. Figure taken from [15]

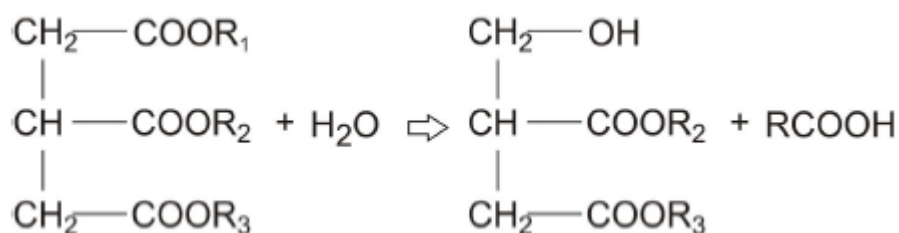


Figure 2.9: Hydrolysis with the formation of a free fatty acid: third possibility for destructive reaction. Figure taken from [15]

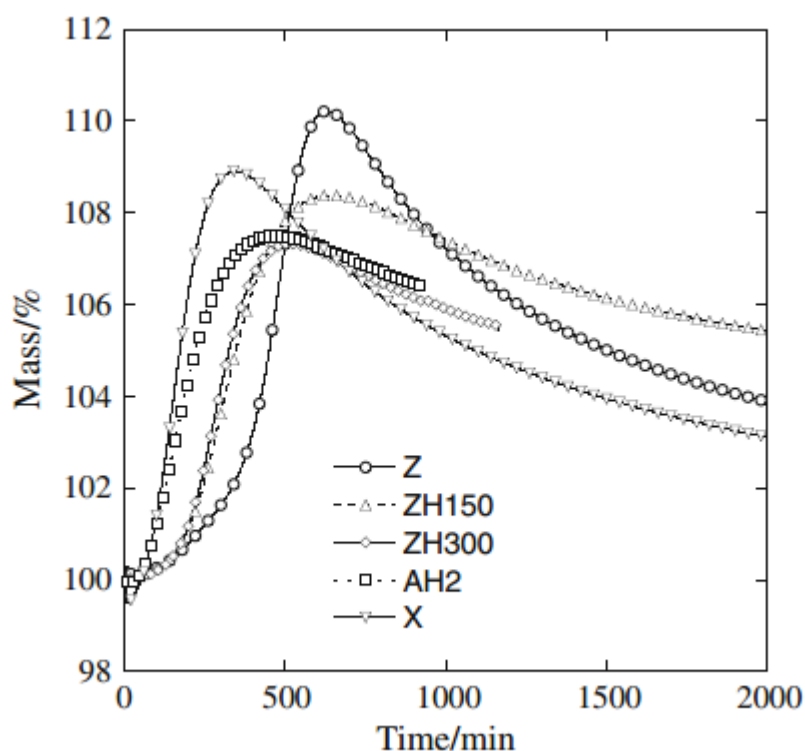


Figure 2.10: Percent mass changes of several linseed oils (Z = untreated oil; ZH150 = Z oil heated to 150 °C; ZH300 = Z oil heated to 300 °C; AH2 = Z oil + Lead (II) oxide then heated to 150 °C; X = water-washed Z oil) treated under air flow at a constant temperature 80 °C versus time of treatment. Figure taken from [6]

## 2.4.2 Observed positive ions

At small masses (below  $m/z$  100), a lot of hydrocarbon fragments are observed. They are fragments of larger molecules present in the oil samples and are not specific enough to be meaningful (see also [5]). Fatty acids are visible in the positive ion spectrum through two different kind of fragments: a protonated form (through the addition of a hydrogen atom:  $[RCOOH + H]^+$ ) and acylium ion form (through the subtraction of  $OH$ :  $[RCOOH - OH]^+$ ). [15][5] In the different samples, following fragments have been observed:

- acylium ions of the dicarboxylic suberic ( $C_8H_{13}O_3^+$ ), azelaic ( $C_9H_{15}O_3^+$ ) and sebacic ( $C_{10}H_{17}O_3^+$ ) acids (at  $m/z$  157, 171 and 185),
- acylium ions of the saturated palmitic ( $C_{16}H_{31}O^+$ ) and stearic ( $C_{18}H_{35}O^+$ ) acids (at  $m/z$  239 and 267),
- protonated ions of the saturated palmitic ( $C_{16}H_{33}O_2^+$ ) and stearic ( $C_{18}H_{37}O_2^+$ ) acids (at  $m/z$  257 and 285),
- acylium ions of unsaturated linoleic ( $C_{18}H_{31}O^+$ ) and oleic  $C_{18}H_{33}O^+$  acids (at  $m/z$  263 and 265),
- protonated ions of unsaturated linolenic ( $C_{18}H_{31}O_2^+$ ), linoleic ( $C_{18}H_{33}O_2^+$ ) and oleic ( $C_{18}H_{35}O_2^+$ ) acids (at  $m/z$  279, 281 and 283),
- acylium ions of monoglycerides (or monoacylglycerols) of azelaic ( $C_{12}H_{21}O_5^+$ ), palmitoleic<sup>3</sup> ( $C_{19}H_{35}O_3^+$ ), palmitic ( $C_{19}H_{37}O_3^+$ ), linoleic ( $C_{21}H_{37}O_3^+$ ), oleic ( $C_{21}H_{39}O_3^+$ ) and stearic ( $C_{21}H_{41}O_3^+$ ) acid (at  $m/z$  245, 311, 313, 337, 339 and 341),
- acylium ions of diglycerides (or diacylglycerols) of palmitic acid on one branch and suberic ( $C_{27}H_{49}O_6^+$ ), azelaic ( $C_{28}H_{51}O_6^+$ ), sebacic ( $C_{29}H_{53}O_6^+$ ), palmitic ( $C_{35}H_{67}O_4^+$ ), linoleic ( $C_{37}H_{67}O_4^+$ ), oleic ( $C_{37}H_{69}O_4^+$ ) and stearic ( $C_{37}H_{71}O_4^+$ ) acid on the other (at  $m/z$  469, 483, 497, 551.5, 575.5, 577.5, 579.5),
- acylium ions of diglycerides of stearic acid on one branch and suberic ( $C_{29}H_{53}O_6^+$ ), azelaic ( $C_{30}H_{55}O_6^+$ ), linolenic ( $C_{39}H_{69}O_4^+$ ), linoleic ( $C_{39}H_{71}O_4^+$ ), oleic ( $C_{39}H_{73}O_4^+$ ) and stearic ( $C_{39}H_{75}O_4^+$ ) acid on the other (at  $m/z$  497, 511, 601.5, 603.5, 605.5 and 607.5),
- acylium ions of diglycerides with linolenic acid on one branch and linolenic ( $C_{39}H_{63}O_4^+$ ) and oleic ( $C_{39}H_{67}O_4^+$ ) acid on the other (at  $m/z$  595.5 and 599.5),
- acylium ions of diglyceride with linoleic acids on both branches ( $C_{39}H_{67}O_4^+$ ) (at  $m/z$  599.5)

Fragments such as glycerol, triglycerols or other possible mono- and diglycerols are not observed and neither are any triglycerides. Measurements of reference standards of a triglyceride, containing stearic and palmitic acids, ([5]) shows indeed only diglyceride, monoglyceride and free fatty acid fragments (containing palmitic and stearic acid) in the form of acylium ions, not in protonated fragments, which is consistent with our observations. A measurement of a reference of free stearic acid ([5]), however, shows both acylium and protonated fragments, in a ratio 1:1,2.

## 2.4.3 Observed negative ions

Fatty acids are visible in the negative ion spectrum through two different kinds of fragments: a deprotonated form (through the loss of a hydrogen atom:  $[RCOOH - H]^-$ ) and aliphatic chain fragments, which are visible in ions of the type  $C_2H_3(CH_2)_xCOO^-$ . [15][5] In the different samples, following fragments have been observed:

---

<sup>3</sup>Palmitoleic acid ( $C_{16}H_{30}O_2$ ) is a monounsaturated fatty acid.

- deprotonated ions of octanoic ( $C_8H_{16}O_2$ ), nonanoic ( $C_9H_{18}O_2$ ) and decanoic acid ( $C_{10}H_{20}O_2$ ) ( $C_8H_{15}O_2^-$ ,  $C_9H_{17}O_2^-$  and  $C_{10}H_{19}O_2^-$  at  $m/z$  143, 157 and 171). These short chains are products of oxidation and degradation processes ([5]), but these could also correspond to larger molecules that have fragmented during the ionisation process,
- deprotonated ions of aliphatic chain fragments of fatty acids from the type  $C_2H_3(CH_2)_xCOO^-$ , separated by 14 amu. We observed fragments for  $x$  ranging from 0 to 12 (at  $m/z$  71, 85, 99, 113, 127, 141, 155, 169, 183, 197, 211, 225 and 239),
- deprotonated ions of dicarboxylic suberic ( $C_8H_{13}O_4^-$ ) and azelaic ( $C_9H_{15}O_4^-$ ) acids (at  $m/z$  173 and 187),
- deprotonated ions of saturated palmitic ( $C_{16}H_{31}O_2^-$ ) and stearic ( $C_{18}H_{35}O_2^-$ ) acids (at  $m/z$  255 and 283),
- deprotonated ions of unsaturated palmitoleic ( $C_{16}H_{29}O_2^-$ ), linolenic ( $C_{18}H_{29}O_2^-$ ), linoleic ( $C_{18}H_{31}O_2^-$ ) and oleic ( $C_{18}H_{33}O_2^-$ ) acids (at  $m/z$  253, 277, 279 and 281).

Measurement of reference standards of triglyceride has shown that ester-bound and free fatty acids both produce deprotonated ions. The yield however, should be two times higher for the ester-bound than for the free fatty acids.[5] An example of a ToF-SIMS spectrum is shown in Figure

#### 2.4.4 Discussion of the results for dried and aged non boiled and boiled linseed oil (sample series A and B)

The legenda for the following figures is found in Figure 2.12.

##### Linolenic acid

Looking at the deprotonated ions from linolenic acid (Figure 2.13), we see that the yield in samples A1 and A3 is almost five times lower than that of sample A2. We must stress that ToF-SIMS is not a quantitative technique, however as we are comparing the same ion for very similar samples, we believe that it is possible that quantitative conclusions can be drawn from these results. If that is true, this means that linolenic acid (in both bound and free form) is less present in sample A1 than in A3. This conclusion is surprising at first sight. As we know, linolenic acid is a triple unsaturated fatty acid, very present in fresh linseed oil (48%-60% according to 2.1), that will disappear gradually through the auto-oxidation process. This would lead to the conclusion that that samples A1 and A3 have undergone a more far-reaching auto-oxidation process than sample A2. This process is induced by light ([6]) and needs of course the presence of oxygen. Sample A1 (as sample B1) has undergone some days of mild heat treatment to make it dry (a necessary step to allow the characterisation by ToF-SIMS) and sample A3 (as sample B3) were aged artificially, involving exposure to (UV) light and air (due to the presence of a fan in the ageing oven). These factors could explain why the auto-oxidation was stronger in samples A1 and A3 than in the sample A2 which was present in the same oven as sample A3 but was covered with aluminium foil, blocking it from UV light and (partly) from contact with oxygen. No difference in the yield levels is detected between samples A1, A3, B1 and B3. This seems to suggest that the linolenic presence has reached a minimal level and has almost completely disappeared in these samples. Secondly, this process must have taken place quite rapidly, as the effect is the same for samples that have merely dried (A1 and B1) as for samples that have undergone some weeks of ageing (samples A3 and B3).

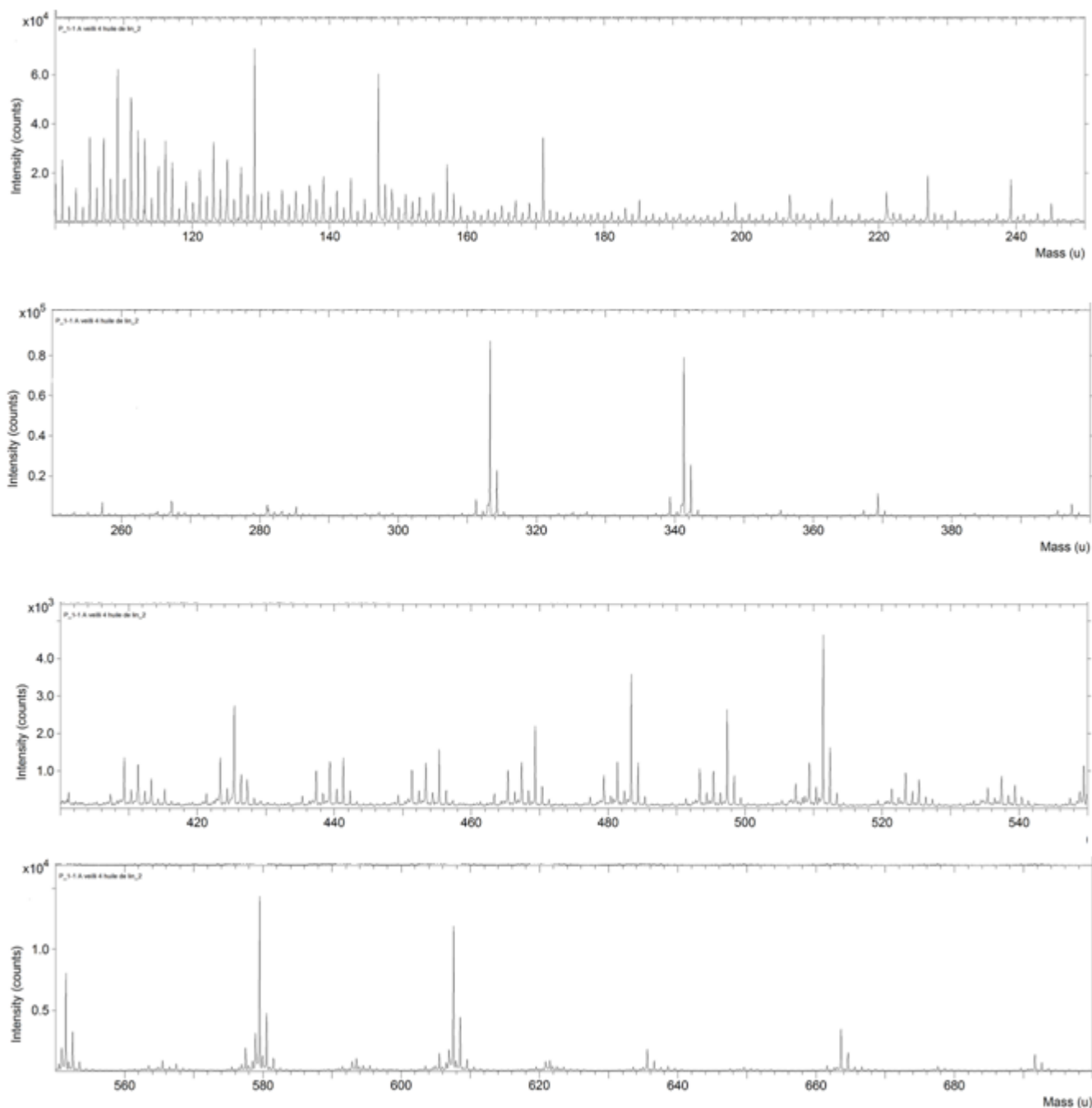


Figure 2.11: ToF-SIMS spectrum for positive ions an aged sample of linseed oil (A3): we see the peaks of the acylium ions of monoglycerides with palmitic and stearic fatty acid at  $m/z$  313 and 341, many diglycerides (in the zone  $m/z$  420-600) such as diglycerides palmitic-palmitic, palmitic-stearic, stearic-stearic at  $m/z$  551.5, 579.5 and 607.5

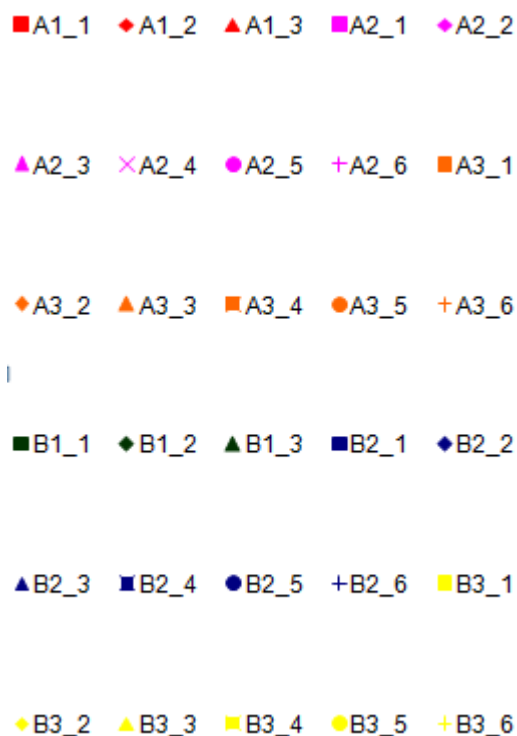


Figure 2.12: Legend used for Figures 2.13 to 2.37

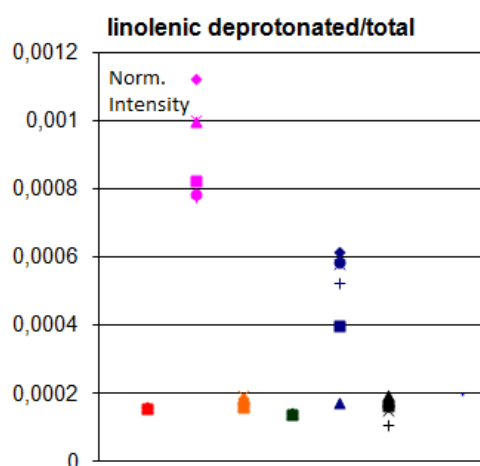


Figure 2.13: Negative deprotonated ions of linolenic acid  $C_{18}H_{29}O_2^-$  at  $m/z$  277 in linseed oil

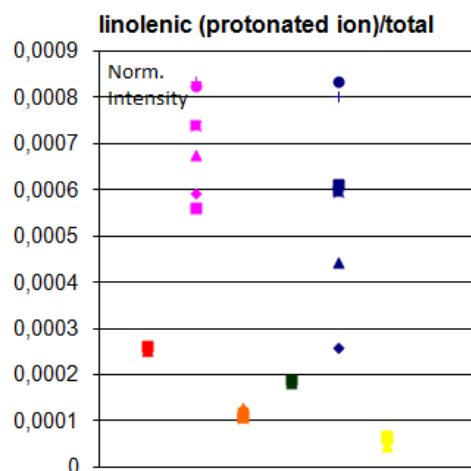


Figure 2.14: Positive protonated ions of linolenic acid  $C_{18}H_{31}O_2^+$  at  $m/z$  279 in linseed oil

It seems strange however, that the auto-oxidation process has gone further in sample A1 than in sample A2 as this last sample has been exposed to direct sunlight for 35 days before artificial ageing. Another possible interpretation for the low intensities of deprotonated ion in A1 (and B1) could be due to the fact that there is a considerable difference in fatty acid's deprotonated ion yield between free and ester bound fatty acids. Keune ([5]) reports that for free stearic acid, the deprotonated ion yield is twice as high than for triglyceride with three stearic acid molecules on its branches. No reference measurement was done to check this assertion for linolenic acid, but if we suppose that the effect is similar, the low yield for A1 could be due

to the fact that the present linolenic acids are bound and therefore much less ionised in SIMS. The fact remains however that, even if we suppose that all linolenic acid molecules are bound in A1 and all are free in A2, the factor five remains high (compared to the factor 2 reported for stearic acid). We believe that in any case, the low yield in A3 must be due to the loss of linolenic acid in both bound and free form in the film as it is difficultly conceivable that this sample shows more bound fatty acids than its counterpart that has not been irradiated by the Xenon lamp during the artificial ageing. A second caveat we would like to add is that we must remember that ToF-SIMS is a surface sensitive technique and that the conclusions above are only valid for a thin oil film. It is possible that through ageing certain molecules migrate in the sample and that there is an important difference between the surface and the bulk. However, literature suggests that in fresh oil free acids are mostly present in the surface. If we still think of sample A1 as being 'fresh' oil, this effect would rather enhance the ion yield and is therefore no explanation for our observations. In any case, this can be further investigated with a depth profile.

Sample B2 shows a yield above this level (although we must acknowledge that there is a considerable spread on the results). As A2 and B2 have been treated under the same circumstances, we can follow the same logic: the lesser contact with light and oxygen has not allowed the auto-oxidation process to fully take place. However we see that the yield in B2 is only half of that of A2. We believe we can conclude that linolenic is less present in boiled oil. This is in line with the literature, suggesting that pre-heated oil is more oxidised ([6]).

The protonated ion originates from free fatty acids ([5])(see Figure 2.14). The ion yield is much less for A3 than for A2, but is the highest for A2. We believe that we can draw the conclusion that A2 and B2 are less oxidised than A3 and B3. The yield of A1 is higher than A3. This is not easily interpretable. We would expect that the protonated ion rises with hydrolysis, but the oxidation process makes the linolenic acids disappear, which may explain the low yield in A3. An other possible explication lies in the observation reported in literature that in fresh oil, free fatty acids are present on the surface, while in aged oil, the fatty acids are more abundant in the bulk ([5]). ToF-SIMS is indeed a surface sensitive technique, sensing only the upper layers of a material and not its bulk. The B samples follow the same rationale as the A series, although showing always a lower yield than their counterparts. We suggest that the pre-heating reinforces the effect of ageing on the distribution of fatty acids on the surface or in the bulk.

### **Linoleic acid**

We recognise in the yield of the deprotonated ion (Figure 2.15) the same pattern as for the deprotonated ion of linolenic acid, which would corroborate the hypothesis that A3 and B3 have undergone a further-reaching auto-oxidation than samples A2 and B2. The explanation of the yield of A1 and B1 poses the same problem as before and it is unclear whether the low yield is due to further auto-oxidation, less ionisation by bound fatty acids or due to migration. A2 has 2,5 times higher yield than A1 and A3; B2 has a 3 times higher yield. As before with the linolenic acid (5 times and 2,5 times higher respectively), the difference is more pronounced for the A series, but in both cases this difference is smaller. This may be because of the fact that linoleic is twice unsaturated and would therefore be (slightly) less susceptible to the auto-oxidation process. Additionally, linoleic acid can only form external hydroperoxides, while on linolenic acid hydroperoxide is formed on external as well as on internal positions.[23] As with the linolenic acid ions, B2 shows significant lower yield than A2 and here this trend is also visible in B1 and B3 versus A1 and A3. This means that linoleic acid has already partly disappeared during boiling, and that (at least for the A series) the minimal level has not been reached yet. The yield of the linoleic acid's deprotonated ion is in general about four times larger than that of linolenic acid. This is in spite of the abundance of this last acid in fresh linseed oil (about four times less present, according to Table 2.1). Linolenic, as mentioned before, reacts more strongly to

the auto-oxidation process and will disappear more quickly. It is doubtful that this is the only explanation for the difference. Different ionisation probabilities could play as well, although both fatty acids have a comparable structure. A third possibility is that together with ions originating from the fatty acids themselves, we also observe fragments of higher mass molecules, such as oleic acid. It is however unclear why this contribution would be larger for the linoleic peak than for the linolenic peak.

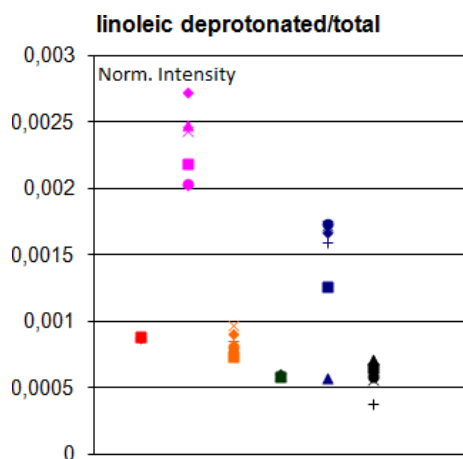


Figure 2.15: Negative deprotonated ions of linoleic acid  $C_{18}H_{31}O_2^-$  at  $m/z$  279 in linseed oil

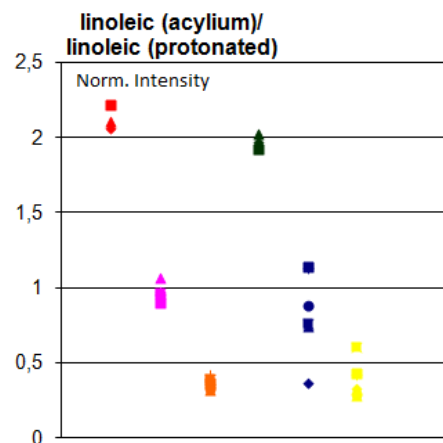


Figure 2.16: Ratio of positive acylium and protonated ions of linoleic acid in linseed oil

ToF-SIMS measurements of reference standards have shown that free fatty acids are visible in the positive spectrum through protonated and acylium ions in a ratio of 1.2 to 1. (Ester)-Bound fatty acids however, only give rise to an acylium ion.[5] We believe therefore that we can use the ratio of the yield of the acylium ion to that of the protonated ion to investigate whether the free fatty acids in a sample are more or less bound. For linoleic acid, this ratio is represented in Figure 2.16. We see steadily decreasing ratio for A1, A2 and A3. B1, B2 and B3 show roughly the same values as their counterparts in series A. This decreasing acylium/protonated ratio indicates in our opinion a progressing hydrolysis (as the free fatty acid content shifts from bound to being unbound). We know that hydrolysis is a reaction that is stimulated by temperature and the presence of water. It is active from the beginning of the drying and ageing process, but it is only after a while that it becomes dominant over the auto-oxidation and cross-linking reaction. We believe that the fact that A1 (as B1) has only undergone a drying treatment, limited in time, can explain why it shows less hydrolysis than samples A2 (B2) and A3 (B3). The difference between samples A2 and A3 (and between samples B2 and B3) must be attributed to the fact that the covering with aluminium foil inhibits the hydrolysis slightly: we believe that it diminishes the exposure of the sample to water and that the exposure to heat is roughly unaffected.

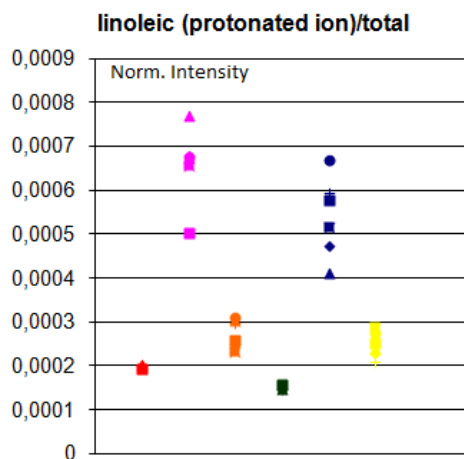


Figure 2.17: Positive protonated ions of linoleic acid  $C_{18}H_{33}O_2^+$  at  $m/z$  281 in linseed oil

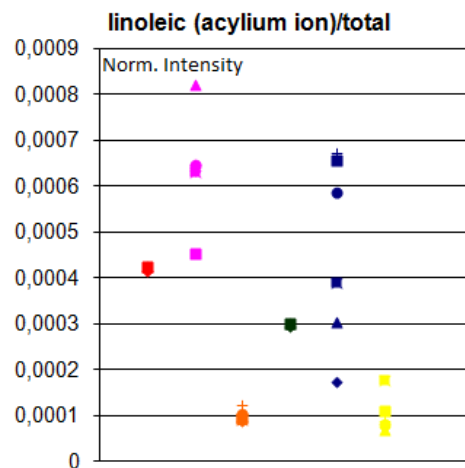


Figure 2.18: Positive acylium ions of linoleic acid  $C_{18}H_{31}O^+$  at  $m/z$  263 in linseed oil

The acylium ion yield will decrease when a sample has undergone more auto-oxidation and hydrolysis. The auto-oxidation process tends to decrease also the protonated yield, but the hydrolysis reaction tends to increase it. This makes the final protonated ion yield the result of a trade-off between the auto-oxidative and the hydrolysis process. The fact that the protonated ion yield of linoleic acid (Figure 2.17) is lower for sample A3 than for sample A2 shows that although in A3 the hydrolysis process has gone further than in A2 (as proven by the acylium/protonated ratio), still the auto-oxidative process, far stronger in A3 than in A2 (as shown by the deprotonated ion yield) dominates in the trade-off. The same conclusion can be drawn for the B series of boiled oil.

The B series follows the same patterns as the A series. The acylium/protonated ratio is about the same for counterparts in the same sample. A substantive difference can be seen in the yield of deprotonated ions of A2 and B2 samples (boiling has an auto-oxidative effect). The same difference is visible in the acylium and protonated ion yields, however more pronounced in the first. We remark that the A3 and B3 show the same values, which seems to corroborate the assertion that linoleic acid is affected early on in the drying and ageing process and that the ageing process has levelled out differences between the boiled (B3) and the non-boiled (A3) oil.

### Oleic acid

In the light of what we have seen for the deprotonated ions of linolenic and linoleic acids, the deprotonated ion yield for oleic acid (Figure 2.19) shows a strange behaviour. The yield for A1 is higher than for A2 and A3, although our hypothesis said that the auto-oxidation process in A2 had less far than in A1 and A3. For the heated oils however, the levels of B1 and B2 are comparable. A1 and A2 show clearly a higher yield than A3 (the same holds for B1, B2 and B3). This may lead to the conclusion that the disappearance of oleic acid is a far slower process than that of linolenic and linoleic acids. This may be due to the fact that the energetically most advantageous carbon configuration for the auto-oxidation process, more specifically the hydroperoxide formation, is present in linolenic and linoleic acid and not in oleic acid.[23] This could also be the reason that the deprotonated yield is remarkably higher for oleic acid than for linoleic acid, although they are present in fresh linseed oil in broadly the same quantities (see Table 2.1). The yields of A1 and A2 are about double those of B1 and B2. This shows that oleic

acid is lost in boiled oil, which is in line with the observation in literature that pre-heated oil is more oxidised and has fewer double bonds.[6] Clearly oleic acid is further lost during ageing, both for boiled and non-boiled oil.

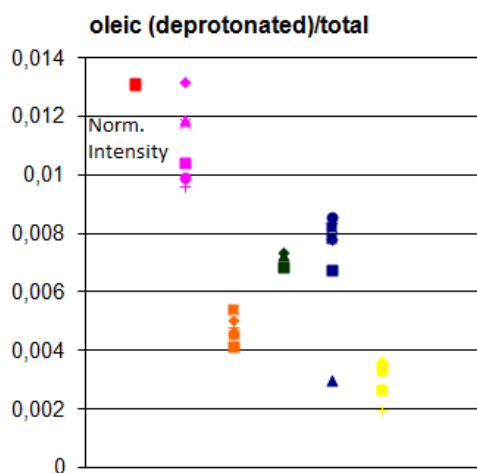


Figure 2.19: Negative deprotonated ions of oleic acid  $C_{18}H_{33}O_2^-$  at  $m/z$  281 in linseed oil

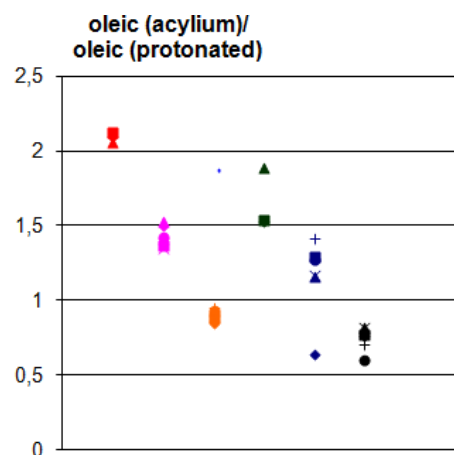


Figure 2.20: Ratio of positive acylium and protonated ions of oleic acid in linseed oil

Looking at the acylium/protonated ratio for oleic acid (Figure 2.20), we see the same rationale as for linoleic acid: A3 shows more hydrolysis than A2, A2 more than A1 and the same holds for the B series. It seems that the boiled oil has also undergone more hydrolysis than its non-boiled counterpart. Literature states indeed that pre-treatment enhances hydrolysis ([6]) and the effect is also slightly visible for linoleic acid.

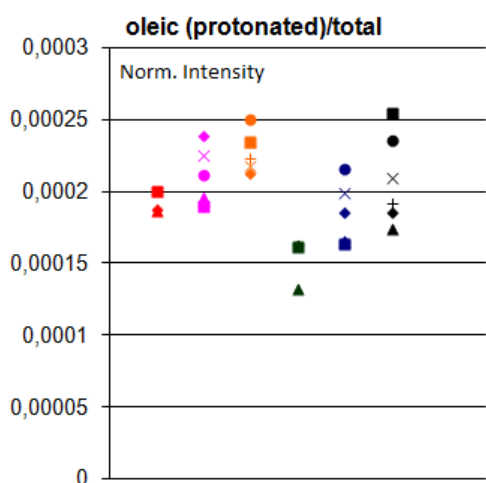


Figure 2.21: Positive protonated ions of oleic acid  $C_{18}H_{35}O_2^+$  at  $m/z$  283 in linseed oil

The yield of protonated ions has increased from A1 (B1) over A2 (B2) to A3 (B3). As

explained above the yield of these ions is the result of a competition between the auto-oxidation and the hydrolysis processes. In Figure 2.21 we see that the hydrolysis process becomes more dominant versus the auto-oxidation process in samples A1 to A3 (and B1 to B3). Combining the information from the deprotonated ions and the acylium/protonated ratio we can say that A1 (and B1) and A2 (and B2) show the roughly the same amount of auto-oxidation, but hydrolysis has gone further in A2 and B2 than in A1 and B1. We know that A3 (and B3) presents both further reaching auto-oxidation and hydrolysis than A2 (and B2), but the hydrolysis seems stronger than the auto-oxidation. The difference between the pattern of the protonated ion yield of linoleic acid and oleic acid can be explained by the stronger auto-oxidation process in the doubly unsaturated linoleic acid. The boiled counterparts show the same pattern, at lower magnitudes (implicating more auto-oxidation, as mentioned above).

The acylium ion yield for the oleic acid shows a systematic decrease through samples A1, A2 and A3. This is in contrast with the protonated ion, discussed above. We believe this is due to the hydrolysis process combined with the auto-oxidation process. The difference between A1 and A2 is wholly due to the hydrolysis process, as we know from the deprotonated ions that auto-oxidation is roughly at the same level. As was the case for the protonated ion, the boiled samples show the same pattern but at a lower magnitude due to further auto-oxidation.

### Palmitic and stearic acid

The results of the deprotonated ion yield of both palmitic and stearic acids (Figures 2.22 and 2.23) are interesting. Literature sometimes suggests that palmitic and stearic acids, due to the fact that they are saturated acids, are (almost) not effected by the pre-treatments or ageing processes.[5][25] The results show otherwise: there is quite a large dispersion with A2 at a yield about twice that of A3 and 7 to 8 times that of A1. For the B series, a similar pattern arises, with B1 at the same yield as A1, B2 at the same yield as A3 and B3 at about the half of the yield of B2. There seems to be some a loss of ionisation of palmitic and stearic acid through the heating pre-treatment. In general the similarity with the patterns of the yield of deprotonated ions for linolenic and linoleic acid is striking with the higher yield of A3 (B3) compared to A1 (B1) as main difference. The reasoning that we applied in those cases, namely that the pattern is attributable to the different stages of the auto-oxidation process, is not applicable here as it concerns saturated molecules. The similarity could also suggest that a similar process is behind all four patterns, which would defeat the previous explanation of the linolenic and linoleic acid deprotonated ions yield.<sup>4</sup> The explanation cannot be found in the hydrolysis process either as an increase of free fatty acids would mean a higher yield.

---

<sup>4</sup>One could suggest that looking at the relative ion yields (that is, the total counts per peak divided by the total counts of the measurement) gives a distorted image. Just looking at the total counts would not offer a solution as different measurements (even of the same sample) can give a very different ion yields. Ideally the ion yield would have to be taken relative to the number of counts of a specific peak of a compound that is not affected by the different treatments. However, no such compound is known to us and we therefore decide to continue to use the ion yield relative to the total number of counts of the measurement.

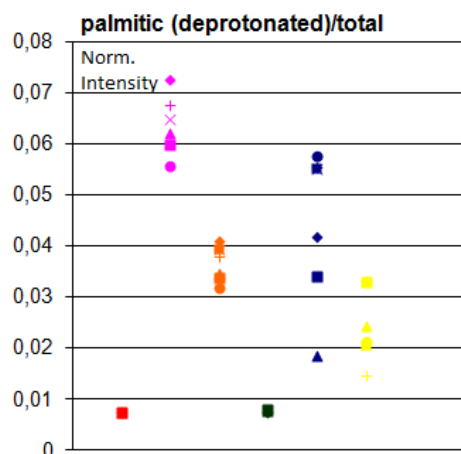


Figure 2.22: Negative deprotonated ions of palmitic acid  $C_{16}H_{31}O_2^-$  at  $m/z$  255 in linseed oil

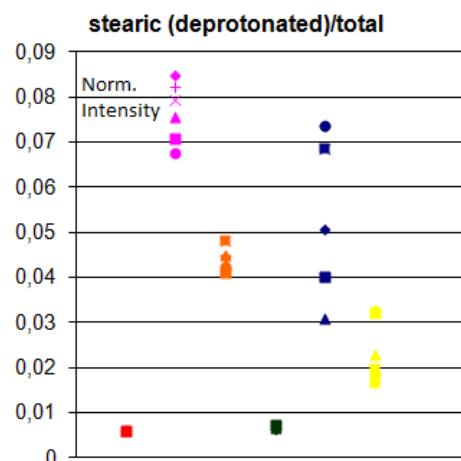


Figure 2.23: Negative deprotonated ions of stearic acid  $C_{18}H_{35}O_2^-$  at  $m/z$  283 in linseed oil

Looking at the acylium/protonated ion ratio for stearic acid (Figure 2.25), we see a pattern that is similar with the previous ratios (of linoleic and oleic acid): it seems that hydrolysis increases from samples A1 through A2 and A3. However, the spread on the results is considerable and we should be careful. The B series shows the same pattern, but tends to be more hydrolysed, a conclusion also reached for previous ratios. Concerning the acylium/protonated ratio for palmitic acid (Figure 2.24), roughly the same pattern is visible, but A2 seems to be at the same level as A3.

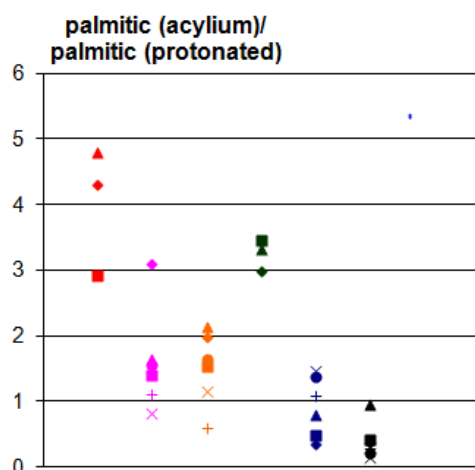


Figure 2.24: Ratio of positive acylium and protonated ions of palmitic acid in linseed oil

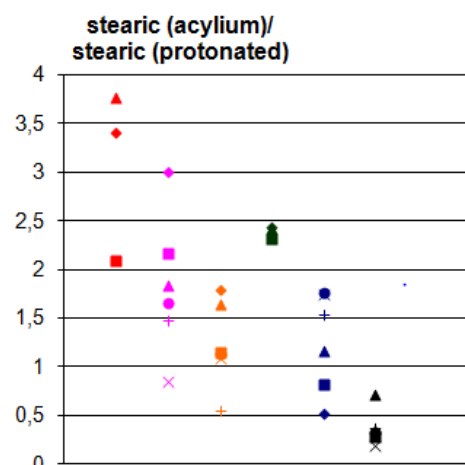


Figure 2.25: Ratio of positive acylium and protonated ions of stearic acid in linseed oil

The protonated ion yields for palmitic and stearic acid (Figures 2.26 and 2.27) show the same behaviour as that of oleic acid, showing the increasing hydrolysis (stronger than the unaccounted 'loss' that is visible in the deprotonated ion yield). It is striking to see that both palmitic and stearic acid protonated ion oil are practically absent in A1 and B1, this can be related to the generally low palmitic and stearic acid content and to the fact that the existing compounds are integrated in a bound form. Boiled samples show higher yield in protonated ions, except for B1,

implying further hydrolysis, as suggested by the acylium/protonated ratio. In broad outline the acylium ion yield for both palmitic and stearic acids (Figures 2.28 and 2.29) is similar to the deprotonated ions and therefore generates the same questions: A1 and B1 have almost five times lower yield than A2 and A3 or B2 and B3. The B series are, as before lower in acylium ion yield.

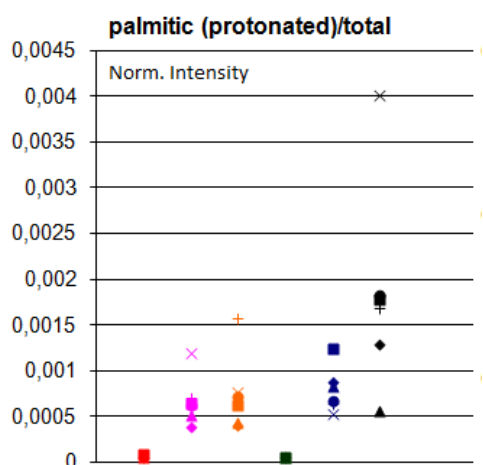


Figure 2.26: Positive protonated ions of palmitic acid  $C_{16}H_{33}O_2^+$  at  $m/z$  257 in linseed oil

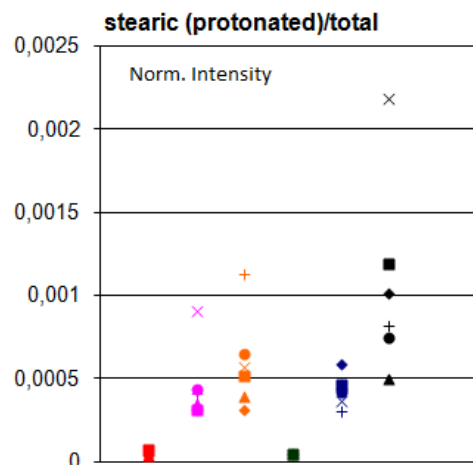


Figure 2.27: Positive protonated ions of stearic acid  $C_{18}H_{37}O_2^+$  at  $m/z$  285 in linseed oil

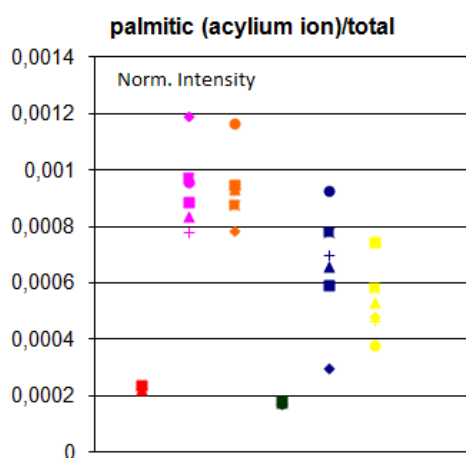


Figure 2.28: Positive acylium ions of palmitic acid  $C_{16}H_{31}O^+$  at  $m/z$  239 in linseed oil

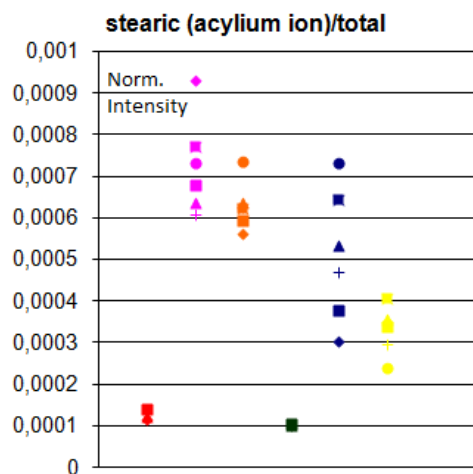


Figure 2.29: Positive acylium ions of stearic acid  $C_{18}H_{35}O^+$  at  $m/z$  267 in linseed oil

### Suberic acid

The deprotonated ion yield pattern of suberic acid (Figure 2.30) seems consistent with the hypothesis that samples A2 has undergone a less far reaching auto-oxidation than A1 and A3. We know that suberic acid is a product of the auto-oxidation of linolenic, linoleic and oleic acid followed by a hydrolysis process.[6][25] It is therefore logical to find suberic acid present in those samples who show the most auto-oxidation. The B series, however, shows almost no variation in the deprotonated ion yield. The fact that this variation would be less than for the A series seems logical: from the differences in deprotonated ion yield of linolenic, linoleic and oleic acid between samples A2 and B2 we deduced that the auto-oxidation process already started with the

heating pre-treatment. The subsequent variation in the deprotonated ion yield of the mentioned acids through drying and ageing (samples B1 and B3 as compared to sample B2) was already smaller than for the A series and this also holds for the ion yield of suberic acid. The fact that the auto-oxidation process already started also explains the fact that the yields for the B series are all higher than for A2 and at about the same level as A1. B3 seems to show a slightly higher yield than B1 and B2, which can be a faint indication of the effect of further auto-oxidation.

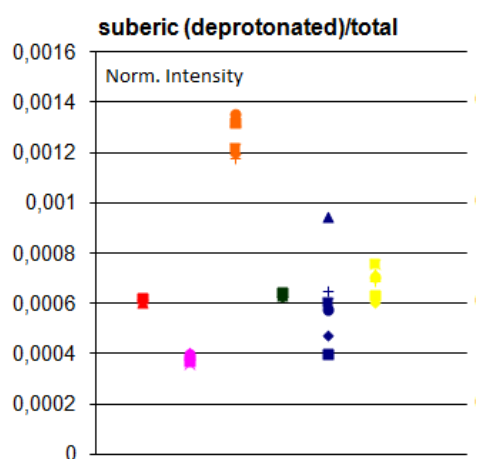


Figure 2.30: Negative deprotonated ions of suberic acid  $C_8H_{13}O_4^-$  at  $m/z$  173 in linseed oil

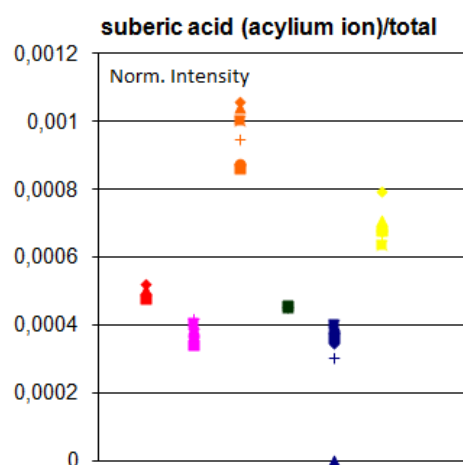


Figure 2.31: Positive acylium ions of suberic acid,  $C_8H_{13}O_3^+$  at  $m/z$  157 in linseed oil

Protonated ions of suberic acid were not observed. The acylium ion yield of suberic acid is shown in Figure 2.31. At first sight, we come to the same conclusion as for the deprotonated ion: suberic acid is indeed a product of auto-oxidation and follows an inverse pattern as the same ion for linolenic and linoleic acid. The difference between the series A and B that we thought to discern for the deprotonated ion yield disappears, however: they appear on the same level, only B3 showing a lower yield than A3. This goes somewhat against our previous assertion that the B series have already undergone some oxidation during the pre-treatment. A possibility is however that this pre-treatment effect would express itself rather in the free fatty acids than in the bound ones.

### Azelaic acid

The pattern of the deprotonated ion yield of azelaic acid (Figure 2.32), is less easily interpretable. At first sight, we would expect it to be similar to that of suberic acid, as azelaic is also a product of auto-oxidation followed by hydrolysis.[6][25] In fact, azelaic should be the most present oxidation product, more than suberic and sebacic acid. We indeed remark that the ion yield is generally about three times higher than that of suberic acid discussed above. But one other difference with the deprotonated ion yield of suberic acid is striking: the yield of A3 is much closer to the yields of A1 and A2 than in suberic acid. The same holds for the B series on an even more dramatical scale: B3's yield is significantly lower than that of B1 or B2. A possible explanation is found in literature: it has been noted that heating treatments can make the amounts of suberic and sebacic acid increase with respect to azelaic acid through double bond

isomerisation.[25][6][26] Such a loss of azelaic acid could explain why the deprotonated yield is lower for A3 than for A1 and lower for B3 than for B1 and B2. In our experiments, however, this effect clearly is not solely related to the heat treatment as it is as present in the A series as in the B series although it could be said that it seems stronger in the boiled sample B3 than in A3.

As for suberic acid no protonated ions were observed. The acylium ion yield (Figure 2.33) shows a behaviour very similar to that of suberic acid and the kind of behaviour we would expect for a resulting product of the auto-oxidation process: more present in samples that show higher oxidation. It is not entirely clear how the conclusions for the deprotonated ion yield and the acylium ion yield should be connected, but it may be that the described double bond isomerisation process preferentially takes place with the free or with bound azelaic acids.

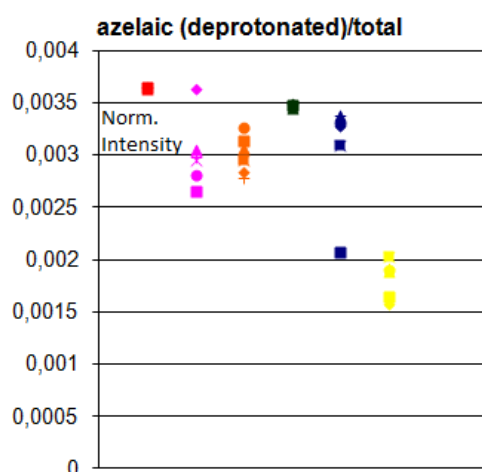


Figure 2.32: Negative deprotonated ions of azelaic acid  $C_9H_{15}O_4^-$  at  $m/z$  187 in linseed oil

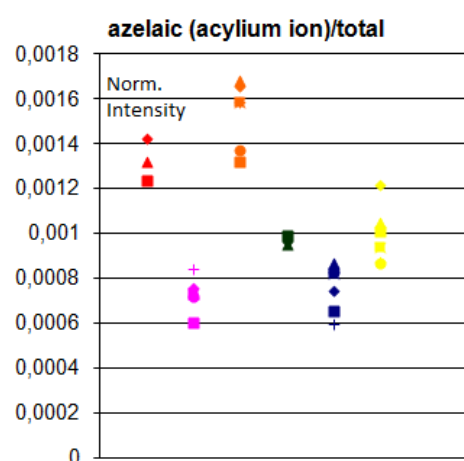


Figure 2.33: Positive acylium ions of azelaic acid  $C_9H_{15}O_3^+$  at  $m/z$  171 in linseed oil

### Palmitic/Stearic (P/S) ratio

In literature different ratios are used in the hope that they reveal general properties of the material or its (pre-)treatment. The most used ratio is that of palmitic acid with respect to stearic acid (P/S). P/S ratios are used to distinguish the type of oil used in a paint sample: the P/S ratio for linseed oil is expected to be lower than 2, between 2 and 3 for walnut oil and higher than 3 for poppy seed oil.[25][5] Often this ratio is measured through GC/MS analysis (Gas Chromatography-Mass Spectrometry), but in SIMS it is obtained by dividing the deprotonated ion yields of both fatty acids.[25][5] This ratio is expected to remain fairly constant during pre-treatment or ageing. Even if the palmitic and stearic acids are changed by the treatments, it is assumed that they have the same reactivity and that therefore the ratio in itself would not be affected.[5] However, changes with ageing are observed, but there seems to be no agreement about the trend of the changes. Some sources report a rise of the P/S ratio for aged samples ([5]). Others predict that the P/S ratio would fall with ageing, due to preferential loss of palmitic.[25]

An important difference between the measurement of the P/S ratio by GC/MS or SIMS is that GC/MS obtains an average value of the ratio over the whole bulk of the sample, whereas SIMS only gives the value at the surface. The value in the bulk is typically higher than on the surface.[5]

Looking at the measurements for our samples (Figure 2.34), we see indeed a variation in P/S ratio. It seems that the ratio is rather rising with ageing, although it is unclear why A1 (B1)

shows a higher value than A3 (B3). It seems that the pre-treated and aged (with UV radiation) oil has a higher P/S value than its non-heated counterpart, but this trend is not general for the B series, as B2 is at the same level as A2 and B1 is even lower than A1. These variations, however, do not hinder a clear qualification of the samples as being linseed oil based: all values are well below 2.

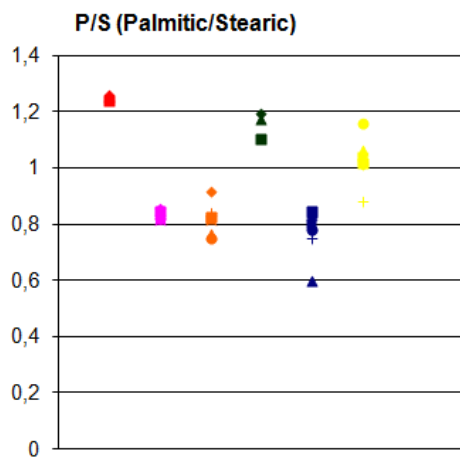


Figure 2.34: Ratio of negative deprotonated palmitic and stearic acid ions in linseed oil

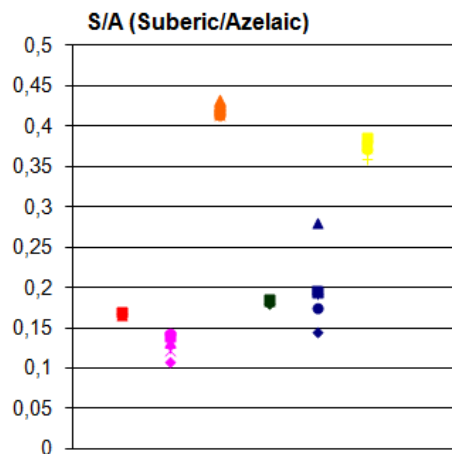


Figure 2.35: Ratio of negative deprotonated suberic and azelaic acid ions in linseed oil

### Suberic/Azelaic (S/A) ratio

The suberic acid to azelaic acid ratio (S/A) is reported in literature as being indicative for pre-treatment, such as heating. This is because azelaic acid is lost in favour of suberic acid due to second bond isomerisation.[25] We see indeed in our measurements (Figure 2.35) that suberic acid increases with respect to azelaic acid in the samples that we believe to be more auto-oxidised (A1 and A3 versus A2). The same effect is visible in the B series, although there does not seem to be a difference between B1 and B2. The S/A ratio seems to be more influenced by ageing than by pre-treatment. This is an observation that has been reported before ([7]).

### Oleic/Stearic (O/S) ratio

The oleic acid to stearic acid ratio (O/S) should be indicative of the auto-oxidation process: oleic acid, being unsaturated, would disappear while the saturated stearic acid remains almost constant.[25] The results (Figure 2.36) are contra-intuitive, however. The sample for which we expect the most auto-oxidation (A3 or B3) is at the same level with the sample for which we expect the least (A2 or B2). It seems that the pattern is most of all influenced by the very low yield of stearic acid in A1 and B1 in comparison to the other samples and it is doubtful that it gives a faithful image of the auto-oxidation.

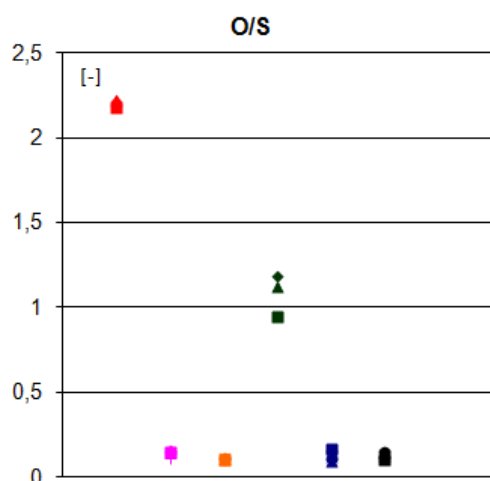


Figure 2.36: Ratio of negative deprotonated oleic and stearic acid ions in linseed oil

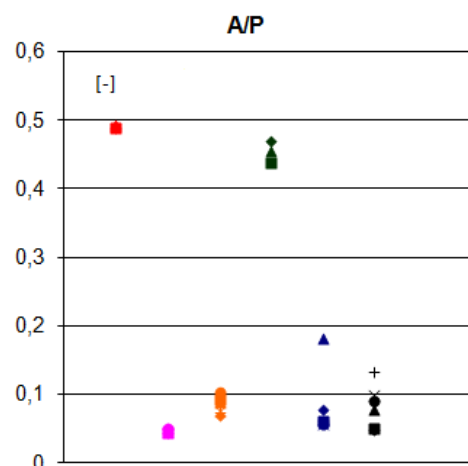


Figure 2.37: Ratio of negative deprotonated azelaic and palmitic acid ions in linseed oil

### Azelaic/Palmitic (A/P) ratio

The azelaic to palmitic ratio (A/P, see Figure 2.37) is used to distinguish oils from egg lipids. The A/P ratio should be higher than 1 for drying oil and lower than 0.3 for egg lipids, with intermediate values indicating a mixture of the two, known as *tempera grassa*.<sup>[25]</sup> We see however that all our samples show a value below 1, even below 0.3 with the exception of A1 and B1 although no egg lipids whatsoever were added to the samples. We are under the impression that once more the pattern is disturbed by the very low palmitic yield for A1 and B1, as seen before. An increasing A/P can also be indicative of ongoing auto-oxidation. This could explain the slight increase from A2 to A3, but is not corroborated by the B series.

### Other ions

We will limit our discussion to the previous ions. They are the most significant and are of most interest to our discussion. The results of the other peaks are sometimes less clear. A discussion of the observations can be found in Appendix A

### Conclusions

- nature of the dried fresh oil (sample A1): the interpretation of the results for this sample is somewhat problematic. Some results seem to suggest that the sample is more auto-oxidated than the sample that has been aged without being exposed to UV light. The yield of linolenic and linoleic acid is very low, but oleic acid shows a normal yield. Palmitic and stearic deprotonated ions have also a very low yield.
- nature of the aged linseed oil sample
- linolenic acid: the ion yield for the triply unsaturated linolenic acid disappears with ageing and under the influence of pre-heating. This can be explained as an effect of the auto-oxidative process.
- linoleic acid: the ion yield for the doubly unsaturated linoleic acid disappears with ageing and under the influence of pre-heating. As for linolenic acid, we believe that this can be explained by the auto-oxidation process.

- oleic acid: the deprotonated ion yield for mono-unsaturated oleic acid disappears with ageing and under the influence of pre-heating. We believe that the protonated ion yield reflects the influence of hydrolysis.
- palmitic and stearic acids: the ionisation for the deprotonated and acylium ion of palmitic and stearic acids seems to decrease both with ageing and with pre-treatment. The low yield for the sample that is not aged is not easy to explain. The protonated ion seems to reflect the effect of hydrolysis.
- suberic acid: suberic acid shows a higher yield for the aged sample, which seems to confirm its role as a oxidation product.
- azelaic acid: the deprotonated ion yield does not show the increase we would expect for an oxidation product. This can be due to double bond isomerisation.
- palmitic/stearic ratio: the P/S ratio corresponds to the values reported for linseed oil ([5]). There is no clear effect of ageing or pre-treatment.
- suberic/azelaic: This value is sometimes used to identify pre-treatment, but this ratio seems to be more influenced by ageing than by pre-treatment (this criticism on the use of S/A to indicate pre-treatment has already been formulated [7]).
- oleic/stearic and azelaic/palmitic ratios: we believe that the unusual low deprotonated ion yield for palmitic and stearic acid for the non-aged sample renders the interpretation of these ratios doubtful.
- hydrolysis: we have introduced the ratio of the acylium ion to the protonated ion of a fatty acid as an indication for hydrolysis. This parameter seems to follow well what we would expect. The samples that have not been aged (samples A1 and B1) show the highest value. It seems that their short drying process has not allowed hydrolysis to go as far as for the aged samples. The samples that have aged with exposure to UV show a lower value than those who have not been into contact with UV. A possible explanation is that the aluminium cover diminishes the exposure to water and therefore inhibits the hydrolysis process.

#### 2.4.5 Discussion of the results for linseed oil pre-treated with lead driers (samples C and D)

Samples C and D have been pre-treated with lead based driers. The samples originate from the KIK-IRPA laboratory. Sample D has been heated together with *litharge* ( $PbO$ ). How exactly sample C has been treated is unclear (the etiquette mentions ageing in an oven at  $45^{\circ}C$ , with exposure to infrared light). The details of the artificial ageing that they have undergone are also unknown. GC-MS and thermogravimetric analysis has shown that such oils are more oxidised (with a higher amount of dicarboxylic acids) and less cross-linked.[6]

The legend for the figures in this section is found in Figure 2.38.

##### Linolenic acid

The deprotonated ion of linolenic acid (Figure 2.39) is more present in samples C and D than in A1 (and even A3), in D even at comparable levels as for A2. This is contrary to what we would expect from a sample that has been aged and that, based on literature ([6]) is more oxidised. The protonated ion (Figure 2.40) shows a lower yield for C and D than for A. These two observations combined could suggest that linolenic acid is mostly present in its bound form in C and D, which is once more contrary to the expectations.

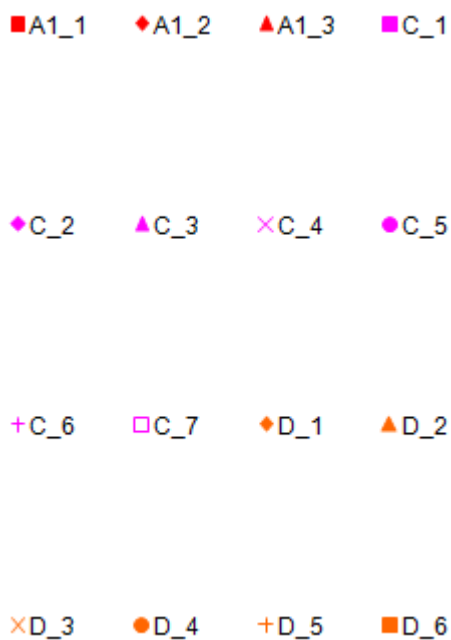


Figure 2.38: Legend used for Figures 2.39 to 2.52

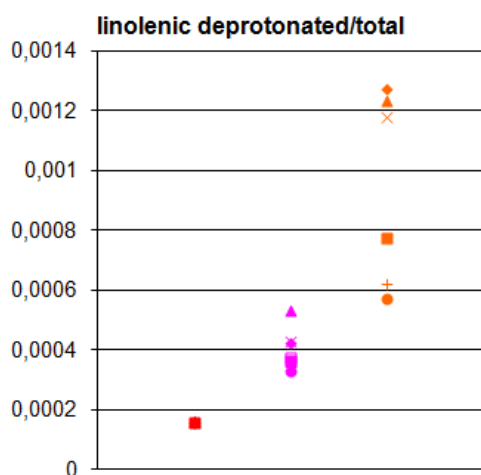


Figure 2.39: Negative deprotonated ions of linolenic acid in linseed oil pre-treated with lead driers

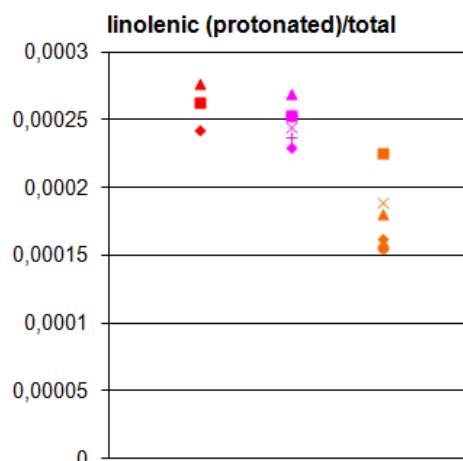


Figure 2.40: Positive protonated ions of linolenic acid in linseed oil pre-treated with lead driers

### Linoleic and Oleic acids

The deprotonated ion yield for linoleic and oleic acids shows the same, contra-intuitive behaviour as for linolenic acid (see Figure 2.41). Sample C seems to be the most hydrolysed and A1 the least.

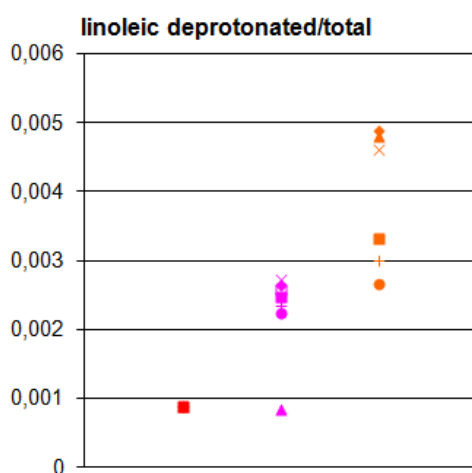


Figure 2.41: Negative deprotonated ions of linoleic acid in linseed oil pre-treated with lead driers

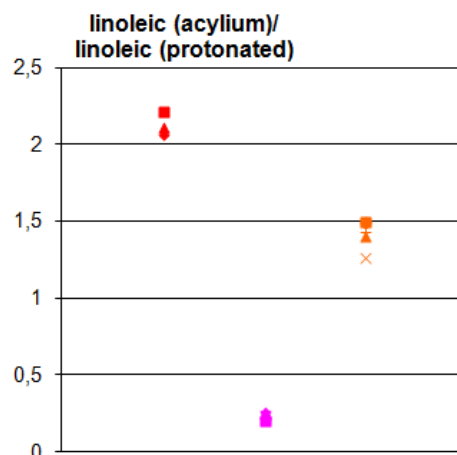


Figure 2.42: Ratio of positive acylium and protonated ions of oleic acid

### Palmitic and Stearic acid

Samples C and D show a much more higher yield of the deprotonated ion of palmitic (see Figure 2.43) and stearic acids than A1. The reason is unclear. The acylium/protonated ratio (Figure 2.44) for these fatty acids seems to suggest that A1 and D are more hydrolysed than C, which is contradictory to what we saw for linoleic and oleic acid. The protonated ion (Figure 2.45) shows a higher yield for C than for A1 and D, who are not detected.

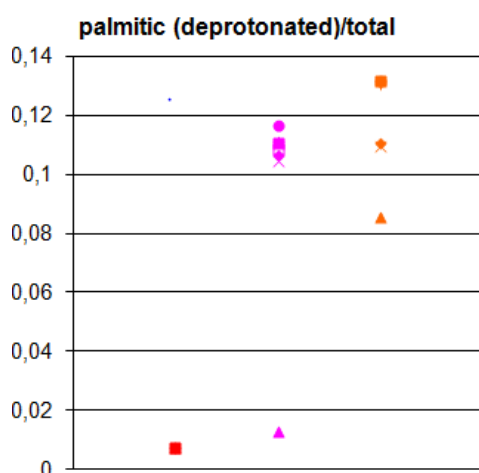


Figure 2.43: Negative deprotonated ions of palmitic acid  $C_{16}H_{31}O_2^-$  at  $m/z$  255 in linseed oil pre-treated with lead driers

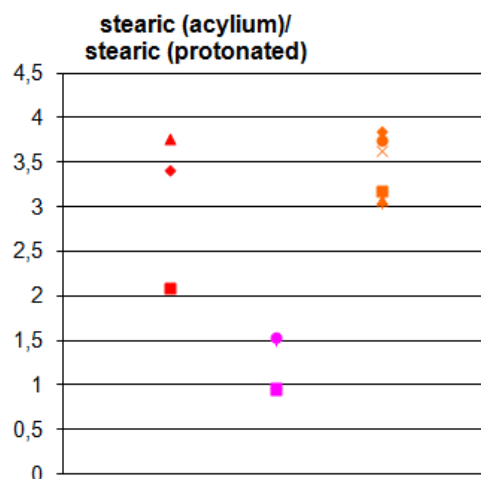


Figure 2.44: Ratio of positive acylium and protonated ions of stearic acid in linseed oil pre-treated with lead driers

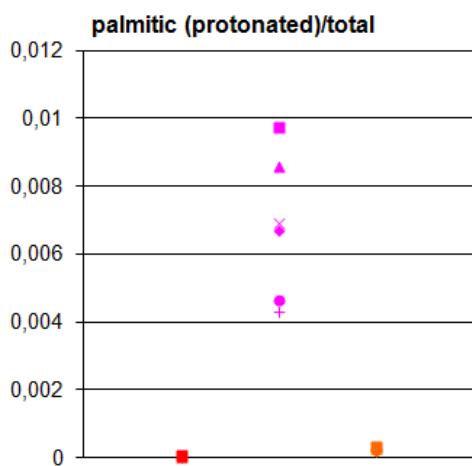


Figure 2.45: Positive protonated ions of palmitic acid  $C_{16}H_{33}O_2^+$  at  $m/z$  257 in linseed oil pre-treated with lead driers

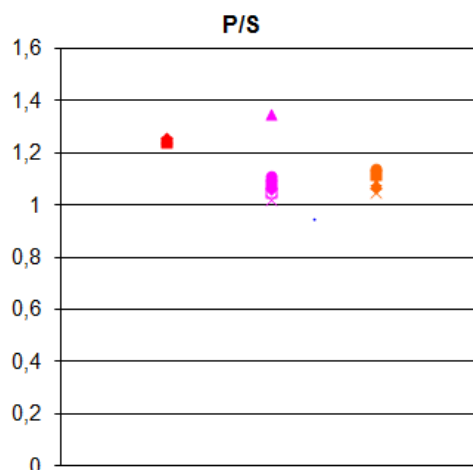


Figure 2.46: Ratio of negative deprotonated palmitic and stearic acid ions in linseed oil pre-treated with lead driers

### Palmitic/Stearic (P/S) ratio

Despite the problems with the interpretation of the ion yields for palmitic and stearic acid, the P/S ratio (Figure 2.46) seems to give a very acceptable result: the ratio is fairly constant over all samples at a value of 1.1. This is lower than 2, what we expect for linseed oil ([5]).

### Suberic and Azelaic acid

The deprotonated ion yield of suberic (Figure 2.47) and of azelaic (2.48) diminishes in both cases with treatment. This is contra-intuitive as well, as it has been reported that in samples that have been treated with driers, more dicarboxylic acids are present. This does not seem to be the case.

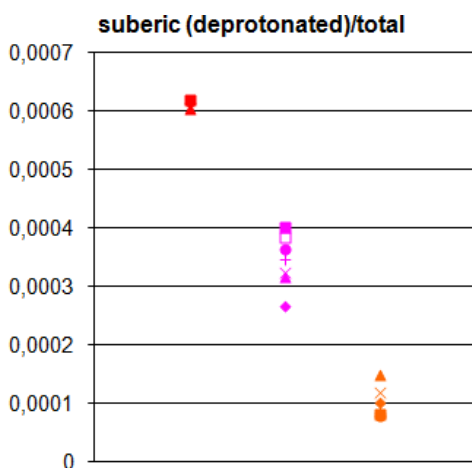


Figure 2.47: Negative deprotonated ions of suberic acid  $C_8H_{13}O_4^-$  at  $m/z$  173 in linseed oil pre-treated with lead driers

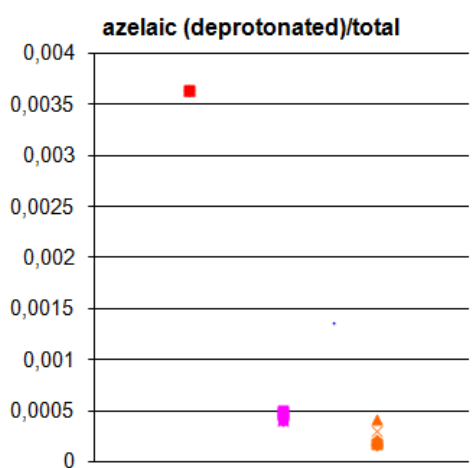


Figure 2.48: Negative deprotonated ions of azelaic acid  $C_9H_{15}O_4^-$  at  $m/z$  187 in linseed oil pre-treated with lead driers

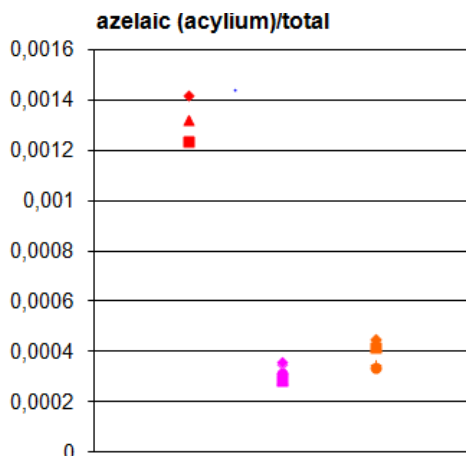


Figure 2.49: Positive acylium ions of azelaic acid  $C_9H_{15}O_3^+$  at  $m/z$  171 in linseed oil pre-treated with lead driers

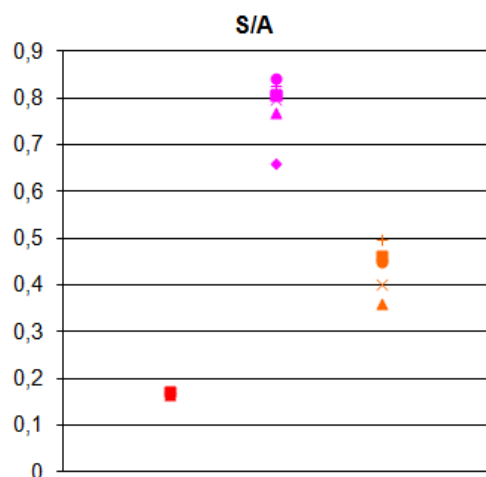


Figure 2.50: Ratio of negative deprotonated suberic and azelaic acid ions in linseed oil pre-treated with lead driers

### Suberic/Azelaic (S/A) ratio

The pre-treatment leads to a higher S/A ratio. S/A ratio is normally expected to rise for heat-treated samples, which might be the case.

### Oleic/Stearic (O/S) ratio

The pre-treatment seems to enhance the effect of auto-oxidation.

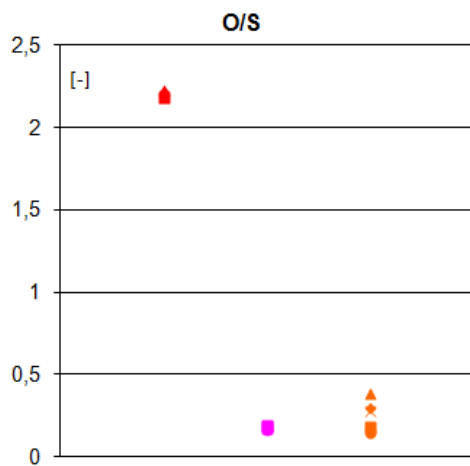


Figure 2.51: Ratio of negative deprotonated oleic and stearic acid ions in linseed oil pre-treated with lead driers

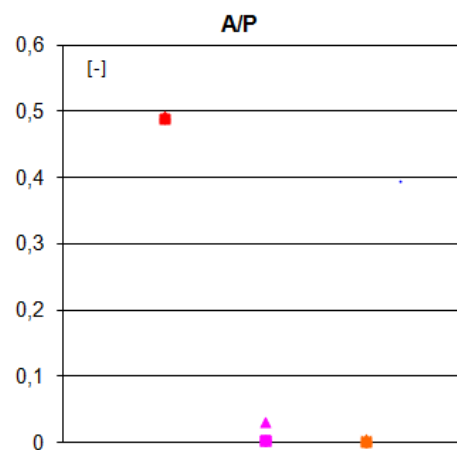


Figure 2.52: Ratio of negative deprotonated azelaic and palmitic acid ions in linseed oil pre-treated with lead driers

### Azelaic/Palmitic (A/P) ratio

This ratio is contradictory to the previous one as it suggests that the pre-treated samples are less auto-oxidated.

## 2.4.6 Conclusion

- Nature of the oils treated with lead driers: The samples show a behaviour that is contrary to what we expected. Previous analysis showed that samples of linseed oil that had been pre-heated with oxygen and (lead based) driers or for fresh linseed oil to which driers are added (without heating) are more oxidised and less cross-linked. The linolenic acid deprotonated (-) and protonated (+) ions suggest that the samples, pre-treated with driers and aged afterwards, are less auto-oxidated and less free fatty acids. For linoleic and oleic, the samples with driers seem to be more hydrolysed, but this is contradicted by the acylium/protonated ion ratios for palmitic and stearic acid. The yield for azelaic and suberic acids is lower for the pre-treated samples than for the non-treated sample in both the deprotonated and azelaic ion yield, which contradicts the statement ([6]) that those pre-treated sample show more dicarboxylic acids. The O/S and A/P ratio seem to contradict one another. It is reported ([6]) that the A/P ratio rises with pre-treatment with lead driers, but this is not the case.
- Ionisation of palmitic and stearic acid: the yield for the deprotonated ion is higher for the oils treated with driers. However, the protonated ion is not visible in one of the sample that have been boiled with *litharge* (sample D), just as in the non treated oil and as was the case in the pre-heated oil (sample B).
- Palmitic/Stearic ratio: The ratio seems not influenced by the pre-treatment and clearly identifies the samples as being linseed oil-based.

As very little is known about the exact provenance, processing and ageing of the samples, it is very difficult to interpret these data. They certainly do not proof that linseed oil samples become more oxidised and less cross-linked when they are treated with (lead) driers. In spite of these difficulties, we see that the P/S ratio has a constant value of about 1.1 for all these samples.

# Chapter 3

## Pigments

### 3.1 Introduction

In order to obtain colours, pigments are mixed with the paint medium, being linseed oil in this study.[20] The sources of historic pigments can be mineral, vegetal or animal. Cennino Cennini (ca.1360-1427) mentions seven 'natural' colours and distinguishes between 'mineral' colours and colours that 'have to be helped artificially'. The first category includes: black (made out of black stone), red (from red ochre or from sinopia), yellow (from for example yellow ochre) and green (from green earth). Colours requiring 'artificial help' are white (lime white, a pigment on the basis of chalk, or white lead), blue (ultramarine, on the basis of ground lapis lazuli, or azurite, on the basis of a copper mineral) and a yellow color called '*giallorino*' (probably lead-tin-yellow). Cennini also mentions some pigments from vegetal origin: burnt vine twigs for black, saffron for yellow and rose madder (also known under the French name *laque de garance*, from the plant *Rubia tinctorum*). He does not make mention of any animal pigments but bone char (from bones or from charred ivory) was already used in ancient times for example.[19][27]

### 3.2 Samples

In this study, we will obtain the ToF-SIMS spectra from a number of pigments that are often found in paintings from the period of Van Eyck. We have focused on lead based pigments as they are known to react particularly strongly with the oil medium they are mixed in.[6] As a comparison, one non-lead based pigment was studied as well. Three different lead whites, with different production processes, were selected, because of their frequent occurrence in historical paintings. Lead white was the most used white pigment until it was replaced by titanium white during the XX<sup>th</sup> century. Lead carbonate and hydrocerussite are compounds that are believed to be present in most lead whites and lead chloride can occur as a reaction product of lead whites. Minium and the copper based azurite are two pigments that are also frequently found in historical paintings.

- Lead white and related samples: lead white is available in a whole range of varieties. In most cases its chemical composition is  $Pb_3(CO_3)_2(OH)_2$  (lead carbonate hydroxide or basic lead carbonate). The following samples were studied:
  - Hydrocerussite: a mineral with formula  $Pb_3(CO_3)_2(OH)_2$  (a lead carbonate hydroxide) in the form of white crystals. This natural form is rare which prevents its practical use for pigments.[28]
  - *Blanc de Saturne*: it is not entirely clear what this sample from KIK-IRPA, labelled '*Blanc de Saturne, Blanc de plomb traditionnel, formule Paul Arsic, Ent. Vermeer*' (traditional lead white) contains. It is probably lead white produced with the traditional 'stack process' (or a slight variant, the 'Dutch process'). In this process a pot

- of acetic acid or vinegar is surrounded with fermenting material, mostly dung, which gives heat and produces carbon dioxide. Above the pots, lead sheets (or lead coils in the Dutch process) are placed. Several of those sequences (pots with acetic acid, dung and lead sheets) are repeatedly stacked the one on the other, separated by floorboards, until they fill a room. The lead reacts with the air, the carbon dioxide and the acetic acid and finally in lead carbonate hydroxide. After three to four months, lead white has appeared on the lead sheets and can be scraped off. The process is not very precise and often the reaction is not entirely completed.[28]
- Flake white: a lead white produced according to the Cremnitz process, developed in the town of Krems in Austria. The reactions are similar to those described above, but the materials and techniques are different. The result is more pure.[28] The sample originates from the stocks of KIK-IRPA.
  - *Blanc d'argent* or silver white is a very pure lead white, obtained via the so-called 'French process'.[28] The sample is taken from the stocks of KIK-IRPA and is labelled ('*Blanc d'argent mou, Blocqx*'). The Blocqx process consists of precipitating lead acetate in carbonic acid. One obtains a very pure neutral lead carbonate ( $PbCO_3$ ).[19]
  - Lead carbonate: This sample contains lead(II) carbonate ( $PbCO_3$ ), but the purity is unknown. It comes from the stock of KIK-IRPA. Natural lead carbonate can be found in the mineral cerussite.
- Minium: minium, or 'red lead' is lead(III,IV)oxide ( $Pb_3O_4$  or  $[2PbO].[PbO_2]$ ), an orange-red pigment. It was known to painters since ancient time and Pliny the Elder describes already its production.[19] It is obtained by oxidising a white lead sample or a lead(II) oxide sample ( $PbO$ )(also known as *litharge*).[20] It can be found in its natural state in weathering zones of lead ore deposits, but it is not very common.[28] It is possible that in minium, there is an excess of  $PbO$ . [20] The sample was obtained from the stocks of KIK-IRPA.
  - Lead chloride: it is not entirely certain what this white coloured sample, taken from the stocks of KIK-IRPA, exactly contains. It could be pure lead(II) chloride ( $PbCl_2$ ). In literature, we also find mention of lead chloride hydroxide ( $[Pb(OH)_2].[PbCl_2]$ ). This compound has been found for example in the painting *The Anatomy Lesson of Dr. Nicolaes Tulp* (1632) by Rembrandt van Rijn (1606-1669). A hypothesis is that it is a product of a reaction that is caused when oil is purified with salt water and a lead based drier is added.[28]
  - Azurite: azurite, also known as 'mountain blue' is a dark blue copper(II) carbonate mineral following the formula  $Cu_3(CO_3)_2(OH)_2$ . It is known since times immemorial and was extensively used by the Egyptians.[20] Its conservation properties are representative for other copper based pigments ([20]), which makes it a very interesting as the only non lead based sample in this study.

### 3.3 XPS study of lead based pigments

To gain a better understanding of the differences between the lead based pigments, we will study them first with the X-ray Photoelectron Spectroscopy (XPS) technique. In XPS, the sample is irradiated with X-rays (in our case with an energy of 1486 eV, corresponding to the  $K\alpha$  line of aluminum) and core level electrons are ejected. These photoelectrons are analysed in a spectrometer and plotted as intensity versus electron energy. The binding energy,  $E_B$  can then be calculated via its relation with the photoelectron's kinetic energy,  $E_k$ , the energy of the incoming X-ray,  $h\nu$  and the work function of the spectrometer,  $W$ :

$$E_B = h\nu - E_k - W$$

Electrons that do not undergo any energy loss after being excited form the peaks of the spectrum. Each peak has a 'tail', due to background noise of electrons that undergo inelastic collisions and do lose energy before reaching the spectrometer. The strength of XPS, however, is that, next to the elemental composition of a sample, it also gives information about the chemical state that these elements are in (for example in which compounds they are bound).[29] This is especially interesting for our purpose. Furthermore, XPS is a quantitative technique, which ToF-SIMS is not.

The analyses were performed on a SSX 100/206 photoelectron spectrometer from Surface Science Instruments (USA) equipped with a monochromatised micro focused Al X-ray source (powered at 20 mA and 10 kV). The powder samples were fixed with a piece of insulated double sided tape onto small copper troughs of 6 mm diameter, disposed on a ceramic carousel. The pressure in the analysis chamber was around  $1 \times 10^{-8}$  mbar. The angle between the surface normal and the axis of the analyser lens was  $55^\circ$ . The analysed area was approximately 1.4 mm and the pass energy was set at 150 eV for the survey scans (in these conditions, the full width at half maximum (FWHM) of the Au 4f<sub>7/2</sub> peak of a clean gold standard sample was about 1.6 eV) and 50 eV for the high resolution narrow scans. A flood gun set at 8 eV and a Ni grid placed 3 mm above the sample surface were used for charge stabilisation. The following sequence of spectra was recorded: survey spectrum, C 1s, O 1s, Pb 4f, Na 1s, Ba 3d Cr 2p and C 1s again to check the stability of charge compensation with time. The  $C - (C, H)$  component of the C1s peak of adventitious carbon has been fixed to 284.8 eV to set the binding energy scale. Data treatment was performed with CasaXPS program (Casa Software Ltd, UK). Some spectra were decomposed with the least squares fitting routine provided by the software with a Gaussian/Lorentzian (85/15) product function after subtraction of a non linear baseline (Shirley). Molar fractions were calculated using peak areas normalised on the basis of acquisition parameters and sensitivity factors provided by the manufacturer.<sup>1</sup>

The resulting spectra are shown for lead carbonate, minium, lead chloride and flake white in Figure 3.3. Figure 3.4 shows the chemical shift between peaks of *Pb*, *O* and *C*. We see two peaks in lead because the 4f state is a doublet (with  $j = 7/2$  and  $5/2$ ). Depending on whether the spin-orbit coupling is parallel or anti-parallel, the binding energy is lower or higher, with the peak areas proportionate to the degeneracy. The shift in the peaks is due to the chemical environment of the *Pb*-atoms of which electrons gave rise to the peaks. When lead is bound with the very electronegative oxygen, the screening of the core electrons by the valence electrons diminishes and the core electrons are bound more strongly to the nucleus: the binding energy will increase. Sometimes however, the shifts are weak and the peaks are convoluted, making it difficult to separate the different contributions. With the XPS technique we were able to distinguish between electrons from *Pb*-atoms in *PbSO*<sub>4</sub>, *PbCl*<sub>2</sub>, *Pb*<sub>3</sub>*O*<sub>4</sub> compounds, in *PbO*<sub>*x*</sub> or *Pb(OH)*<sub>2</sub> or *PbCO*<sub>3</sub>-compounds (we are not able to distinguish between those three contributions) or from metallic *Pb*. This is visible in the details of the spectra of lead carbonate, minium, lead chloride and flake white.

The elemental composition and the decomposition for the O-peaks and Pb-peaks in the different contributions, are shown in Figures 3.1 and 3.2.

Comparing the different lead-based pigments, we reach the following conclusions:

- Hydrocerussite: 96.5% of the lead stems from *PbO*<sub>*x*</sub>, *Pb(OH)*<sub>2</sub> or *PbCO*<sub>3</sub> compounds, the rest is metallic lead. The ratio of the *CO*<sub>3</sub> peak with respect to the *PbO*<sub>*x*</sub> or *Pb(OH)*<sub>2</sub> or *PbCO*<sub>3</sub> peak is 0.69. This is close to the 2/3 we would expect if hydrocerussite corresponds indeed to the formula *Pb*<sub>3</sub>(*CO*<sub>3</sub>)<sub>2</sub>(*OH*)<sub>2</sub>. Starting from the assumption that all the carbonates in the sample are lead carbonates, then the other 31% of the peak of *PbO*<sub>*x*</sub>-*Pb(OH)*<sub>2</sub>-*PbCO*<sub>3</sub> compounds must be attributable to *PbO*<sub>*x*</sub> (we assume *PbO*) or to *Pb(OH)*<sub>2</sub>. In order to separate those peaks, we calculate the ratio between the peak of *O* bound to *Pb* (thus excluding the carbonates, only taking into account oxygen from *PbO*<sub>*x*</sub>

---

<sup>1</sup>Description from Mr. Pierre Eloy

	a	Na	Ba	Cr	O	C			Cl <sup>[b]</sup>	S <sup>[d]</sup>	Pb				P				
	b	Na 1s	Ba 3d <sub>5/2</sub>	Cr 2p <sub>3/2</sub>	O 1s	C 1s			Cl 2p <sub>3/2</sub>	S 2p	Pb 4f <sub>7/2</sub>				P 2p				
	c	Na <sup>+</sup>	BaSO <sub>4</sub> ?	[3]		Carbonates, O=C-O	C-O	C-(C,H)	Cl <sup>-</sup>	Sulfates	PbSO <sub>4</sub>	PbCl <sub>2</sub>	PbO <sub>x</sub>	Pb(OH) <sub>2</sub>	PbCO <sub>3</sub>	Pb <sub>3</sub> O <sub>4</sub>	Pb <sup>δ</sup>	Pb tot.	
Blanc d'argent	d	1071,5			531,1	289,0	287,8	286,3	284,8	~199			138,4				136,9		
	e	1,8			1,6	1,4	1,4	1,4	1,4				1,4				1,4		
	f	5,9			45,0	12,9	0,4	1,4	15,5	2,0			16,1				0,8		16,9
Flake White	d	1071,5			531,2	289,1	287,8	286,3	284,8	~199			138,5				136,9		
	e	1,8			1,5	1,4	1,4	1,4	1,4				1,4				1,4		
	f	3,2			45,2	12,8	0,9	1,8	16,5	2,0			16,9				0,7		17,6
Blanc de Saturne	d				531,2	289,1	287,8	286,3	284,8	~199			138,5				136,9		
	e				1,6	1,5	1,5	1,5	1,5				1,5				1,5		
	f				43,5	12,0	1,4	1,8	20,1	1,5			19,0				0,7		19,7
Lead Chloride	d				531,6	288,9	287,8	286,3	284,8	198,1		138,9	138,0				136,7		
	e				1,8	1,4	1,4	1,4	1,4	1,2		1,1	1,1				1,1		
	f				7,5	1,3	2,3	3,8	26,8	37,0		18,2	1,8				1,2		21,3
Minium	d				531,9	288,8	287,8	286,3	284,8		~169	139,4					137,6		134,0
	e				1,7	1,6	1,6	1,6	1,6								1,3		1,1
	f				39,4	1,1	1,5	1,3	39,2								1,8		0,8
Lead Carbonate	d				531,3	289,1	287,8	286,3	284,8	~199			138,6				136,9		
	e				1,6	1,4	1,4	1,4	1,4				1,5				1,5		
	f				43,2	11,9	1,1	1,6	20,8	2,6			18,3				0,6		18,9
Hydrocerussite	d	1071,4			531,1	289,0	287,8	286,3	284,8	~199			138,5				136,9		
	e	1,9			1,6	1,4	1,4	1,4	1,4				1,4				1,4		
	f	1,3			44,6	11,4	0,6	0,8	22,7	1,3			16,6				0,7		17,2

Figure 3.1: Elemental composition of the analysed samples. With 'a' the element, 'b' the XPS peak, 'c' the attribution, 'd' the binding energy (eV), 'e' FWHM (Full Width at Half Maximum) of the peak and 'f' the Surface atomic fraction (in % with H excluded)



and  $Pb(OH)_2$  compounds) with respect to the remainder of the  $PbO_x$ - $Pb(OH)_2$ - $PbCO_3$  peak. A ratio of 1 would suggest that the whole peak is attributable to  $PbO$  and a ratio of 2 would suggest the same for  $Pb(OH)_2$ . The ratio appears to be 1.73, which indicates a mix: 22.6% of the  $PbO_x$ - $Pb(OH)_2$ - $PbCO_3$  peak stems from  $Pb(OH)_2$  and the remaining 8.4% from  $PbO$ . The ratio between  $PbCO_3$  and  $Pb(OH)_2$  is not 2 however, as we should expect, but 3, which indicates that there is also free  $PbCO_3$  present. We will make the assumption that all the  $Pb(OH)_2$  compounds are part of the bigger  $Pb_3(CO_3)_2(OH)_2$  compound.

- Lead carbonate: 96.8% of the lead stems from  $PbO_x$ ,  $Pb(OH)_2$  or  $PbCO_3$  compounds, the rest is metallic lead. The ratio of the  $CO_3$  peak with respect to the  $PbO_x$ - $Pb(OH)_2$ - $PbCO_3$  peak is 0.65. This means that there is less  $PbCO_3$  with respect to  $PbO_x$  and  $Pb(OH)_2$  than in hydrocerussite! We once more take the assumption that all the carbonates in the sample are lead carbonates. Calculating the ratio between the peak of  $O$  bound to  $Pb$  (thus excluding lead carbonates) with respect to the remainder of the  $PbO_x$ - $Pb(OH)_2$ - $PbCO_3$  peak yields a value of 0.77. It is strange to acquire a value that is lower than 1. This can be due to errors, but it certainly seems to suggest that not much  $Pb(OH)_2$  is present and we therefore assume that the rest of the  $PbO_x$ - $Pb(OH)_2$ - $PbCO_3$  peak is attributable to  $PbO$ .
- *Blanc de Saturne*: 96.4% of the lead stems from  $PbO_x$ ,  $Pb(OH)_2$  or  $PbCO_3$  compounds, the rest is metallic lead. The ratio of the  $CO_3$  peak with respect to the  $PbO_x$ - $Pb(OH)_2$ - $PbCO_3$  peak is 0.63. Assuming that all the carbonates in the sample are lead carbonates, the ratio between the peak of  $O$  bound to  $Pb$  (thus excluding lead carbonates) and the remainder of the  $PbO_x$ - $Pb(OH)_2$ - $PbCO_3$  peak is 0.6. This is even lower than before and once more we make the conclusion that not much  $Pb(OH)_2$  is present and that the rest of the  $PbO_x$ - $Pb(OH)_2$ - $PbCO_3$  peak is attributable to  $PbO$ .
- Flake white: 96% of the lead stems from  $PbO_x$ ,  $Pb(OH)_2$  or  $PbCO_3$  compounds, the rest is metallic lead. The ratio of the  $CO_3$  peak with respect to the  $PbO_x$ - $Pb(OH)_2$ - $PbCO_3$  peak is 0.75. We assume that all the carbonates are lead carbonates. The ratio of  $O$  (from bonds with  $Pb$ ) to the remainder of the  $PbO_x$ - $Pb(OH)_2$ - $PbCO_3$  peak is 1.02. This value suggests that the remainder of the  $PbO_x$ - $Pb(OH)_2$ - $PbCO_3$  peak is solely attributable to  $PbO$ .
- *Blanc d'argent*: 95.3% of the lead stems from  $PbO_x$ ,  $Pb(OH)_2$  or  $PbCO_3$  compounds, the rest is metallic lead. The ratio of the  $CO_3$  peak with respect to the  $PbO_x$ - $Pb(OH)_2$ - $PbCO_3$  peak is 0.80. We once more take the assumption that all the carbonates in the sample are lead carbonates. Calculating the ratio between the peak of  $O$  bound to  $Pb$  with respect to the remainder of the  $PbO_x$ - $Pb(OH)_2$ - $PbCO_3$  peak yields a value of 1.41, implying a mix of  $PbO$  and  $Pb(OH)_2$ : 8.2 % of the  $PbO_x$ - $Pb(OH)_2$ - $PbCO_3$  peak is attributable to  $Pb(OH)_2$  and the remaining 11.8% to  $PbO$ . The ratio between  $PbCO_3$  and  $Pb(OH)_2$  is about 10, which suggests that there is a lot of free  $PbCO_3$  present as well. We will make the assumption that all the  $Pb(OH)_2$  compounds are part of the bigger  $Pb_3(CO_3)_2(OH)_2$  compound.
- Minium: minium is the only sample that shows quite a strong presence of two non-lead atoms: electrons from barium atoms take 6.5% of the total intensity of the spectrum and sulphur takes 7.3%. We therefore suggest that the barium is bound in a  $BaSO_4$  compound. The lead presence is also much weaker than in the other samples (merely 2% of the total intensity, in contrast to 17 to 21% in the other samples). From this lead presence, 80.59% is attributable to  $Pb_3O_4$  and 12.48% to  $PbSO_4$ , the rest stems from metallic lead.
- Lead chloride: lead chloride is easily distinguishable. It shows a chloride presence that is 20 times stronger than in the other samples. 86% of the lead present stems from a  $PbCl_2$ -compound. As the amount of oxygen atoms bound to carbon already makes up the

Pigment	Lead compounds	Lead atomic fraction
Hydrocerussite	$Pb_3(CO_3)_2(OH)_2$ (65.43%), $PbCO_3$ (22.97%), $PbO$ (8.11%), $Pb$ (4.1%)	17.2%
Lead carbonate	$PbCO_3$ (62.94%), $PbO$ (33.89%), $Pb$ (3.17%)	18.9%
<i>Blanc de saturne</i>	$PbCO_3$ (60.67%), $PbO$ (35.69%), $Pb$ (3.55%)	19.7%
Flake white	$PbCO_3$ (72.02%), $PbO$ (24.01%), $Pb$ (3.98%)	17.6%
<i>Blanc d'argent</i>	$Pb_3(CO_3)_2(OH)_2$ (23.43%), $PbCO_3$ (60.59%), $PbO$ (11.24%), $Pb$ (4.73%)	16.9%
Minium	$Pb_3O_4$ (80.59%), $PbSO_4$ (12.48%), $Pb$ (6.93%)	2.2%
Lead chloride	$PbCl_2$ (85.59%), $PbCO_3$ (8.56%), $Pb$ (5.85%)	21.3%

Table 3.1: Composition of the different lead-based samples, with the fraction of the total lead presence that is attributable to each compound, based on the XPS measurements and the made assumptions, and the lead atomic fraction (in % with H excluded)

total amount of oxygen, the presence of  $PbO_x$  or  $Pb(OH)_2$  compounds is excluded. The rest of the lead presence therefore stems from lead(II) carbonate compounds and metallic lead.

In general, the sodium presence is weak (and only noticeable in hydrocerussite, flake white and *blanc d'argent*). This is in contrast to what the SIMS data suggest, showing once more that sodium is very receptive in ToF-SIMS. The conclusions of the XPS measurements are summarised in Table 3.1. We see that neither hydrocerussite nor lead carbonate are pure samples. *blanc de saturne* and flake white seem to be very similar to lead carbonate, rather than to hydrocerussite. *blanc d'argent* resembles hydrocerussite, but there is also an important presence of lead carbonate. The total presence of lead does not vary greatly between the samples, with minium as an important exception. This is shown in Figure 3.5.

## 3.4 Study of lead-based pigments with ToF-SIMS

### 3.4.1 Observed positive ions

In the positive ion spectra of the lead based samples (hydrocerussite, *blanc de Saturne*, flake white, *blanc d'argent*, lead carbonate, minium and lead chloride) we observe the following significant peaks (other peaks are due to contamination, for example from organic compounds or the very receptive polydimethylsiloxane (PDMS) or they could not be attributed):

- lead:
  - pure lead ions ( $Pb^+$ ) are observed for the isotopes of lead at  $m/z$  204,206,207 and 208 (main isotope),
  - $Pb_2^+$  at  $m/z$  412, 413, 414, 415 and 416,
- lead hydride:  $PbH^+$  at  $m/z$  205, 207, 208 and 209,
- lead oxide:
  - $Pb_2O^+$  at  $m/z$  428, 429, 430, 431 and 432,
  - $Pb_3O_2^+$  at  $m/z$  650, 651, 652, 653, 654, 655 and 656,
  - $Pb_4O_3^+$  at  $m/z$  874, 875, 876, 877, 878, 879 and 880,
- lead hydroxide and oxides with hydrogen:
  - $PbOH^+$  at  $m/z$  223, 224 and 225,

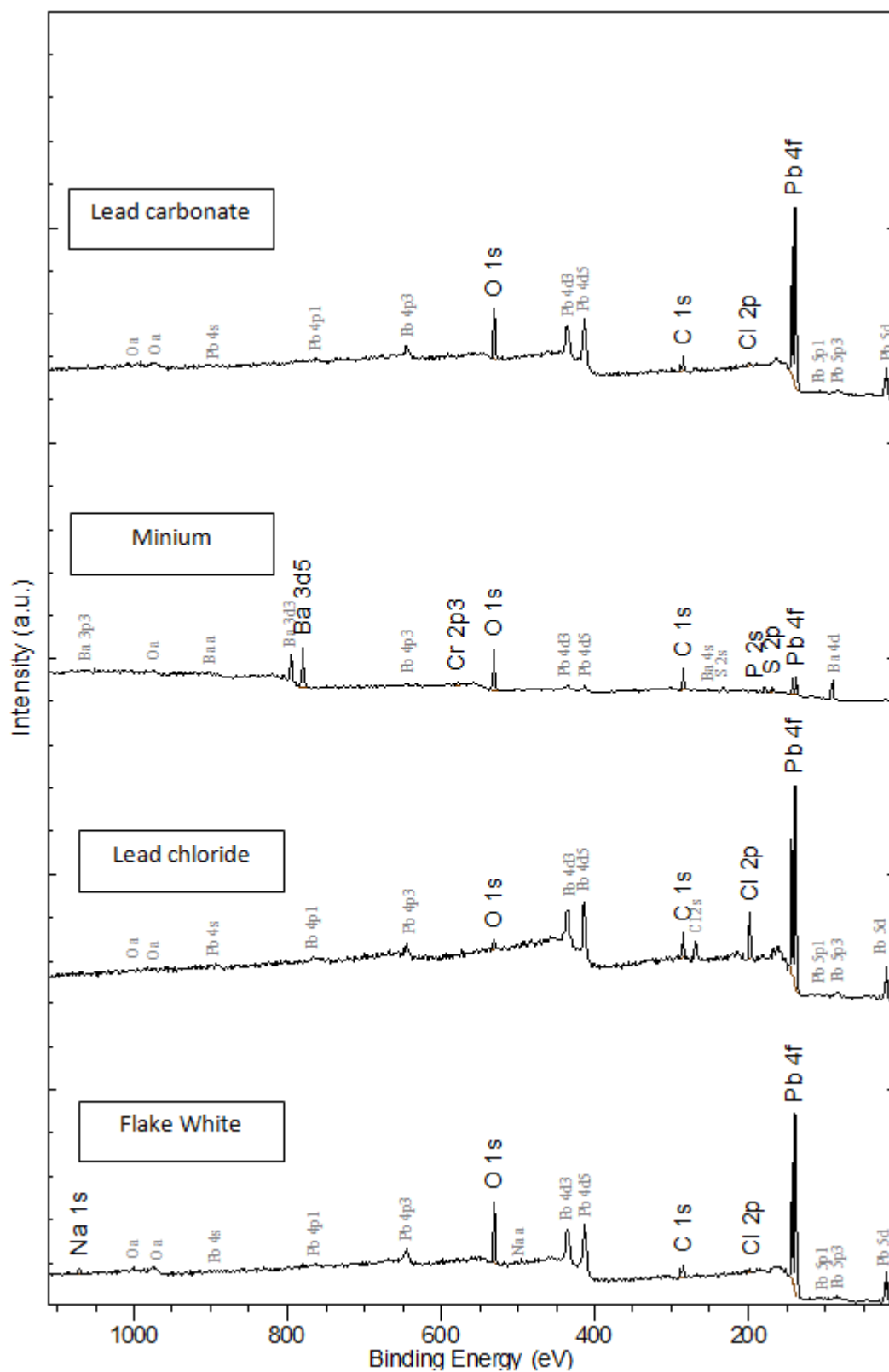


Figure 3.3: XPS spectra for lead carbonate, minium, lead chloride and flake white (intensity versus binding energy)

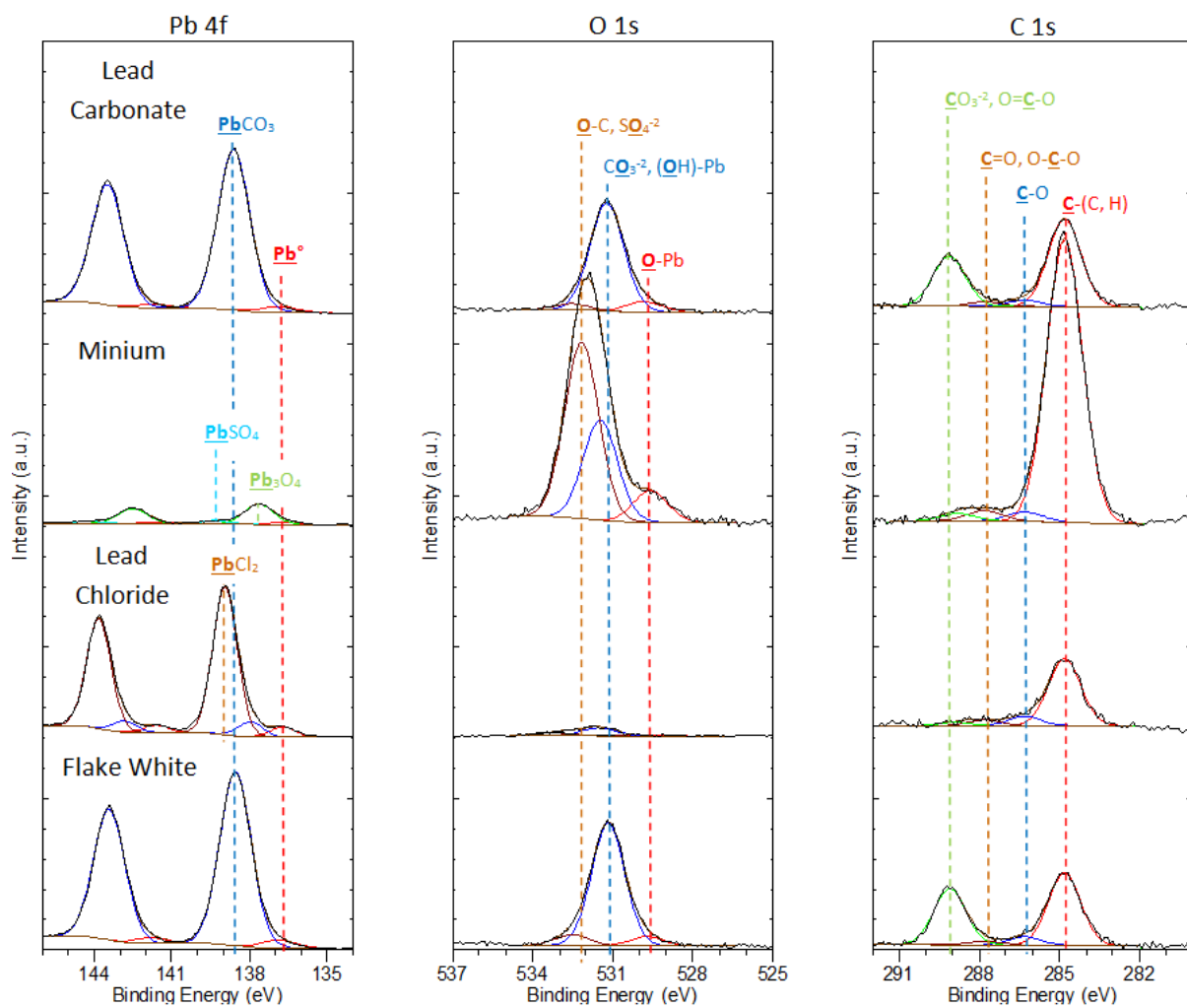


Figure 3.4: Details of the XPS spectra for lead carbonate, minium, lead chloride and flake white (intensity versus binding energy)

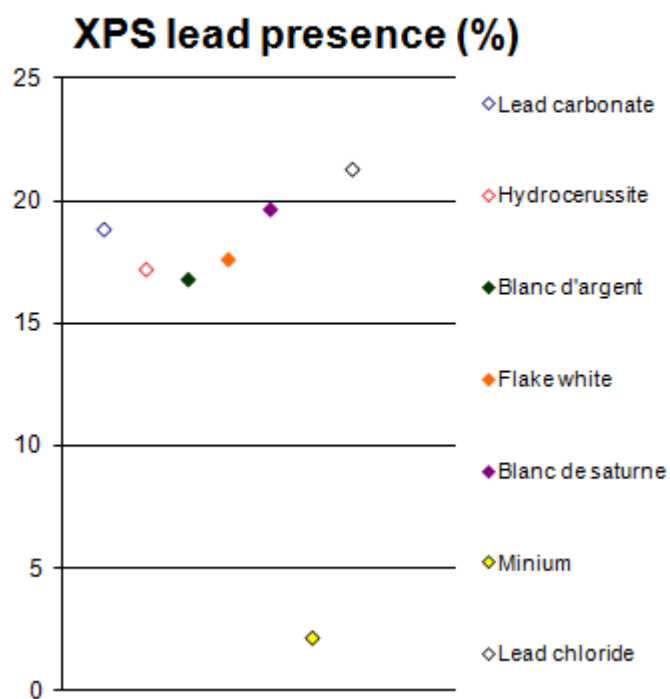


Figure 3.5: Lead presence according to XPS measurements, relative to the total intensity of the spectrum

- $Pb_2O_2H^+$  at  $m/z$  445, 446, 447, 448 and 449,
- $Pb_3O_3H^+$  at  $m/z$  667, 668, 669, 670, 671, 672 and 673,
- $Pb_4O_4H^+$  at  $m/z$  891, 892, 893, 894, 895, 896 and 897.

It is striking that a number of sodium related peaks are very present in the positive ion spectra. It is well known that sodium is very receptive to ionisation in ToF-SIMS and only a small amount must be present in a sample to lead to a very significant peak. Following sodium related peaks were observed:

- sodium:  $Na^+$  at  $m/z$  23,
- sodium oxides and oxides with hydrogen:
  - $Na_2O^+$  and  $Na_2OH^+$  at  $m/z$  62 and 63,
  - $NaO_3H^+$  at  $m/z$  72,
- sodium-sulfur compounds:  $Na_2H_3SO_3^+$  and  $Na_3SO_4^+$  at 129 and 165,
- sodium-lead compounds:
  - $NaPbO^+$  at  $m/z$  245, 246 and 247,
  - $Na_2PbO^+$  at  $m/z$  268, 269 and 270,
  - $Na_2PbO_2H^+$  at  $m/z$  285, 286 and 287,
  - $Na_3PbO_2^+$  at  $m/z$  307, 308 and 309,
  - $NaPb_2O_2^+$  at  $m/z$  467, 468, 469, 470 and 471,
  - $Na_2Pb_2O_3H^+$  at  $m/z$  507, 508, 509, 510 and 511,
  - $NaPb_3O_3^+$  at  $m/z$  689, 690, 691, 692, 693, 694 and 695,
  - $Na_3Pb_3O_4^+$  at  $m/z$  753, 754, 755, 756 and 757.

In the minium sample a series of chromium and barium related peaks dominate the spectrum. They are:

- $Cr^+$  at  $m/z$  52,
- $Ba^+$  with its isotopes at  $m/z$  134, 135, 136, 137 and 138 (main isotope),
- barium oxide and oxide with hydrogen
  - $BaOH^+$  at  $m/z$  151, 152, 153, 154 and 155,
  - $Ba_2O^+$  at  $m/z$  288, 289, 290, 291 and 292,
  - $Ba_2O_2^+$  at  $m/z$  304, 305, 306, 307 and 308,
  - $Ba_2O_2H^+$  at  $m/z$  305, 306, 307, 308 and 309,
  - $Ba_2O_3^+$  at  $m/z$  320, 321, 322, 323 and 324,
  - $Ba_2O_5^+$  at  $m/z$  352, 353, 354, 355 and 356,
  - $Ba_3O_2^+$  at  $m/z$  442, 443, 444, 445 and 446,
  - $Ba_3O_3^+$  at  $m/z$  458, 459, 460, 461 and 462,
  - $Ba_4O_3^+$  at  $m/z$  595, 596, 597, 598, 599 and 600,
  - $Ba_4O_4^+$  at  $m/z$  611, 612, 613, 614, 615 and 616,
- barium-sodium compounds:  $BaNaO^+$  at  $m/z$  177
- barium-sulfur compounds:  $BaSO_2^+$  at  $m/z$  202.

### 3.4.2 Observed negative ions

The following (significant) peaks were discerned in the negative spectrum:

- lead oxides and oxides with hydrogen:
  - $PbO^-$  at  $m/z$  222, 223 and 224 and  $PbOH^-$  at  $m/z$  223, 224 and 225,
  - $PbO_2^-$  at  $m/z$  238, 239 and 240 and  $PbO_2H^-$  at  $m/z$  239, 240 and 241,
  - $Pb_2O_2^-$  at  $m/z$  444, 445, 446, 447 and 448 and  $Pb_2O_2H^-$  at  $m/z$  445, 446, 447, 448 and 449,
  - $Pb_2O_3^-$  at  $m/z$  460, 461, 462, 463 and 464, and  $Pb_2O_3H^-$  at  $m/z$  461, 462, 463, 464 and 465,

In the lead chloride sample we observe, as could be expected, some chlorine and lead-chlorine compounds:

- chlorine:
  - $Cl^-$  with two isotopes at  $m/z$  35 (main isotope) and 37,
  - $Cl_2^-$  at  $m/z$  70, 72 and 74,
- lead chloride:
  - $PbCl^-$  at  $m/z$  241, 242, 243, 244 and 245,
  - $PbCl_2^-$  at  $m/z$  276, 277, 278, 279, 280, 281 and 282,
  - $PbCl_3^-$  at  $m/z$  311, 312, 313, 314, 315, 316 and 317,
  - $Pb_2Cl_3O^-$  at  $m/z$  533, 534, 535, 536, 537, 538, 539, 540 and 541,
  - $Pb_2Cl_5^-$  at  $m/z$  587, 588, 589, 890, 591, 592, 593, 594, 596, and 597.

In the minium sample we observe some dominant chromium and barium based peaks:

- chromium oxides:
  - $CrO_3^-$  at  $m/z$  100,
  - $Cr_2O_5^-$  at  $m/z$  184,
  - $Cr_2O_6^-$  at  $m/z$  200,
- barium-sulfur compounds:
  - $BaSO_4^-$  at  $m/z$  234
  - $BaSO_5^-$  at  $m/z$  250.

An example of a ToF-SIMS spectrum is shown in Figure 3.6.

### 3.4.3 Discussion of the results

#### Lead peaks

Looking at the  $Pb^+$  (Figure 3.8) yield, we see that there is quite some variation between the samples. This corresponds partly to the variation in total lead as measured with XPS (see Figure 3.5), but there are important differences: hydrocerussite would be expected to be slightly lower than flake white, but it is not. The biggest difference is in minium, which shows a lead presence much too high for its real presence. It may be that its low real lead presence will be reflected in the yield of ions with higher mass, or the contradiction between the XPS and the SIMS result may be due to matrix effects, as we know that SIMS is not a quantitative technique. On the

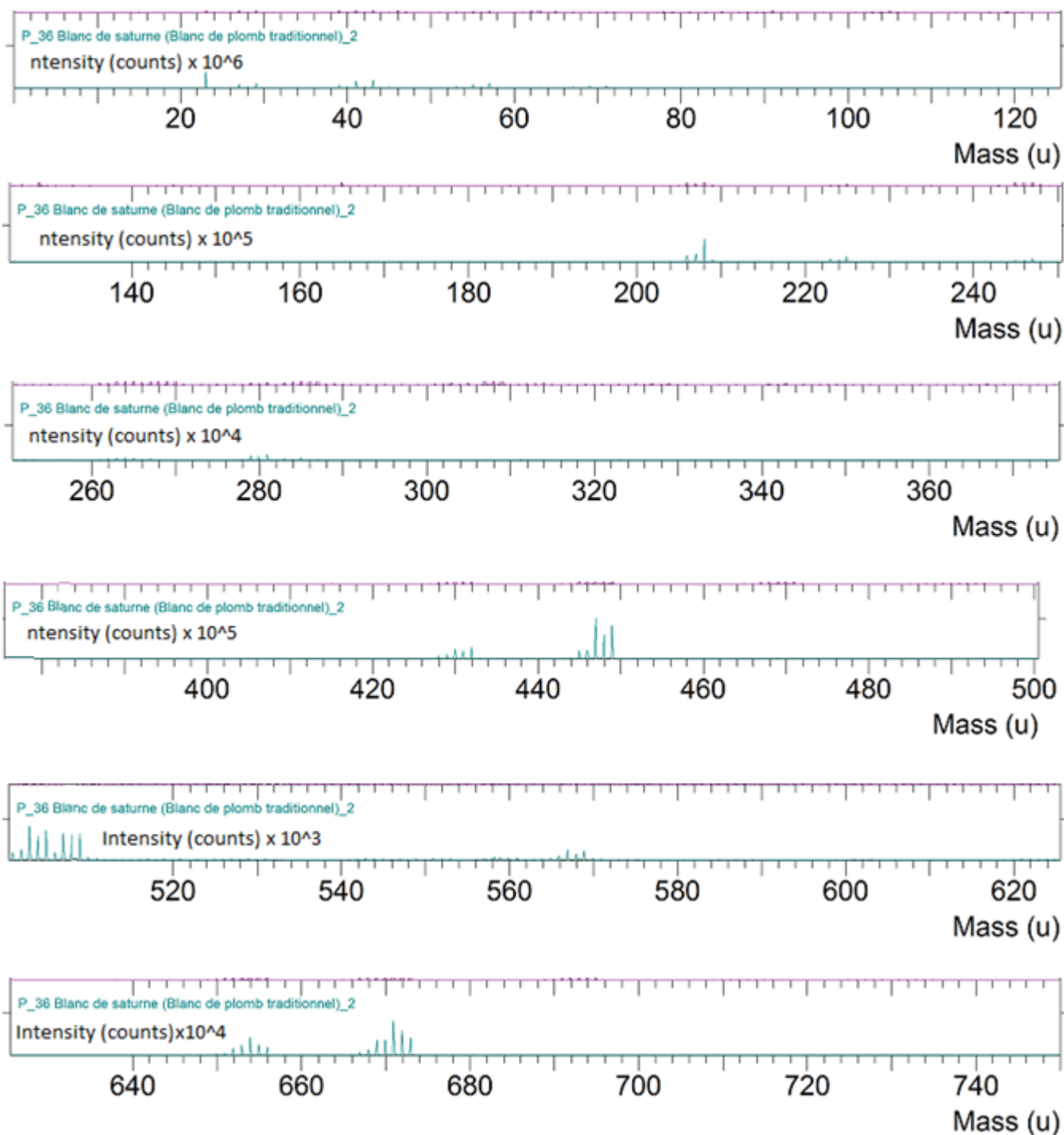


Figure 3.6: ToF-SIMS spectrum for positive ions of the sample *Blanc de Saturne*: we see  $Pb^+$  at  $m/z$  204,  $Pb_2O_2H^+$  at  $m/z$  445,  $Pb_3O_2^+$  at  $m/z$  650 and  $Pb_3O_3H^+$  at  $m/z$  670

basis of this plot, the distinction between *blanc d'argent* or flake white on the one hand and *blanc de saturne* on the other could be made, as well as a distinction between hydrocerussite and the rest. It is however questionable to base such conclusions on such plots as they depend on the total presence of lead, something that can change from one preparation to another and is not specific to the type of pigment. It seems therefore logical to look in the following paragraphs to lead related peaks that have been scaled relative to this  $Pb^+$  peak. The  $PbOH^+$  peak (Figure 3.9) seems to give the same pattern as the  $Pb^+$  peak, the main difference being for lead chloride. It is logical that lead oxides will be much less present in lead chloride, than in the other samples. Looking at the peak relative to the  $Pb^+$  peak (Figure 3.10), the differences are much smaller, but it confirms our intuition with respect to the low yield for lead oxides in lead chloride. The explanation for the rest of the pattern, however, is not clear.

- ◆ Lead carbonate\_1
- Lead carbonate\_2
- ▲ Lead carbonate\_3
- ◆ Hydrocerussite\_1
- Hydrocerussite\_2
- ▲ Hydrocerussite\_3
- ◆ Blanc d'argent\_1
- Blanc d'argent\_2
- ▲ Blanc d'argent\_3
- ◆ Flake white\_1
- Flake white\_2
- ▲ Flake white\_3
- ◆ Blanc de saturne\_1
- Blanc de saturne\_2
- ▲ Blanc de saturne\_3
- ◆ Minium\_1
- Minium\_2
- ▲ Minium\_3
- ◇ Lead chloride\_1
- Lead chloride\_2
- △ Lead chloride\_3

Figure 3.7: Legend used for Figures 3.8 to 3.17

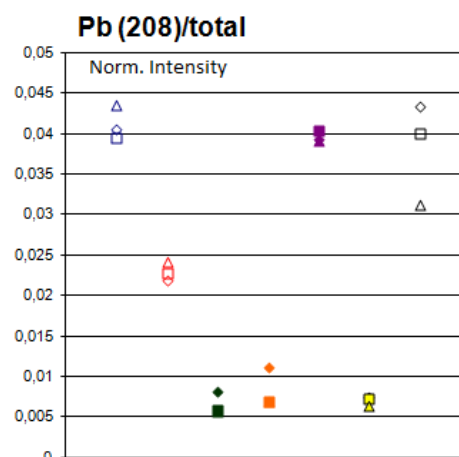


Figure 3.8: Positive  $Pb^+$  ions at  $m/z$  208

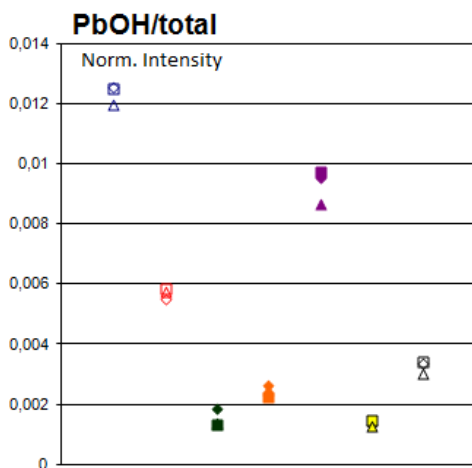


Figure 3.9: Positive  $PbOH^+$  ion at  $m/z$  225

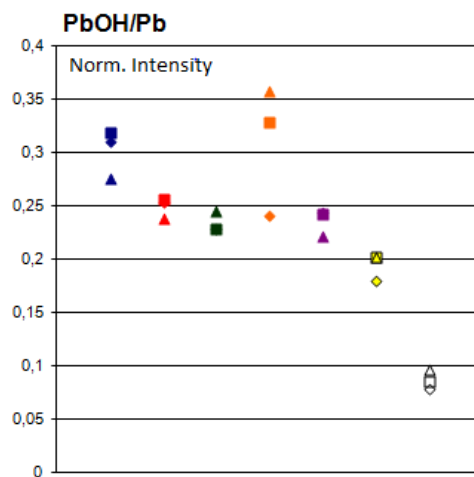


Figure 3.10: Positive  $PbOH^+$  ion at  $m/z$  225 relative to the counts of the  $Pb^+$  peak

The  $Pb_2^+$  peak, relative to the  $Pb^+$  peak, shows more dispersion, which could be used to distinguish between the different samples. The exact reason for the pattern is unclear.

### Lead oxide peaks

All positive peaks (the  $Pb_2O^+$  peaks, the  $Pb_2O_2H^+$  peaks and the  $Pb_3O_2^+$  and  $Pb_3O_3H^+$  peaks, see Figures 3.11 and 3.12) all show the same pattern, somewhat similar to the patterns of the  $PbOH^+$  and  $Pb_2^+$  peaks, the only difference between them being the lack of presence of minimum (even in the plots relative to the  $Pb^+$  peak) for the  $Pb_2O_2H^+$ ,  $Pb_3O_2^+$  and  $Pb_3O_3H^+$  peaks. As pointed out before, lead chloride shows almost no presence of lead oxides. Why the flake white yield is higher than the others in all these plots, is unclear.

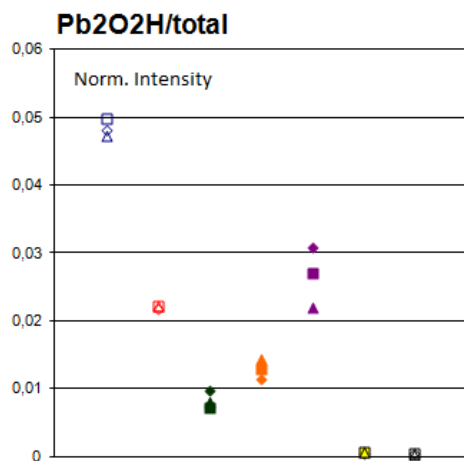


Figure 3.11: Positive  $Pb_2O_2H^+$  ion at  $m/z$  447

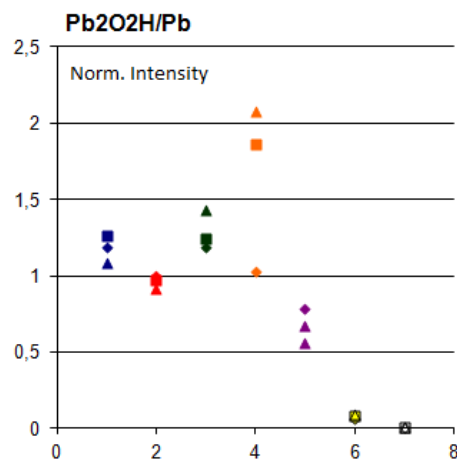


Figure 3.12: Positive  $Pb_2O_2H^+$  ion relative to the counts of the  $Pb^+$  peak at  $m/z$  447

In the negative peaks, the  $PbO^-$  peak (see Figure H.19) seems to reflect fairly well the total lead presence established through XPS. The only exception is that lead chloride has a much lower yield than we would expect from the XPS measurements. The reason is clear: as already seen above, the presence of lead oxides is very low in lead chloride. The  $PbOH^-$  peak (Figure

3.14) shows the same pattern. For the same reasons as before, we decide to look at the yield normalised by the  $PbO^-$  peak. This normalisation however, has no sense for lead chloride. In the plot of  $PbOH^-$  relative to the  $PbO^-$  peak (Figure 3.15) we see that all samples show almost the same value.

The other negative peaks ( $PbO_2^-$ ,  $PbO_2H^-$ ,  $Pb_2O_2H^-$ ,  $Pb_2O_3^-$  and  $Pb_2O_3H^-$ , see Figures 3.16 to 3.17), show roughly the same pattern. In the uncorrected peak, we see that the yields of hydrocerussite, *blanc d'argent* and flake white are decreasing with increasing mass of the ions. The peaks relative to the  $PbO^-$  peak does not show that much variation, except for minium, the yield of which is diminished for the  $PbO_2^-$ ,  $PbO_2H^-$ ,  $Pb_2O_3^-$  and  $Pb_2O_3H^-$  peaks (all relative to the  $PbO^-$  peak). This is not the case in the  $Pb_2O_2H^-$  peak however. This peak is also much lower in intensity than the other negative peaks.

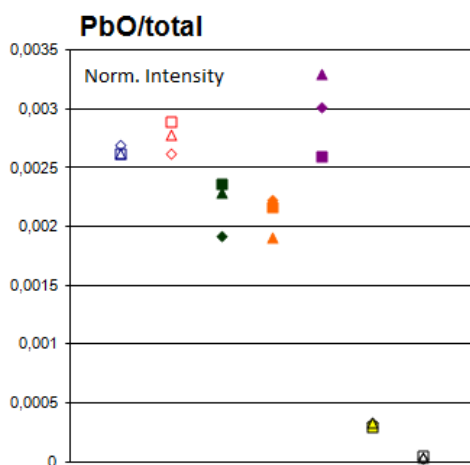


Figure 3.13: Negative  $PbO^-$  ion at  $m/z$  224

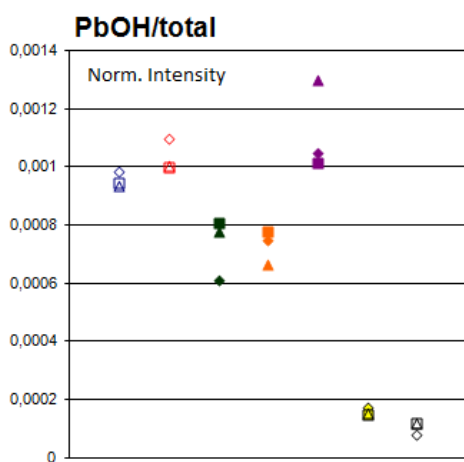


Figure 3.14: Negative  $PbOH^-$  ion at  $m/z$  225

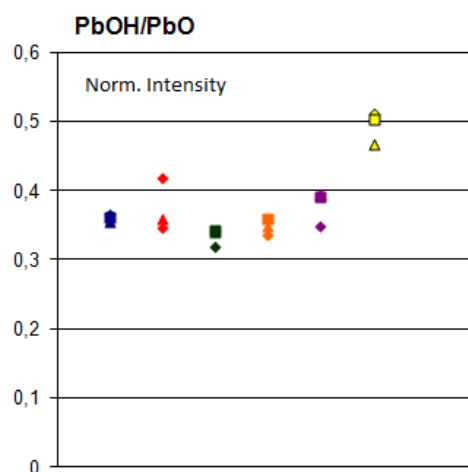


Figure 3.15: Negative  $PbOH^-$  ion at  $m/z$  225 relative to the counts of the  $PbO^-$  peak

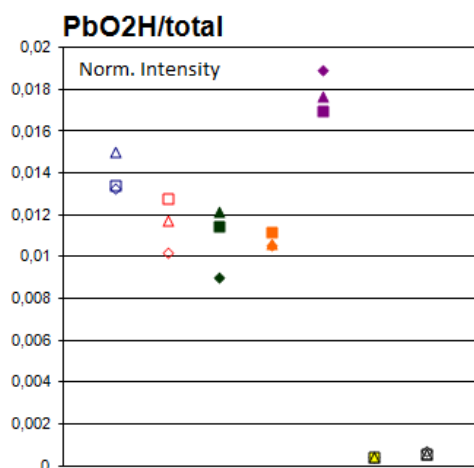


Figure 3.16: Negative  $PbO_2H^-$  ion at  $m/z$  241

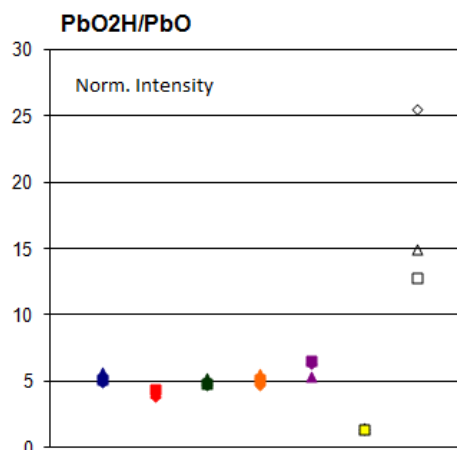


Figure 3.17: Negative  $PbO_2H^-$  ion at  $m/z$  241 relative to the counts of the  $PbO^-$  peak

### Other peaks

The peaks of lead-chlorine peaks (mentioned above) are very present in the lead chloride sample, both in the positive as in the negative spectrum, and totally absent in the other samples. Lead chloride is thus easily identifiable in SIMS.

Minium shows a whole range of barium related peaks (mentioned above). The presence of the element is confirmed through the XPS measurements. We find indeed an important peak for  $BaSO_4^-$ . This barium presence is however not an identifying feature of minium in general. Often other minerals are added to pigments as extenders. This is probably the reason why we find barium in this specific sample, but it does not imply that this will be the case in other minium samples.

The sodium peaks are very present for the *blanc d'argent*, flake white and, to a lesser extent, hydrocerussite samples and not present in the others. This indeed corresponds exactly to the findings in XPS which showed only a sodium presence in those three samples with less sodium in hydrocerussite than in the other two. We have also looked at the effect of eroding the samples (to get rid of surface contamination). This was done in three different ways: with 60 keV  $Bi^{3++}$  ions during 360 seconds, with large 10 keV *Ar*-clusters (with up to 3000 atoms) and with 1 keV *Cs* ions. With neither of these erosion techniques, the sodium presence disappears, which clearly shows that, corresponding to the XPS results, sodium is present in three of the samples.

### Conclusion

As mentioned above, it is possible to distinguish between different samples based on the lead peaks. This difference only partly correspond to the conclusions of the XPS experiments. Furthermore, an eventual similarity between the samples hydrocerussite and *blanc d'argent* and between the samples *blanc de saturne* flake white and lead carbonate, is not evidenced by the SIMS data. All non lead-based peaks are only specific to a certain sample and not to the pigment in general and are therefore not fit to use for identification.

### 3.5 Study of lead isotope abundance ratios in lead based pigments

Natural lead has four isotopes:  $^{204}\text{Pb}$ ,  $^{206}\text{Pb}$ ,  $^{207}\text{Pb}$  and  $^{208}\text{Pb}$ . The first one is not radiogenic, but the last three stem partly from the decay of uranium ( $^{235}\text{U}$  and  $^{238}\text{U}$ ) and thorium ( $^{232}\text{Th}$ ). The concentration of those last three therefore grows with time, while the  $^{204}\text{Pb}$  concentration remains constant.[30]

The abundance of the different lead isotopes in metals (such as silver or copper) in archaeological and historical artefacts (for example coins or glass) has been used successfully to determine the provenance of the metal.[31] The first attempts, in the 1930s, to establish the geological provenance of metals were based on chemical analysis. Such methods fail, however, in distinguishing provenance because of two reasons: first of all the ore deposits, from which the metals are mined, show chemical heterogeneities. Secondly, the chemical composition is changed through the processing.[31] Starting in the 1960s, two laboratories, at the universities of Oxford and Heidelberg, started to look at the lead isotope abundance ratio of materials to determine provenance. The first studies were done on ancient Greek coins, tracing them back to the silver mines in the Aegean where the metal ores stemmed from. A new breakthrough was reached when next to lead isotopes, also copper and copper based alloys were analysed.[31] The technique has already been applied on white lead pigments in the paintings of Rubens, van Dyck and others. In many cases their white leads could be traced back to ores in England, Belgium (Ardennes), Germany, Poland, the Alps, Spain or Italy.[30][32] For an example, see Figure 3.22.

The first reason why lead isotope analysis is effective in determining the provenance of lead samples is that lead, contrary to most elements, shows a large variation in isotopic composition.[30] Secondly, research shows that this isotopic composition is uniform throughout one ore deposit. Thirdly, the isotope composition of the metal directly won from the ore deposit is not changed throughout the entire metallurgical process (smelting, refining, working, casting or cupellation) nor by corrosion or weathering processes. This assertion has been called into question, but experiments have shown that the eventual variation in isotope composition falls well within the experimental error ( $\pm 0.05\%$ ).<sup>2</sup>[31] Furthermore, lead, due to its abundance and inexpensiveness, has been extensively used throughout history and therefore the method can be applied to a great many objects.[30]

The majority of the ore deposits are formed through the separation of the lead from the parent uranium and thorium through fluids. The isotopic composition is thus frozen-in and depends on the  $U/Pb$  and  $Th/Pb$  ratios in the initial source and the time of the final separation of the lead from this source. However, there exists some few ore deposits where this separation has not fully taken place and where the lead isotope composition is not homogeneous throughout.[31][30]

The classic technique for measuring lead isotope ratios is Thermal Ionisation Spectrometry (TIMS): the sample is put under vacuum and heated by an electric current until ionises. A high positive potential (several kilovolts) relative to an anode plate is needed to extract the ions after which the mass analysis happens with a magnetic sector mass spectrometer. To acquire the high precision that is required for the measurement of isotope ratios, the sample must be treated chemically (ion exchange separations prevent isobaric interferences) and often some hours of data acquisition is necessary. This method was advanced by the introduction of multi-collector magnetic sector mass spectrometers, which allow for data acquisition for all the isotopes simultaneously.[33] A newer technique, which offers even better resolution, is Inductively

---

<sup>2</sup>This does not seem to be a general characteristic: it is reported that the isotopic composition of tin does change through the metallurgical processes.[31]

Coupled Plasma Mass Spectrometry (ICPMS).[34] Here, an atomic ionisation is obtained by putting the sample in an inductively coupled plasma. The advantage of this atomisation is that the yield is no longer dependent on the different species containing the element.[35] Coupled with the use of a multi-collector magnetic sector mass spectrometry, this technique is called MS-ICPMS and is currently the best available technique.[31] The manufacturer CAMECA also produces Mass Spectrometry-SIMS machines that show an outstanding reproducibility for isotope ratios.[36]

### 3.5.1 ToF-SIMS study of isotope abundancy ratios in lead based pigments

We will try to apply the lead isotope analysis on the above mentioned lead based samples, using the results from the ToF-SIMS measurements. This firstly implies the hypothesis that there is no difference in ionisation probability between the different isotopes. The main problem, however, is that the samples have not been treated chemically to prevent isobaric interferences. In the first place, there will be an interference between the  $PbH^+$  peaks. Assuming that those are the only interferences, we have tried to separate them making the hypothesis that each isotope is as reactive to binding with a hydrogen atom. With  $A_{204}$  the area under the peak at  $m/z$  204 and  $Q_{204Pb}$  the area attributed to the  $^{204}Pb^+$  ion we can write our assumptions as follows:

$$A_M = Q_{MPb} + Q_{M-1PbH} = Q_{MPb} + \alpha Q_{M-1Pb}$$

With these notations we can write the following:

$$A_{204} = Q_{204Pb}$$

$$A_{205} = \alpha Q_{204Pb}$$

$$A_{206} = Q_{206Pb}$$

$$A_{207} = Q_{207Pb} + \alpha Q_{206Pb}$$

$$A_{208} = Q_{208Pb} + \alpha Q_{207Pb}$$

$$A_{209} = \alpha Q_{208Pb}$$

Which leaves two possible ways to extract  $\alpha$ :

$$\alpha_1 = \frac{A_{205}}{A_{204}}$$

$$A_{209} = \alpha_2[A_{208} - \alpha_2(A_{207} - \alpha_2 A_{206})] \Rightarrow A_{206}\alpha_2^3 - A_{207}\alpha_2^2 + A_{208}\alpha_2 - A_{209} = 0$$

If our assumptions are correct and these equations correctly describe the system, than, of course, both values for  $\alpha$  should be the same. The lead isotope analysis is then based on the comparison of two graphs: one with the  $^{208}Pb/^{206}Pb$  ratio versus  $^{207}Pb/^{206}Pb$  and the other with  $^{206}Pb/^{204}Pb$  versus  $^{207}Pb/^{206}Pb$ . Those ratios are chosen because  $^{204}Pb$  is the only non radiogenic isotope and because the ratios give results in different orders of magnitude, which makes them easily distinguishable.[31] Other articles base their conclusions on a  $^{206}Pb/^{204}Pb$  versus  $^{207}Pb/^{204}Pb$  graph.[32] We have chosen to use the first method and the two graphs with the correction  $\alpha_1$  are given in Figures 3.18 and 3.19. The same calculations with correction factor  $\alpha_2$  are shown in Figures 3.20 and 3.21.

Comparing the two results, we see that the difference between the use of  $\alpha_1$  or  $\alpha_2$  as correction factor influences greatly the  $^{207}Pb/^{206}Pb$  ratio (ranging between 0,18 and 0,88 for  $\alpha_1$  and between 0,83 and 0,99 for  $\alpha_2$ ). The difference is the most dramatic for samples *blanc d'argent* and minium. The  $^{208}Pb/^{206}Pb$  ratio is much less influenced (as only  $Q_{208Pb}$  depends on  $\alpha$ ). Ratio  $^{206}Pb/^{204}Pb$  has no  $\alpha$ -dependence. More importantly, the  $^{207}Pb/^{206}Pb$  ratio for

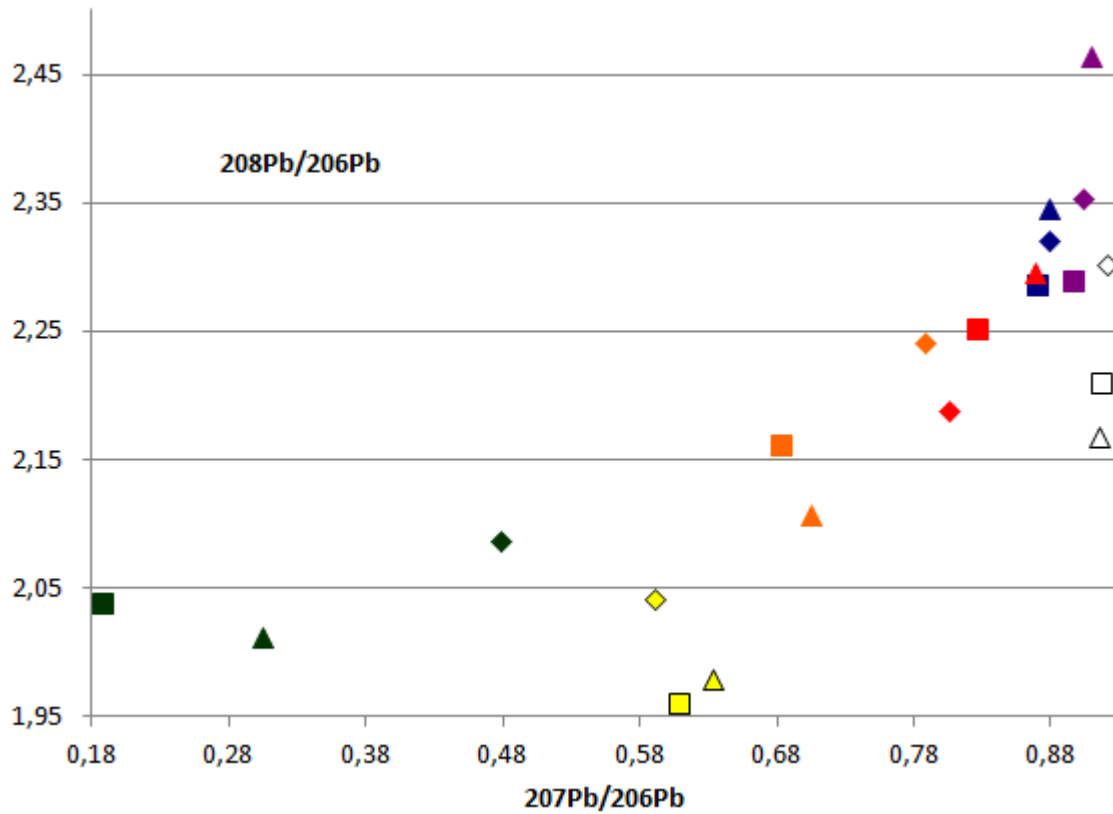


Figure 3.18:  $^{208}\text{Pb}/^{206}\text{Pb}$  versus  $^{207}\text{Pb}/^{206}\text{Pb}$  with  $\alpha_1$ -correction; legenda: see Figure H.1

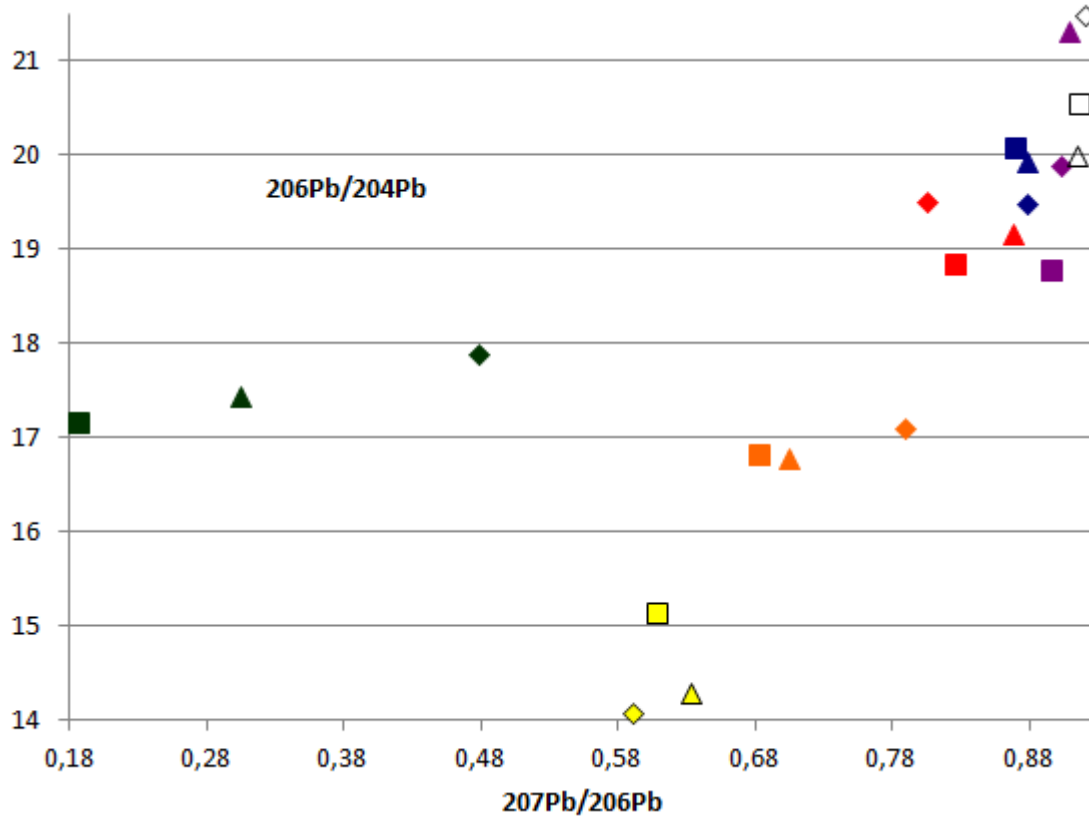


Figure 3.19:  $^{206}\text{Pb}/^{204}\text{Pb}$  versus  $^{207}\text{Pb}/^{206}\text{Pb}$  with  $\alpha_1$ -correction; legenda: see Figure H.1

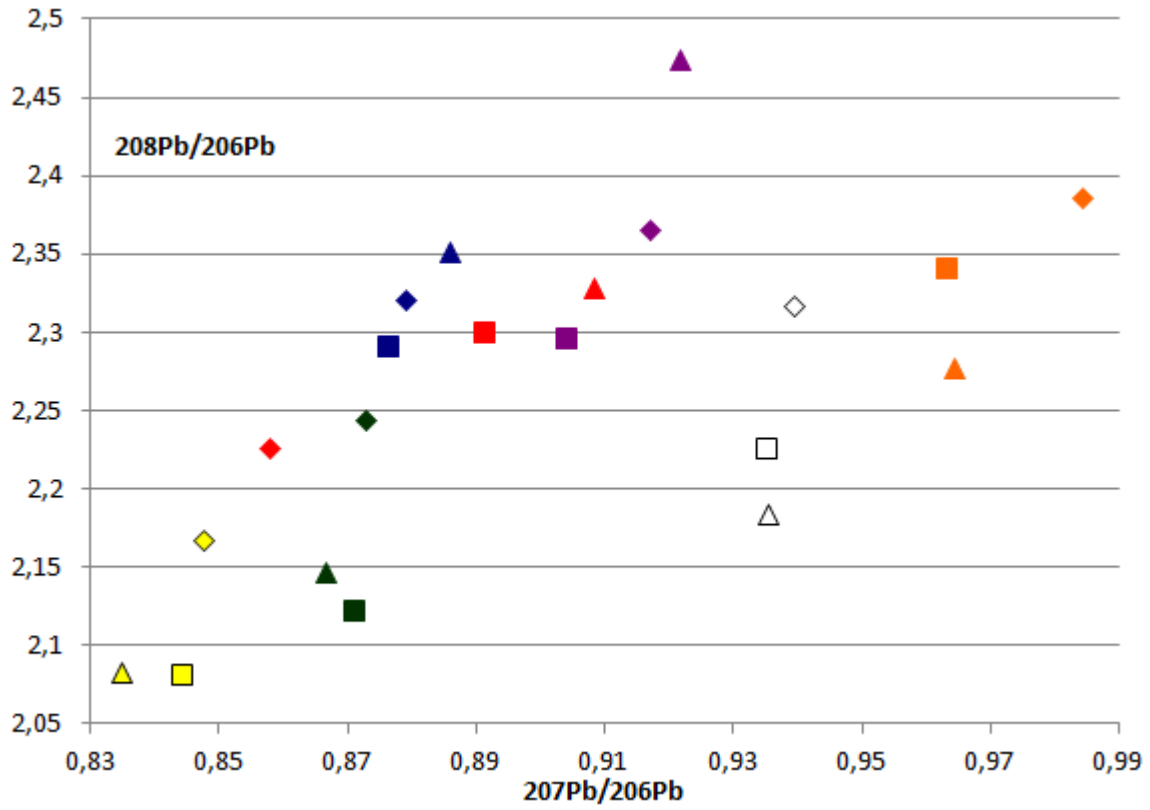


Figure 3.20:  $^{208}\text{Pb}/^{206}\text{Pb}$  versus  $^{207}\text{Pb}/^{206}\text{Pb}$  with  $\alpha_2$ -correction; legenda: see Figure H.1

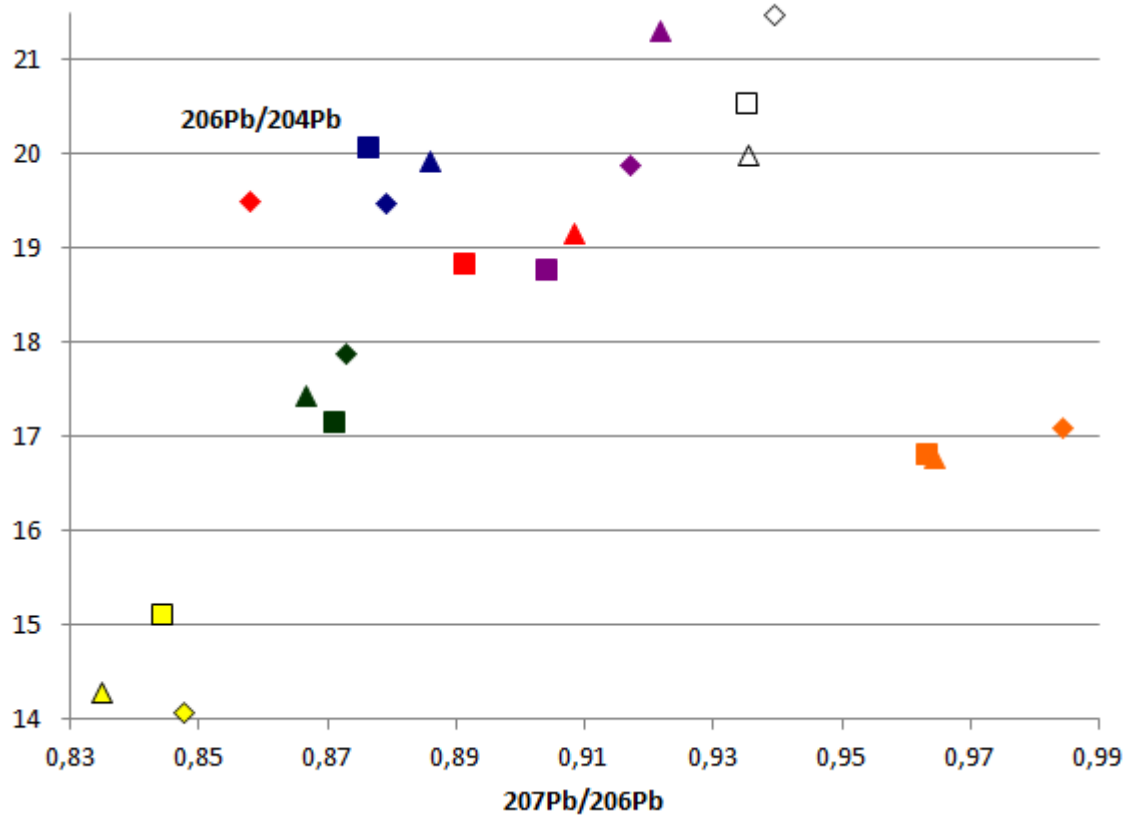


Figure 3.21:  $^{206}\text{Pb}/^{204}\text{Pb}$  versus  $^{207}\text{Pb}/^{206}\text{Pb}$  with  $\alpha_2$ -correction; legenda: see Figure H.1

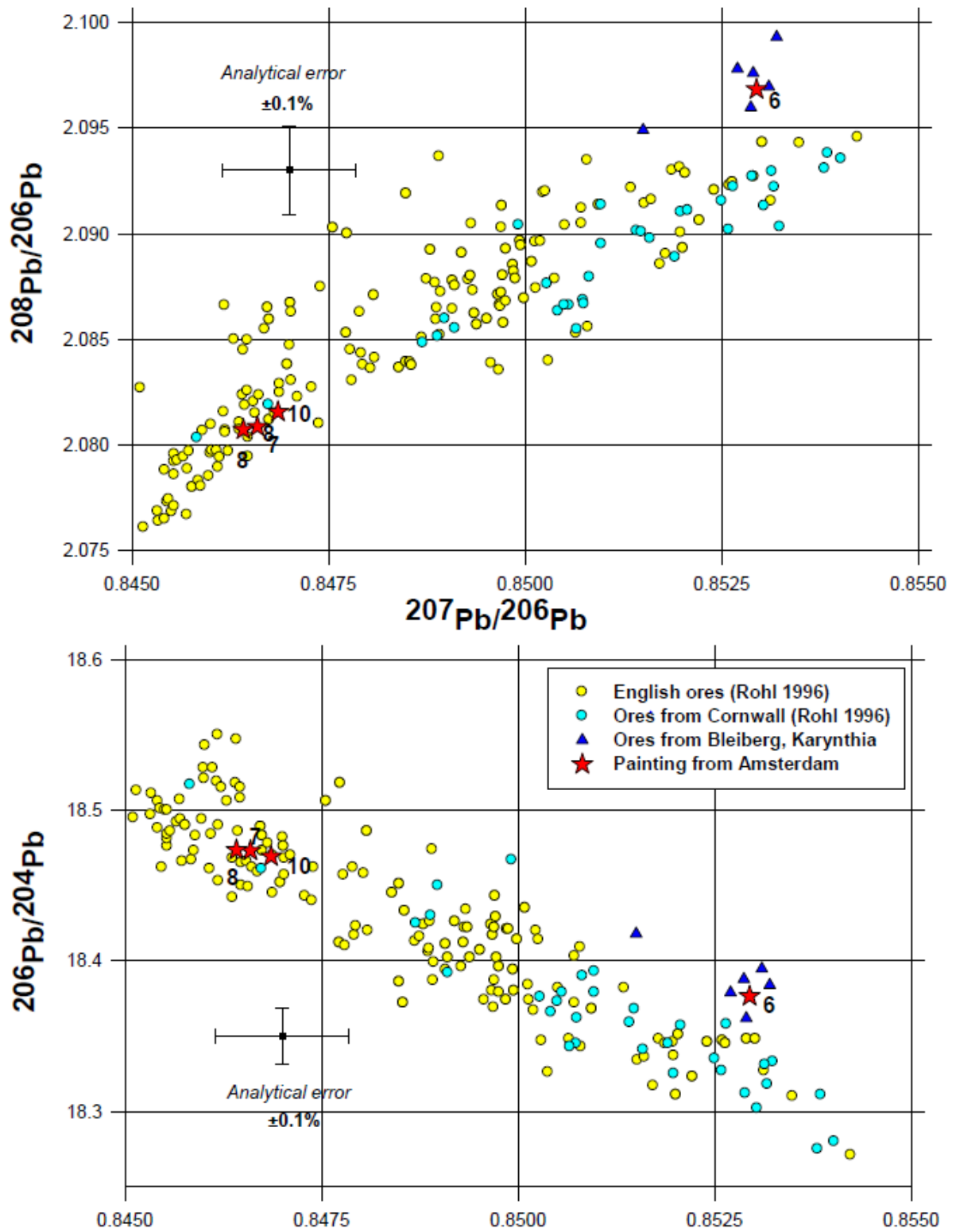


Figure 3.22:  $^{208}\text{Pb}/^{206}\text{Pb}$  and  $^{206}\text{Pb}/^{204}\text{Pb}$  versus  $^{207}\text{Pb}/^{206}\text{Pb}$  for different ores and for an unknown painting from Amsterdam. Taken from [37]

$\alpha_2$ -correction is in the range of what we find in literature([31], [37]): see also Figure 3.22. We therefore believe that this correction factor makes more sense. Its calculation is also based on sharper peaks, whereas the calculation of  $\alpha_1$  depends on two relatively low peaks, which might influence its exactness. However, the fact that there is an important difference between the two correction factors is a reason to call into question the correctness of our method to separate isobaric interference. Nevertheless, for the  $\alpha_2$ -correction, most pigment samples seem to form some sort of cluster which makes them distinguishable with respect to the others. The two exceptions are hydrocerussite and *blanc d'argent* who are more disperse. However, comparing our results with those of Figure 3.22, we see that the spread on our measurements is much larger for all three ratios. We can therefore conclude that the ToF-SIMS technique applied as such, without any efforts to enhance the resolution or to prevent isobaric interferences, has not the required precision to establish the provenance of the samples based on isotope abundance ratios. The fact that most pigments seem to be distinguishable between them as they form separate groups, can help in the identification of an unknown sample. To that end, the three ratios for such a sample should be plotted against each other and compared with the results of Figures 3.20 and 3.21.

## 3.6 Study of azurite with ToF-SIMS

In order to study later on the effect of lead pigments on the ageing of the oil binder, we also want to examine a non-lead-based pigment to make a comparison. This pigment will be azurite,  $Cu_3(CO_3)_2(OH)_2$ . In the ToF-SIMS spectra no traces of lead are found, as would be expected and instead peaks of copper compounds are clearly distinguishable.

### 3.6.1 Observed positive ions

We observe:

- copper: pure copper ions ( $Cu^+$ ) are observed for the isotopes of copper at  $m/z$  63 (main isotope) and 65,
- copper oxide:
  - $Cu_2O^+$  at  $m/z$  142, 144 and 146,
  - $Cu_3O^+$  at  $m/z$  205, 207 and 209
  - $Cu_4O_2^+$  at  $m/z$  284, 286, 288 and 290,
  - $Cu_4O_3^+$  at  $m/z$  300, 302, 304 and 306,
  - $Cu_5O_2^+$  at  $m/z$  347, 349, 351, 353 and 355,
  - $Cu_5O_3^+$  at  $m/z$  363, 365, 367, 369 and 371,
  - $Cu_6O_3^+$  at  $m/z$  426, 428, 430, 432 and 434,
  - $Cu_6O_4^+$  at  $m/z$  442, 444, 448 and 450,
  - $Cu_7O_4^+$  at  $m/z$  504, 506, 508, 510, 512 and 514,
- copper hydroxide and oxides with hydrogen:
  - $Cu_2OH^+$  at  $m/z$  143, 145 and 147,
  - $Cu_4O_2H$  at  $m/z$  285, 287, 289 and 290,
  - $Cu_5O_3H^+$  at  $m/z$  364, 366, 368, 370 and 372.

### 3.6.2 Observed negative ions

The following (significant) peaks were discerned in the negative spectrum:

- copper: pure copper ions ( $Cu^-$ ) at  $m/z$  63 (main isotope) and 65,
- copper oxides and oxides with hydrogen:
  - $Cu_2O_3^-$  at  $m/z$  174, 176 and 178,
  - $Cu_3O_3^-$  at  $m/z$  237, 239 and 241 and  $Cu_3O_3H^-$  at  $m/z$  238, 240 and 242,
  - $Cu_4O_4^-$  at  $m/z$  316, 318, 320 and 322, and  $Cu_4O_4H^-$  at  $m/z$  317, 319, 321 and 323,
  - $Cu_5O_4^-$  at  $m/z$  379, 381, 383, 385 and 387,
  - $Cu_5O_5^-$  at  $m/z$  395, 397, 399, 401 and 403,
  - $Cu_6O_5^-$  at  $m/z$  458, 460, 462, 464 and 466,
  - $Cu_7O_5^-$  at  $m/z$  520, 522, 524, 526, 528 and 530,
  - $Cu_8O_6^-$  at  $m/z$  599, 601, 603, 605, 607 and 609,
- copper sulfate:  $CuSO_4^-$  at  $m/z$  159.

## Chapter 4

# Study of oil-pigment mixtures

### 4.1 Introduction

The process of the drying and ageing of (linseed) oil was described in Chapter 2. The presence of pigments, however, can alter this process considerably. Cations (zinc, copper, lead or other) from the pigments can convert the fatty acids into metal carboxylate anions which later form insoluble metal soap.[7] This saponification can change the appearance of a painting and makes the compounds less volatile. Oil films with pigments present have a tendency to be more oxidised. This is first of all due to the fact that the dispersion of pigment particles increases the contact of the binder with oxygen. Secondly, it is a known effect that lead has a catalysing influence on the oxidation of the fatty acids.

### 4.2 Study of linseed oil-flake white mixtures in ToF-SIMS

In the following, we will study a mixture of linseed oil (Fresh linseed oil, refined, (product number 5840 650) from Maimeri, Mediglia, Italy; taken from the stocks of KIK-IRPA, used for samples A1, A2 and A3 in Chapter 2) with flake white (see Chapter 3) and an analogous mixture of the same pigment with boiled linseed oil (boiled for two hours on a low heat from Le Lion; taken from the stocks of KIK-IRPA, used for the samples B1, B2 and B3 in Chapter 2). Samples of this mixture have undergone simulated ageing in the same way as in Chapter 2. A part was covered with aluminium foil during the ageing process. We will thus compare following samples:

- Sample A2 (see Chapter 2): fresh linseed oil, undergone simulated ageing treatment while being covered with aluminium foil.
- Sample A3 (see Chapter 2): fresh linseed oil, undergone simulated ageing treatment.
- Fresh linseed oil mixed with flake white (ratio about 1:1), undergone simulated ageing treatment while being covered with aluminium foil. We will call this sample A2FW.
- Fresh linseed oil mixed with flake white (ratio about 1:1), undergone simulated ageing treatment. We will call this sample A3FW.
- Sample B2 (see Chapter 2): boiled linseed oil, undergone simulated ageing treatment while being covered with aluminium foil.
- Sample B3 (see Chapter 2): boiled linseed oil, undergone simulated ageing treatment.
- Boiled linseed oil mixed with flake white (ratio about 1:1), undergone simulated ageing treatment while being covered with aluminium foil. We will call this sample B2FW.
- Boiled linseed oil mixed with flake white (ratio about 1:1), undergone simulated ageing treatment. We will call this sample B3FW.

### 4.2.1 Observed positive ions

The observed ions that are related to the linseed, are the same as those mentioned in Chapter 2. Furthermore we observe peaks that are related to the pigment. For the lead white, there are lead-based peaks:

- lead:
  - pure lead ions ( $Pb^+$ ) are observed for the isotopes of lead at  $m/z$  204,206,207 and 208 (main isotope),
  - $Pb_2^+$  at  $m/z$  412, 413, 414, 415 and 416,
- lead oxide:
  - $Pb_2O^+$  at  $m/z$  228, 229, 230, 231 and 232,
  - $Pb_3O_2^+$  at  $m/z$  650, 651, 652, 653, 654, 655 and 656,
  - $Pb_4O_3^+$  at  $m/z$  874, 875, 876, 877, 878, 879 and 880,
- lead hydroxide and oxides with hydrogen:
  - $PbOH^+$  at  $m/z$  223, 224 and 225,
  - $Pb_2O_2H$  at  $m/z$  445, 446, 447, 448 and 449,
  - $Pb_3O_3H^+$  at  $m/z$  667, 668, 669, 670, 671, 672 and 673,
  - $Pb_4O_4H$  at  $m/z$  891, 892, 893, 894, 895, 896 and 897.

The sodium related peaks of  $NaPbO^+$  and  $Na_2Pb_2O_2^+$

### 4.2.2 Observed negative ions

The observed ions are the same as for the linseed oil samples of Chapter 2.

## 4.3 Study of linseed oil-lead carbonate mixtures in ToF-SIMS

Analogously, we will now examine a mixture of linseed oil (the same as before) with lead carbonate (see Chapter 3). Samples of this mixture have undergone simulated ageing in the same way as in Chapter 2. A part was covered with aluminium foil during the ageing process. We will thus compare following samples:

- Sample A2 (see Chapter 2 and Section 4.2).
- Sample A3 (see Chapter 2 and Section 4.2).
- Fresh linseed oil mixed with lead carbonate (ratio about 1:1), undergone simulated ageing treatment while being covered with aluminium foil. We will call this sample A2LC.
- Fresh linseed oil mixed with lead carbonate (ratio about 1:1), undergone simulated ageing treatment. We will call this sample A3LC.
- Sample B2 (see Chapter 2 and Section 4.2).
- Sample B3 (see Chapter 2 and Section 4.2).
- Boiled linseed oil mixed with lead carbonate (ratio about 1:1), undergone simulated ageing treatment while being covered with aluminium foil. We will call this sample B2LC.
- Boiled linseed oil mixed with lead carbonate (ratio about 1:1), undergone simulated ageing treatment. We will call this sample B3LC.

### 4.3.1 Observed positive ions

The observed positive ions are the same as for the mixture with flake white, although the ions  $Pb_4O_3^+$  and  $Pb_4O_4H^+$  are less visible.

### 4.3.2 Observed negative ions

The observed negative ions originating from the linseed binder are the same as for flake white (Section 4.2), but following lead ions are visible:

- $PbO^-$  at  $m/z$  222, 223 and 224 and  $PbOH^-$  at  $m/z$  223, 224 and 225 although very weakly and only in A3LC,
- $PbO_2^-$  at  $m/z$  238, 239 and 240 and  $PbO_2H^-$  at  $m/z$  239, 240 and 241 although weakly,
- $Pb_2^-$  at  $m/z$  412, 413, 414, 415 and 416, although only in A3LC,
- $Pb_2OH^-$  at  $m/z$  429, 430, 431, 432 and 433, clearly visible in A3LC but weaker in A2LC,
- $Pb_2O_3^-$  at  $m/z$  460, 461, 462, 463 and 464, and  $Pb_2O_3H^-$  at  $m/z$  461, 462, 463, 464 and 465,

## 4.4 Study of linseed oil-lead chloride mixtures in ToF-SIMS

In the same way as before, we will now examine a mixture of linseed oil (the same as before) with lead chloride (see Chapter 3). We will thus compare following samples:

- Sample A2 (see Chapter 2 and Section 4.2).
- Sample A3 (see Chapter 2 and Section 4.2).
- Fresh linseed oil mixed with lead chloride (ratio about 1:1), undergone simulated ageing treatment while being covered with aluminium foil. We will call this sample A2LCl.
- Fresh linseed oil mixed with lead chloride (ratio about 1:1), undergone simulated ageing treatment. We will call this sample A3LCl.
- Sample B2 (see Chapter 2 and Section 4.2).
- Sample B3 (see Chapter 2 and Section 4.2).
- Boiled linseed oil mixed with lead chloride (ratio about 1:1), undergone simulated ageing treatment while being covered with aluminium foil. We will call this sample B2LCl.
- Boiled linseed oil mixed with lead chloride (ratio about 1:1), undergone simulated ageing treatment. We will call this sample B3LCl.

### 4.4.1 Observed positive ions

The peaks related to the linseed are the same as in Chapter 2. From the lead-based ions, only the following are visible (only in A3LCl, nothing is visible in A2LCl):

- pure lead ions ( $Pb^+$ ) are observed very weakly for the isotopes of lead at  $m/z$  204,206,207 and 208 (main isotope),
- $Pb_2^+$  very weakly at  $m/z$  412, 413, 414, 415 and 416,
- $Pb_2O^+$  at  $m/z$  228, 229, 230, 231 and 232,
- $PbOH^+$  at  $m/z$  223, 224 and 225,
- $Pb_2O_2H$  at  $m/z$  445, 446, 447, 448 and 449.

#### 4.4.2 Observed negative ions

The observed ions related to the linseed binder are the same as before. From the pigment related ions, only  $Cl^-$  is visible at  $m/z$  35 and 37.

### 4.5 Study of linseed oil-minium mixtures in ToF-SIMS

We will study a mixture of linseed oil (the same as before) with minium (see Chapter 3). We will thus compare following samples:

- Sample A2 (see Chapter 2 and Section 4.2).
- Sample A3 (see Chapter 2 and Section 4.2).
- Fresh linseed oil mixed with minium (ratio about 1:1), undergone simulated ageing treatment while being covered with aluminium foil. We will call this sample A2M.
- Fresh linseed oil mixed with minium (ratio about 1:1), undergone simulated ageing treatment. We will call this sample A3M.
- Sample B2 (see Chapter 2 and Section 4.2).
- Sample B3 (see Chapter 2 and Section 4.2).
- Boiled linseed oil mixed with minium (ratio about 1:1), undergone simulated ageing treatment while being covered with aluminium foil. We will call this sample B2M.
- Boiled linseed oil mixed with minium (ratio about 1:1), undergone simulated ageing treatment. We will call this sample B3M.

#### 4.5.1 Observed positive ions

The peaks related to the linseed binder are the same as before. For the lead based ions, we observe:

- pure lead ions ( $Pb^+$ ) at  $m/z$  204,206,207 and 208 (main isotope),
- $Pb_2O^+$  at  $m/z$  228, 229, 230, 231 and 232,
- $PbOH^+$  at  $m/z$  223, 224 and 225,
- $Pb_2O_2H$  at  $m/z$  445, 446, 447, 448 and 449. And the sodium peak of  $NaPbO^+$ .

#### 4.5.2 Observed negative ions

Once more, the linseed related negative ions are the same as in Chapter 2. However, quite some negative lead related ions are visible in A3M, but not in A2M:

- $Pb^-$  at  $m/z$  206, 207 and 208,
- $PbO^-$  at  $m/z$  222, 223 and 224 and  $PbOH^-$  at  $m/z$  223, 224 and 225,
- $PbO_2^-$  at  $m/z$  238, 239 and 240 and  $PbO_2H^-$  at  $m/z$  239, 240 and 241,
- $C_3H_4O_3Pb^-$  at  $m/z$  294, 295 and 296,
- $PbSO_4^-$  at  $m/z$  302, 303 and 304.

## 4.6 Discussion of results of ToF-SIMS measurements of mixtures of linseed oil and lead-based pigments

### 4.6.1 Pigment related ions

For the flake white mixture, we see that the positive lead ions (Figures C.2 to C.5) are much less present in A2FW (it is barely distinguishable from A2 or A3, samples that do not contain lead). There is however one measurement that forms an exception (measurement P\_A2FW\_2) and does show a lead presence at the level of A3FW for the  $Pb_2O^+$  and  $Pb_3O_3^+$  ions. In the B series, the pigment ions seem even more difficultly distinguishable, even in B3FW. This same pattern is also visible in the other mixtures. The minium samples show almost exactly the same results as the flake white ones for series A, but are the only ones to show a B3 sample with clear pigment ions present. In the mixture with lead carbonate, for example is the lead almost invisible in the A2LC series. We also have to note that there is a very high spread on the measurements for A3LC and to a lesser extent for B3LC. For some measurements no lead can be found in A3LC either. The effect seems the strongest in the lead chloride mixture: although it seems that in the A series  $Pb^+$  and  $PbOH^+$  are slightly more present in A3LCI than in A2, A2LCI and A3, compared to the B series, we see that the lead pigments are not distinguishable at all. As mentioned the  $Pb_3O_3^+$  ion is totally absent.

Secondly, it is remarkable that neither for the A2FW nor for the A3FW sample, any lead related ions are visible in the negative spectrum. Lead carbonate and minium mixtures do show negative lead related ions. These differences cannot be directly traced back to the composition of the pigments themselves: our SIMS study (see Chapter 3) showed that they all present a similar intensity for those negative ions. The same observation is done for negative ions as for the positive ones: they are much less visible in series A2Pigment than in A3Pigment.

We must remark as well that in all mixtures the A3Pigment sample shows a great spread for measured intensities of the lead ions, the minium mixture here as well being the exception. This shows that there is an important spatial variation in the sample. We suspect that there are spots in the sample where the pigment is gathered, and other spots where almost no pigment is present (in the film at least). It is also unclear why the lead ions are almost not visible in the A2Pigment samples. In order to solve these questions, we will measure a depth profile of the A2FW and A3FW samples later on.

### 4.6.2 Fatty acids: oil binder related ions

The legend for the following figures is shown in Figure 4.1

#### Linolenic acid

In series A, the deprotonated ion yield decreases due to the pre-treatment, with ageing and with the presence of the lead pigments (see Figure 2.13). The ageing process seems thus to be reinforced by the pigments, but in most cases this decrease seems rather related to ageing (as A2Pigment shows a yield closer to A2 than to A3). In the B series the behaviour is similar, but less pronounced (there is also a large spread). Only the flake white mixture shows remarkably a higher intensity for B3FW than for B3. The reason is unclear.

#### Linoleic and Oleic acid

The deprotonated ions of linoleic and oleic acid (see Figure 4.3) decrease both through the effect of ageing and through the presence of lead-based ions, just as for linolenic acid. Here as well, the

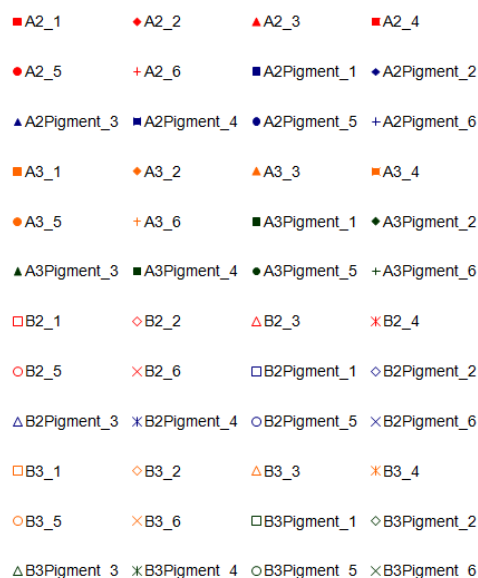


Figure 4.1: Legend used for Figures 4.2 to 4.14

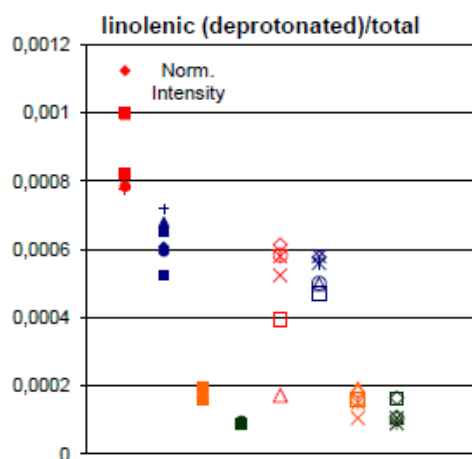


Figure 4.2: Negative deprotonated ions of linolenic acid  $C_{18}H_{29}O_2^-$  at  $m/z$  277 in the linseed oil-minium mixture

lead pigments seem to enhance the auto-oxidation process. As before, the pre-heated oil with flake white shows a deviant behaviour that is difficultly interpretable.

The ratio of the acylium ion yield and the protonated ion yield for oleic acid (see Figure 4.4), shows that in the A series the presence of lead promotes hydrolysis, although this effect is quite weak in the mixtures with minium and lead chloride. In the B series this seems to be the case to except for B3Pigment. The conclusions for linoleic acid are broadly the same.

### Palmitic and Stearic acid

The deprotonated ion yield for both palmitic and stearic (see Figure 4.5) shows roughly the same pattern for all the mixtures: a decrease with ageing and with the presence of lead-based pigment. In Chapter 2, we saw that the deprotonated ion yield decreased with ageing for both fatty acids. The presence of the pigment seems to enhance this effect.

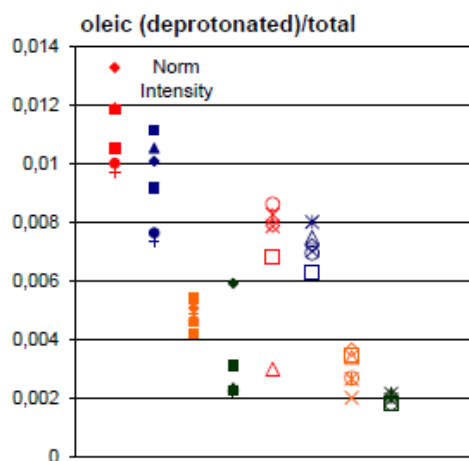


Figure 4.3: Negative deprotonated ions of oleic acid  $C_{18}H_{33}O_2^-$  at  $m/z$  281 in the linseed oil-lead chloride mixture

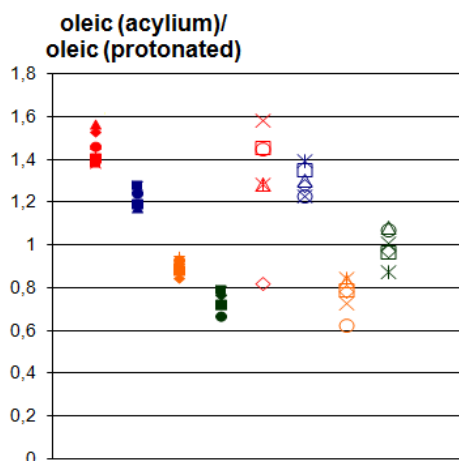


Figure 4.4: Ratio of positive acylium and protonated ions of oleic acid in the linseed oil-flake white mixture

Comparing the ratios of acylium and protonated ion yield for palmitic and stearic acids (see Figure 4.6), the effect of lead pigment is less clear. All samples show a similar pattern, but the spread on the results is for many samples so large, that conclusions are difficult to make. In general, it seems that the presence of lead pigment has only a small influence on the hydrolysis. For A2, A2Pigment and A3 the ratios are very comparable. A3FW shows an advanced hydrolysis. For the B series, on the other hand, the presence of lead has sometimes even a slightly inhibiting effect on hydrolysis. The protonated ion yield reflects this behaviour: except for the mixture with flake white, the hydrolysis is only slightly influenced by the presence of lead pigments and in the B series there is sometimes even an decelerating effect (see Figure 4.7).

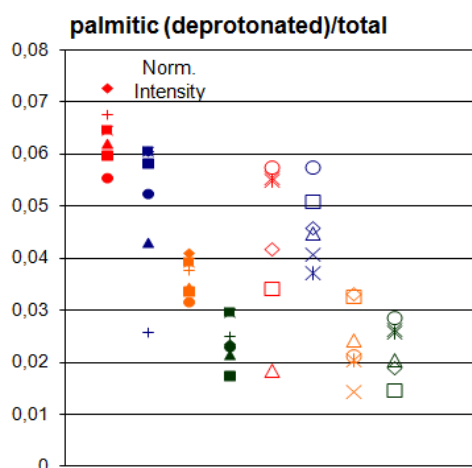


Figure 4.5: Negative deprotonated ions of palmitic acid  $C_{16}H_{31}O_2^-$  at  $m/z$  255 in the linseed oil-flake white mixture

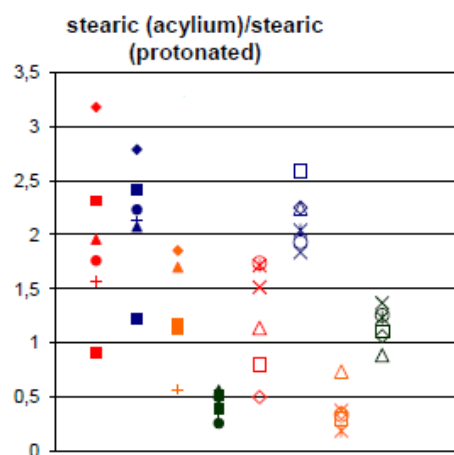


Figure 4.6: Ratio of positive acylium and protonated ions of stearic acid in the linseed oil-lead chloride mixture

### Palmitic/Stearic (P/S) ratio

The P/S ratio is for all the samples fairly constant (see Figure 4.8). This is what is often repeated in literature and this ratio of saturated fatty acids is therefore often used for the identification of an oil binder.[5][25] The same rise in P/S ratio as reported for B3 before, is in some sample also seen in B3Pigment. In general the presence of the pigment does not influence the P/S ratio.

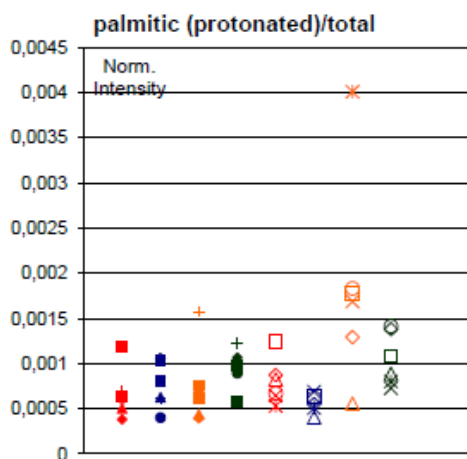


Figure 4.7: Positive protonated ions of palmitic acid  $C_{16}H_{33}O_2^+$  at  $m/z$  257 in the linseed oil-minium mixture

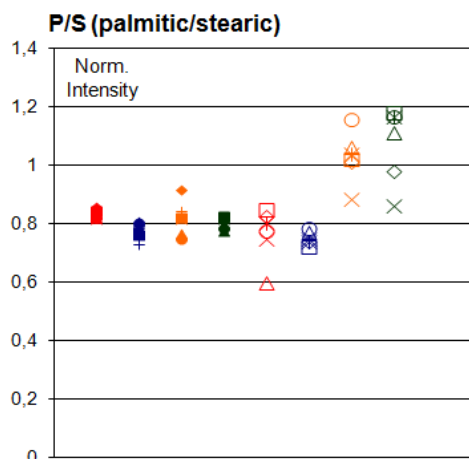


Figure 4.8: Ratio of negative deprotonated palmitic and stearic acid ions in the linseed oil-flake white mixture

### Suberic acid

As mentioned in Chapter 2, suberic acid is a product of the auto-oxidation reaction and is produced by double bond transposition from azelaic acid. For its deprotonated ion (see Figure 4.9), a similar pattern is visible in all mixtures, the clearest in those with minium and lead chloride: there is a rising tendency in the A series. This shows that the presence of lead pigments accelerates the auto-oxidation and probably as well transposition. This effect is also visible between A2 and A2Pigment, although they have been covered during the ageing process. In the flake white and lead carbonate the influence seems to be that strong that there A2FW reaches the suberic intensities of A3 and A3FW. The B series seem to show a similar effect, although the difference between B2 and B3 are small, as already mentioned in Chapter 2. Only the flake white sample shows a more strange behaviour as B3FW shows a lower intensity than all the others (with the exception of one measurement). The same conclusions can be made from the yields of the positive acylium ion of suberic acid.

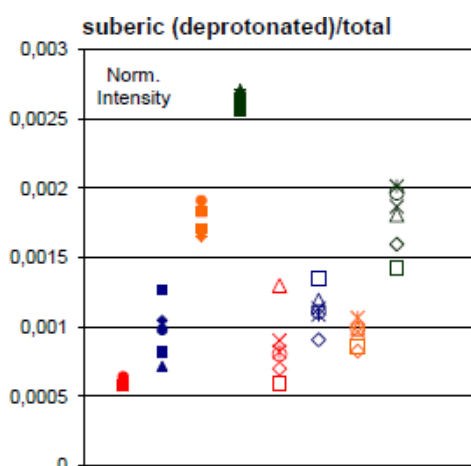


Figure 4.9: Negative deprotonated ions of suberic acid  $C_8H_{13}O_4^-$  at  $m/z$  173 in the linseed oil-minium mixture

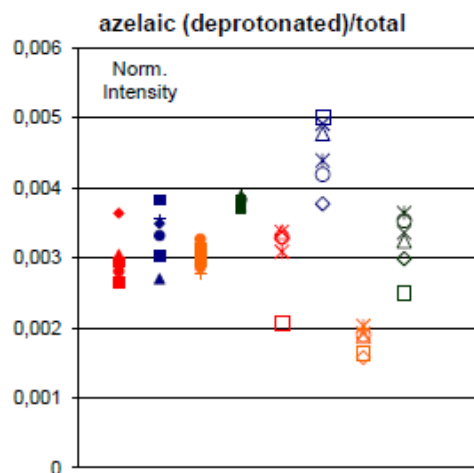


Figure 4.10: Negative deprotonated ions of azelaic acid  $C_9H_{15}O_4^-$  at  $m/z$  187 in the linseed oil-minium mixture

## Azelaic acid

The deprotonated ion of azelaic acid (see Figure 4.10) shows a yield about twice as high as for suberic acid. There is no great variation in the A series. We would expect to see an increase of azelaic analogous to that of suberic acid. However, we have to remember that azelaic decreases through double bond isomerisation (see ratio Suberic/Azelaic). The B series shows an outright decrease with ageing. We made the same observations in Chapter 2 and concluded that the double bond transposition happens in aged samples, but is reinforced in the pre-treated samples. The presence of lead seems to increase the yield of azelaic acid. It seems to reinforce the effect of ageing. There is an exception for the mixture with flake white which shows a lower yield for B3FW than for B3. This is analogous to the observations of suberic acid discussed above. The acylium ion yields (see Figure 4.11) show more the increasing pattern we would expect (once more with an exception for flake white). This was also reported in Chapter 2.

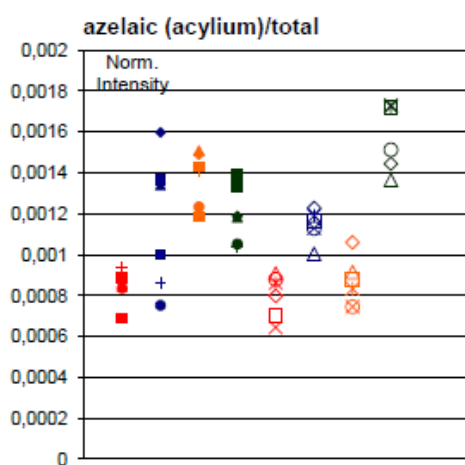


Figure 4.11: Positive acylium ions of azelaic acid  $C_9H_{15}O_3^+$  at  $m/z$  171 in the linseed oil-minium mixture

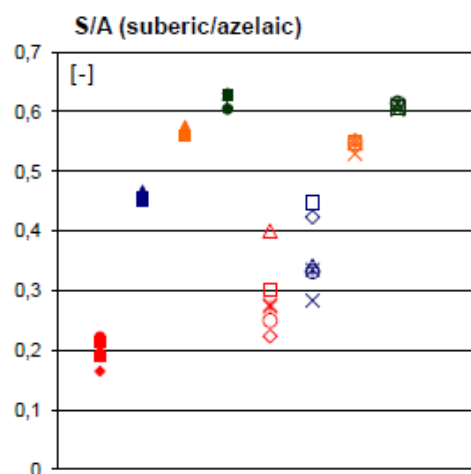


Figure 4.12: Ratio of negative deprotonated suberic and azelaic acid ions in the linseed oil-lead carbonate mixture

## Suberic/Azelaic (S/A) ratio

This ratio indicates double bond transpositions, which increases the amount of suberic and sebacic acid compared to azelaic acid. It is often stated that this is indicative for pre-treatment.[25] However, we see that for all mixtures, these ratios correspond fairly well between the A and B series (see Figure 4.12). The only notable exception is the higher ratio for B2 than for A2 (not the case for the lead chloride mixture). It is thus only in this case, in the absence of lead pigment or ageing that the ratio seems to distinguish between pre-treatments. This corresponds with earlier conclusions in the same sense: double bond transposition is much more influenced by ageing than by pre-treatment.[7] We see indeed that the ratio is higher for aged samples and that the presence of lead containing pigments reinforces the double bond transpositions. Most non-pre-treated samples A3 and A3Pigment show even a higher ratio than their pre-treated counterparts B3 and B3Pigment. The presence of the pigment increases the ratio even in the non-aged samples.

## Oleic/Stearic (O/S) ratio

The O/S ratio (see Figure 4.13) is said to be indicative of the auto-oxidation process ([25]) as the oleic acid is expected to decrease with auto-oxidation. This ratio supposes that the stearic acid yield is more stable, but we have seen that is not always the case. Nevertheless, we see indeed a

decreasing pattern in both A and B series, in accordance with the previous conclusions that the presence of lead pigments seems to reinforce the ageing trend.

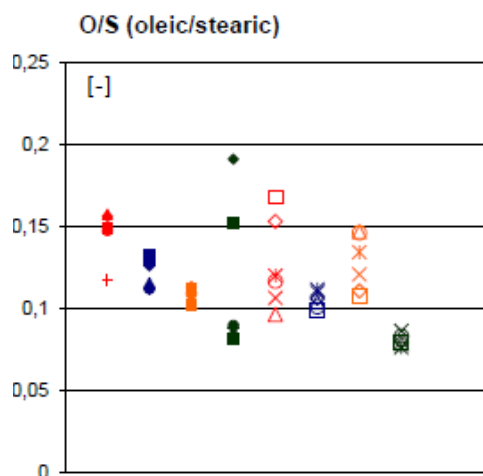


Figure 4.13: Ratio of negative deprotonated oleic and stearic acid ions in the linseed oil-lead chloride mixture

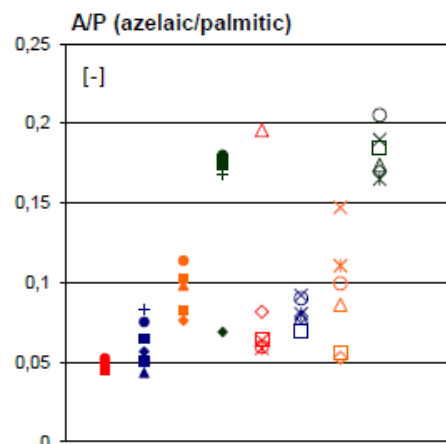


Figure 4.14: Ratio of negative deprotonated azelaic and palmitic acid ions in the linseed oil-lead chloride mixture

#### Azelaic/Palmitic (A/P) ratio

The A/P ratio (see Figure 4.14) is sometimes used to distinguish oil from proteinaceous binders (see Chapter 2), but as before, this identification does not seem to work: all values are below 0,2 which would identify them as being proteinaceous.[25] However, the A/P ratio can also give interesting information on the ageing process, as azelaic acid is a compound created during auto-oxidation and palmitic acid theoretically remains untouched by ageing (that this is not the case has been clearly established). However, the A/P ratios for all samples and in both the A and B series show indeed a rising pattern, as is expected. The only exception is once more B2FW which shows a lower ratio than B2.

#### 4.6.3 Lead Soaps

It is well known that in aged paint samples an interaction between the oleaginous binder and reactive pigments such as lead and copper can lead to saponification. Keune ([5]) mentions the presence of palmitic acid lead soap ( $PbOOC(CH_2)_{14}CH_3^+$  or  $PbO_2C_{16}H_{31}^+$  at  $m/z$  461-463 in the positive spectrum) and of stearic acid lead soap ( $PbOOC(CH_2)_{16}CH_3^+$  or  $PbO_2C_{18}H_{35}^+$  at  $m/z$  489-491 in the positive spectrum). We have tried to find these, or other soap peaks, but we have not found any presence of lead soaps. The reason for this difference between our observations and the reported peaks in the literature is unclear.

### 4.7 Depth Profiling and Imaging

In order to get a better understanding of the reasons why the lead ions are not really visible in the spectra of the A2FW sample, we decide to make a profile measurement. We may not forget that ToF-SIMS is a surface sensitive technique, therefore to get information from the bulk of a sample, we must first remove atoms from the surface. We will thus first erode the surface with a sputtering beam and than make a SIMS-spectrum measurement as we did before. This cycle is repeated different times. The sputtering beam (or Gas Cluster Ion Beam, GCIB) is an  $Ar_{3000}$ -beam (clusters with 3000 atoms on average) with an energy of 10 keV. A spectrum is taken during a 3 second-bombarding with  $Bi_3^{++}$ -ions (with an energy of 60 keV), the argon

sputtering beam is then switched on for 3 seconds. Afterwards, the flood gun bombards the surface for 8 seconds, to remove any positive charges that maybe left during the sputtering. This cycle is repeated 264 times for the A2FW sample and 54 times for the A3FW sample. The bombardment takes place on an area of  $600\ \mu\text{m}$  on  $600\ \mu\text{m}$ , while we measure a surface of  $200\ \mu\text{m}$  on  $200\ \mu\text{m}$ . The depth profile evolution of the  $\text{Na}^+$ ,  $\text{Pb}^+$  and the acylium ions of palmitic and stearic acid ( $\text{C}_{16}\text{H}_{31}\text{O}^+$  and  $\text{C}_{18}\text{H}_{35}\text{O}^+$ ) is shown in Figures 4.15 and 4.16 for sample A2FW and in Figure 4.17 for sample A3FW. In the graphs the intensity is expressed in function of the ion fluence (the number of sputtering  $\text{Ar}_{3000}$  clusters per square centimeter). It is not straightforward to relate this parameter directly to the depth of the crater, but in our case this will correspond to crater depths in the order of  $100\ \text{nm}$ .

We clearly see that the lead ion yield increases the deeper we dig. The intensity doubles for the A3FW sample. For the same fluence, the  $\text{Pb}^+$  intensity in A2FW doubles as well, but the ion remains 20 times less present. The ions of the fatty acids related to the oil (the acylium ions of palmitic ( $\text{C}_{16}\text{H}_{31}\text{O}^+$ ) and stearic ( $\text{C}_{18}\text{H}_{35}\text{O}^+$ ) acid) decrease with the sputtering. Polydimethylsiloxane (PDMS) is a well known contamination product that has, unfortunately, a very high ionisation probability. We see that the PDMS contribution diminishes for A3FW but remains fairly constant for A2FW. The sodium ion ( $\text{Na}^+$ ) is another ion that is very sensitive to secondary ionisation. We see that in both cases it seems to follow the pattern of the lead ion. We can indeed expect to find sodium in zones with a high presence of the pigment, rather than in oleaginous zones.

The depth profiling seems to indicate that both for A2FW as for A3FW the lead pigment is covered with a oil film. It seems that the oil film covering the lead particles in the A2FW sample is thicker than in the A3FW sample.

We will also take images of both samples before and after the sputtering. The images (see Figure 4.18 to 4.23) are taken of a surface of  $200\ \mu\text{m}$  by  $200\ \mu\text{m}$  with a resolution of  $1024 \times 1024$ , but to display the images  $16 \times 16$  binning is applied. They seem to affirm the conclusions from the depth profile. The surface of A2FW is much smoother than that of A3FW where we see a shadowing effect. Looking at the Pb-yield (Figure 4.22) we see indeed two bright spots and we feel that we can conclude that those are effectively lead particles. As can be expected, fatty acids seem to be less present on those spots. The particles have a diameter in the order of  $10\ \mu\text{m}$ . In A2FW we see that lead is absent before sputtering and becomes a little visible afterwards. The fatty acids disappear, but not entirely.

We can conclude that the depth profile and the images have shown that there are grains of lead pigment, which can be covered by an oil film. This oil film is thicker in the case of A2FW than for A3FW. When measuring a spectrum on a spot away from such a grain, or on a grain that is largely covered, almost no lead traces will be found. For the other mixtures of oil and lead based pigments, the same observation was made: lead ions are almost invisible in the spectra of the A2Pigment samples. We assume that the conclusions for A2FW are equally valid for the other mixtures. All pigments have indeed a similar consistence and, as just mentioned, they show the same behaviour in SIMS.

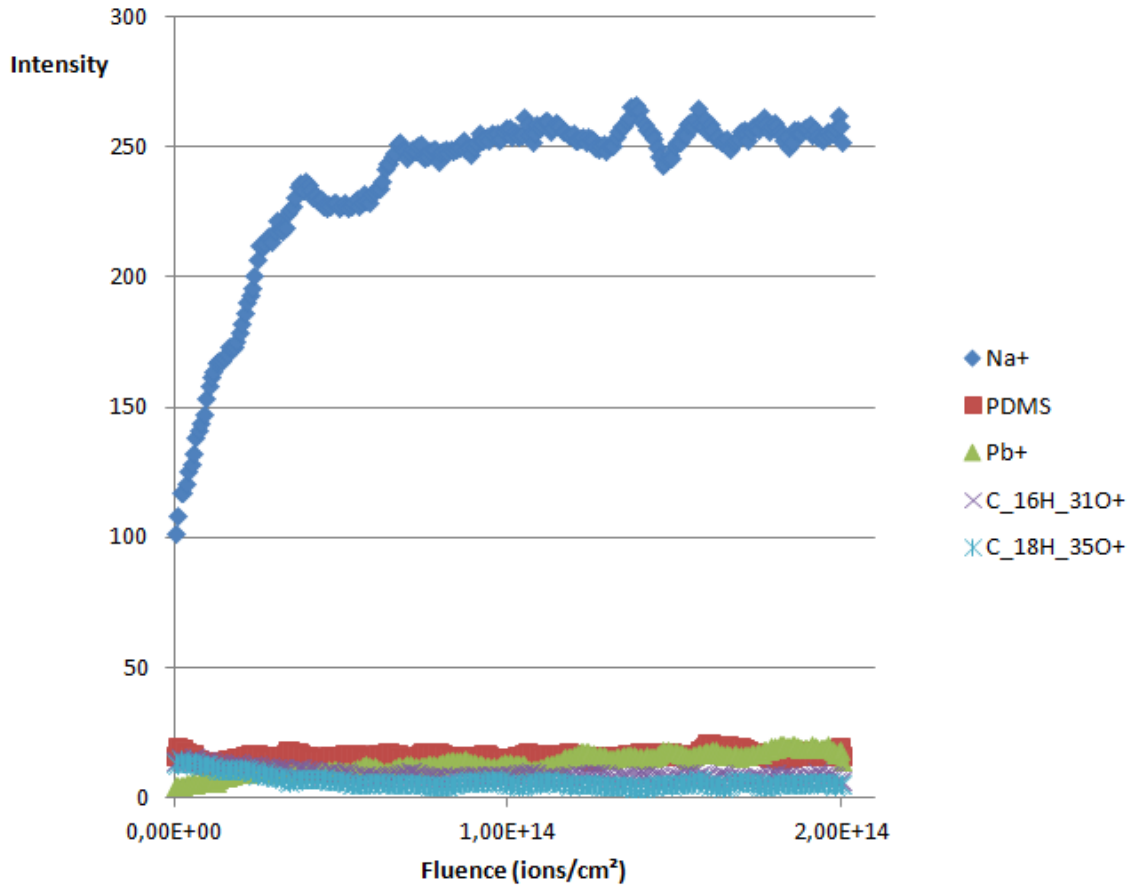


Figure 4.15: Profile of sample A2FW

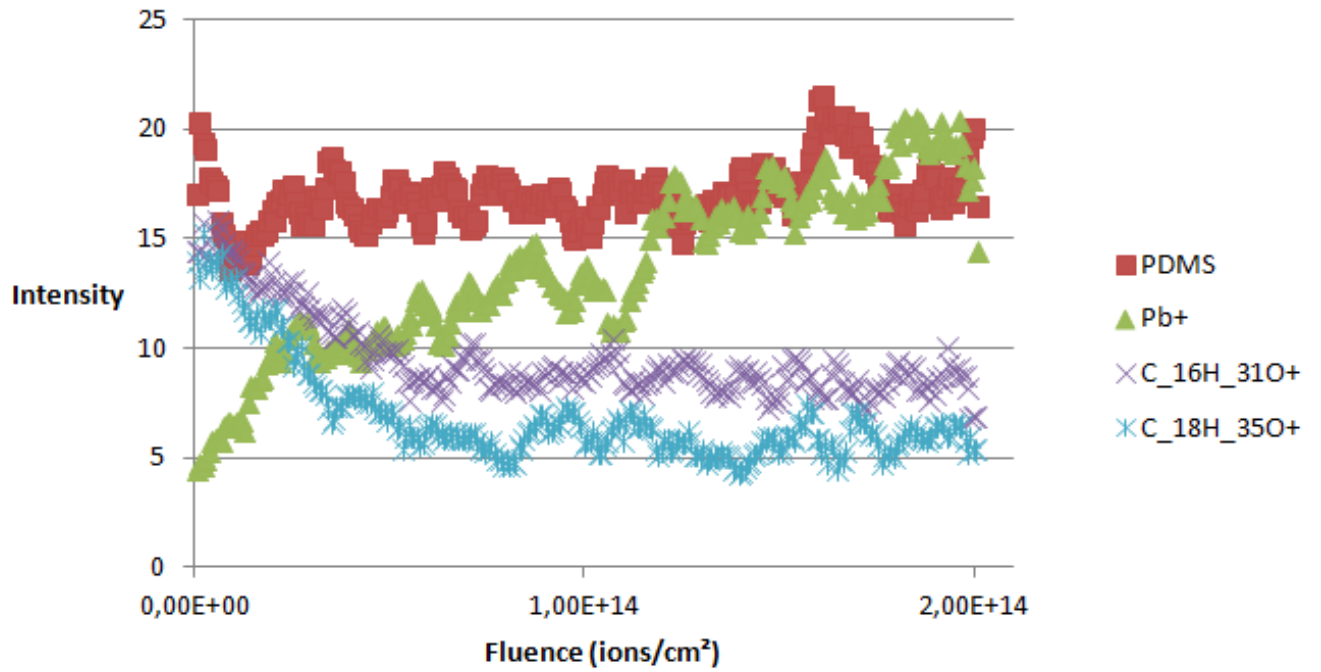


Figure 4.16: Profile of sample A2FW: detail

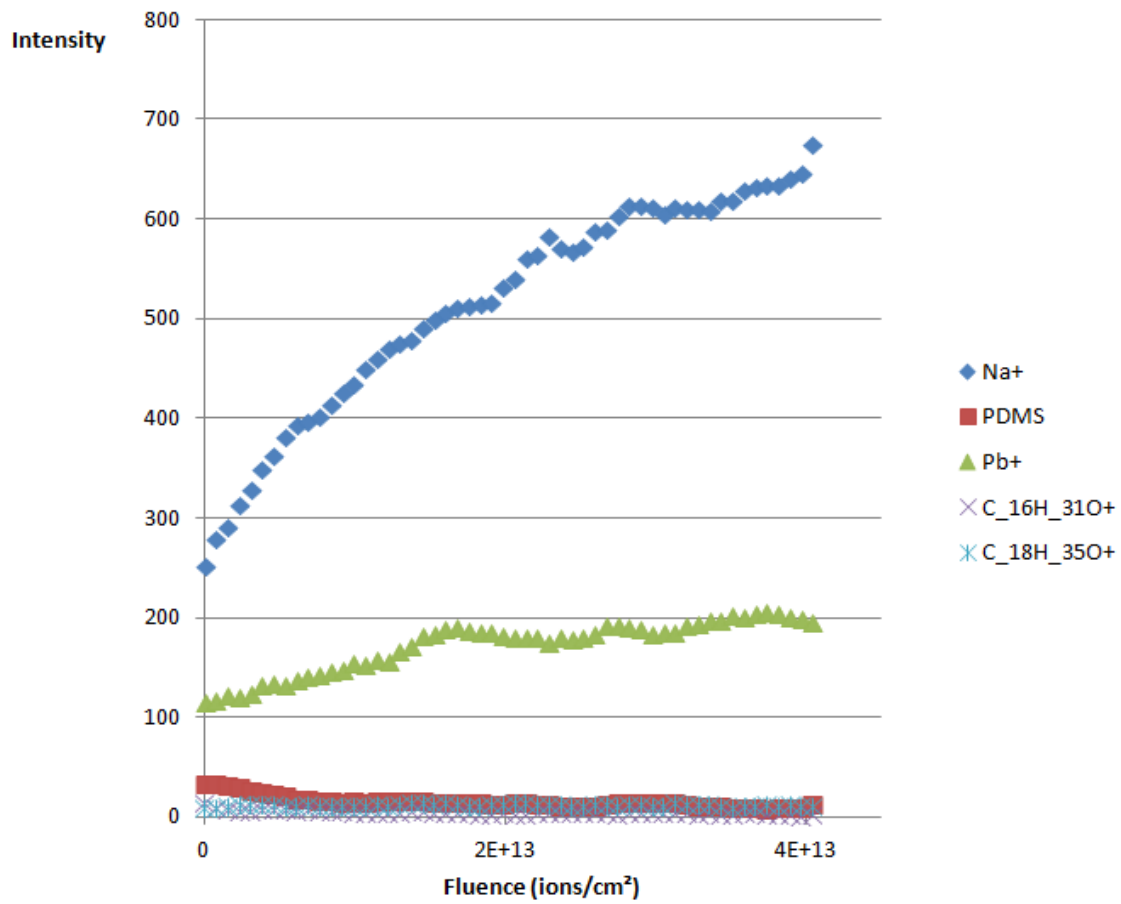


Figure 4.17: Profile of sample A3FW

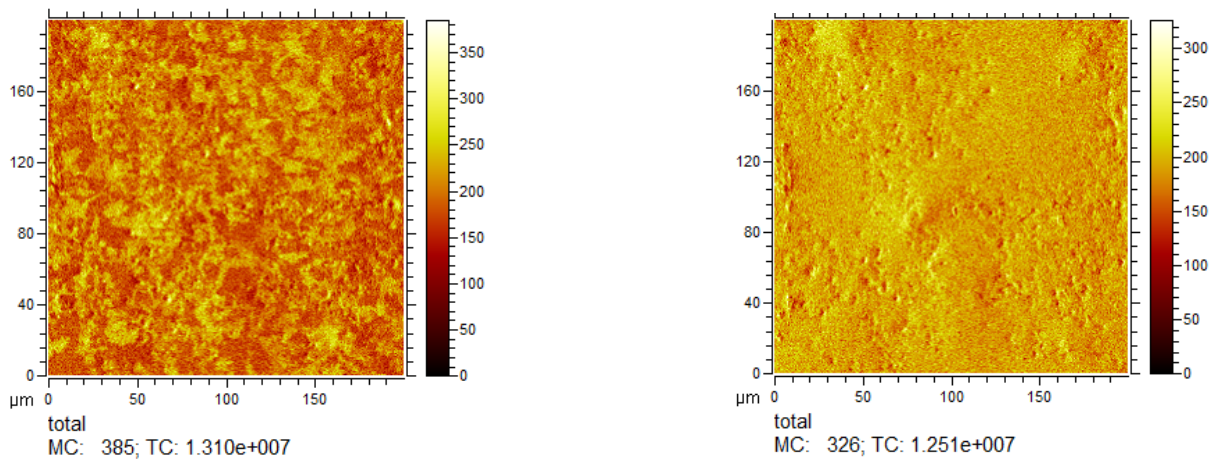


Figure 4.18: Total ion yield of A2FW before (left) and after (right) sputtering

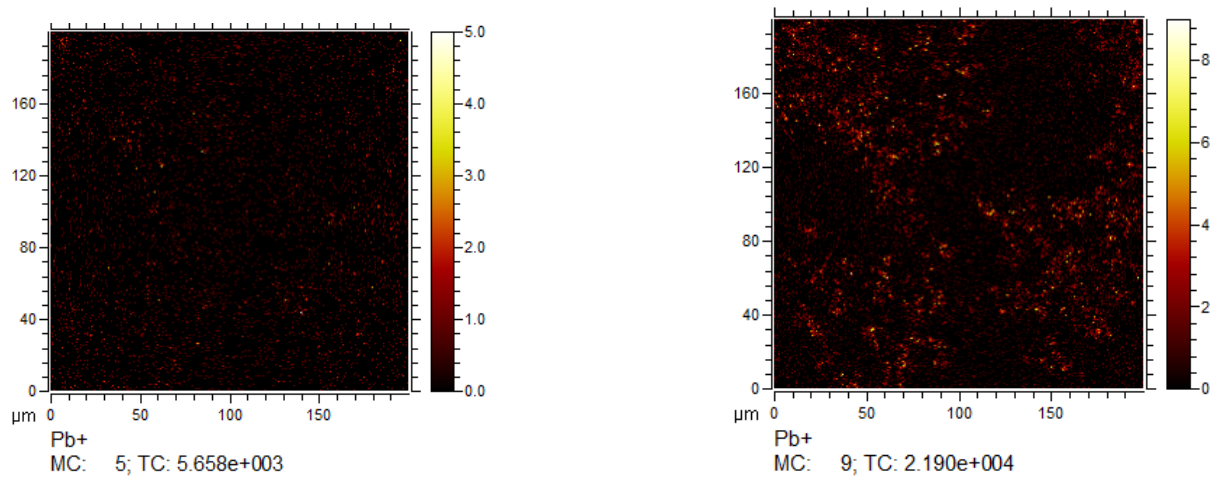


Figure 4.19: Yield of the  $Pb^+$  ion in A2FW before (left) and after (right) sputtering

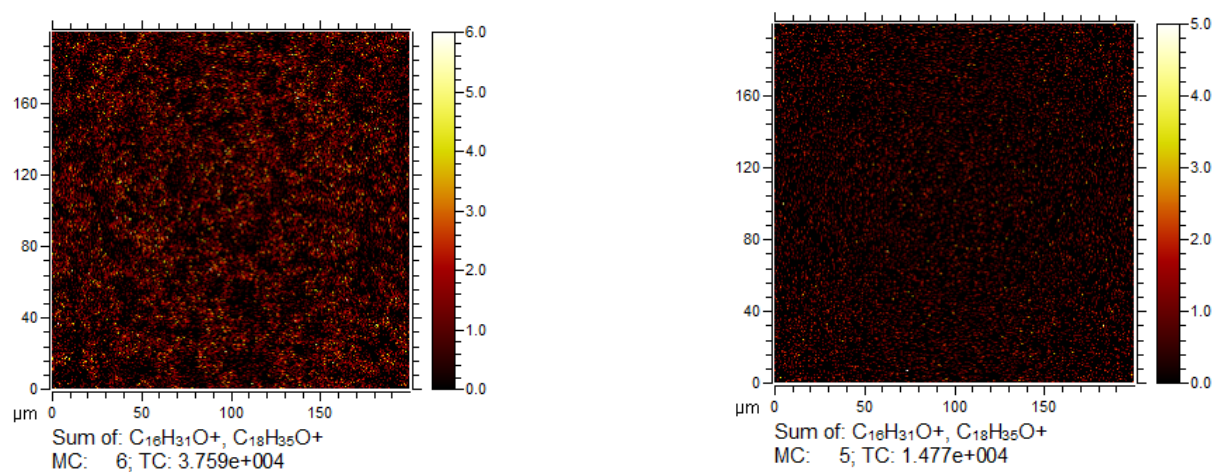


Figure 4.20: Sum of the yield of the acylium ions of palmitic ( $C_{16}H_{31}O^+$ ) and stearic ( $C_{18}H_{35}O^+$ ) acid in A2FW before (left) and after (right) sputtering

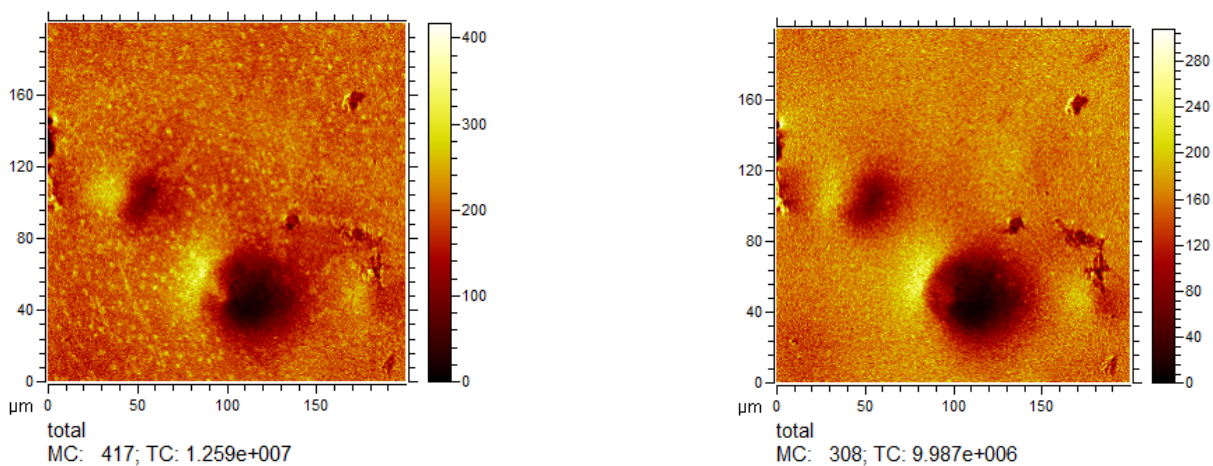


Figure 4.21: Total ion yield of A3FW before (left) and after (right) sputtering

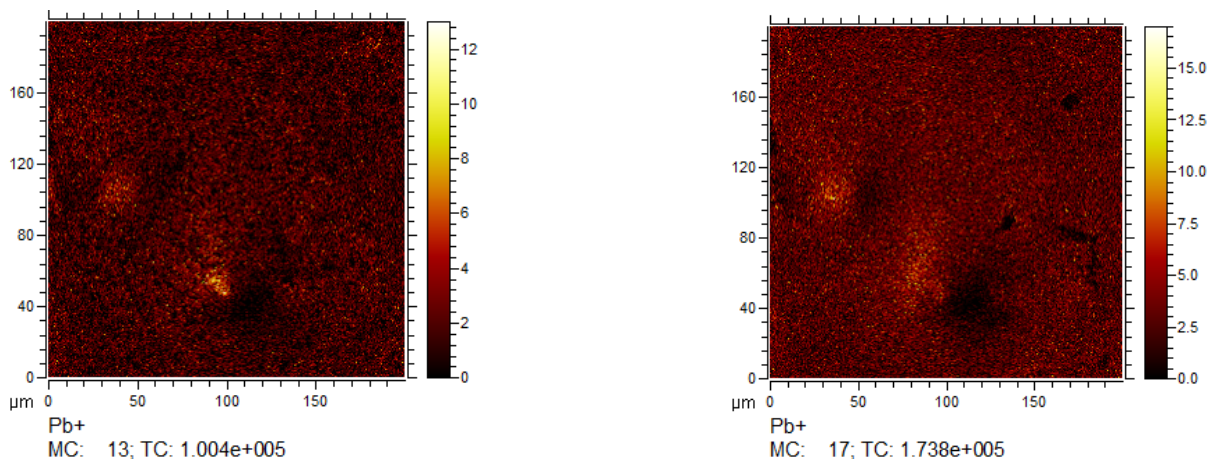


Figure 4.22: Yield of the  $Pb^+$  ion in A3FW before (left) and after (right) sputtering

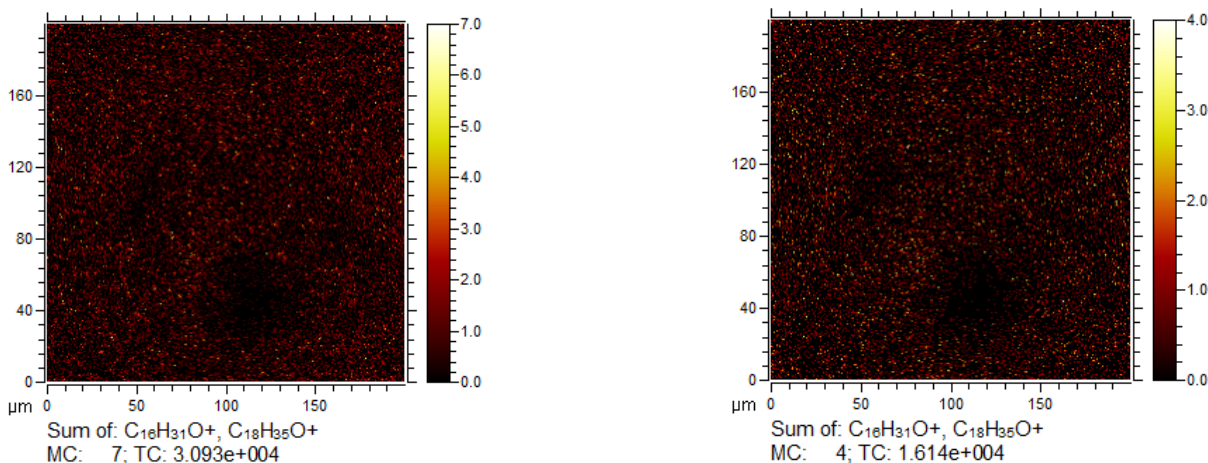


Figure 4.23: Som of the yield of the acylium ions of palmitic ( $C_{16}H_{31}O^+$ ) and stearic ( $C_{18}H_{35}O^+$ ) acid in A23W before (left) and after (right) sputtering

## 4.8 Study of linseed oil-azurite mixtures in ToF-SIMS

We will study a mixture of linseed oil (the same as before) with azurite (see Chapter 3). We will thus compare following samples:

- Sample A2 (see Chapter 2 and Section 4.2).
- Sample A3 (see Chapter 2 and Section 4.2).
- Fresh linseed oil mixed with azurite (ratio about 1:1), undergone simulated ageing treatment while being covered with aluminium foil. We will call this sample A2Az.
- Fresh linseed oil mixed with azurite (ratio about 1:1), undergone simulated ageing treatment. We will call this sample A3Az.
- Sample B2 (see Chapter 2 and Section 4.2).
- Sample B3 (see Chapter 2 and Section 4.2).
- Boiled linseed oil mixed with azurite (ratio about 1:1), undergone simulated ageing treatment while being covered with aluminium foil. We will call this sample B2Az.

- Boiled linseed oil mixed with azurite (ratio about 1:1), undergone simulated ageing treatment. We will call this sample B3Az.

#### 4.8.1 Observed positive ions

The peaks related to the linseed binder are the same as before. For the copper based ions, we only observe the following:

- copper: pure copper ions ( $Cu^+$ ) are observed for the isotopes of copper at  $m/z$  63 (main isotope) and 65,
- $Cu_2OH^+$  at  $m/z$  143, 145 and 147,
- $Cu_4O_2H$  at  $m/z$  285, 287, 289 and 290,
- $Cu_5O_3H^+$  at  $m/z$  364, 366, 368, 370 and 372.

#### 4.8.2 Observed negative ions

Once more, the linseed related negative ions are the same as in Chapter 2. We find only one clear copper ion:  $Cu^-$  at  $m/z$  63 and 65. However, there seems to be a whole series of compounds containing carbon, hydroxide, oxide and copper. For example:

- $C_2H_2OCu^-$  at  $m/z$  106 and 108,
- $C_3H_7Cu_2^-$  at  $m/z$  169 and 171,
- $C_3HOCu_2^-$  at  $m/z$  179 and 181.

### 4.9 Discussion of results of ToF-SIMS of a mixture of linseed oil and azurite

#### 4.9.1 Fatty acids: oil binder related ions

The legenda for the following figures is shown in Figure 4.24.

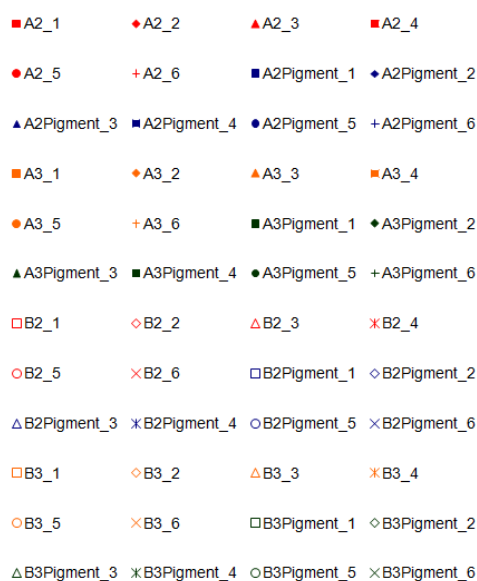


Figure 4.24: Legend used for Figures 4.25 to 4.37

## Linolenic acid

The deprotonated ion of linolenic acid (see Figure 4.25) shows in the A series the same pattern as for the lead based pigments. A stranger behaviour is visible for B2Az.

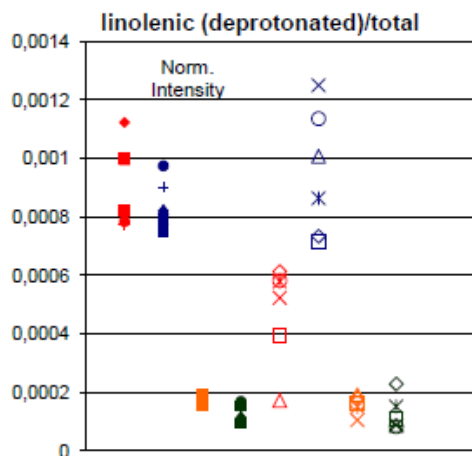


Figure 4.25: Negative deprotonated ions of linolenic acid  $C_{18}H_{29}O_2^-$  at  $m/z$  277 in the linseed oil-azurite mixture

## Linoleic and Oleic acid

The pattern for the deprotonated ion is very similar to that of linolenic acid (see Figure 4.26). The B series shows here as well a higher yield for B2Az. The acylium/protonated ion ratio (see Figure 4.27) shows the same behaviour as for the mixtures with lead pigments: the copper pigment also seems to promote hydrolysis in the A series.

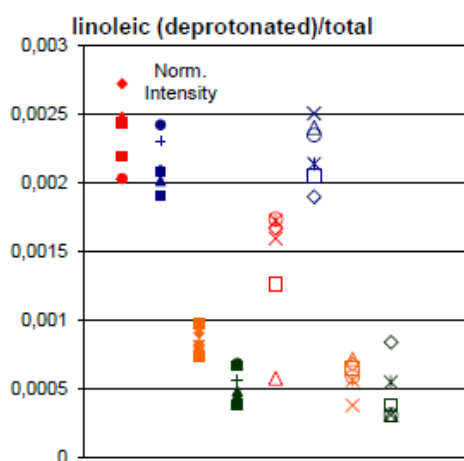


Figure 4.26: Negative deprotonated ions of linoleic acid  $C_{18}H_{31}O_2^-$  at  $m/z$  279 in the linseed oil-azurite mixture

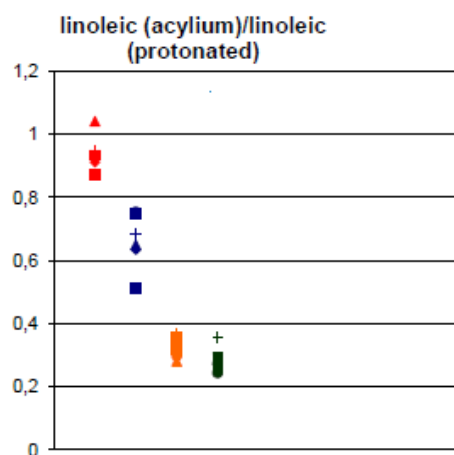


Figure 4.27: Ratio of positive acylium and protonated ions of linoleic acid in the linseed oil-azurite mixture

## Palmitic and Stearic acid

The deprotonated ion yield (see Figure 4.28) for palmitic and stearic acid shows one important difference with the lead-based mixtures: in the sample that has not been exposed to UV, there

is a (small) increase. The A3AZ sample shows a decrease with respect to A3, as in the other mixtures. This difference shows that the presence of a pigment does not always decrease the ionisation of palmitic or stearic acid.

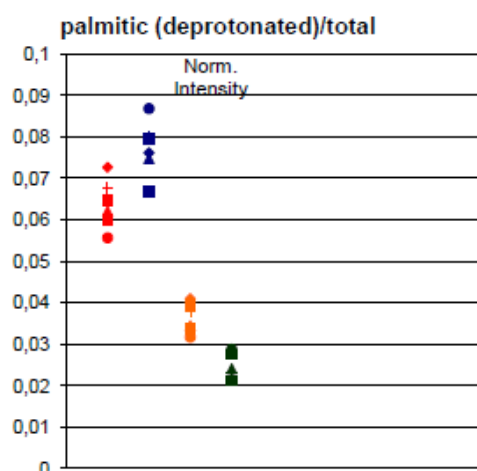


Figure 4.28: Negative deprotonated ions of palmitic acid  $C_{16}H_{31}O_2^-$  at  $m/z$  255 in the linseed oil-azurite mixture

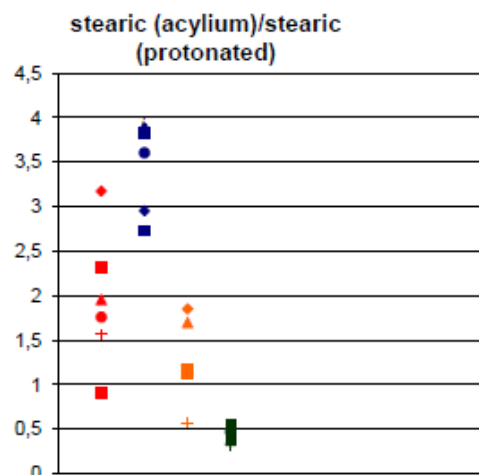


Figure 4.29: Ratio of positive acylium and protonated ions of stearic acid in the linseed oil-azurite mixture

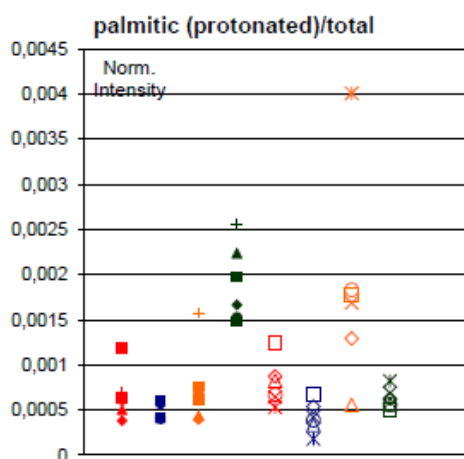


Figure 4.30: Positive protonated ions of palmitic acid  $C_{16}H_{33}O_2^+$  at  $m/z$  257 in the linseed oil-minium mixture

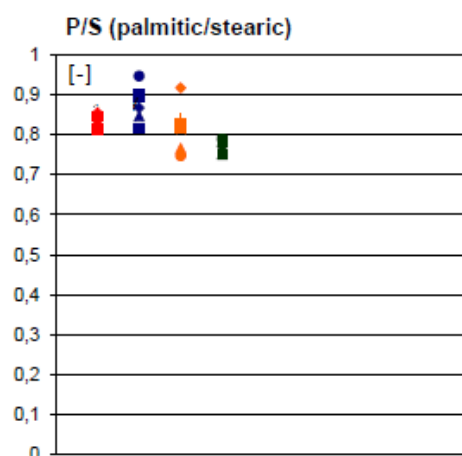


Figure 4.31: Ratio of negative deprotonated palmitic and stearic acid ions in the linseed oil-azurite mixture

### Palmitic/Stearic (P/S) ratio

The P/S ratio (see Figure 4.31) is also fairly constant, as was the case in the mixtures with lead containing pigments. The value is similar: around 0.8, which is within the range reported for linseed oil.[5]

### Suberic acid

The deprotonated ion yield of suberic acid (see Figure 4.32) shows the same rising pattern as for the mixtures with lead pigment. The presence of a pigment reinforces the effect of ageing.

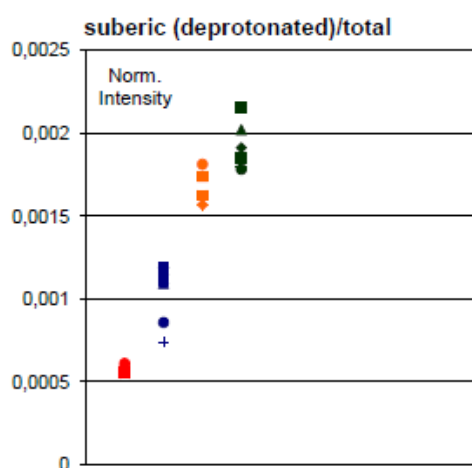


Figure 4.32: Negative deprotonated ions of suberic acid  $C_8H_{13}O_4^-$  at  $m/z$  173 in the linseed oil-azurite mixture

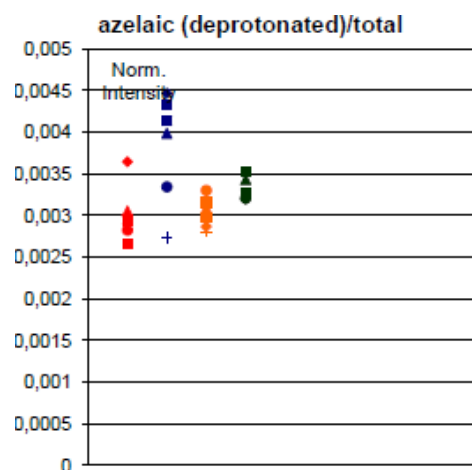


Figure 4.33: Negative deprotonated ions of azelaic acid  $C_9H_{15}O_4^-$  at  $m/z$  187 in the linseed oil-azurite mixture

### Azelaic acid

The same conclusions as for the mixtures with lead based pigments are valid: the deprotonated ion (see Figure 4.33) seems to reflect the double bond transpositions, but the pigment seems to reinforce the effect of ageing. In the positive acylium ion yield (see Figure 4.34), no effect of the bond transposition is observable. As mentioned in Chapter 2, we do not have an explanation for this divergence between the patterns of the positive and negative ions.

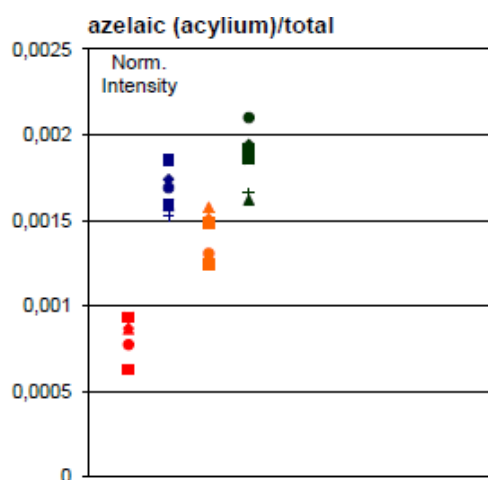


Figure 4.34: Positive acylium ions of azelaic acid  $C_9H_{15}O_3^+$  at  $m/z$  171 in the linseed oil-azurite mixture

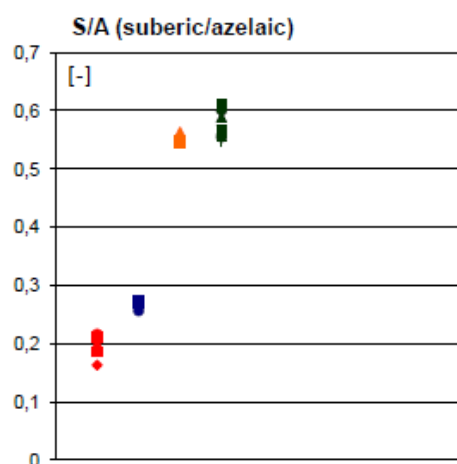


Figure 4.35: Ratio of negative deprotonated suberic and azelaic acid ions in the linseed oil-azurite mixture

### Suberic/Azelaic (S/A) ratio

The same conclusions are in place as for the mixtures with lead based pigments (see Figure 4.34): double bond transposition seems to be reinforced both by ageing and the presence of pigments.

### Oleic/Stearic (O/S) ratio

The same conclusions can be made as for the lead pigment mixtures: the presence of lead seems to enhance the effects of auto-oxidation.

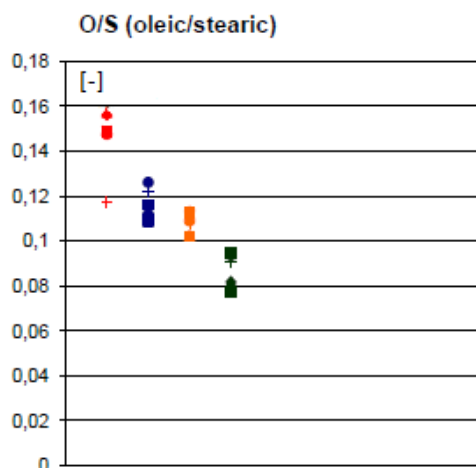


Figure 4.36: Ratio of negative deprotonated oleic and stearic acid ions in the linseed oil-azurite mixture

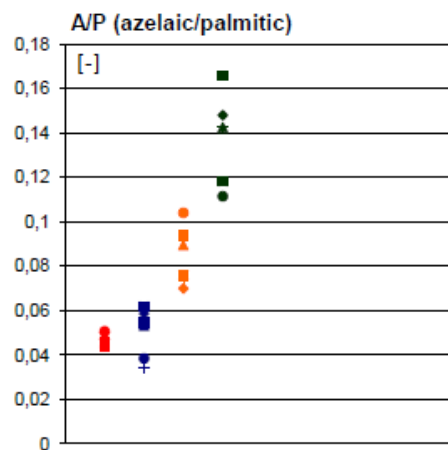


Figure 4.37: Ratio of negative deprotonated azelaic and palmitic acid ions in the linseed oil-azurite mixture

### Azelaic/Palmitic (A/P) ratio

The A/P ratio shows the same values as for the mixtures with lead based pigments and the same pattern: an increase with ageing and with the presence of pigment.

## 4.10 Conclusions

- Hydrolysis: in most cases the presence of the lead pigments seems not to influence the hydrolysis process in an important way, certainly not for palmitic and stearic acid. In the pre-treated oil, it is sometimes even observed that it inhibits the hydrolysis (slightly).
- Ionisation of palmitic and stearic fatty acids: the yield of palmitic and stearic in the negative spectrum is reduced due to the presence of lead based pigments, they tend to reinforce the trend of ageing. The only deviation is observed for the sample not exposed to UV of the azurite mixture.
- P/S ratio: the ratio seems fairly stable for all samples, around 0.8, which is in the range reported for linseed oil ([5], [25]). There is a rise until a value of 1 for B3 and, in some samples, in B3Pigment.
- Ionisation of suberic acid: the yield of suberic acid in the negative spectrum increases under the influence of ageing and of the presence of lead or copper based pigments.
- Ionisation of azelaic acid: the yield of azelaic acid in the negative spectrum shows a less big increase with ageing than we should expect and even a decrease is visible in the pre-treated series. We believe this is due to the loss of azelaic acid in favour of suberic and sebamic acid through double bond isomerisation. Both ageing and pre-treatment seem to give rise to this reaction. The presence of pigments reinforces the trends of the aged samples (increasing the deprotonated ion yield). The divergence with the positive ion yield, which shows no sign of a decrease of azelaic acid is difficult to explain. As mentioned before (Chapter 2), it might be due to a difference in preference for free or bound azelaic acid for the isomerisation reaction. A more detailed study with the use of reference samples should be done.
- S/A ratio: the double bond transposition reaction seems to be reinforced both by ageing and by the presence of pigments (lead and copper based) and their effect is much more

important than the influence of pre-treatments. Using this ratio to distinguish between different pre-treatments ([6]) is only possible in the case of A2 versus B2 (no contact with UV and no pigments present).

- A/P ratio: the expected values (higher than 1, [25]) for linseed oil for this ratio are not observed at all. However the increasing ratio seems to indicate an increasing auto-oxidation with ageing, further reinforced by the presence of lead- or copper-based pigments.
- O/S ratio: this ratio shows a decreasing pattern and seems to confirm the previous observations that the presence of lead and copper pigments reinforces the trends of ageing.
- Profiling: the profiling measurement of the mixture of linseed oil and flake white indicates that in the series that have not been exposed to UV light, the lead pigment is covered by a thicker oil film. This may be because of a higher evaporation in the samples exposed to UV or due to a migration of the pigment particles. We have also observed that the flake white pigment forms a type of grain with a diameter in the order of 10  $\mu\text{m}$ .
- lead soap: no peaks directly related to lead soaps were observed. It is of course possible that other lead related peaks are fragmentations of these soaps. Another possibility is that they are covered under an oil film. To study this subject further, it would be interesting to take a profiling measurement and to look whether lead soaps appear under the oil film.

## Chapter 5

# Study of linseed oil-turpentine mixtures

### 5.1 Introduction

Products derived from natural resins were, and still are, often used in painting. Resins are mainly composed of terpenes, organic molecules that contain linked isoprene ( $C_5H_8$ ) units. Two important products are derived from resins: turpentine oil and rosin. By distillation of the crude resin, volatile terpenes evaporate and then again condensed, forming turpentine oil, used as a thinner or a solvent. The part that rests in the still pot is the rosin, used either in varnish or added directly to the paint. This last use has three major reasons: it reduces the fluidity of the paint, it results in a more uniform surface and it enhances the paint's optical effect. Depending on the vegetal origin (mostly pine trees), different types of turpentine oil and rosin exist. For the oils we can distinguish for example Bordeaux turpentine (from maritime pine, *Pinus pinaster*), Strasbourg turpentine (or turpentine of the Vosges, from silver fir, *Abies alba* also called *Abies pectinata*), turpentine from the Sumatran pine (*Pinus merkusii*) or Venice turpentine (from *Larix decidua*, also called *Pinus larix*, the European larch). For the rosin Strasbourg turpentine, Venice turpentine or Canada turpentine (better known under its name 'Canada balsam', from the balsam fir *Abies balsamea*) are often used. Ancient masters are known to use Venice turpentine oil and rosin.[19][20][38][39]

The purpose of this small chapter is not to study in depth the SIMS analysis of turpentine samples, nor to discuss the influence of ageing or the presence of pigments on the yield for its characteristic ions. The ageing of turpentine is complex and exceeds the limits of this thesis. The goal of this chapter is twofold: we want to list the ions that make it possible to recognise a resinous layer in ToF-SIMS and secondly we want to get a quick idea of the influence of turpentine on the ionisation of the fatty acids.

### 5.2 Chemical composition

In this chapter we will study a sample of a mixture of refined linseed oil with Venice turpentine (rosin) (ratio 1:1) made in the laboratory of KIK-IRPA in 2005. Rosin is known to consist mainly of so-called resin acids, acids derived from terpene through partial oxidation. Two main types exist: abietic type acid (abietic acid, neoabietic acid, palustric acid, levopimaric acid, dehydroabietic acid and oxo-dehydroabietic acid) and the pimaric type (pimaric acid, sandaracopimaric acid and isopimaric acid). The problem for the study of these components in ToF-SIMS is that they are all isomers (with formula  $C_{20}H_{30}O_2$  or  $C_{19}H_{29}COOH$ ), except for dehydroabietic acid ( $C_{20}H_{28}O_2$ ) and oxo-dehydroabietic acid ( $C_{21}H_{28}O_3$ ). Turpentine oil is characterised by volatile monoterpenes such as pinene, cymene or terpineol.[38][25]

Because of the mixture with linseed oil, we expect to find in the sample also diglycerides, monoglycerides and free fatty acids (such as palmitic, stearic, linolenic, linoleic, oleic, azelaic or suberic acids).

## 5.3 Study of oil-turpentine mixture with ToF-SIMS

### 5.3.1 Observed positive ions

The turpentine components observed in the positive ion spectra are derived from resin acids. As was the case with the fatty acids, these acids appear in the positive spectrum as protonated ions ( $[RCOOH + H]^+$ ) and acylium ions ( $[RCOOH - OH]^-$ ). The turpentine components are less visible in the positive spectrum than in the negative spectrum. As the resin acids are mostly isomers, we cannot give more information on which acids they are exactly or to what type (abietic or pimaric) acid they belong. However, we find also dehydrated and oxidised forms:

- protonated ions of dehydro-resin acid (probably dehydroabietic acid):  $C_{20}H_{29}O_2^+$  at  $m/z$  301,
- protonated ions of resin acid (abietic or pimaric type):  $C_{20}H_{31}O_2^+$  at  $m/z$  303,
- acylium and protonated ions of oxidised dehydro-resin acid (probably oxo-dehydroabietic acid):  $C_{20}H_{25}O_2^+$  and  $C_{20}H_{27}O_3^+$  at  $m/z$  297 and 315,
- acylium and protonated ions of oxidised resin acid (abietic or pimaric type):  $C_{20}H_{27}O_2^+$  and  $C_{20}H_{29}O_3^+$  at  $m/z$  299 and 317.

### 5.3.2 Observed negative ions

#### Turpentine components

In the negative ion spectrum, a number of peaks are observed that are related to the resin acids. As before these are mostly isomers but we also find oxidised and dehydrated forms of the resin acids. As with the fatty acids in Chapter 2, we observe the resin acids and their derivations in the negative ion spectrum as deprotonated ions ( $[RCOOH - H]^-$ ):

- dehydro-resin acid (probably dehydroabietic acid):  $C_{20}H_{27}O_2^-$  at  $m/z$  299,
- resin acid (abietic or pimaric type):  $C_{20}H_{29}O_2^-$  at  $m/z$  301,
- oxidised dehydro-resin acid (probably oxo-dehydroabietic acid):  $C_{20}H_{25}O_3^-$  at  $m/z$  313,
- oxidised resin acid (abietic or pimaric type):  $C_{20}H_{27}O_3^-$  at  $m/z$  315.

We also observe some peaks, the provenance of which could not be established. Given the fact that they do not appear in linseed samples and their resemblance in form to the above described peaks, we suggest that they are related to turpentine. These peaks are:

- $C_{20}H_{25}O_4^-$  (suggested by SurfaceLab analysis software) at  $m/z$  329,
- $C_{20}H_{29}O_4^-$  (suggested by SurfaceLab analysis software) at  $m/z$  333,
- $C_{24}H_{29}O_2^-$  (suggested by SurfaceLab analysis software) at  $m/z$  349.

## Linseed oil components

We expect to see the known negative components of fatty acids in their deprotonated form. We observe mainly the following peaks:

- deprotonated ions of dicarboxylic azelaic acid at  $m/z$  187,
- deprotonated ions of saturated palmitic and stearic acids at  $m/z$  255 283,
- deprotonated ions of unsaturated palmitoleic and oleic acids at  $m/z$  253, and 281.

## 5.4 Observations

We will not study the influence of the ageing or the presence of pigments on the yields for the ions that are related to turpentine. We will quickly describe the influence of the presence of Venice turpentine in a mixture with linseed oil on the ionisation of the deprotonated ions of palmitic, stearic and azelaic acid:

- ionisation of palmitic acid in the sample that has been aged without exposure to UV is reduced when venice turpentine is present. In the fully aged sample, the ion yield is even lower.
- ionisation of stearic acid: the same observation can be done for stearic acid: the ion yield decreases with ageing and with the presence of venice turpentine.
- ionisation of azelaic acid: the trend is less clear: azelaic deprotonated yield rises with the presence of Venice turpentine in the samples that have been aged without exposure to UV, but decreases for the series that is fully aged.
- Palmitic/Stearic ratio: The value for the P/S ratio changes significantly: from about 0.5 (aged without exposure to UV) and 0.8 (aged with exposure to UV) to 1.0 (pre-heated oil, aged without exposure to UV) and even 2.0 (pre-heated oil, aged with exposure to UV). The addition of Turpentine and the pre-treatment do change the P/S value significantly. Still, the value just remains within the limits (lower than 2.0) expected for a linseed oil sample.

## Chapter 6

# Conclusion

In this thesis we have undertaken a comprehensive study of linseed oil-pigment systems with Time of Flight-Secondary Mass Spectrometry. This project finds its context in a practical problem that is frequently encountered during the ToF-SIMS measurement of real paint sections of the *Ghent Altarpiece* (1432) by Hubert and Jan Van Eyck: a very important loss of fatty acid signal is observed in these samples. This calls into question the suitability of ToF-SIMS for the identification of the nature of a certain paint layer. The main goal is thus to study the influence of different factors on the ionisation of fatty acids in ToF-SIMS. The studied factors are: pre-treatment with heat and oxygen, pre-treatment by heating with oxygen in the presence of lead driers (*'cuite à la litharge'*), pre-treatment by the addition of driers (for this sample, originating from the laboratory archives of the KIK-IRPA it is unknown whether the sample has been heated during the addition of the driers), ageing and the presence of the pigments in the mixture.

For the mixtures of oil and pigment, four types of oil binder were used: a fresh linseed oil (called A), a linseed oil that has been heated as a pre-treatment (called B), a mixture of fresh linseed oil with a Venice turpentine-linseed oil mix (called AT) and a mixture of heated linseed oil with a Venice turpentine-linseed oil mix (called BT). These samples have been mixed with different pigments, four lead containing pigments (flake white (FW), lead carbonate (LC), minium (MIN) and lead chloride (LCl)) and one copper containing pigment (azurite (AZ)). Those pigments were chosen because they are often found in historical paint samples and because lead and copper based pigments are known to react strongly with the oleaginous binder. These mixtures have been dried in the sunlight and aged in a SUNSET CPS+. A part of the samples was covered by aluminium foil during the ageing, which prevents its exposure to UV light.

The analysis of the samples was based on a group of important fatty acid peaks: the acylium (+) and deprotonated (-) peaks of linolenic acid, the acylium (+), protonated (+) and deprotonated (-) peaks of linoleic and oleic acids, the same peaks for palmitic and stearic acid, and the deprotonated (-) and acylium ion for suberic and azelaic. Furthermore we used a number of ratios derived from these peaks: palmitic/stearic ratio, suberic/azelaic ratio, azelaic/palmitic ratio and oleic/stearic ratio. We have also made use of the ratio of the acylium ion with respect to the protonated ion for a specific fatty acid. As free fatty acids give rise to both a protonated and an acylium ion in the positive spectrum, but bound fatty acids only to an acylium ion, we believe that this ratio can be used to indicate the effect of the hydrolysis in a sample.

For all these ions the influence of ageing, pre-treatment and the presence of pigments was studied. We have concluded that in most cases pre-treatment or the presence of lead and copper pigments reinforces the effect of ageing. This effect can be an increase of the ion yield (such as for azelaic and suberic) or a decrease (such as for palmitic and stearic acid). The P/S ratio seems

surprisingly resistant to ageing, the presence of pigments and pre-treatment. The double bond transposition reaction seems to be reinforced both by ageing and by the presence of pigments (lead and copper based) and their effect is much more important than the influence of pre-treatments.

We have to be careful, because for each of these general trends there are exceptions. We therefore hope that this work, which was mostly one of observation and information gathering, can be used as a modest database on the influence of ageing, pre-treatment and the presence of pigments on the ion yield of the most important fatty acids.

As a final illustration, the results for the negative deprotonated ions for the four most important fatty acid ions (the deprotonated ions of palmitic, stearic, suberic and azelaic acids) are shown together in Figures 6.1, 6.2, 6.3 and 6.4.

The deprotonated ion yield for palmitic and stearic fatty acid (Figure 6.1 and Figure 6.2) show a very similar behaviour throughout all samples. The first and foremost conclusion is that all samples that have been aged show a loss in ionisation with respect to the samples that have been aged without being exposed to UV light. This seems in accordance with the observation of fatty acid signal loss in real historic painting samples. Samples that have been heated as pre-treatment have the tendency to show lower ionisation. In general, the influence of the pre-treatment is parallel with that of ageing. There are four exceptions noted: in the mixtures with lead carbonate pigment the pre-treated sample shows a higher yield. The same is true for the aged mixtures with minium and for the samples of mixtures with Venice turpentine that have not been exposed to UV light and have not been mixed with a pigment. In the mixtures with linseed oil that has undergone no previous treatment, the presence of a lead pigment has the tendency to diminish the yield (with some exceptions). This is in general also the case for the pre-treated variants, but there seem to be more exceptions. The presence of Venice turpentine also diminishes the yield, with the one exception that the yield for samples of turpentine-pre-treated oil mixture that have not been exposed to UV is higher than for the pre-treated oil alone. In most cases, ageing, heating pre-treatment and the presence of pigments or Venice turpentine all reduce the yield for the deprotonated ions of palmitic and stearic acids. The oils that have been pre-treated with lead driers, however, show higher yields. The very low yield for non-aged 1 (both the fresh sample, A1, and the one that has undergone heating pre-treatment, B1) is difficult to explain. Questions have risen whether the drying process that has been applied for this sample has not had a deeper (auto-oxidating) effect than we anticipated.

## 6.1 Future Prospects

It is clear that this study is only a starting point. First of all, a whole number of samples has not been unstudied. Secondly, many questions remains unanswered and hypotheses were made that could not be verified. In this part we will try to formulate some guidelines that can lead future research.

This work has primarily been one of observation. The first, logical, step would be to continue those observations and to analyse, in the same way as before, the remaining samples. Their examination and the confrontation of the results with our findings can be a first step in refining the conclusions. It would be interesting to see, for example, how organic pigments (such as madder lake) influence the ionisation of fatty acids or to see the difference between the linseed oils used and the mixture with stand oil. Later on, new samples can be added. Because we did not know the exact treatment of the samples of linseed oil with lead based driers, not many significant

---

$${}^1\sigma = \sqrt{\frac{\sum_i (x_i - \mu)^2}{n-1}}$$
 with  $n$  the sample size and  $\mu$  the mean

	A2Pigment		A3Pigment		B2Pigment		B3Pigment	
	$\mu$	$\sigma$	$\mu$	$\sigma$	$\mu$	$\sigma$	$\mu$	$\sigma$
<b>no pigment</b>	6.38	0.60	3.63	0.36	4.37	1.54	2.44	0.74
<b>Flake white</b>	5.01	1.37	2.33	0.40	4.62	0.72	2.25	0.53
<b>Lead carbonate</b>	3.40	0.64	2.14	0.21	6.92	1.27	2.80	0.18
<b>Lead chloride</b>	5.88	1.12	2.12	0.61	5.73	0.39	1.94	0.18
<b>Minium</b>	5.48	0.92	1.87	0.16	4.81	0.52	2.43	0.27
<b>Azurite</b>	7.74	0.66	2.44	0.31				

Table 6.1: Intensity relative to the total number of counts (in %) of the peak of the negative deprotonated ion of palmitic acid ( $C_{16}H_{31}O_2^-$  at  $m/z$  255): the mean value ( $\mu$ ) and the standard deviation ( $\sigma$ ) of the different measurements is presented for each sample

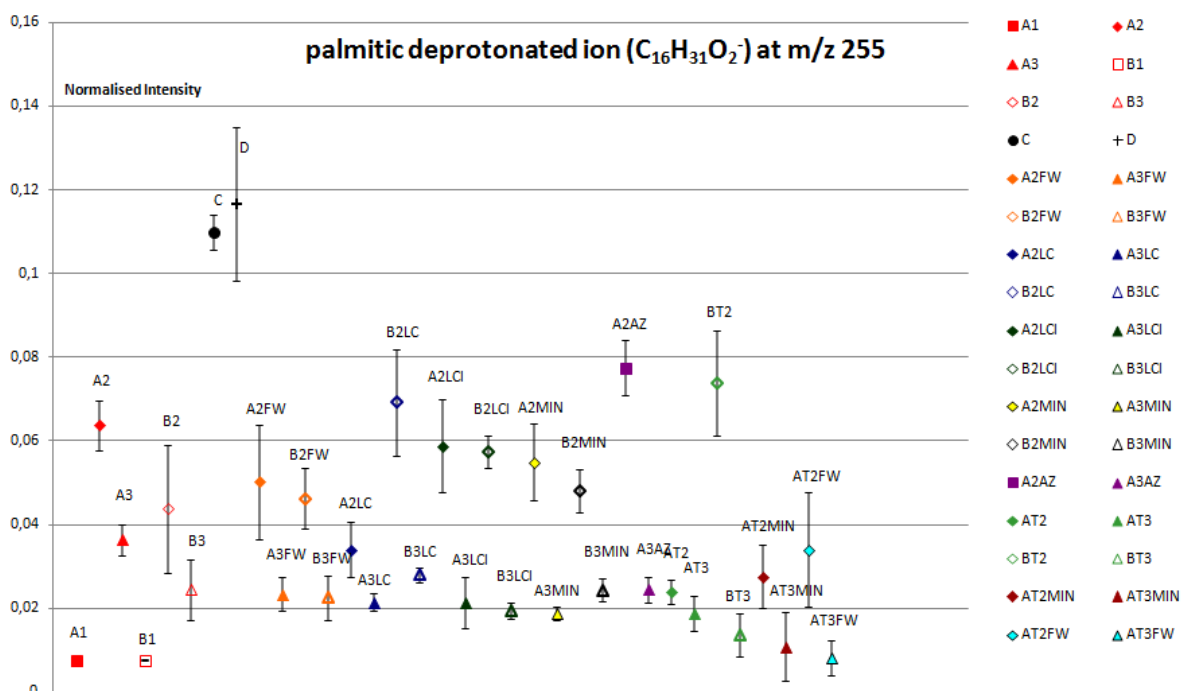


Figure 6.1: Intensity relative to the total number of counts of the peak of the negative deprotonated ion of palmitic acid ( $C_{16}H_{31}O_2^-$  at  $m/z$  255). The mean value of the different measurements is presented for each sample and the standard deviation is shown with the error bars. (A1: Fresh linseed oil; A2: Linseed oil aged without exposure to UV; A3 Linseed oil aged with exposure to UV; B1, B2 and B3 the equivalent samples for a pre-treated oil; and AT (BT) the mixtures of (pre-heated) linseed oil with Venice turpentine; FW: Flake White; LC: Lead Carbonate; LCl: Lead Chloride; MIN: Minium; AZ: Azurite)



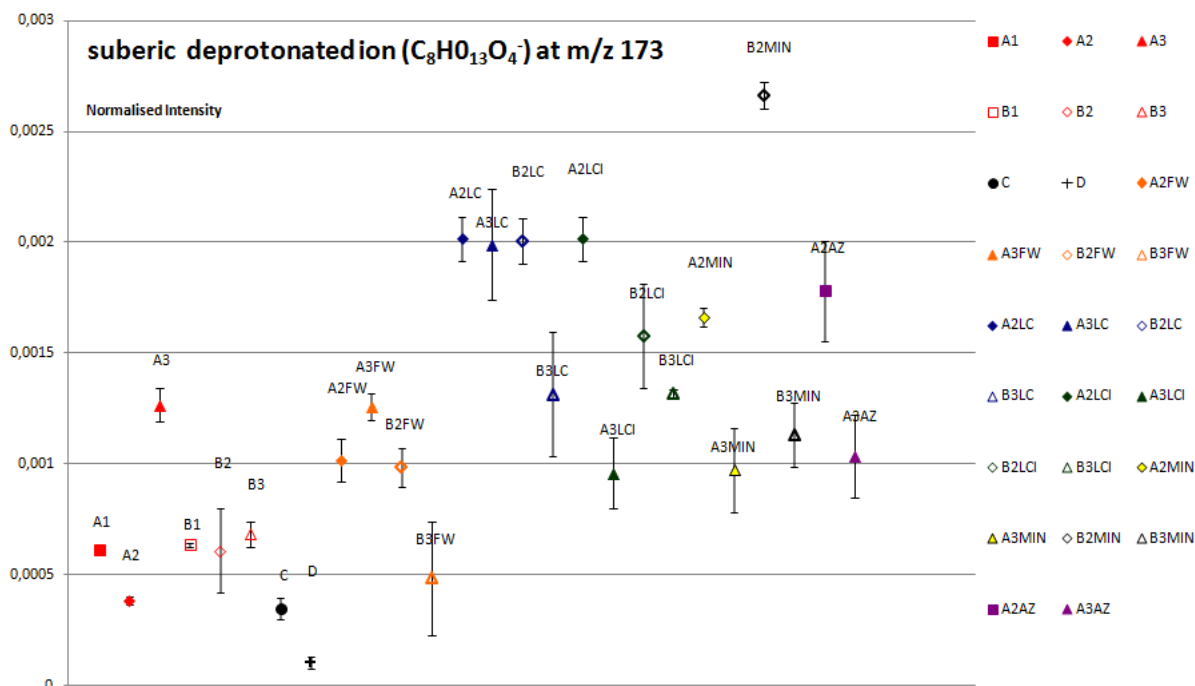


Figure 6.3: Intensity relative to the total number of counts of the peak of the negative deprotonated ion of suberic acid ( $C_8H_{13}O_4^-$  at  $m/z$  173). The mean value of the different measurements is presented for each sample and the standard deviation is shown with the error bars

	A2Pigment		A3Pigment		B2Pigment		B3Pigment	
	$\mu$	$\sigma$	$\mu$	$\sigma$	$\mu$	$\sigma$	$\mu$	$\sigma$
<b>no pigment</b>	0.30	0.03	0.30	0.02	0.31	0.05	0.18	0.02
<b>Flake white</b>	0.33	0.02	0.31	0.02	0.35	0.02	0.14	0.07
<b>Lead carbonate</b>	0.43	0.05	0.32	0.02	0.36	0.03	0.33	0.02
<b>Lead chloride</b>	0.35	0.03	0.31	0.04	0.47	0.06	0.35	0.01
<b>Minium</b>	0.33	0.04	0.38	0.01	0.45	0.05	0.32	0.04
<b>Azurite</b>	0.38	0.07	0.33	0.01				

Table 6.4: Intensity relative to the total number of counts (in %) of the peak of the negative deprotonated ion of azelaic acid ( $C_9H_{15}O_4^-$  at  $m/z$  173): the mean value ( $\mu$ ) and the standard deviation ( $\sigma$ ) of the different measurements is presented for each sample

conclusions could be drawn. Another analysis, of samples of which we do the pre-treatment ourselves and follow also the ageing process from close by, could deliver more information. The study of samples with proteinaceous binders can be very revealing, as such binders were commonly used.

A second possibility is to try to gain a better understanding of the processes we witnessed. We have observed the influence of pre-treatment, the presence of pigments and ageing on the ionisation of oil paint fatty acids, but the mechanisms that lie behind these observations are certainly not fully understood. Discovering these mechanisms is beyond doubt an awesome task. It would require to focus the attention on one very specific effect and its in-depth investigation. As we have seen that the effect of all pigments is very comparable, such a future study could single out one pigment and concentrate on its effect.

A clearer picture of how exactly the named factors influence the ionisation of fatty acids can only be obtained when all other factors that can possibly influence the results are excluded and therefore the experiments must be carried out more rigorously. It is for example common in other studies to take samples of linseed oil that have been pressed from a same lot of linseeds. Attention should be paid to the storage of the samples, this should be a dark and dry place and contact between samples should be avoided. Samples should be handled using latex gloves. In that way, the contamination (for example from PDMS) that was quite present in some of our samples could be (partly) avoided. It is also reported in literature that samples are sometimes cleaned with hexane before measurement([5]), but it should be verified that this procedure does not influence the measurement. During this work, some questions have arisen about the procedure used to dry the oleaginous samples before ToF-SIMS measurement. It seemed that this drying (in an oven at about 35 °C) had a non negligible influence on the sample (see the discussion of samples A1 and B1).

In order to better understand the transformation of the sample with ageing, we could investigate samples at various points in time during this ageing process. We believe that covering samples with aluminium foil and making a comparison between the samples that have been exposed to UV and those who have not could remain an interesting part of such an analysis. Keeping different back-up versions of the same sample can also be of help when certain measurements are not as expected. We believe that in such an attempt it could be very revealing to complement the ToF-SIMS measurements with the application of other techniques, such as GC/MS. This would allow to verify some of the hypotheses made.

A further ToF-SIMS study could be improved in three ways. Firstly, reference standards should be studied in order to get more certainty about the attribution of the peaks in the spectra. This would allow to better discern the fragmentation peaks of different molecules and also to distinguish between the contributions of free or bound fatty acids.

Secondly, we must remember that ToF-SIMS is a surface sensitive technique. A more systematic measurement of depth profiles would allow to compare results for the surface with those of the bulk and to follow the eventual migration of species.

Thirdly, the succesful application of multivariate analysis methods (PCA) in earlier ToF-SIMS studies of paint samples (for example [40]) can be an inspiration. This would help to structure the enormous amount of information stored in a SIMS spectrum and to find the important trends of the data set, which could reveal new information.

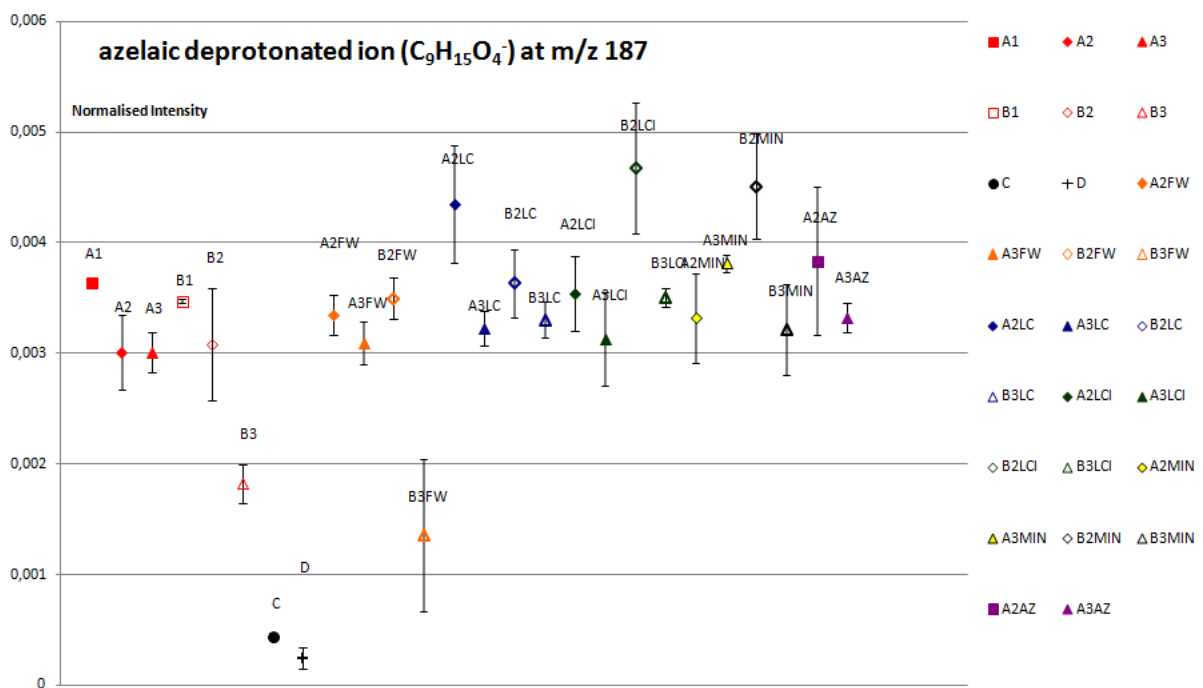


Figure 6.4: Intensity relative to the total number of counts of the peak of the negative deprotonated ion of azelaic acid ( $C_9H_{15}O_4^-$  at  $m/z$  173). The mean value of the different measurements is presented for each sample and the standard deviation is shown with the error bars

# Appendix A

## Results of ToF-SIMS measurements of Linseed oil

### A.1 Discussion of observations

For the discussion of the results for azelaic, suberic, palmitic, stearic, linolenic, linoleic and oleic fatty acid ions: see Chapter 2

#### A.1.1 Aliphatic chain fragments of the type $C_2H_3(CH_2)_xCOO^-$

These aliphatic chain fragments (Figures A.37 to A.43) are results of the auto-oxidation and fragmentation (hydrolysis) processes.[5] Fragments  $C_2H_3(CH_2)_xCOO^-$  with  $x$  ranging from 6 to 12 show roughly the same pattern (see Figures A.42 and A.43). This is not the behaviour we would expect from a auto-oxidation product, samples A2 and B2, having undergone the least auto-oxidation being the highest. The very low yield of A1 and B1 is also remarkable, but could be attributed to the weak hydrolysis in those samples. The B series seem to offer almost the same appearance. The pattern of  $C_5H_7O_2$  looks more promising, but the other fragments show very different patterns. In general, it is difficult to explain the patterns of these aliphatic chain fragments and their role as products of auto-oxidation and hydrolysis processes is not obvious.

#### A.1.2 Decanoic acid

Decanoic acid is also mentioned in literature as a product of auto-oxidation and degradation.[5] This does not seem to be reflected in the deprotonated ion yield showing A2 and B2 having a higher yield than A3 and B3, but lower than A1 and B1. The role of decanoic acid as such a oxidation and degradation product is therefore not obvious.

#### A.1.3 Monoglycerides with palmitic or stearic acid

Monoglycerides are only observed through the acylium ions. The yield for monoglycerides containing palmitic acid and stearic acid (Figures A.15 and A.18) is higher than that of the acylium ion yield of the respective fatty acids (Figures A.5 and A.6). The pattern is however very similar. The outlook of these monoglyceride ion yields thus seems to be attributable to the behaviour of the fatty acid it consists of. We have to be careful, as the spread on the measurements is also very considerable. We remark that the acylium ion is practically absent for A1 and B1, as was the case for the acylium ion of palmitic and stearic acid.

#### **A.1.4 Monoglyceride with linoleic acid**

Just as for the monoglycerides of palmitic and stearic acid, the yield of acylium ions of monoglyceride containing linoleic acid (Figure A.16) follows the pattern of the acylium ion yield of linoleic acid and the behaviour of the monoglyceride seems to be attributable to the behaviour of the fatty acid it consists of. The yields of both ions are on about the same level.

#### **Monoglyceride with oleic acid**

In contrast to the monoglycerides discussed above, the yield of acylium ions of monoglyceride with oleic acid (Figure A.17) does not seem to be attributable to solely the behaviour of the fatty acid it consists of. Once more, the spread on the results is large and the differences are small, but it appears that the following pattern is discernible: A2 has a higher yield than A1, which is higher than A3. For the B series the same pattern holds, but at lower amounts of yield. The lower yield for A3 (B3) than for A1 (B1) can be explained by the further oxidation of oleic acid and to hydrolysis. The further hydrolysis in A2 (B2) with respect to A1 (B1), as illustrated by the acylium/protonated ratio, does not seem to have its effect on this monoglyceride as A2 (B2) are at a higher yield than A1 (B1).

#### **A.1.5 Monoglyceride with azelaic acid**

Once more, the behaviour of the acylium ion yield of monoglyceride containing azelaic acid (Figure A.14) follows the pattern of the (acylium ion of) the fatty acid it contains, in this case explained by azelaic acid's role as a product of the auto-oxidation and hydrolysis processes. The yield is however higher for the acylium ion of azelaic acid than for its monoglyceride.

#### **A.1.6 Diglycerides with palmitic and stearic acids**

Diglycerides with twice palmitic acid (Figure A.21), with twice stearic acid (Figure A.30) and with palmitic and stearic acid (Figure A.24), all seem to follow the same pattern as the fatty acids they contain and their monoglycerides. The yield is on a level comparable to or slightly higher than the acylium ion yields of palmitic and stearic acids but lower than those of the respective monoglycerides of those fatty acids.

#### **A.1.7 Diglycerides with palmitic or stearic acid and oleic acid**

Diglyceride with palmitic and oleic acid and diglyceride with stearic and oleic acid show comparable patterns for their acylium ion yield, much alike to that of the monoglyceride with oleic acid, but quite different from the oleic acid acylium ion yield. The differences between the samples could be explained, as was the case for the monoglyceride, by the hydrolysis effect. We have to remark that the spread is large, even dramatically so for sample B2. The yield is in general about half that of the monoglyceride with oleic acid and at about the same level as oleic acid's acylium ion yield.

#### **A.1.8 Diglyceride with palmitic and linoleic acid**

The pattern of the acylium ion yield of diglyceride with palmitic and linoleic acid (A.22) resembles that of the acylium ion yield of linoleic acid although the difference between the yields of A1 and A2 is bigger and the difference between A2 and A3 has grown; the same holds for the B series. This may be under the influence of the palmitic acid, which shows an extremely low acylium ion yield for A1 (B1) and only a small difference between A2 and A3 (B2 and B3). This seems to suggest that the behaviour of this diglyceride is characterised by an intermediate between the patterns of the two fatty acids it contains. The spread on measurements of A2 and B2 is large, however. The yield is on about the same level as that of the acylium ion of linoleic acid.

### **A.1.9 Diglyceride with stearic and linolenic or linoleic acid**

The interpretation of the acylium ion yield of the diglycerides with stearic on the one hand and linolenic or linoleic acid on the other (Figures A.27 and A.28) is more difficult. The diglyceride of stearic and linoleic acid seems to follow roughly the pattern of the acylium ion of linoleic acid. The difference between A2 and A3 (and between B2 and B3) can be explained by further auto-oxidation of linoleic acid and hydrolysis in A3 (B3). A difference, although a small one, between those patterns is the fact that A1 has a higher yield than A2. The reason why is not clear, certainly not because sample A1 shows an extremely low acylium ion yield of stearic acid. This effect is even more marked in the acylium ion yield of the stearic-linolenic acids diglyceride. We would expect a much lower yield for A1 and B1 as we saw before that the auto-oxidation process had gone further than in A2 (or B2). The difference between A1 and B1 can be explained by the further auto-oxidation due to the pre-treatment.

### **A.1.10 Diglycerides with palmitic or stearic acid and suberic, azelaic or sebacic acid**

The acylium ion yield for diglycerides with palmitic acid on the one hand and suberic, azelaic or sebacic acid on the other (Figures A.19, A.20 and A.25) and for diglycerides with stearic acid on the one hand and suberic or azelaic acid on the other (Figures A.25 and A.20) all show a comparable pattern that seems in the first place to be defined by the acylium ions of the dicarboxylic fatty acids (suberic, azelaic acid) they contain. The mass of monoglyceride with palmitic and sebacic is the same as that with stearic and suberic acid and does not follow the sebacic acid acylium pattern (Figure A.4), but rather that of the suberic acid acylium ion. The yield is in the same order as that of the acylium ions of sebacic acid and of monoglyceride with azelaic acid, but is lower than that of acylium ions of suberic and azelaic acid.

### **A.1.11 Diglyceride with linolenic acid**

We expect diglyceride with twice linolenic acid to disappear rapidly with auto-oxidation and hydrolysis. This is partly visible in Figure A.31: A2 and B2 show a higher yield than the other samples. It is unclear why A3 and B3 show higher yield than A1 and B1. The B series shows no important differences with their A series counterparts. In any case, the yield is strikingly low, which might show the small survival possibilities for linolenic acid.

## **A.2 Results of ToF-SIMS measurements**

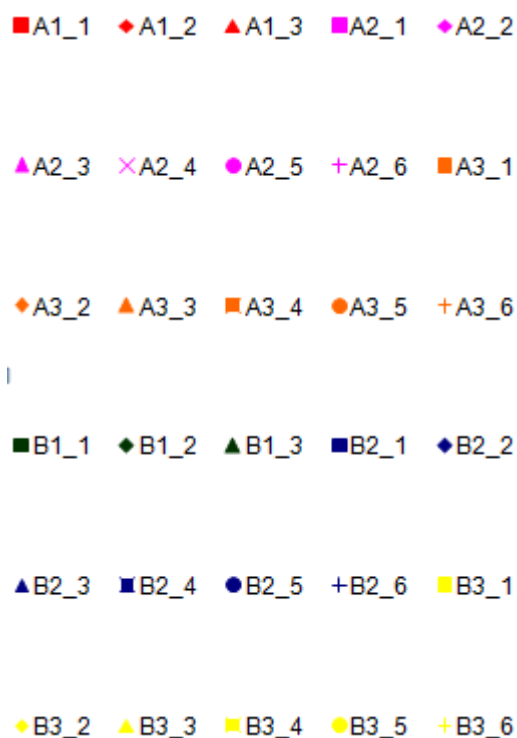


Figure A.1: Legend used for Figures G.1 to A.56

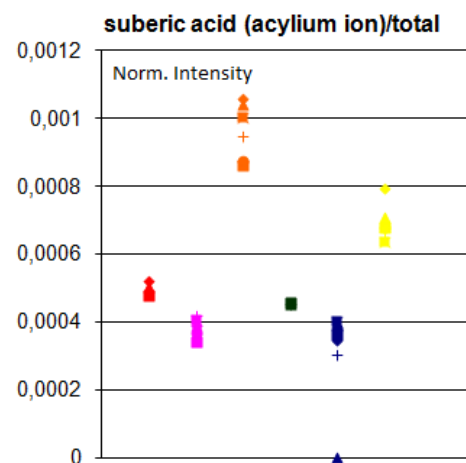


Figure A.2: Positive acylium ions of suberic acid,  $C_8H_{13}O_3^+$  at  $m/z$  157 in linseed oil

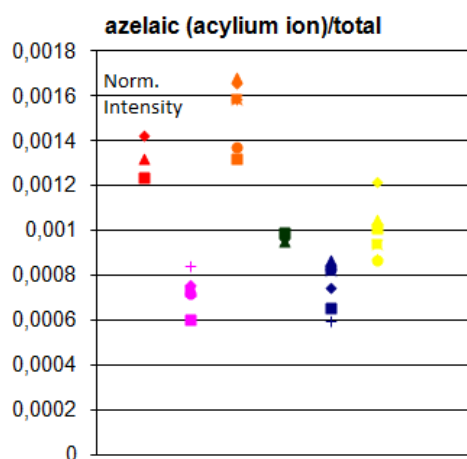


Figure A.3: Positive acylium ions of azelaic acid  $C_9H_{15}O_3^+$  at  $m/z$  171 in linseed oil

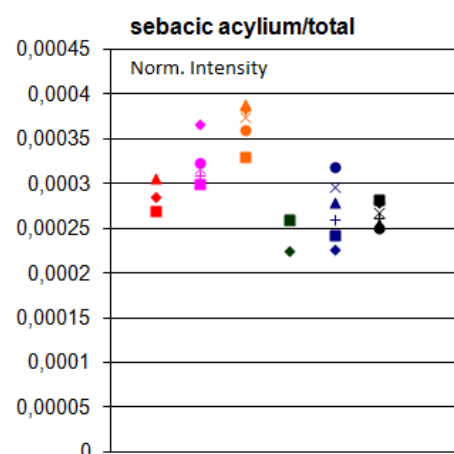


Figure A.4: Positive acylium ions of sebacic acid  $C_{10}H_{17}O_3^+$  at  $m/z$  185 in linseed oil

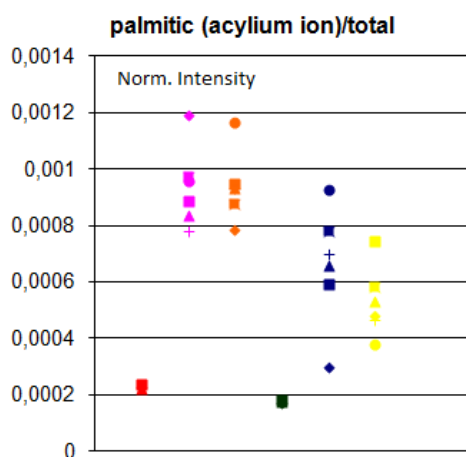


Figure A.5: Positive acylium ions of palmitic acid  $C_{16}H_{31}O^+$  at  $m/z$  239 in linseed oil

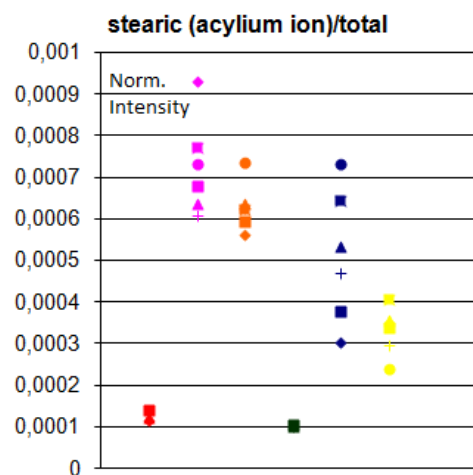


Figure A.6: Positive acylium ions of stearic acid  $C_{18}H_{35}O^+$  at  $m/z$  267 in linseed oil

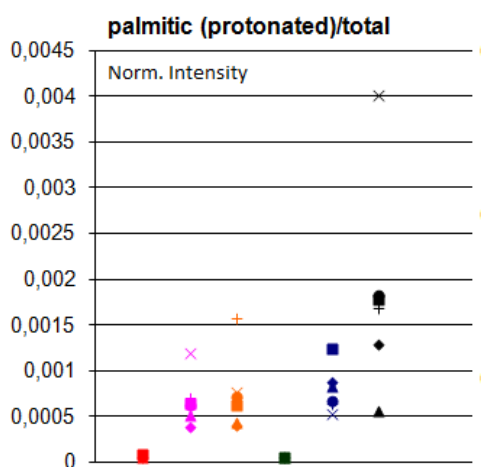


Figure A.7: Positive protonated ions of palmitic acid  $C_{16}H_{33}O_2^+$  at  $m/z$  257 in linseed oil

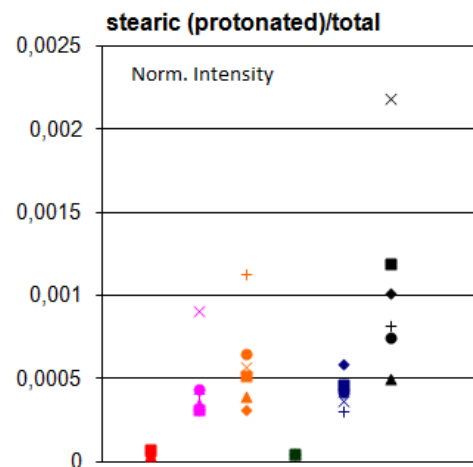


Figure A.8: Positive protonated ions of stearic acid  $C_{18}H_{37}O_2^+$  at  $m/z$  285 in linseed oil

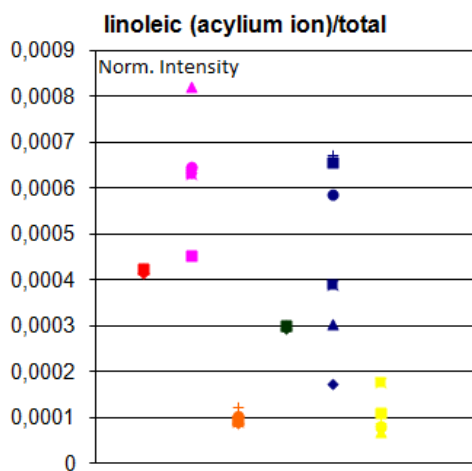


Figure A.9: Positive acylium ions of linoleic acid  $C_{18}H_{31}O^+$  at  $m/z$  263 in linseed oil

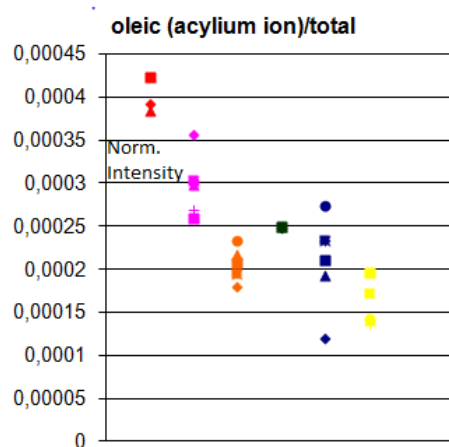


Figure A.10: Positive acylium ions of oleic acid  $C_{18}H_{33}O^+$  at  $m/z$  265 in linseed oil

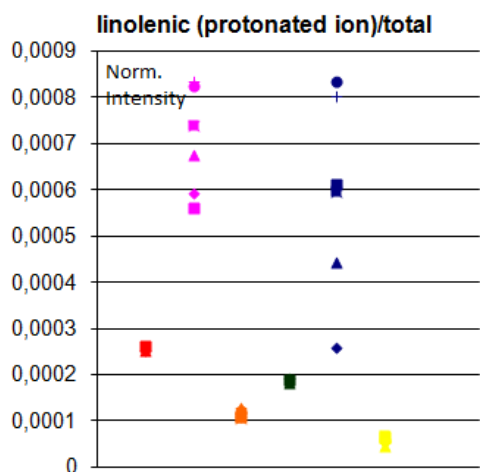


Figure A.11: Positive protonated ions of linolenic acid  $C_{18}H_{31}O_2^+$  at  $m/z$  279 in linseed oil

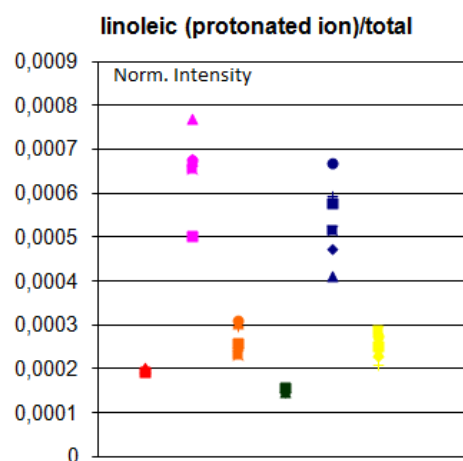


Figure A.12: Positive protonated ions of linoleic acid  $C_{18}H_{33}O_2^+$  at  $m/z$  281 in linseed oil

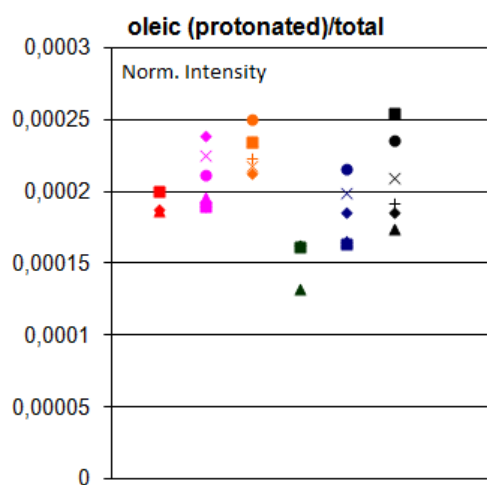


Figure A.13: Positive protonated ions of oleic acid  $C_{18}H_{35}O_2^+$  at  $m/z$  283 in linseed oil

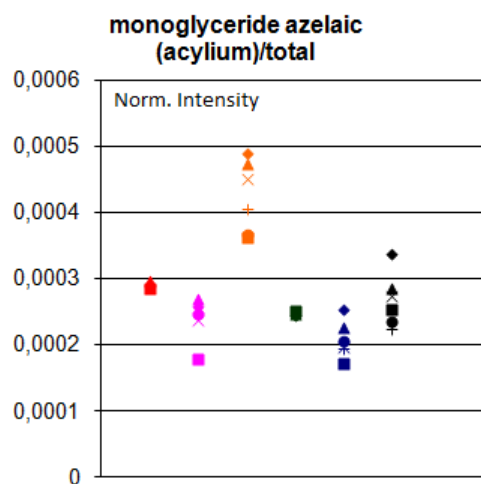


Figure A.14: Positive acylium ions of monoglyceride with azelaic acid  $C_{12}H_{21}O_5^+$  at  $m/z$  245 in linseed oil

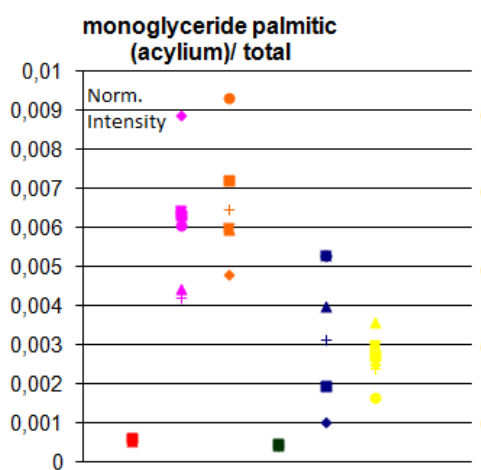


Figure A.15: Positive acylium ions of monoglyceride with palmitic acid  $C_{19}H_{37}O_3^+$  at  $m/z$  313 in linseed oil

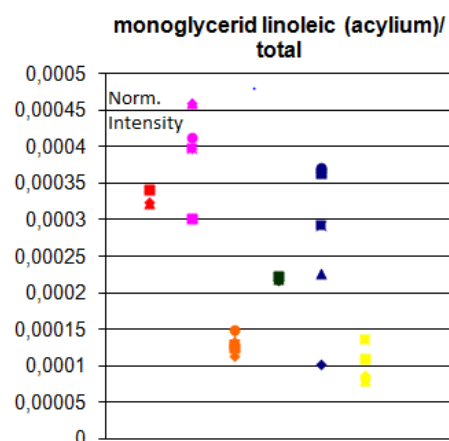


Figure A.16: Positive acylium ions of monoglyceride with linoleic acid  $C_{21}H_{37}O_3^+$  at  $m/z$  337 in linseed oil

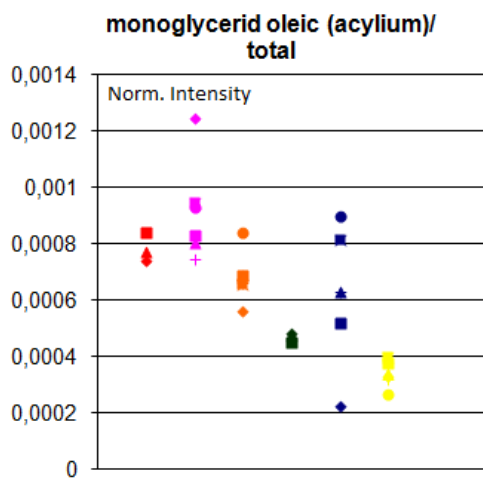


Figure A.17: Positive acylium ions of monoglyceride with oleic acid  $C_{21}H_{39}O_3^+$  at  $m/z$  339 in linseed oil

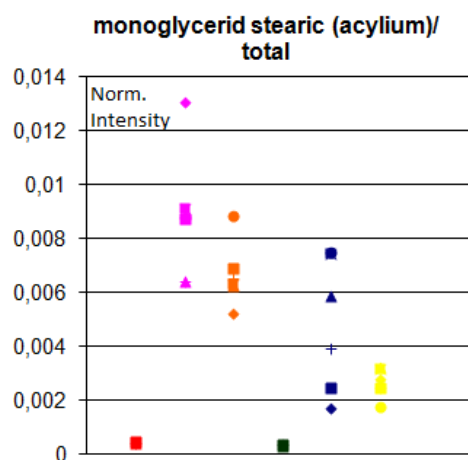


Figure A.18: Positive acylium ions of monoglyceride with stearic acid  $C_{21}H_{41}O_3^+$  at  $m/z$  341 in linseed oil

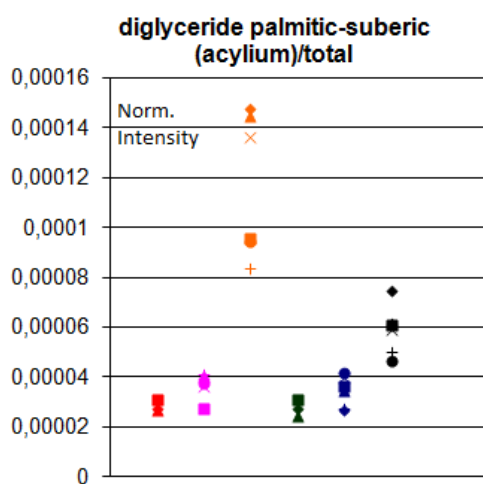


Figure A.19: Positive acylium ions of diglyceride with palmitic/suberic acid  $C_{27}H_{49}O_6^+$  at  $m/z$  469 in linseed oil

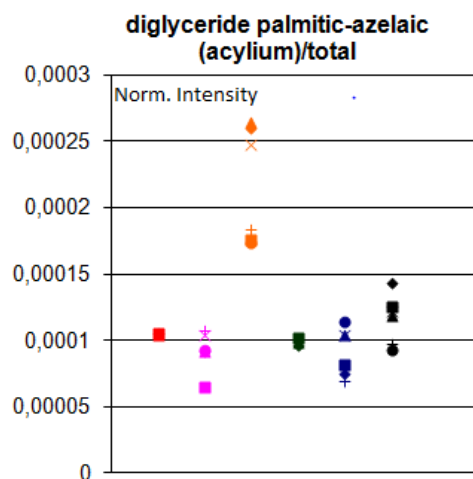


Figure A.20: Positive acylium ions of diglyceride with palmitic/azelaic acid  $C_{28}H_{51}O_6^+$  at  $m/z$  483 in linseed oil

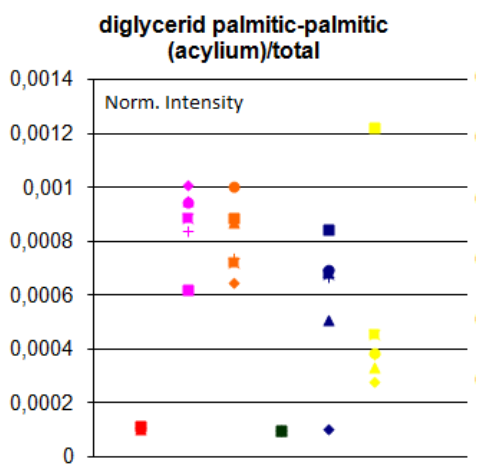


Figure A.21: Positive acylium ions of diglyceride with twice palmitic acid  $C_{35}H_{67}O_4^+$  at  $m/z$  551,5 in linseed oil

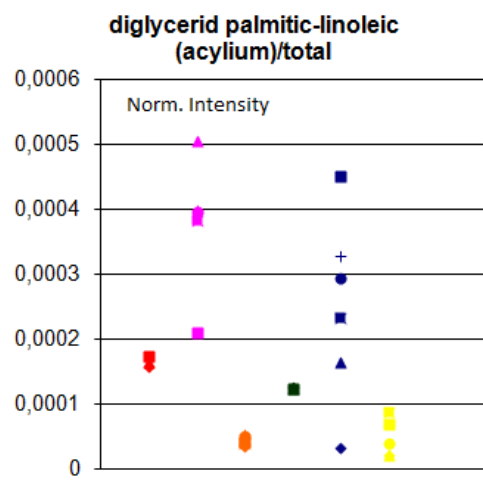


Figure A.22: Positive acylium ions of diglyceride with palmitic/linoleic acid  $C_{37}H_{67}O_4^+$  at  $m/z$  575,5 in linseed oil

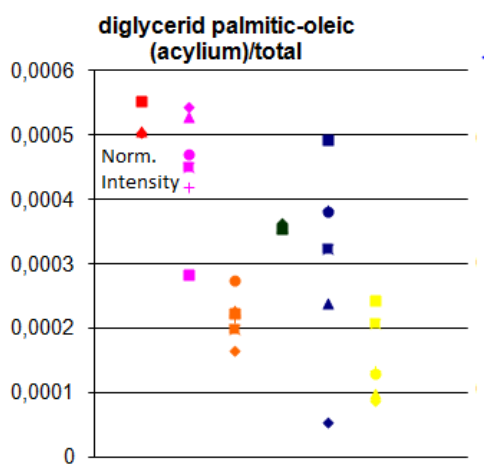


Figure A.23: Positive acylium ions of diglyceride with palmitic/oleic acid  $C_{37}H_{69}O_4^+$  at  $m/z$  577,5 in linseed oil

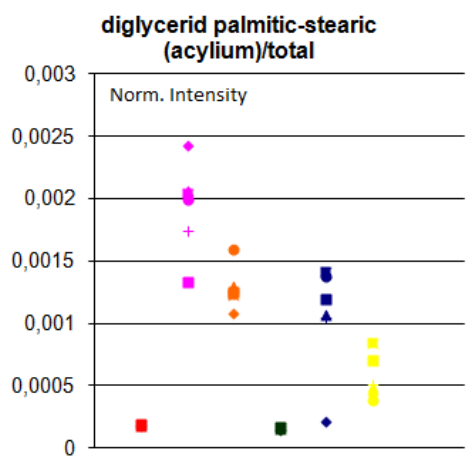


Figure A.24: Positive acylium ions of diglyceride with palmitic/stearic acid  $C_{37}H_{71}O_4^+$  at  $m/z$  579,5 in linseed oil

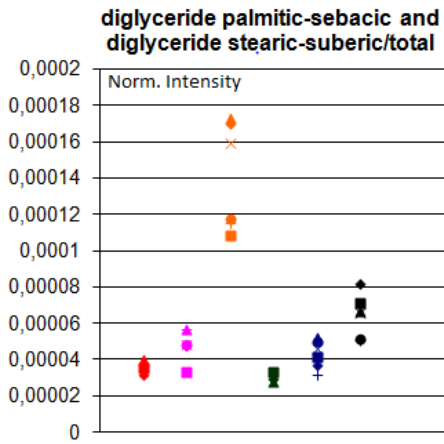


Figure A.25: Positive acylium ions of diglyceride with stearic/suberic acid and of diglyceride with palmitic/sebacic acid  $C_{29}H_{53}O_6^+$  at  $m/z$  497 in linseed oil

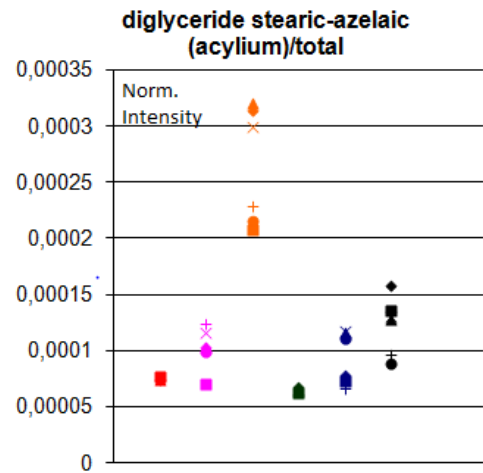


Figure A.26: Positive acylium ions of diglyceride with stearic/azelaic acid  $C_{30}H_{55}O_6^+$  at  $m/z$  511 in linseed oil

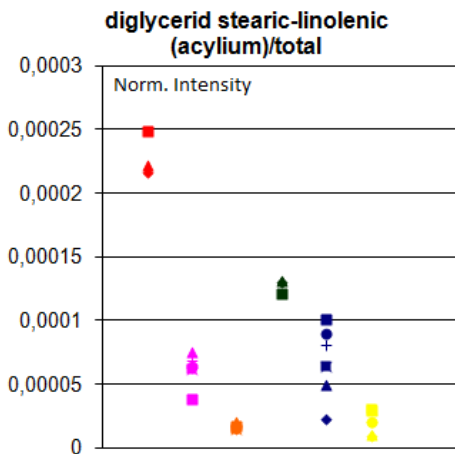


Figure A.27: Positive acylium ions of diglyceride with stearic/linolenic acid  $C_{39}H_{69}O_4^+$  at  $m/z$  601,5 in linseed oil

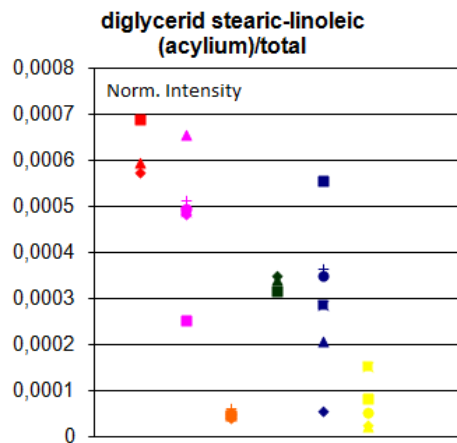


Figure A.28: Positive acylium ions of diglyceride with stearic/linoleic acid  $C_{39}H_{71}O_4^+$  at  $m/z$  603,5 in linseed oil

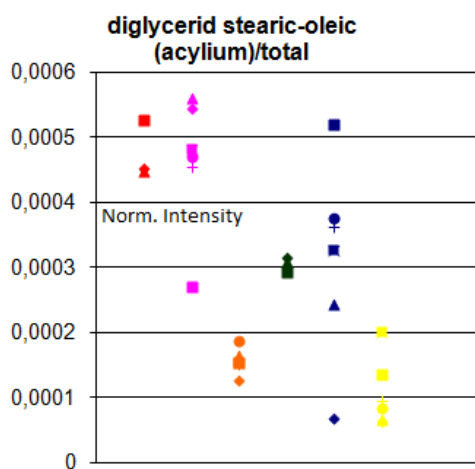


Figure A.29: Positive acylium ions of diglyceride with stearic/oleic acid  $C_{39}H_{73}O_4^+$  at  $m/z$  605,5 in linseed oil

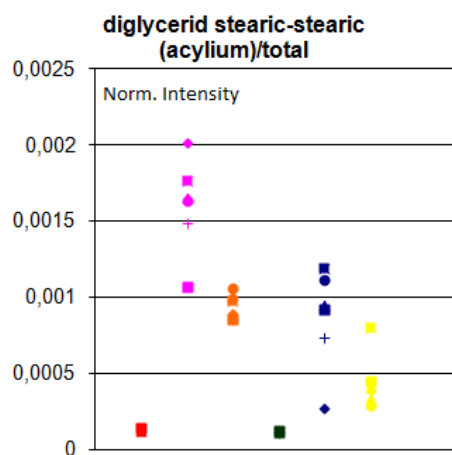


Figure A.30: Positive acylium ions of diglyceride with twice stearic acid  $C_{39}H_{75}O_4^+$  at  $m/z$  607,5 in linseed oil

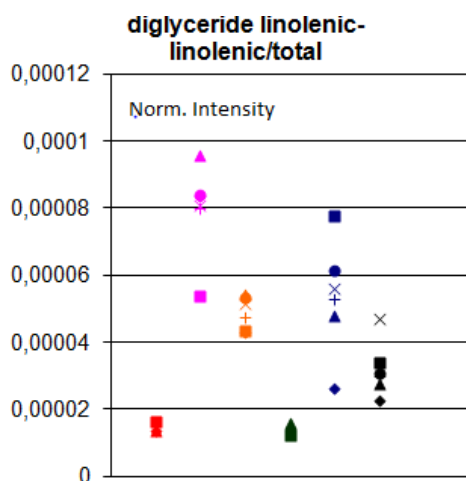


Figure A.31: Positive acylium ions of diglyceride with twice linolenic acid  $C_{39}H_{63}O_4^+$  at  $m/z$  595,5 in linseed oil

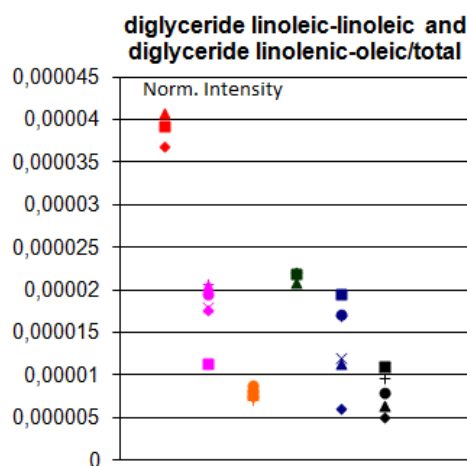


Figure A.32: Positive acylium ions of diglyceride with twice linoleic acid and of diglyceride with linolenic/oleic  $C_{39}H_{67}O_4^+$  at  $m/z$  599,5 in linseed oil

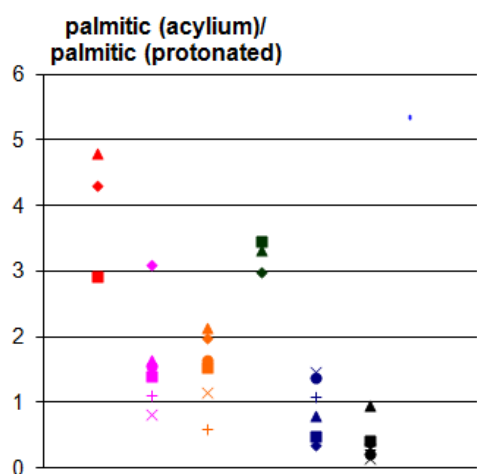


Figure A.33: Ratio of positive acylium and protonated ions of palmitic acid in linseed oil

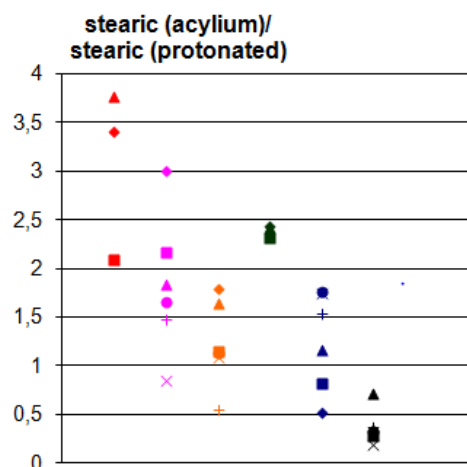


Figure A.34: Ratio of positive acylium and protonated ions of stearic acid in linseed oil

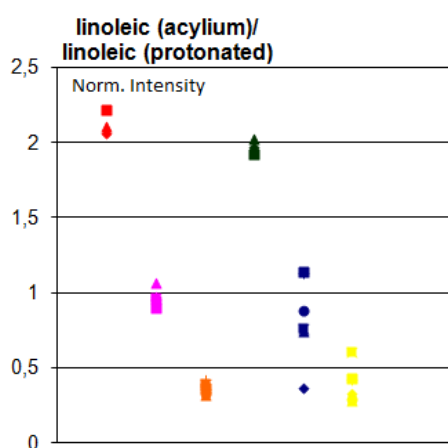


Figure A.35: Ratio of positive acylium and protonated ions of linoleic acid in linseed oil

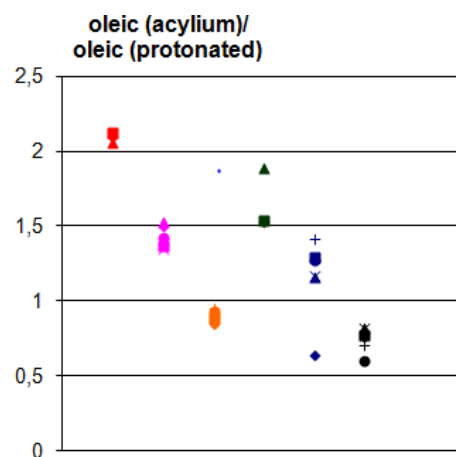


Figure A.36: Ratio of positive acylium and protonated ions of oleic acid in linseed oil

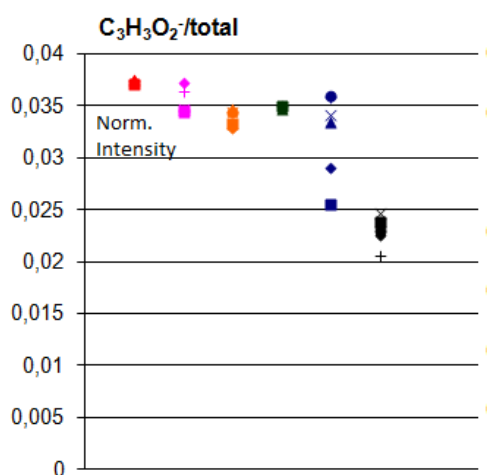


Figure A.37: Negative ions of aliphatic chain fragment with formula  $C_2H_3COO^-$  at  $m/z$  71 in linseed oil

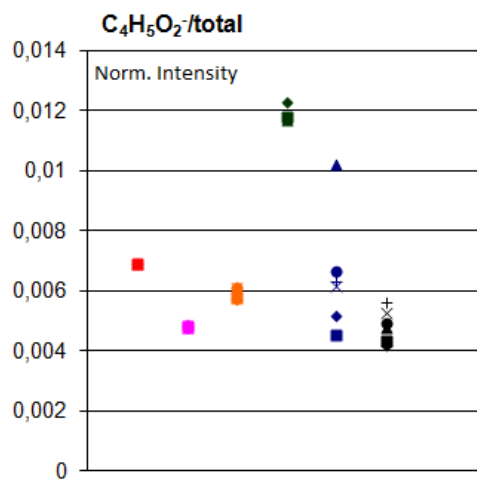


Figure A.38: Negative ions of aliphatic chain fragment with formula  $C_2H_3CH_2COO^-$  at  $m/z$  85 in linseed oil

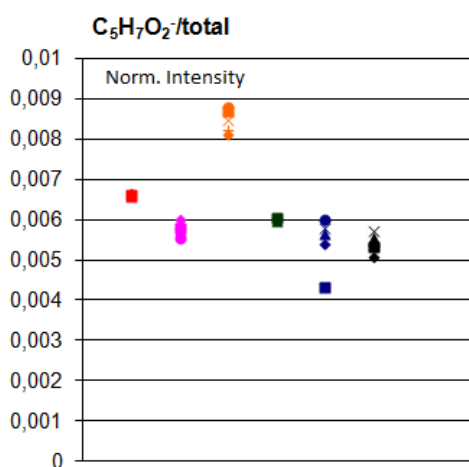


Figure A.39: Negative ions of aliphatic chain fragment with formula  $C_2H_3(CH_2)_2COO^-$  at  $m/z$  99 in linseed oil

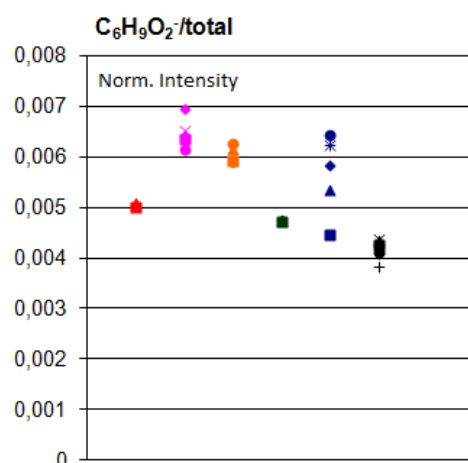


Figure A.40: Negative ions of aliphatic chain fragment with formula  $C_2H_3(CH_2)_3COO^-$  at  $m/z$  113 in linseed oil

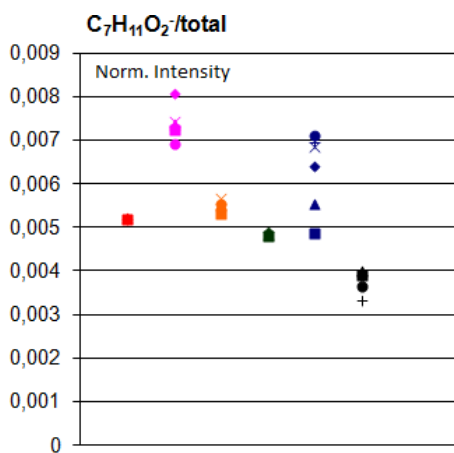


Figure A.41: Negative ions of aliphatic chain fragment with formula  $C_2H_3(CH_2)_4COO^-$  at  $m/z$  127 in linseed oil

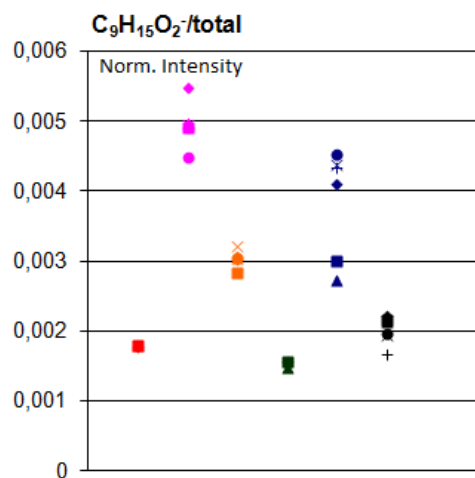


Figure A.42: Negative ions of aliphatic chain fragment with formula  $C_2H_3(CH_2)_6COO^-$  at  $m/z$  155 in linseed oil

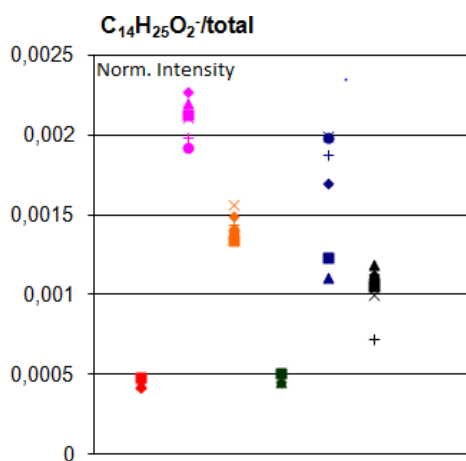


Figure A.43: Negative ions of aliphatic chain fragment with formula  $C_2H_3(CH_2)_{11}COO^-$  at  $m/z$  225 in linseed oil

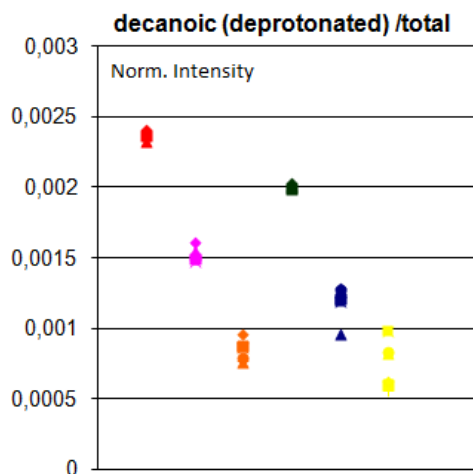


Figure A.44: Negative deprotonated ions of decanoic acid  $C_{10}H_{19}O_2^-$  at  $m/z$  171 in linseed oil

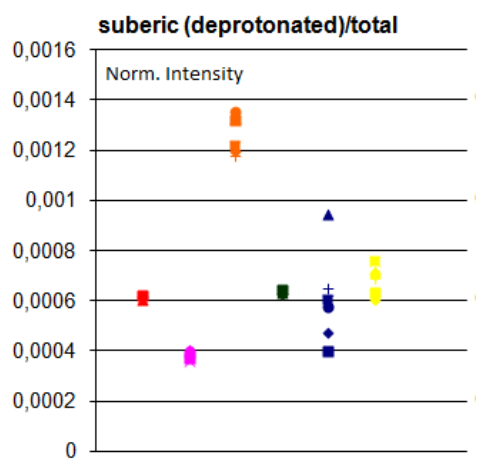


Figure A.45: Negative deprotonated ions of suberic acid  $C_8H_{13}O_4^-$  at  $m/z$  173 in linseed oil

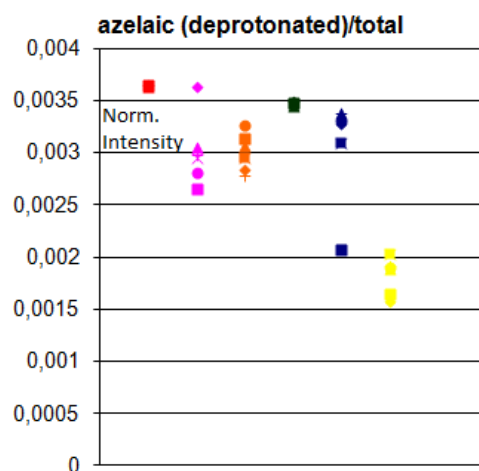


Figure A.46: Negative deprotonated ions of azelaic acid  $C_9H_{15}O_4^-$  at  $m/z$  187 in linseed oil

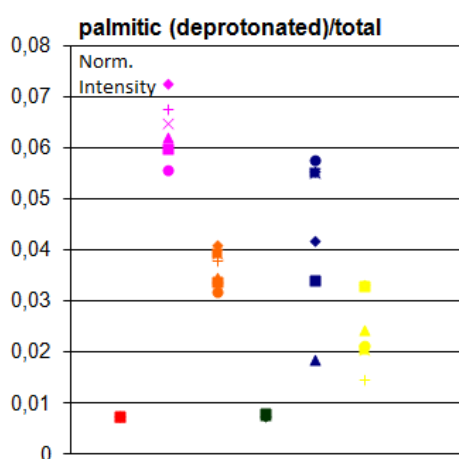


Figure A.47: Negative deprotonated ions of palmitic acid  $C_{16}H_{31}O_2^-$  at  $m/z$  255 in linseed oil

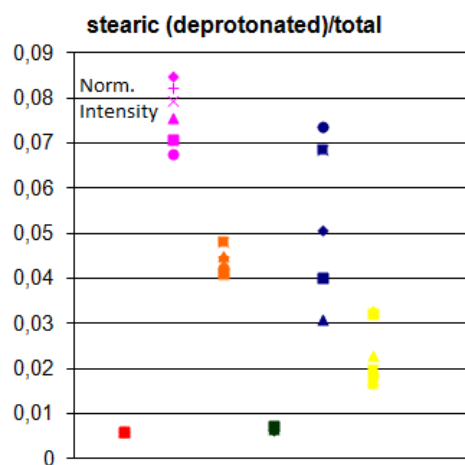


Figure A.48: Negative deprotonated ions of stearic acid  $C_{18}H_{35}O_2^-$  at  $m/z$  283 in linseed oil

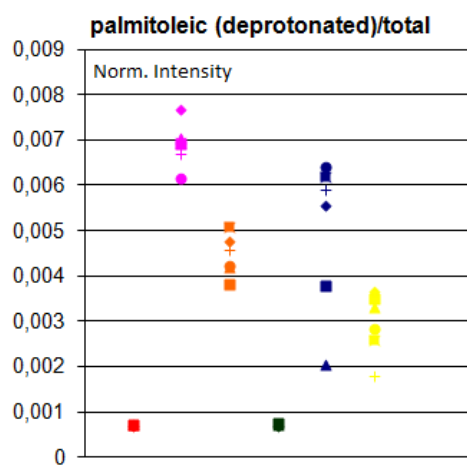


Figure A.49: Negative deprotonated ions of palmitoleic acid  $C_{16}H_{29}O_2^-$  at  $m/z$  253 in linseed oil

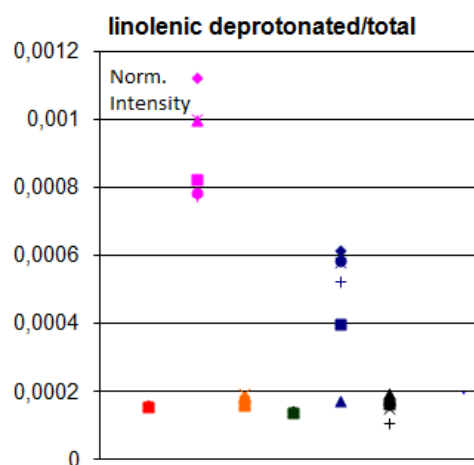


Figure A.50: Negative deprotonated ions of linolenic acid  $C_{18}H_{29}O_2^-$  at  $m/z$  277 in linseed oil

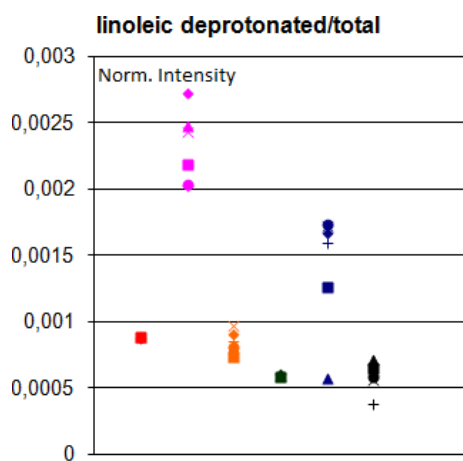


Figure A.51: Negative deprotonated ions of linoleic acid  $C_{18}H_{31}O_2^-$  at  $m/z$  279 in linseed oil

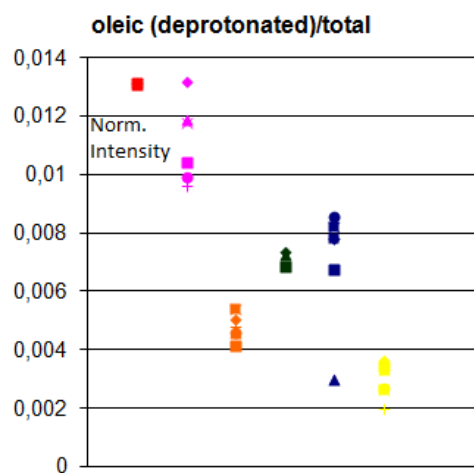


Figure A.52: Negative deprotonated ions of oleic acid  $C_{18}H_{33}O_2^-$  at  $m/z$  281 in linseed oil

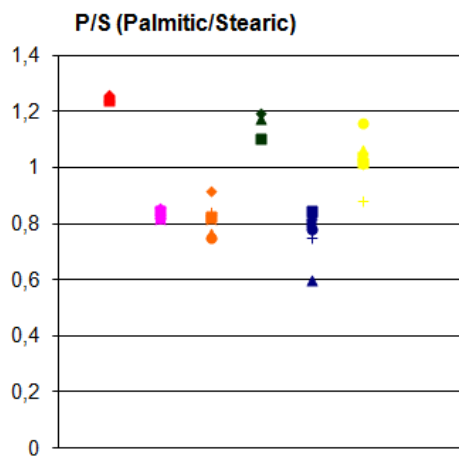


Figure A.53: Ratio of negative deprotonated palmitic and stearic acid ions in linseed oil

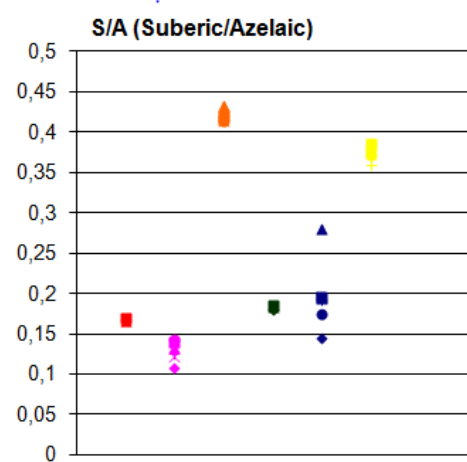


Figure A.54: Ratio of negative deprotonated suberic and azelaic acid ions in linseed oil

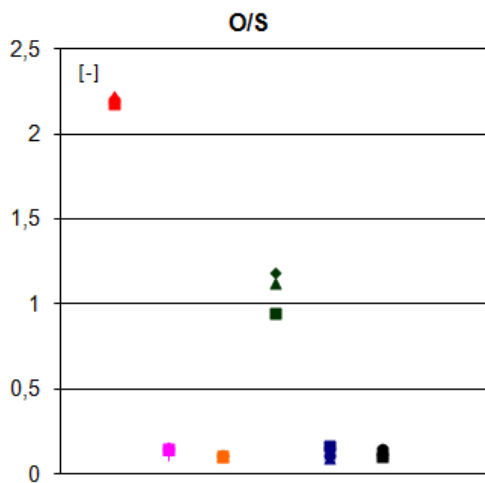


Figure A.55: Ratio of negative deprotonated oleic and stearic acid ions in linseed oil

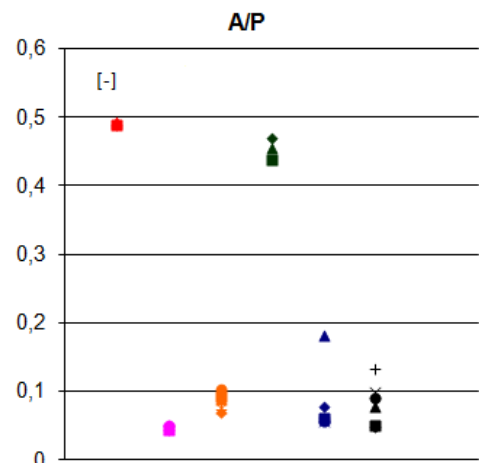


Figure A.56: Ratio of negative deprotonated azelaic and palmitic acid ions in linseed oil

## Appendix B

# Results of ToF-SIMS measurements of Linseed oil pre-treated with lead driers

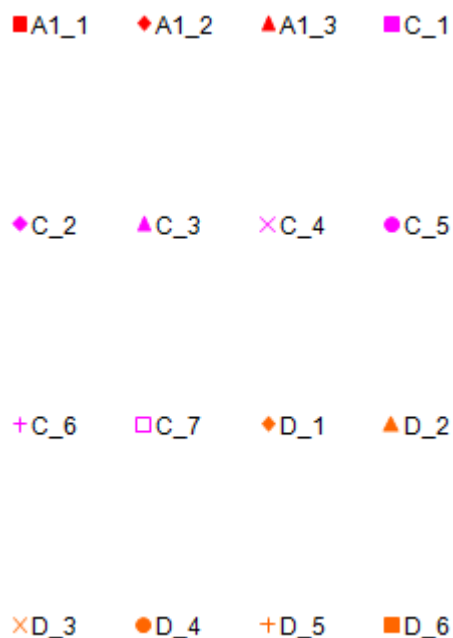


Figure B.1: Legend used for Figures B.2 to B.56

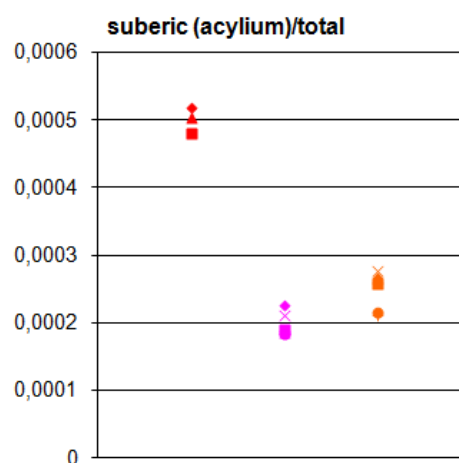


Figure B.2: Positive acylium ions of suberic acid,  $C_8H_{13}O_3^+$  at  $m/z$  157 in linseed oil pre-treated with lead driers

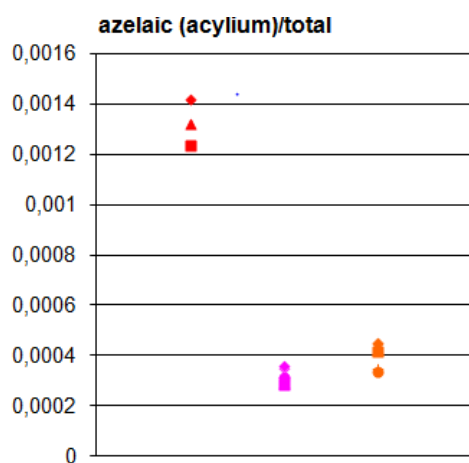


Figure B.3: Positive acylium ions of azelaic acid  $C_9H_{15}O_3^+$  at  $m/z$  171 in linseed oil pre-treated with lead driers

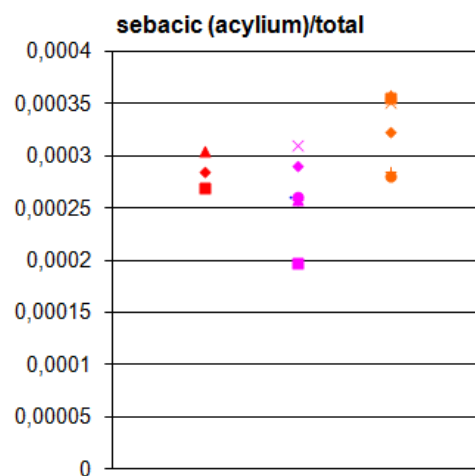


Figure B.4: Positive acylium ions of sebacic acid  $C_{10}H_{17}O_3^+$  at  $m/z$  185 in linseed oil pre-treated with lead driers

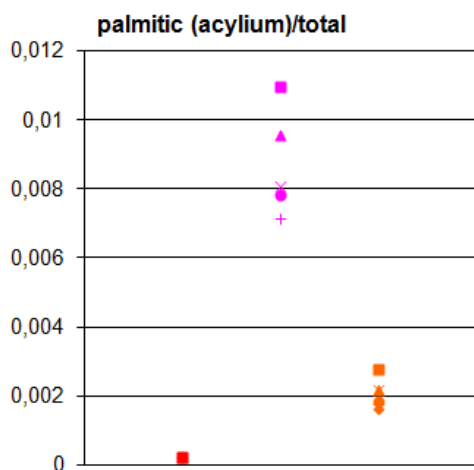


Figure B.5: Positive acylium ions of palmitic acid  $C_{16}H_{31}O^+$  at  $m/z$  239 in linseed oil pre-treated with lead driers

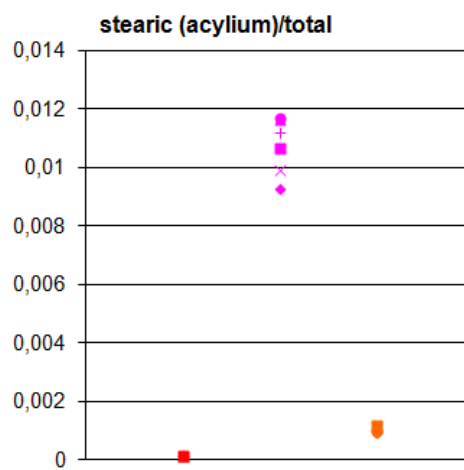


Figure B.6: Positive acylium ions of stearic acid  $C_{18}H_{35}O^+$  at  $m/z$  267 in linseed oil pre-treated with lead driers

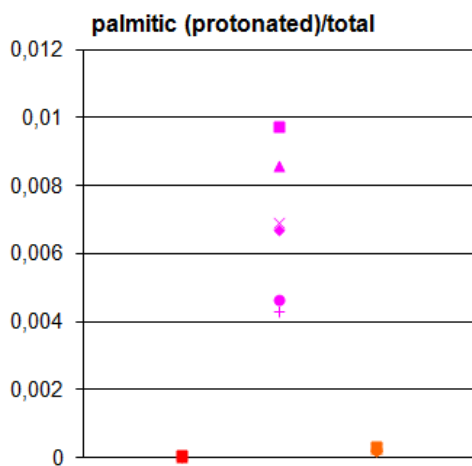


Figure B.7: Positive protonated ions of palmitic acid  $C_{16}H_{33}O_2^+$  at  $m/z$  257 in linseed oil pre-treated with lead driers

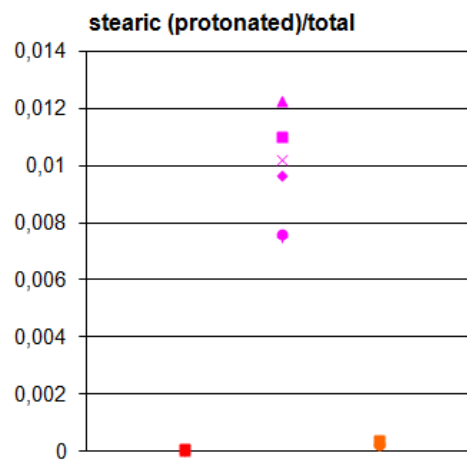


Figure B.8: Positive protonated ions of stearic acid  $C_{18}H_{37}O_2^+$  at  $m/z$  285 in linseed oil pre-treated with lead driers

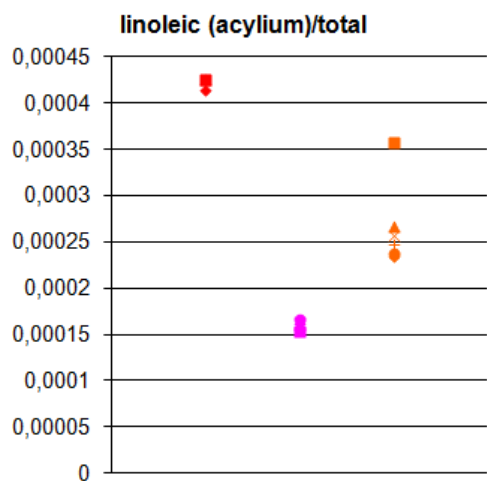


Figure B.9: Positive acylium ions of linoleic acid  $C_{18}H_{31}O^+$  at  $m/z$  263 in linseed oil pre-treated with lead driers

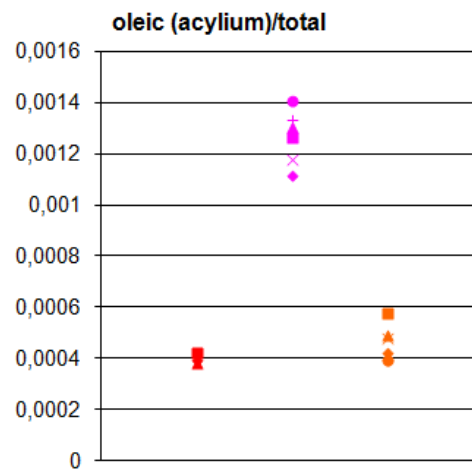


Figure B.10: Positive acylium ions of oleic acid  $C_{18}H_{33}O^+$  at  $m/z$  265 in linseed oil pre-treated with lead driers

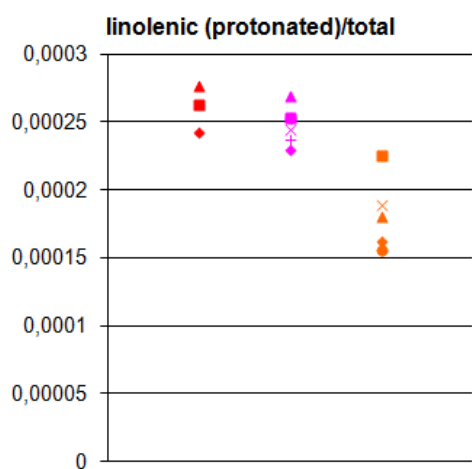


Figure B.11: Positive protonated ions of linolenic acid  $C_{18}H_{31}O_2^+$  at  $m/z$  279 in linseed oil pre-treated with lead driers

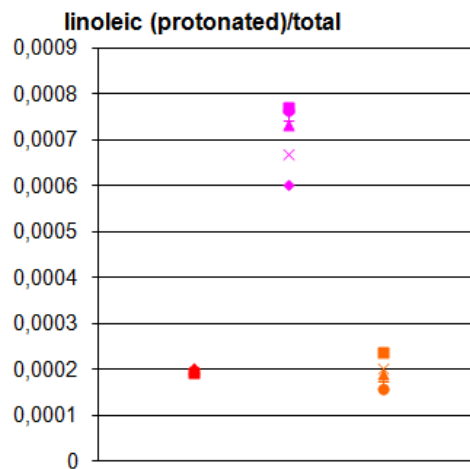


Figure B.12: Positive protonated ions of linoleic acid  $C_{18}H_{33}O_2^+$  at  $m/z$  281 in linseed oil pre-treated with lead driers

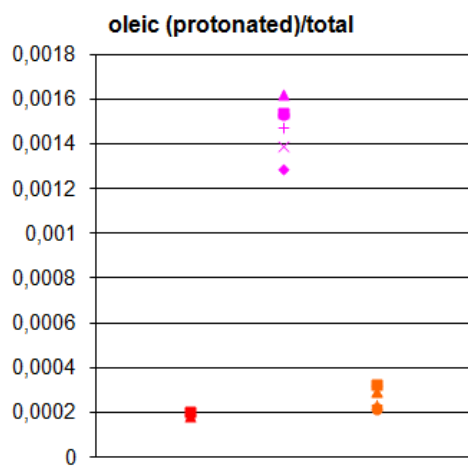


Figure B.13: Positive protonated ions of oleic acid  $C_{18}H_{35}O_2^+$  at  $m/z$  283 in linseed oil pre-treated with lead driers

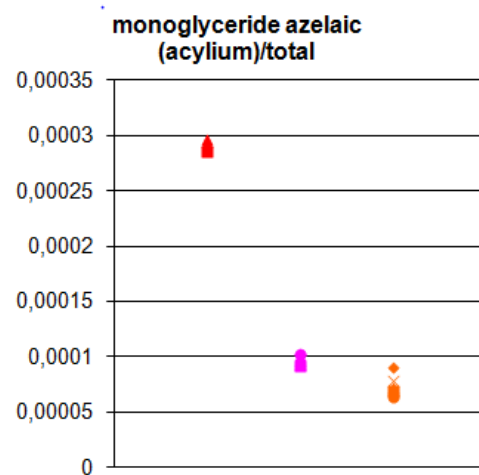


Figure B.14: Positive acylium ions of monoglyceride with azelaic acid  $C_{12}H_{21}O_5^+$  at  $m/z$  245 in linseed oil pre-treated with lead driers

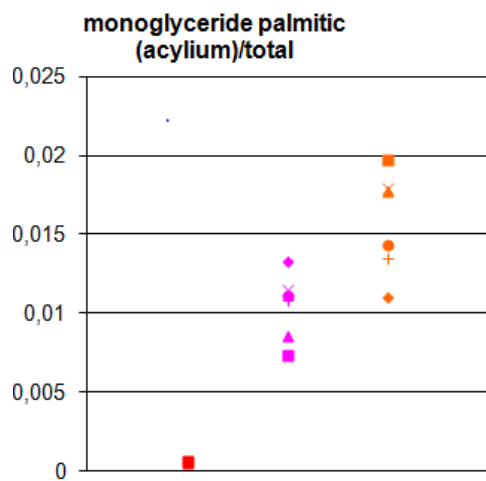


Figure B.15: Positive acylium ions of monoglyceride with palmitic acid  $C_{19}H_{37}O_3^+$  at  $m/z$  313 in linseed oil pre-treated with lead driers

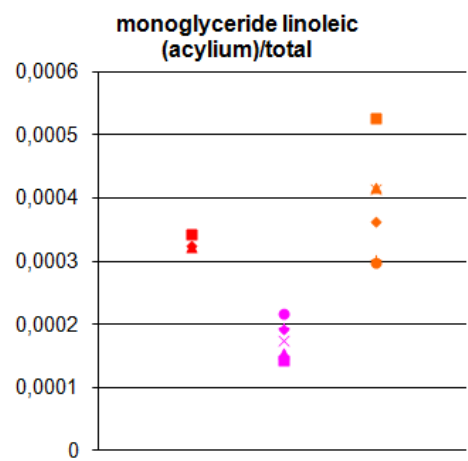


Figure B.16: Positive acylium ions of monoglyceride with linoleic acid  $C_{21}H_{37}O_3^+$  at  $m/z$  337 in linseed oil pre-treated with lead driers

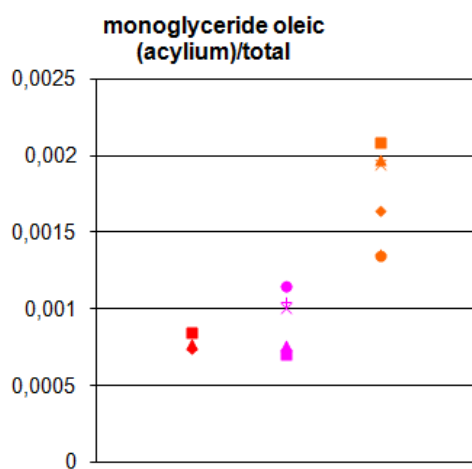


Figure B.17: Positive acylium ions of monoglyceride with oleic acid  $C_{21}H_{39}O_3^+$  at  $m/z$  339 in linseed oil pre-treated with lead driers

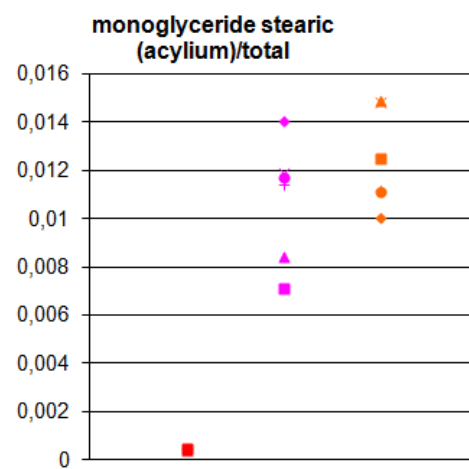


Figure B.18: Positive acylium ions of monoglyceride with stearic acid  $C_{21}H_{41}O_3^+$  at  $m/z$  341 in linseed oil pre-treated with lead driers

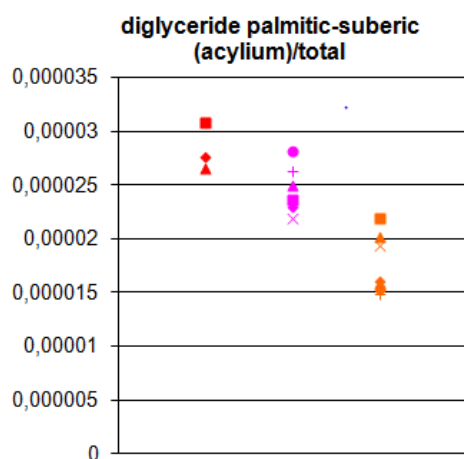


Figure B.19: Positive acylium ions of diglyceride with palmitic/suberic acid  $C_{27}H_{49}O_6^+$  at  $m/z$  469 in linseed oil pre-treated with lead driers

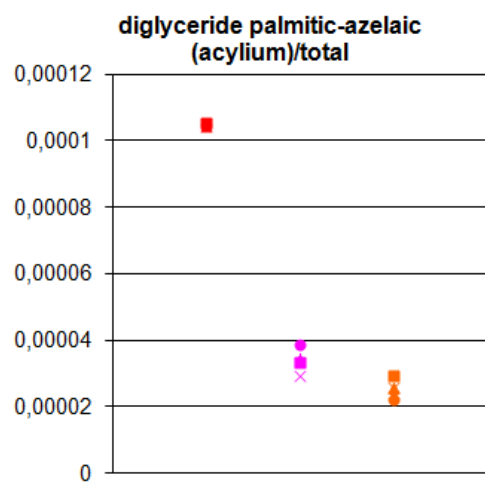


Figure B.20: Positive acylium ions of diglyceride with palmitic/azelaic acid  $C_{28}H_{51}O_6^+$  at  $m/z$  483 in linseed oil pre-treated with lead driers

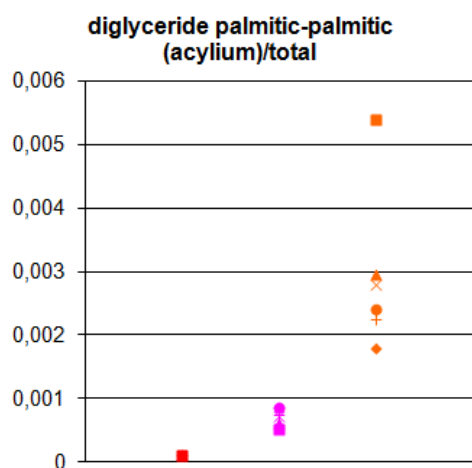


Figure B.21: Positive acylium ions of diglyceride with twice palmitic acid  $C_{35}H_{67}O_4^+$  at  $m/z$  551,5 in linseed oil pre-treated with lead driers

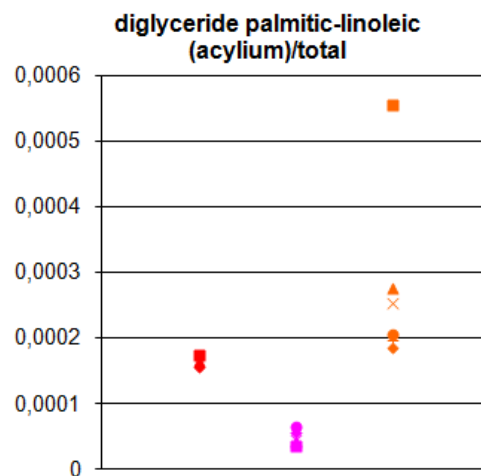


Figure B.22: Positive acylium ions of diglyceride with palmitic/linoleic acid  $C_{37}H_{67}O_4^+$  at  $m/z$  575,5 in linseed oil pre-treated with lead driers

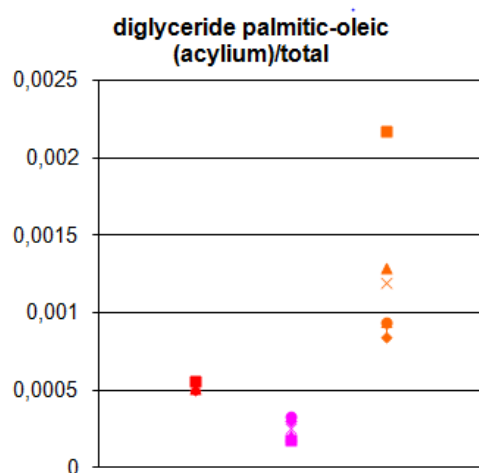


Figure B.23: Positive acylium ions of diglyceride with palmitic/oleic acid  $C_{37}H_{69}O_4^+$  at  $m/z$  577,5 in linseed oil pre-treated with lead driers

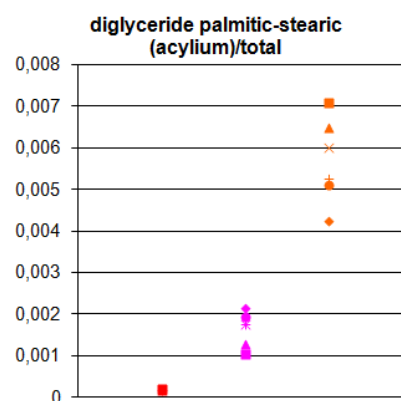


Figure B.24: Positive acylium ions of diglyceride with palmitic/stearic acid  $C_{37}H_{71}O_4^+$  at  $m/z$  579,5 in linseed oil pre-treated with lead driers

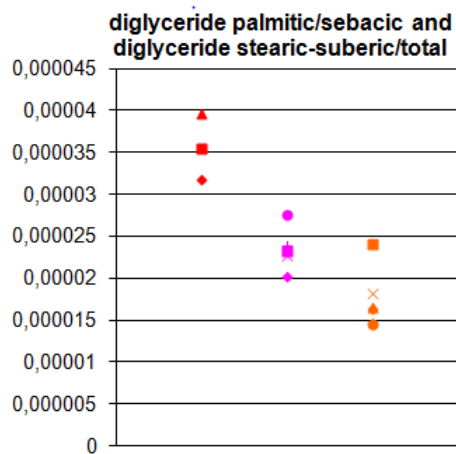


Figure B.25: Positive acylium ions of diglyceride with stearic/suberic acid and of diglyceride with palmitic/sebacic acid  $C_{29}H_{53}O_6^+$  at  $m/z$  497 in linseed oil pre-treated with lead driers

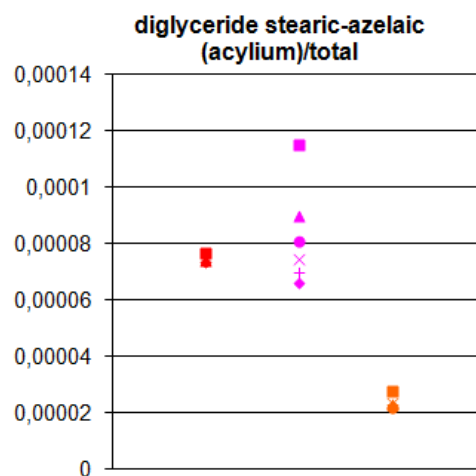


Figure B.26: Positive acylium ions of diglyceride with stearic/azelaic acid  $C_{30}H_{55}O_6^+$  at  $m/z$  511 in linseed oil pre-treated with lead driers

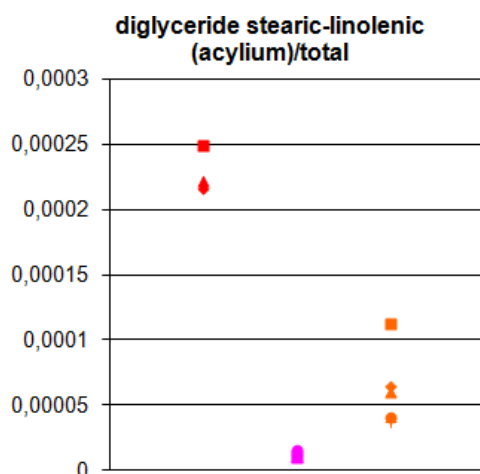


Figure B.27: Positive acylium ions of diglyceride with stearic/linolenic acid  $C_{39}H_{69}O_4^+$  at  $m/z$  601,5 in linseed oil pre-treated with lead driers

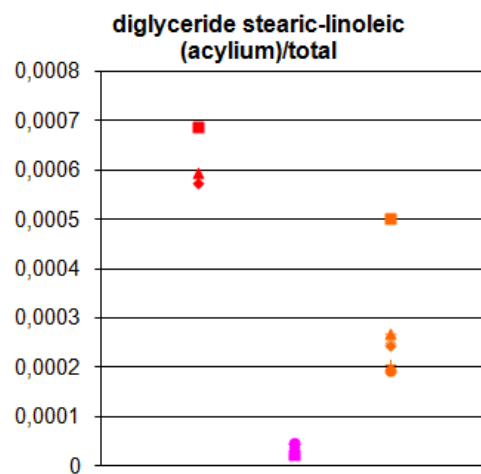


Figure B.28: Positive acylium ions of diglyceride with stearic/linoleic acid  $C_{39}H_{71}O_4^+$  at  $m/z$  603,5 in linseed oil pre-treated with lead driers

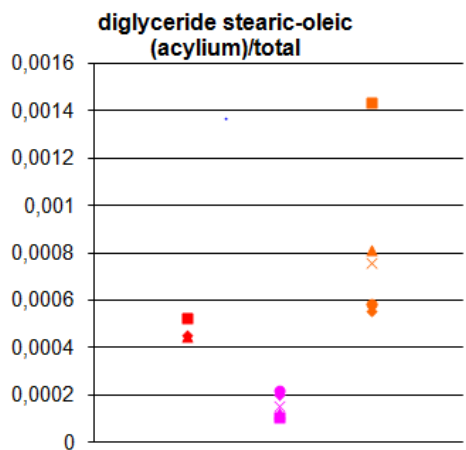


Figure B.29: Positive acylium ions of diglyceride with stearic/oleic acid  $C_{39}H_{73}O_4^+$  at  $m/z$  605,5 in linseed oil pre-treated with lead driers

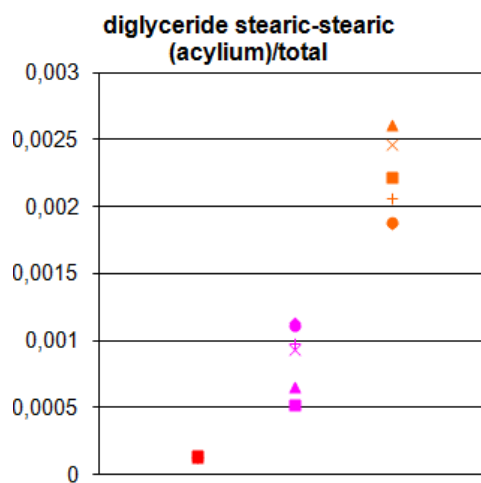


Figure B.30: Positive acylium ions of diglyceride with twice stearic acid  $C_{39}H_{75}O_4^+$  at  $m/z$  607,5 in linseed oil pre-treated with lead driers

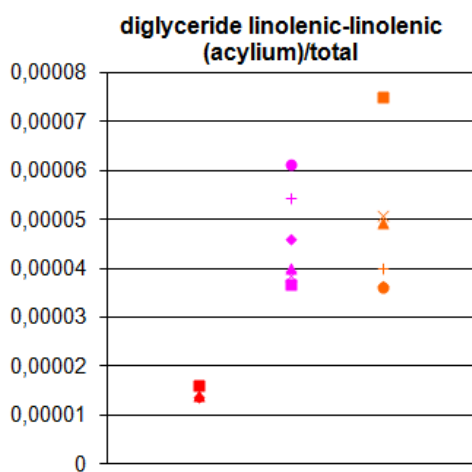


Figure B.31: Positive acylium ions of diglyceride with twice linolenic acid  $C_{39}H_{63}O_4^+$  at  $m/z$  595,5 in linseed oil pre-treated with lead driers

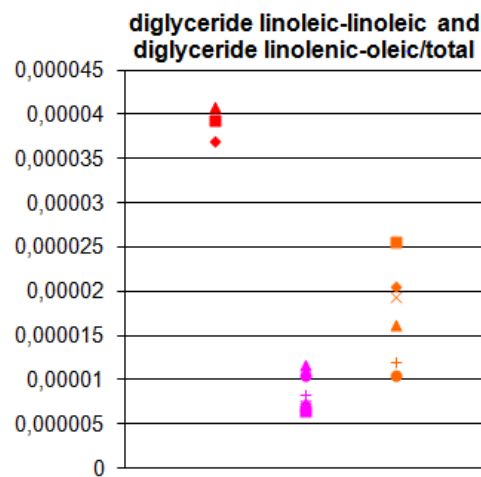


Figure B.32: Positive acylium ions of diglyceride with twice linoleic acid and of diglyceride with linolenic/oleic  $C_{39}H_{67}O_4^+$  at  $m/z$  599,5 in linseed oil pre-treated with lead driers

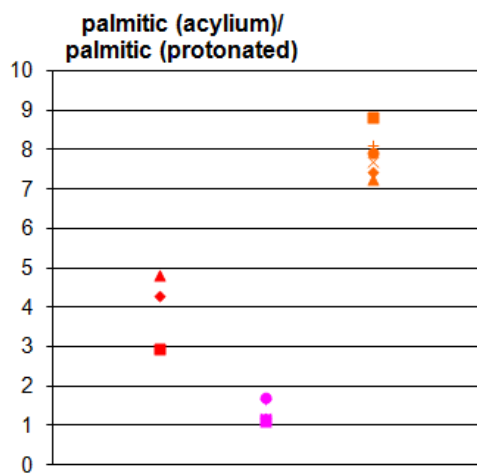


Figure B.33: Ratio of positive acylium and protonated ions of palmitic acid in linseed oil pre-treated with lead driers

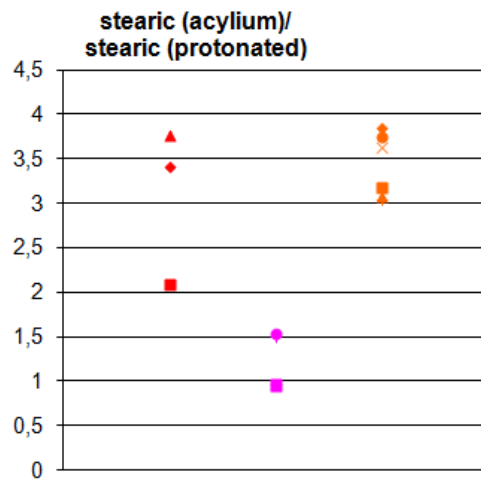


Figure B.34: Ratio of positive acylium and protonated ions of stearic acid in linseed oil pre-treated with lead driers

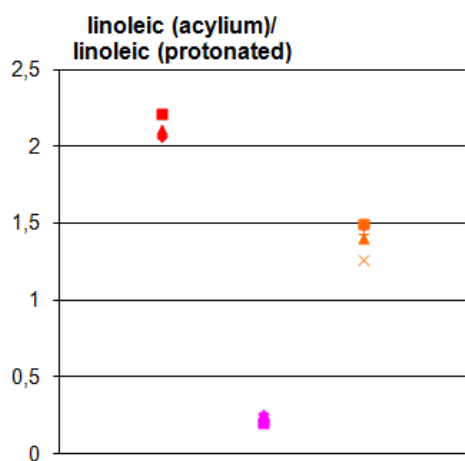


Figure B.35: Ratio of positive acylium and protonated ions of linoleic acid in linseed oil pre-treated with lead driers

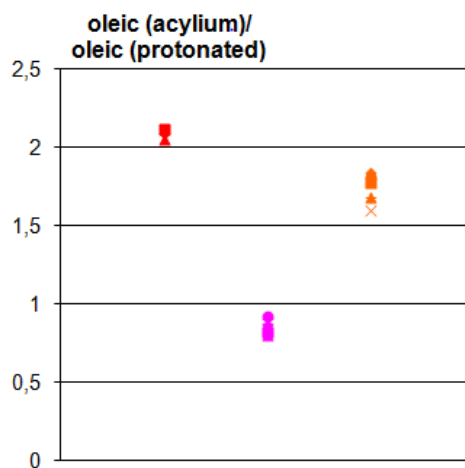


Figure B.36: Ratio of positive acylium and protonated ions of oleic acid in linseed oil pre-treated with lead driers

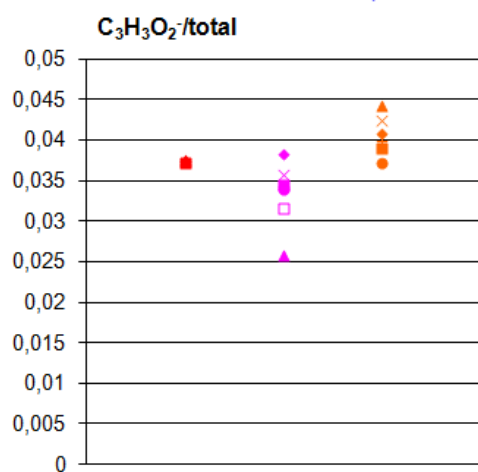


Figure B.37: Negative ions of aliphatic chain fragment with formula  $C_2H_3COO^-$  at  $m/z$  71 in linseed oil pre-treated with lead driers

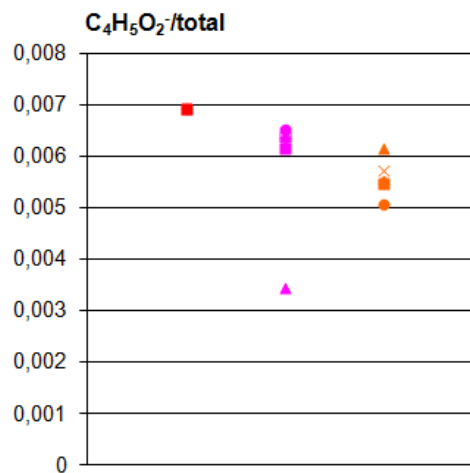


Figure B.38: Negative ions of aliphatic chain fragment with formula  $C_2H_3CH_2COO^-$  at  $m/z$  85 in linseed oil pre-treated with lead driers

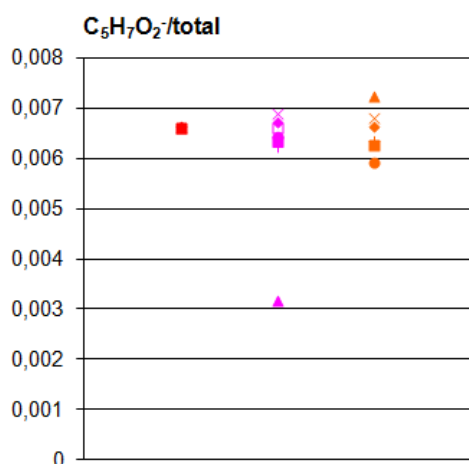


Figure B.39: Negative ions of aliphatic chain fragment with formula  $C_2H_3(CH_2)_2COO^-$  at  $m/z$  99 in linseed oil pre-treated with lead driers

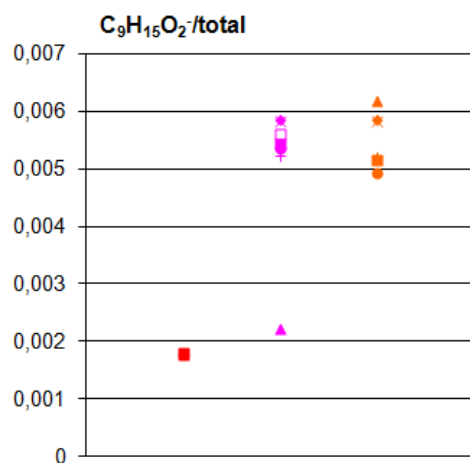


Figure B.40: Negative ions of aliphatic chain fragment with formula  $C_2H_3(CH_2)_3COO^-$  at  $m/z$  113 in linseed oil pre-treated with lead driers

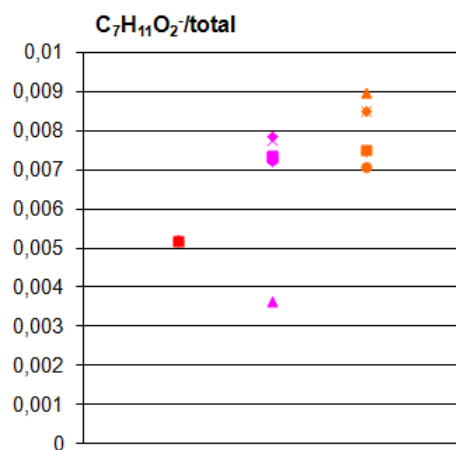


Figure B.41: Negative ions of aliphatic chain fragment with formula  $C_2H_3(CH_2)_4COO^-$  at  $m/z$  127 in linseed oil pre-treated with lead driers

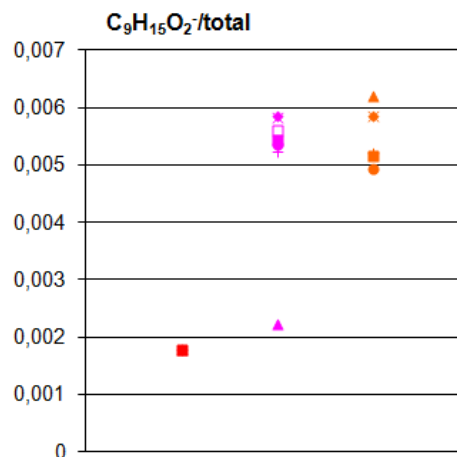


Figure B.42: Negative ions of aliphatic chain fragment with formula  $C_2H_3(CH_2)_6COO^-$  at  $m/z$  155 in linseed oil pre-treated with lead driers

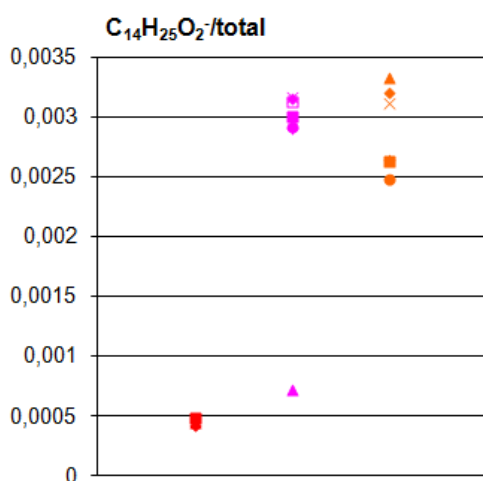


Figure B.43: Negative ions of aliphatic chain fragment with formula  $C_2H_3(CH_2)_{11}COO^-$  at  $m/z$  225 in linseed oil pre-treated with lead driers

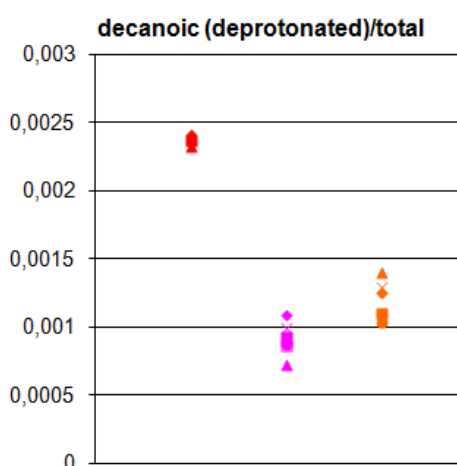


Figure B.44: Negative deprotonated ions of decanoic acid  $C_{10}H_{19}O_2^-$  at  $m/z$  171 in linseed oil pre-treated with lead driers

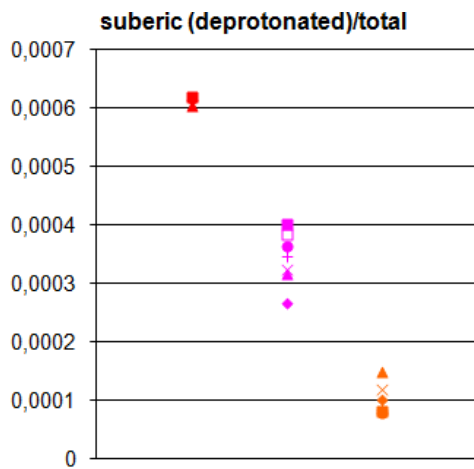


Figure B.45: Negative deprotonated ions of suberic acid  $C_8H_{13}O_4^-$  at  $m/z$  173 in linseed oil pre-treated with lead driers

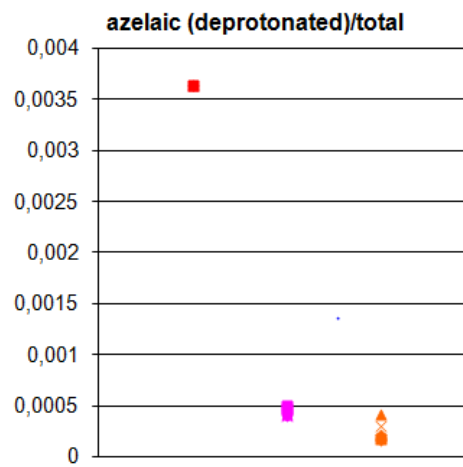


Figure B.46: Negative deprotonated ions of azelaic acid  $C_9H_{15}O_4^-$  at  $m/z$  187 in linseed oil pre-treated with lead driers

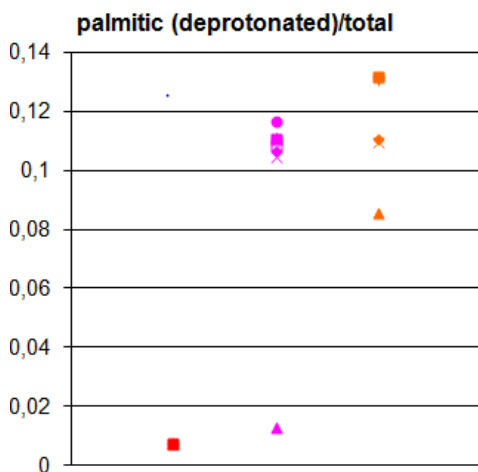


Figure B.47: Negative deprotonated ions of palmitic acid  $C_{16}H_{31}O_2^-$  at  $m/z$  255 in linseed oil pre-treated with lead driers

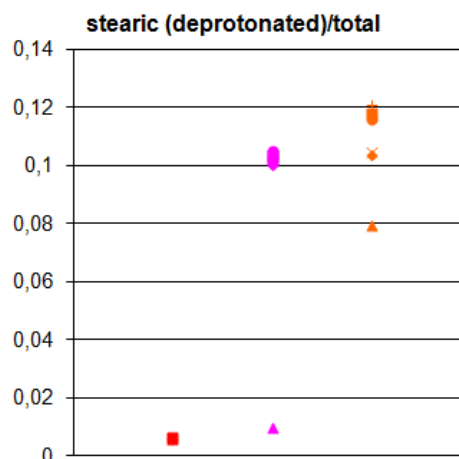


Figure B.48: Negative deprotonated ions of stearic acid  $C_{18}H_{35}O_2^-$  at  $m/z$  283 in linseed oil pre-treated with lead driers

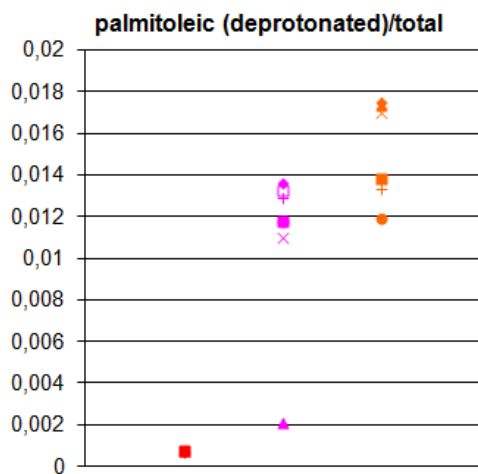


Figure B.49: Negative deprotonated ions of palmitoleic acid  $C_{16}H_{29}O_2^-$  at  $m/z$  253 in linseed oil pre-treated with lead driers

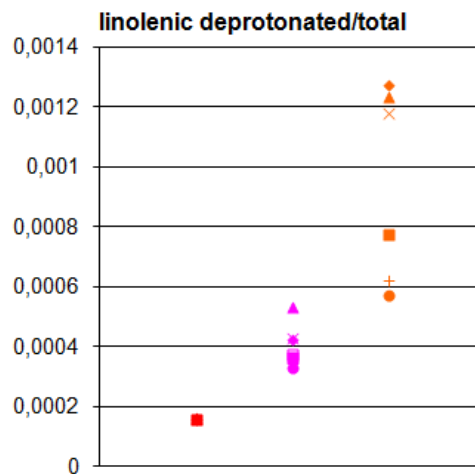


Figure B.50: Negative deprotonated ions of linolenic acid  $C_{18}H_{31}O_2^-$  at  $m/z$  277 in linseed oil pre-treated with lead driers

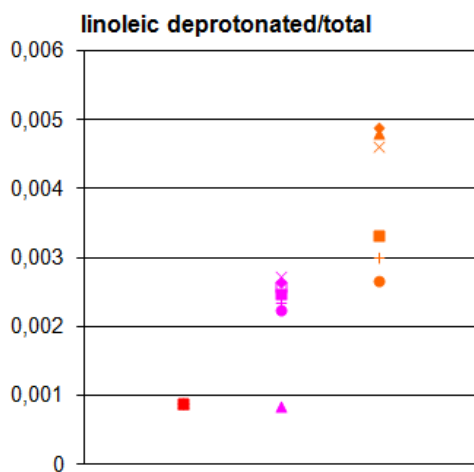


Figure B.51: Negative deprotonated ions of linoleic acid  $C_{18}H_{31}O_2^-$  at  $m/z$  279 in linseed oil pre-treated with lead driers

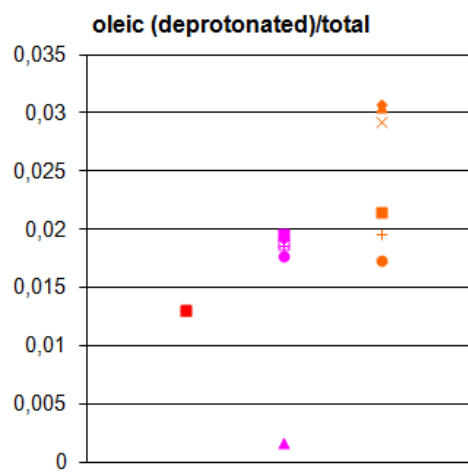


Figure B.52: Negative deprotonated ions of oleic acid  $C_{18}H_{33}O_2^-$  at  $m/z$  281 in linseed oil pre-treated with lead driers

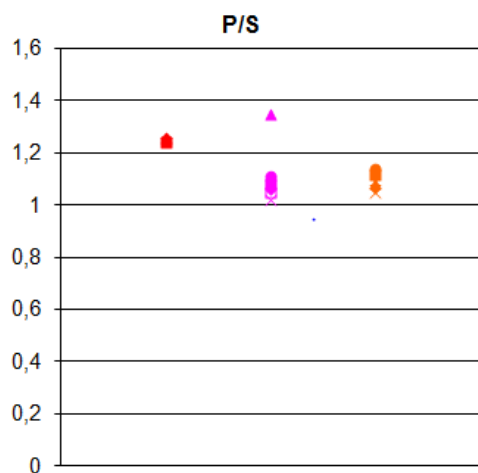


Figure B.53: Ratio of negative deprotonated palmitic and stearic acid ions in linseed oil pre-treated with lead driers

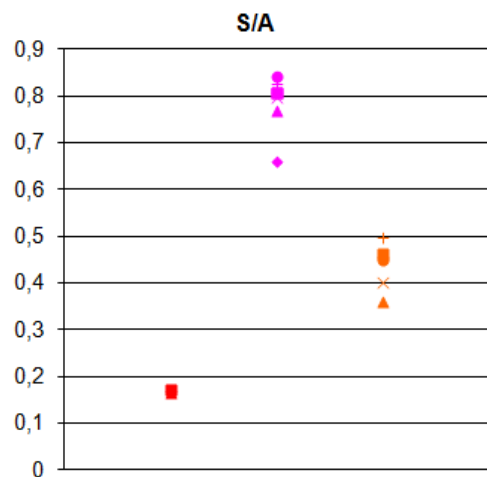


Figure B.54: Ratio of negative deprotonated suberic and azelaic acid ions in linseed oil pre-treated with lead driers

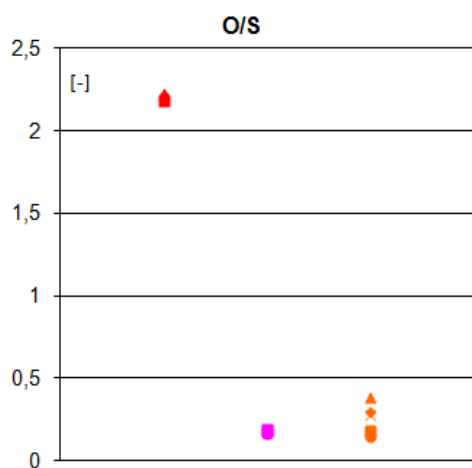


Figure B.55: Ratio of negative deprotonated oleic and stearic acid ions in linseed oil pre-treated with lead driers

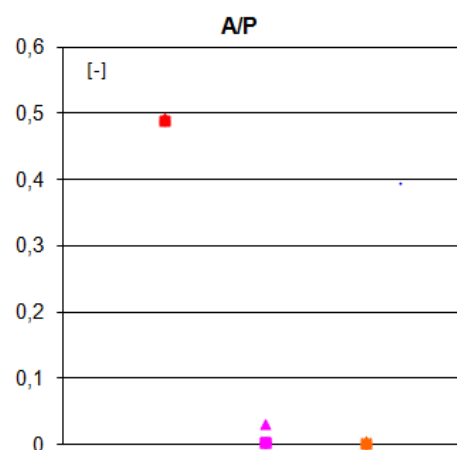


Figure B.56: Ratio of negative deprotonated azelaic and palmitic acid ions in linseed oil pre-treated with lead driers

# Appendix C

## Results of ToF-SIMS measurements of Linseed oil with Flake White

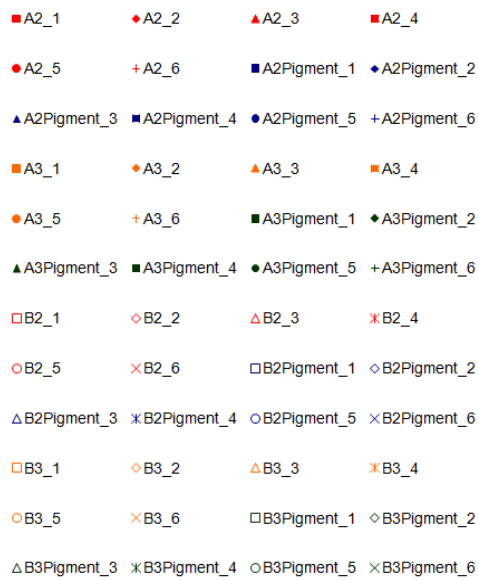


Figure C.1: Legend used for Figures C.2 to C.55

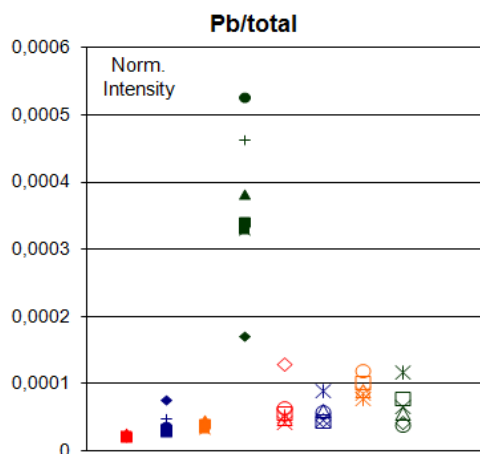


Figure C.2: Positive  $Pb^+$  ions in the linseed oil-flake white mixture at  $m/z$  208

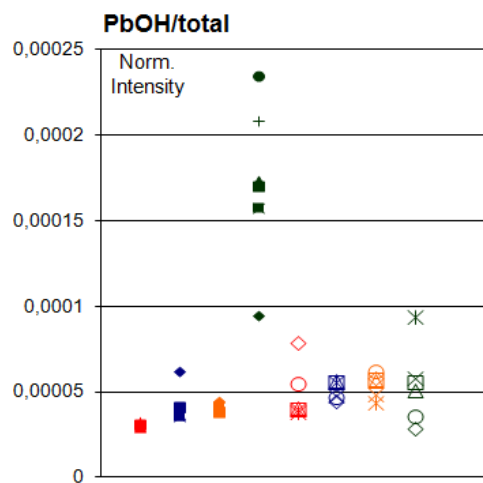


Figure C.3: Positive  $PbOH^+$  ions in the linseed oil-flake white mixture at  $m/z$  225

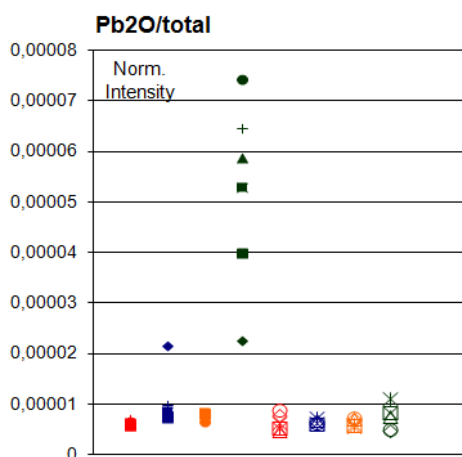


Figure C.4: Positive  $Pb_2O^+$  ions in the linseed oil-flake white mixture at  $m/z$  432

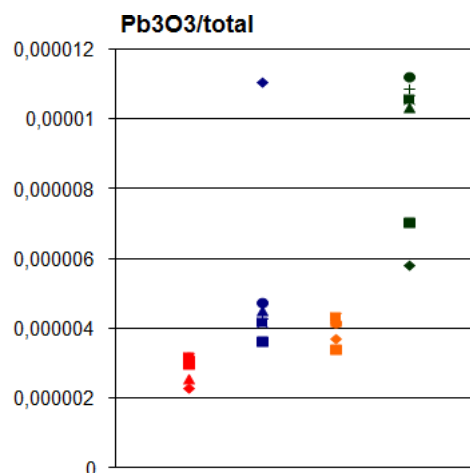


Figure C.5: Positive  $Pb_3O_3^+$  ions in the linseed oil-flake white mixture at  $m/z$  672

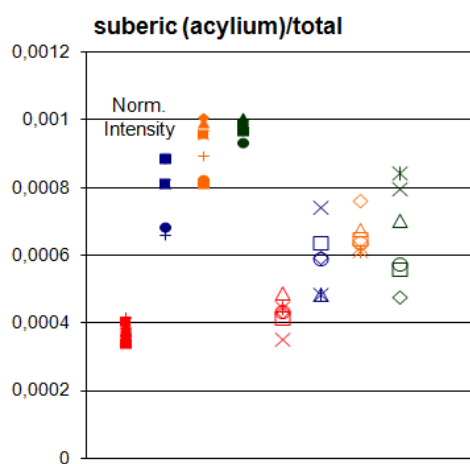


Figure C.6: Positive acylium ions of suberic acid,  $C_8H_{13}O_3^+$  at  $m/z$  157 in the linseed oil-flake white mixture

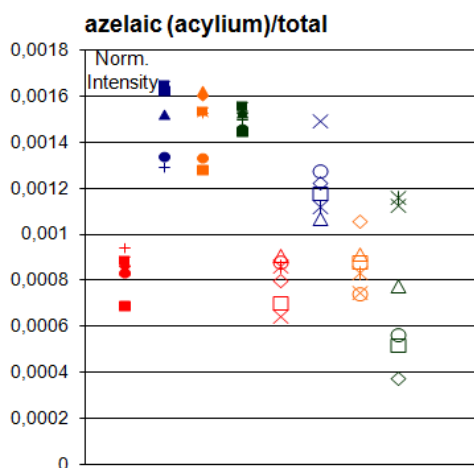


Figure C.7: Positive acylium ions of azelaic acid  $C_9H_{15}O_3^+$  at  $m/z$  171 in the linseed oil-flake white mixture

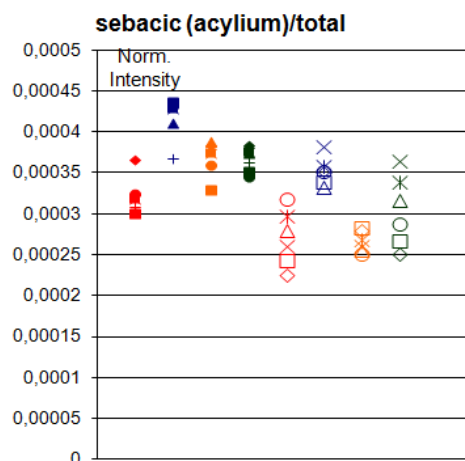


Figure C.8: Positive acylium ions of sebacic acid  $C_{10}H_{17}O_3^+$  at  $m/z$  185 in the linseed oil-flake white mixture

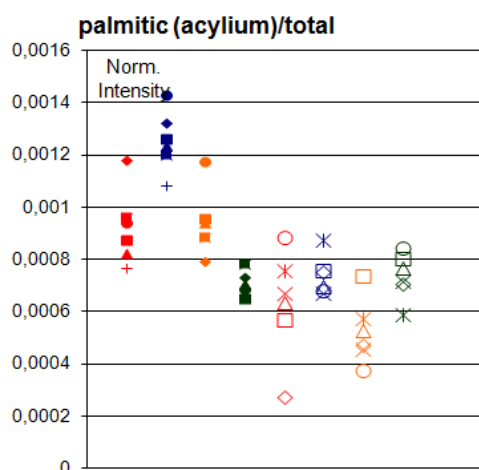


Figure C.9: Positive acylium ions of palmitic acid  $C_{16}H_{31}O^+$  at  $m/z$  239 in the linseed oil-flake white mixture

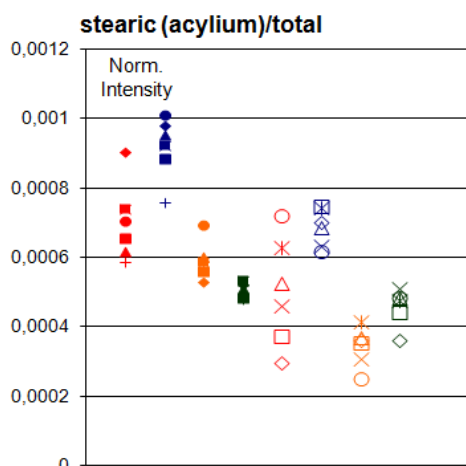


Figure C.10: Positive acylium ions of stearic acid  $C_{18}H_{35}O^+$  at  $m/z$  267 in the linseed oil-flake white mixture

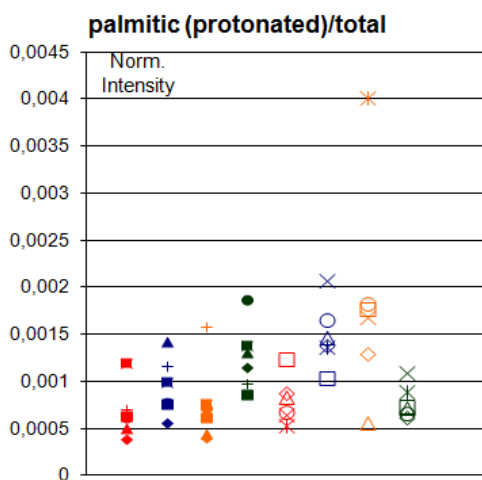


Figure C.11: Positive protonated ions of palmitic acid  $C_{16}H_{33}O_2^+$  at  $m/z$  257 in the linseed oil-flake white mixture

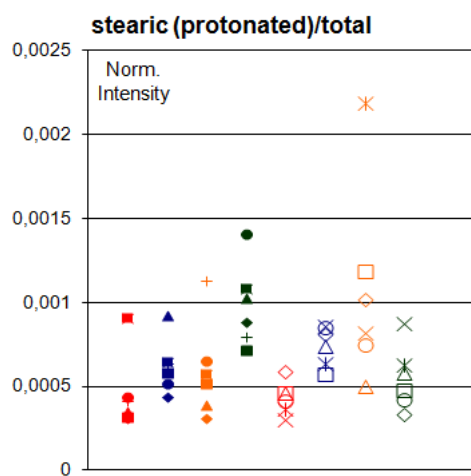


Figure C.12: Positive protonated ions of stearic acid  $C_{18}H_{37}O_2^+$  at  $m/z$  285 in the linseed oil-flake white mixture

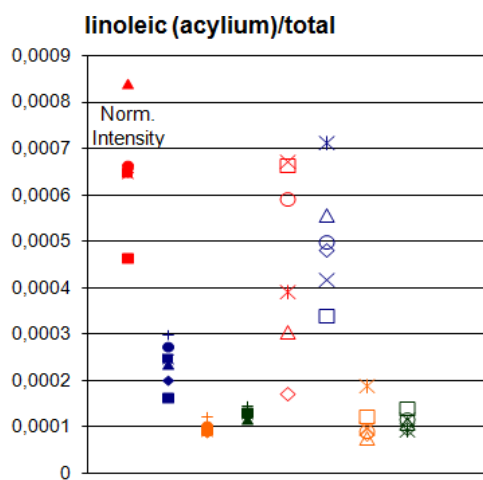


Figure C.13: Positive acylium ions of linoleic acid  $C_{18}H_{31}O^+$  at  $m/z$  263 in the linseed oil-flake white mixture

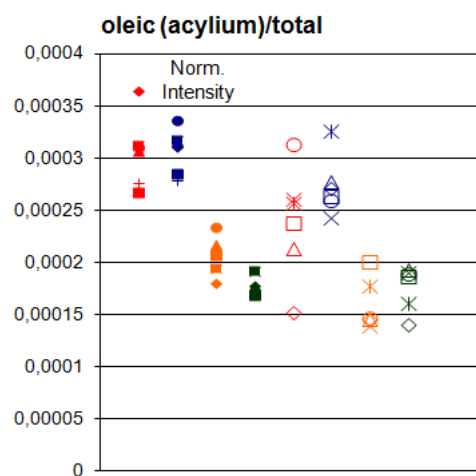


Figure C.14: Positive acylium ions of oleic acid  $C_{18}H_{33}O^+$  at  $m/z$  265 in the linseed oil-flake white mixture

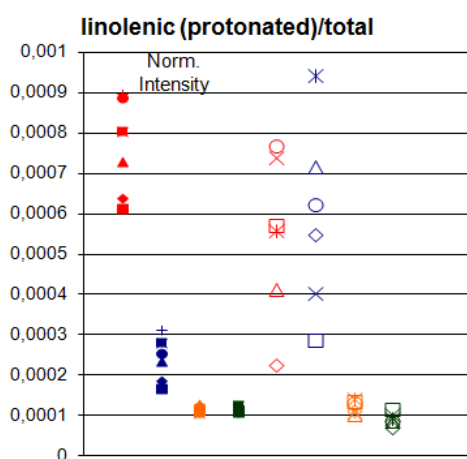


Figure C.15: Positive protonated ions of linolenic acid  $C_{18}H_{31}O_2^+$  at  $m/z$  279 in the linseed oil-flake white mixture

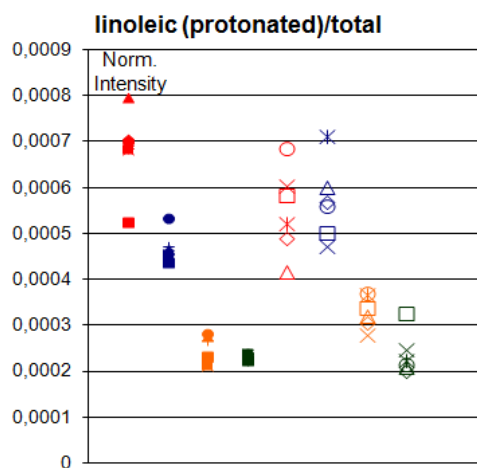


Figure C.16: Positive protonated ions of linoleic acid  $C_{18}H_{33}O_2^+$  at  $m/z$  281 in the linseed oil-flake white mixture

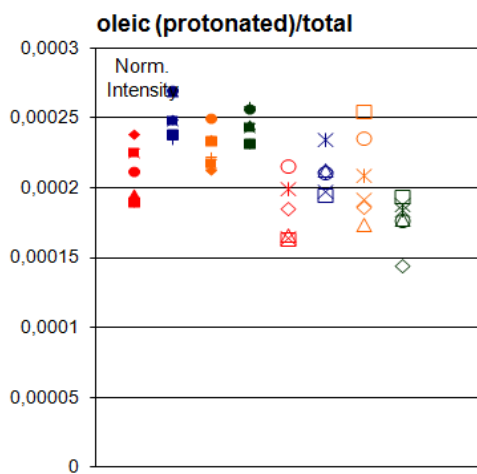


Figure C.17: Positive protonated ions of oleic acid  $C_{18}H_{35}O_2^+$  at  $m/z$  283 in the linseed oil-flake white mixture

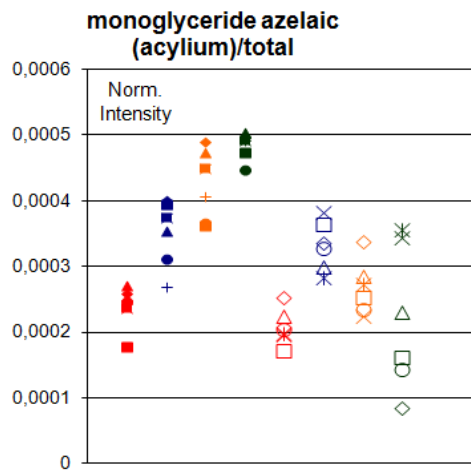


Figure C.18: Positive acylium ions of monoglyceride with azelaic acid  $C_{12}H_{21}O_5^+$  at  $m/z$  245 in the linseed oil-flake white mixture

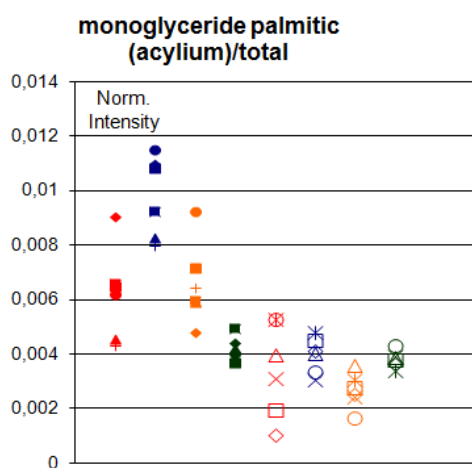


Figure C.19: Positive acylium ions of monoglyceride with palmitic acid  $C_{19}H_{37}O_3^+$  at  $m/z$  313 in the linseed oil-flake white mixture

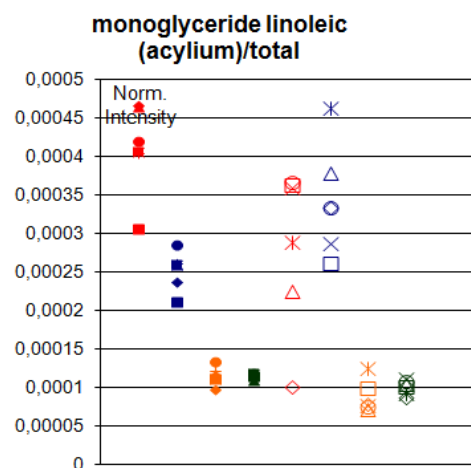


Figure C.20: Positive acylium ions of monoglyceride with linoleic acid  $C_{21}H_{37}O_3^+$  at  $m/z$  337 in the linseed oil-flake white mixture

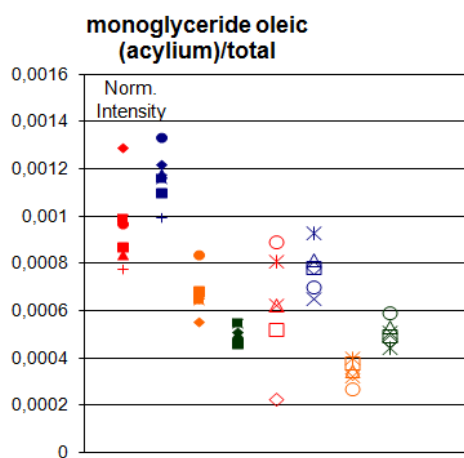


Figure C.21: Positive acylium ions of monoglyceride with oleic acid  $C_{21}H_{39}O_3^+$  at  $m/z$  339 in the linseed oil-flake white mixture

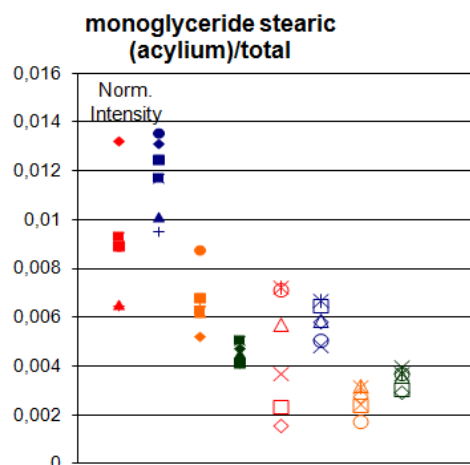


Figure C.22: Positive acylium ions of monoglyceride with stearic acid  $C_{21}H_{41}O_3^+$  at  $m/z$  341 in the linseed oil-flake white mixture

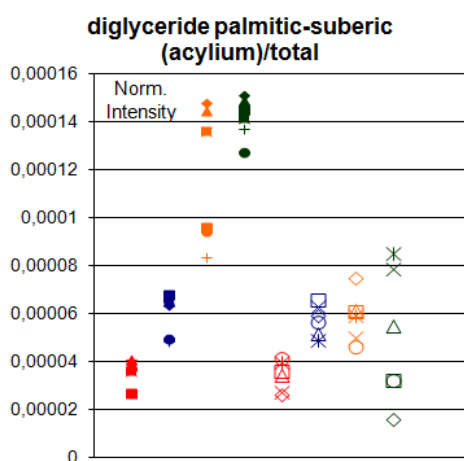


Figure C.23: Positive acylium ions of diglyceride with palmitic/suberic acid  $C_{27}H_{49}O_6^+$  at  $m/z$  469 in the linseed oil-flake white mixture

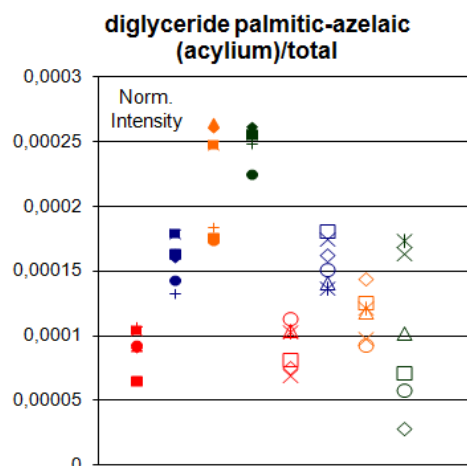


Figure C.24: Positive acylium ions of diglyceride with palmitic/azelaic acid  $C_{28}H_{51}O_6^+$  at  $m/z$  483 in the linseed oil-flake white mixture

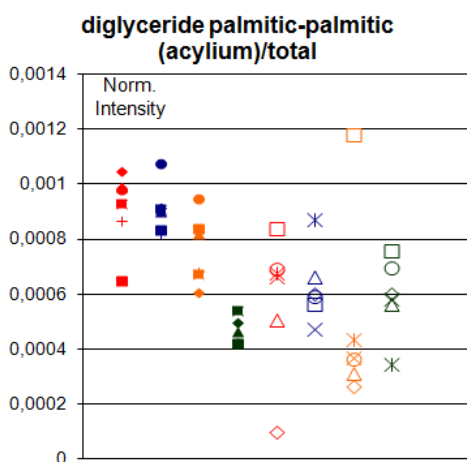


Figure C.25: Positive acylium ions of diglyceride with twice palmitic acid  $C_{35}H_{67}O_4^+$  at  $m/z$  551,5 in the linseed oil-flake white mixture

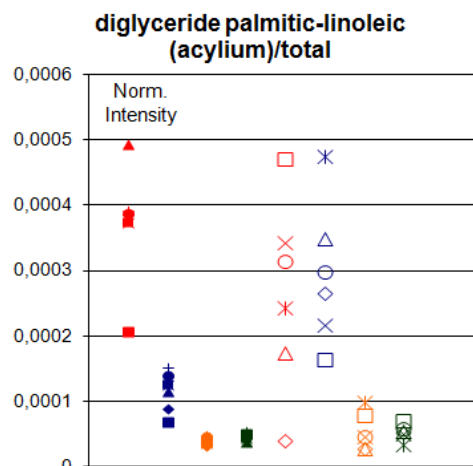


Figure C.26: Positive acylium ions of diglyceride with palmitic/linoleic acid  $C_{37}H_{67}O_4^+$  at  $m/z$  575,5 in the linseed oil-flake white mixture

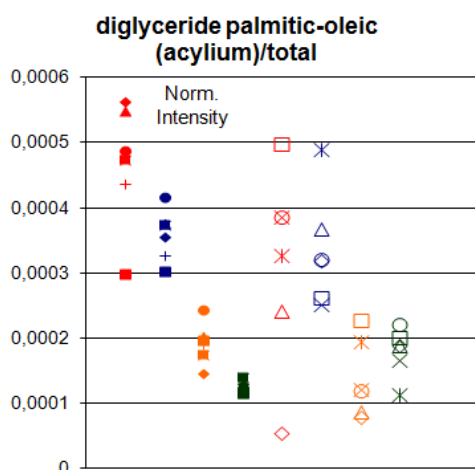


Figure C.27: Positive acylium ions of diglyceride with palmitic/oleic acid  $C_{37}H_{69}O_4^+$  at  $m/z$  577,5 in the linseed oil-flake white mixture

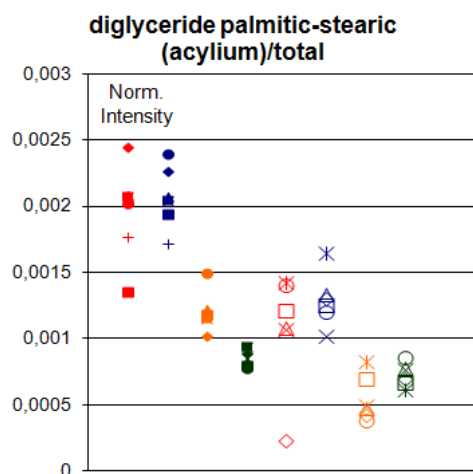


Figure C.28: Positive acylium ions of diglyceride with palmitic/stearic acid  $C_{37}H_{71}O_4^+$  at  $m/z$  579,5 in the linseed oil-flake white mixture

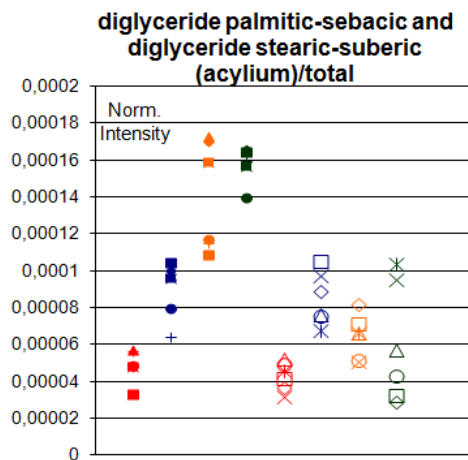


Figure C.29: Positive acylium ions of diglyceride with stearic/suberic acid and of diglyceride with palmitic/sebaric acid  $C_{29}H_{53}O_6^+$  at  $m/z$  497 in the linseed oil-flake white mixture

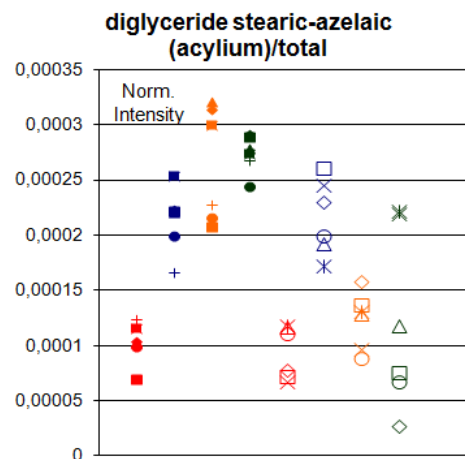


Figure C.30: Positive acylium ions of diglyceride with stearic/azelaic acid  $C_{30}H_{55}O_6^+$  at  $m/z$  511 in the linseed oil-flake white mixture

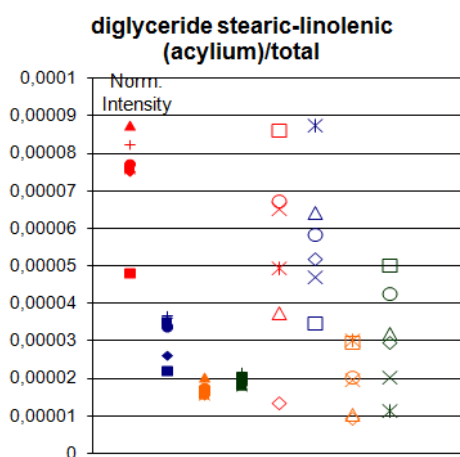


Figure C.31: Positive acylium ions of diglyceride with stearic/linolenic acid  $C_{39}H_{69}O_4^+$  at  $m/z$  601,5 in the linseed oil-flake white mixture

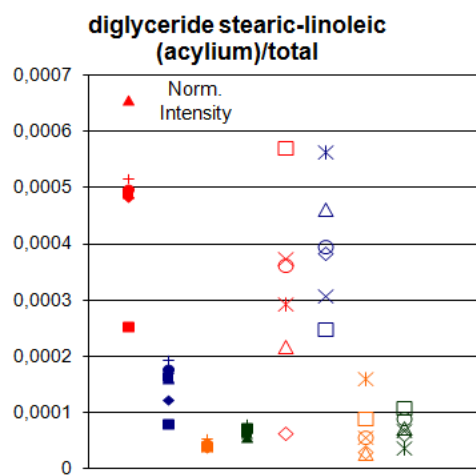


Figure C.32: Positive acylium ions of diglyceride with stearic/linoleic acid  $C_{39}H_{71}O_4^+$  at  $m/z$  603,5 in the linseed oil-flake white mixture

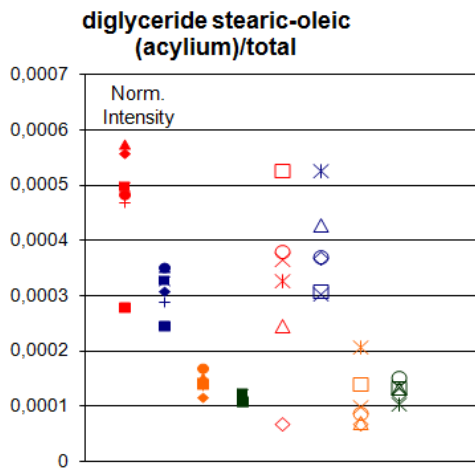


Figure C.33: Positive acylium ions of diglyceride with stearic/oleic acid  $C_{39}H_{73}O_4^+$  at  $m/z$  605,5 in the linseed oil-flake white mixture

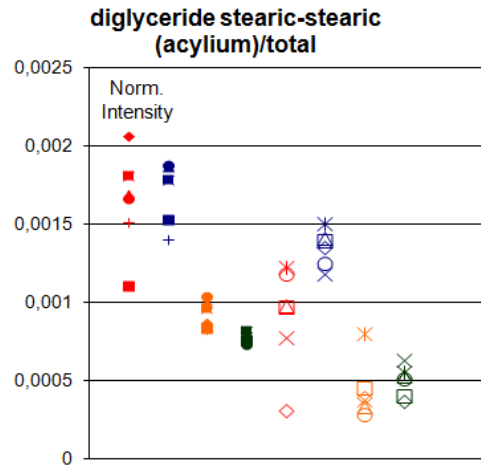


Figure C.34: Positive acylium ions of diglyceride with twice stearic acid  $C_{39}H_{75}O_4^+$  at  $m/z$  607,5 in the linseed oil-flake white mixture

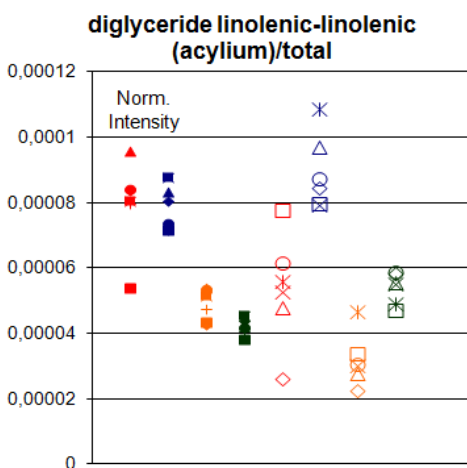


Figure C.35: Positive acylium ions of diglyceride with twice linolenic acid  $C_{39}H_{63}O_4^+$  at  $m/z$  595,5 in the linseed oil-flake white mixture

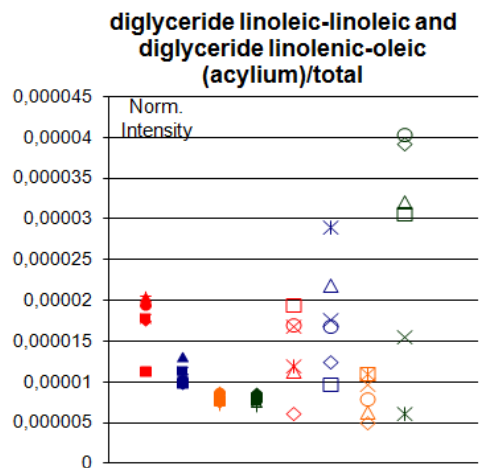


Figure C.36: Positive acylium ions of diglyceride with twice linoleic acid and of diglyceride with linolenic/oleic  $C_{39}H_{67}O_4^+$  at  $m/z$  599,5 in the linseed oil-flake white mixture

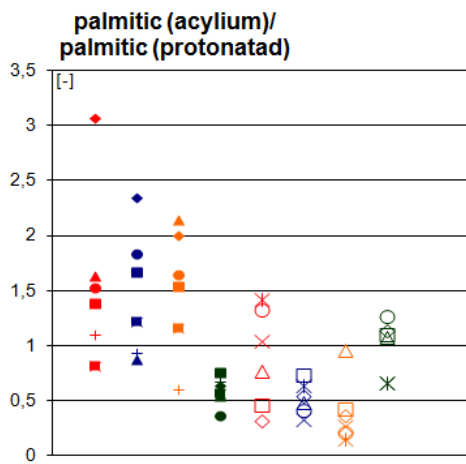


Figure C.37: Ratio of positive acylium and protonated ions of palmitic acid in the linseed oil-flake white mixture

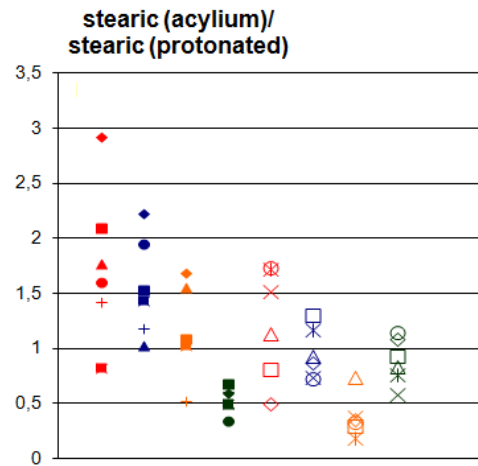


Figure C.38: Ratio of positive acylium and protonated ions of stearic acid in the linseed oil-flake white mixture

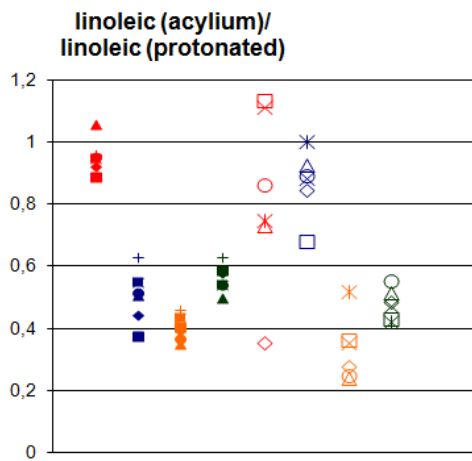


Figure C.39: Ratio of positive acylium and protonated ions of linoleic acid in the linseed oil-flake white mixture

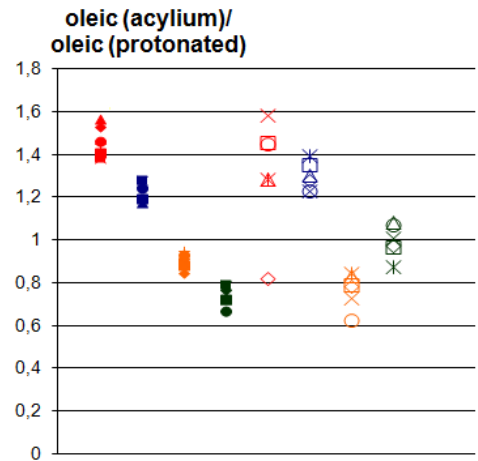


Figure C.40: Ratio of positive acylium and protonated ions of oleic acid in the linseed oil-flake white mixture



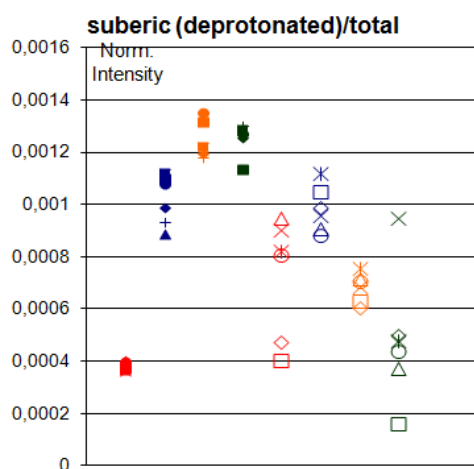


Figure C.44: Negative deprotonated ions of suberic acid  $C_8H_{13}O_4^-$  at  $m/z$  173 in the linseed oil-flake white mixture

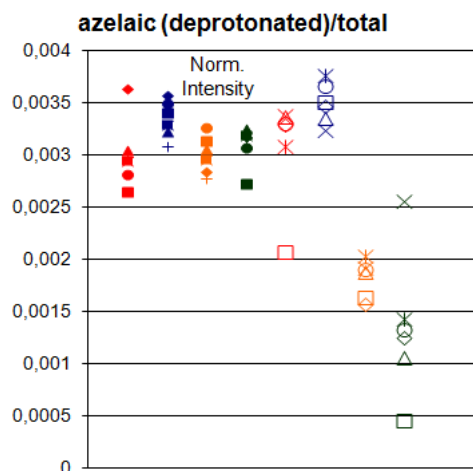


Figure C.45: Negative deprotonated ions of azelaic acid  $C_9H_{15}O_4^-$  at  $m/z$  187 in the linseed oil-flake white mixture

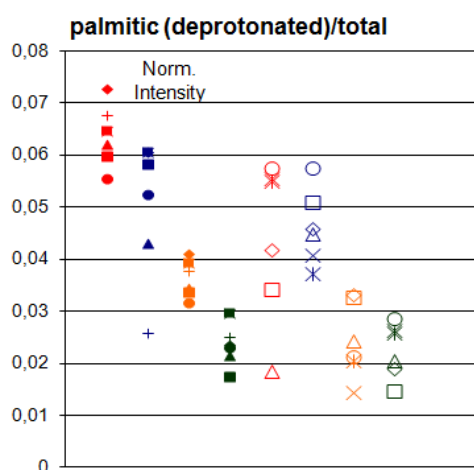


Figure C.46: Negative deprotonated ions of palmitic acid  $C_{16}H_{31}O_2^-$  at  $m/z$  255 in the linseed oil-flake white mixture

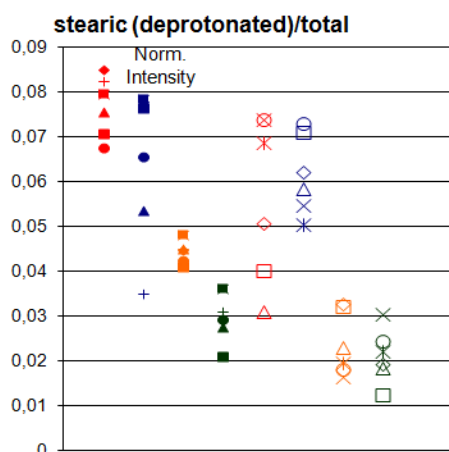


Figure C.47: Negative deprotonated ions of stearic acid  $C_{18}H_{35}O_2^-$  at  $m/z$  283 in the linseed oil-flake white mixture

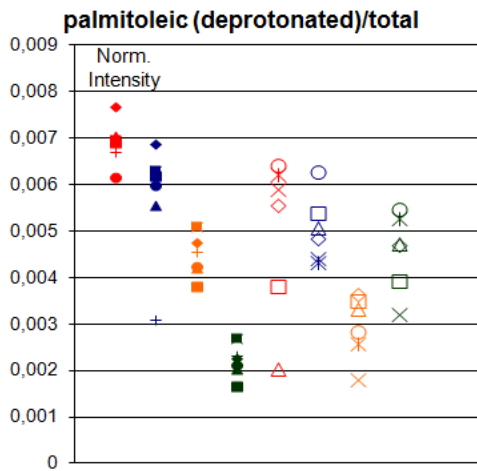


Figure C.48: Negative deprotonated ions of palmitoleic acid  $C_{16}H_{29}O_2^-$  at  $m/z$  253 in the linseed oil-flake white mixture

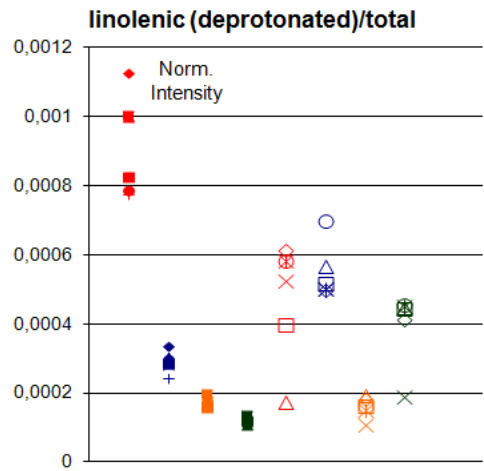


Figure C.49: Negative deprotonated ions of linolenic acid  $C_{18}H_{29}O_2^-$  at  $m/z$  277 in the linseed oil-flake white mixture

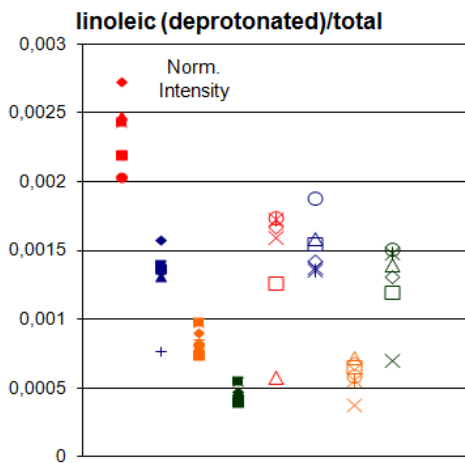


Figure C.50: Negative deprotonated ions of linoleic acid  $C_{18}H_{31}O_2^-$  at  $m/z$  279 in the linseed oil-flake white mixture

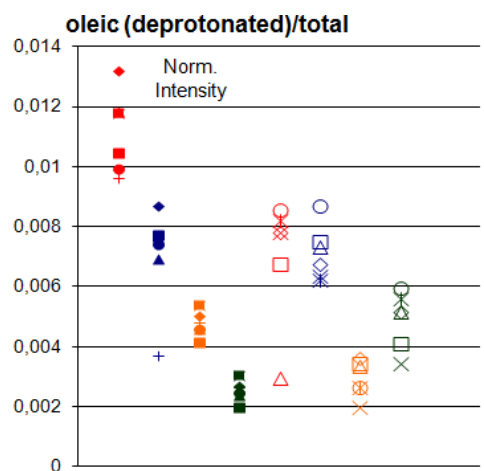


Figure C.51: Negative deprotonated ions of oleic acid  $C_{18}H_{33}O_2^-$  at  $m/z$  281 in the linseed oil-flake white mixture

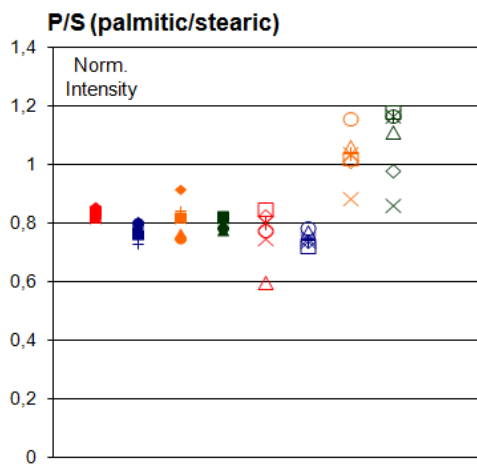


Figure C.52: Ratio of negative deprotonated palmitic and stearic acid ions in the linseed oil-flake white mixture

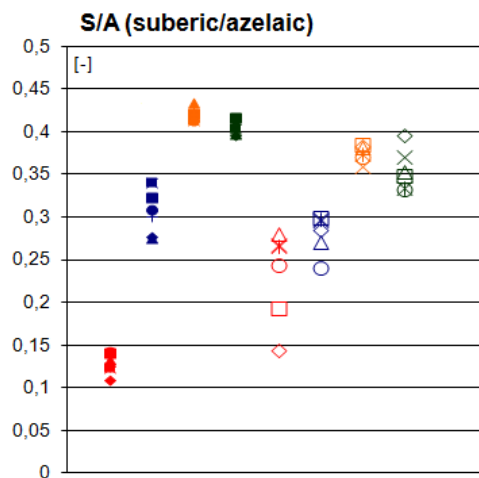


Figure C.53: Ratio of negative deprotonated suberic and azelaic acid ions in the linseed oil-flake white mixture

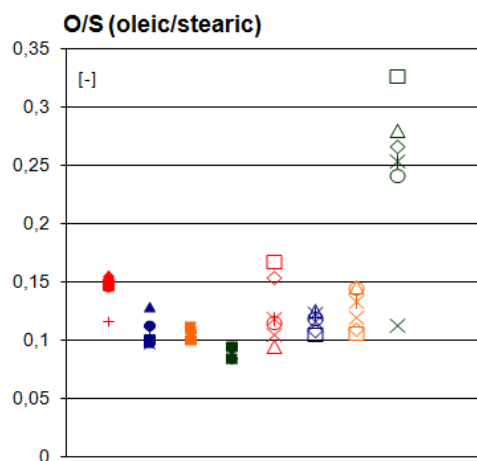


Figure C.54: Ratio of negative deprotonated oleic and stearic acid ions in the linseed oil-flake white mixture

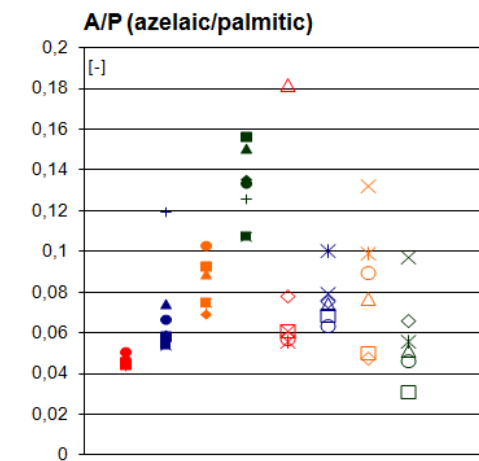


Figure C.55: Ratio of negative deprotonated azelaic and palmitic acid ions in the linseed oil-flake white mixture

## Appendix D

# Results of ToF-SIMS measurements of Linseed oil with Lead Carbonate

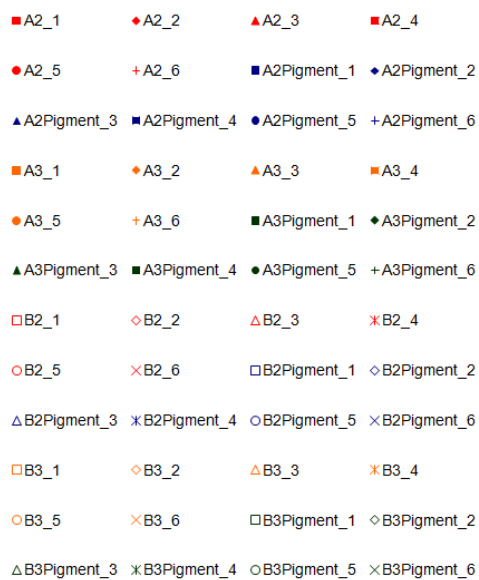


Figure D.1: Legend used for Figures D.2 to D.55

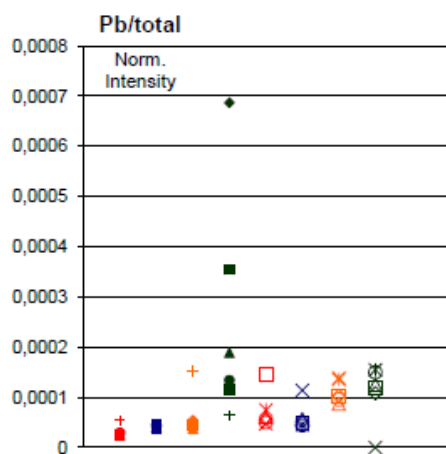


Figure D.2: Positive  $Pb^+$  ions in the linseed oil-lead carbonate mixture at  $m/z$  208

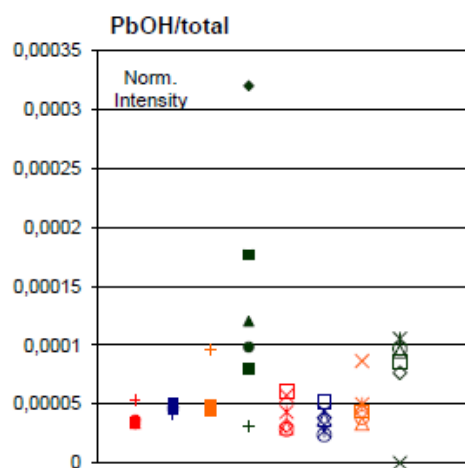


Figure D.3: Positive  $PbOH^+$  ions in the linseed oil-lead carbonate mixture at  $m/z$  225

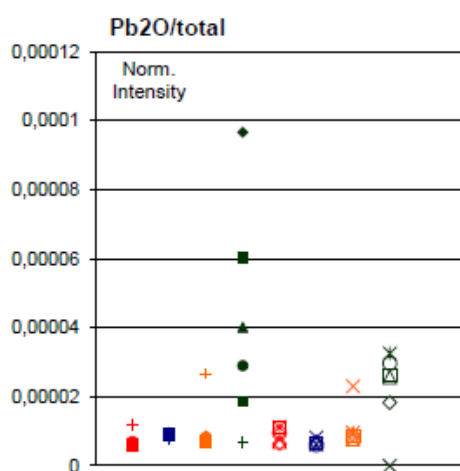


Figure D.4: Positive  $Pb_2O^+$  ions in the linseed oil-lead carbonate mixture at  $m/z$  432

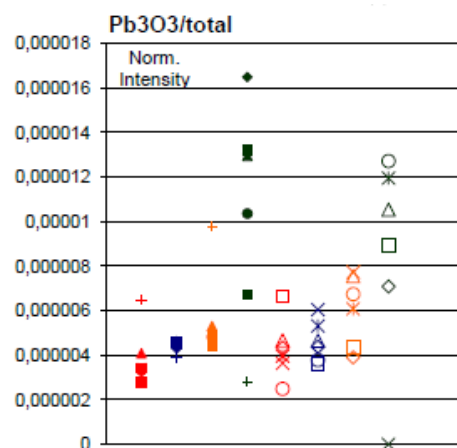


Figure D.5: Positive  $Pb_3O_3^+$  ions in the linseed oil-lead carbonate mixture at  $m/z$  672

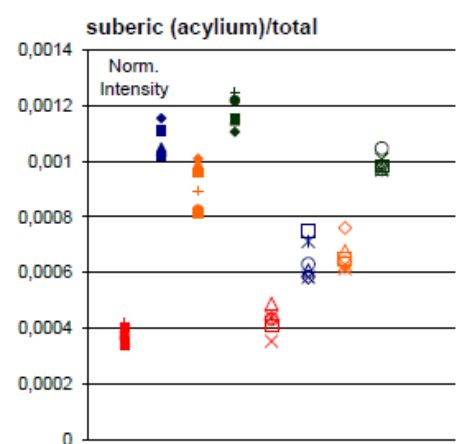


Figure D.6: Positive acylium ions of suberic acid,  $C_8H_{13}O_3^+$  at  $m/z$  157 in the linseed oil-lead carbonate mixture

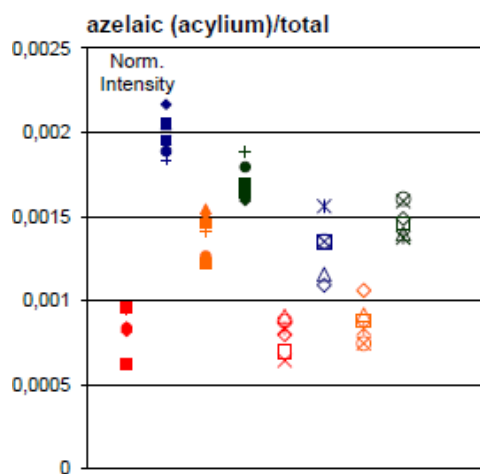


Figure D.7: Positive acylium ions of azelaic acid  $C_9H_{15}O_3^+$  at  $m/z$  171 in the linseed oil-lead carbonate mixture

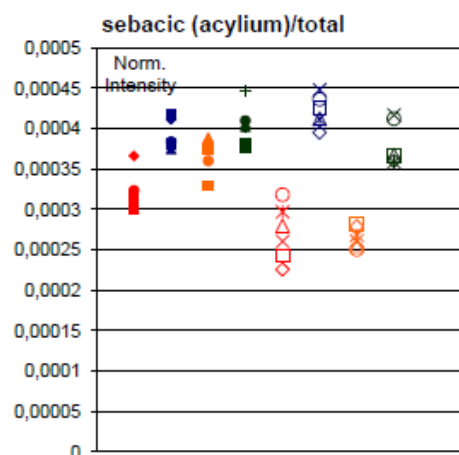


Figure D.8: Positive acylium ions of sebacic acid  $C_{10}H_{17}O_3^+$  at  $m/z$  185 in the linseed oil-lead carbonate mixture

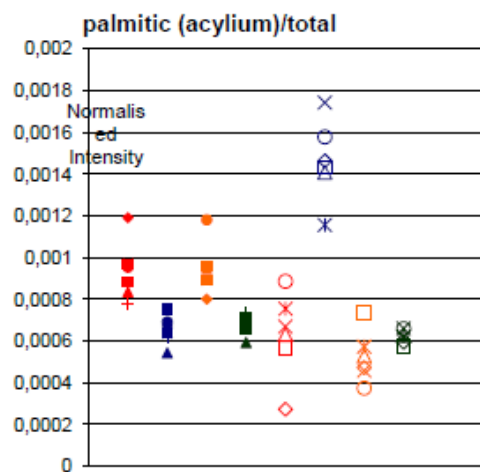


Figure D.9: Positive acylium ions of palmitic acid  $C_{16}H_{31}O^+$  at  $m/z$  239 in the linseed oil-lead carbonate mixture

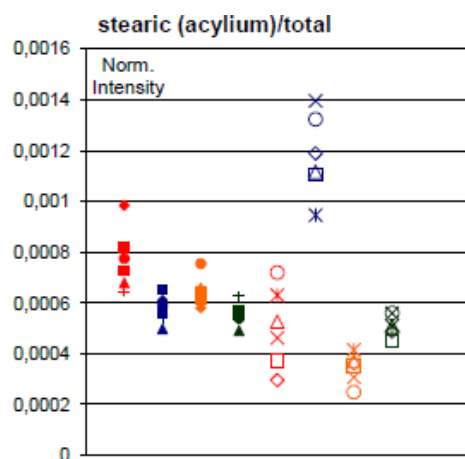


Figure D.10: Positive acylium ions of stearic acid  $C_{18}H_{35}O^+$  at  $m/z$  267 in the linseed oil-lead carbonate mixture

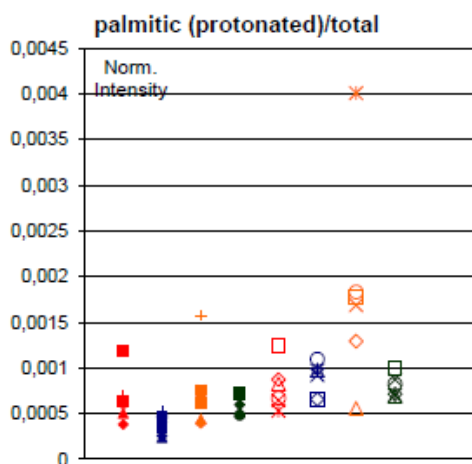


Figure D.11: Positive protonated ions of palmitic acid  $C_{16}H_{33}O_2^+$  at  $m/z$  257 in the linseed oil-lead carbonate mixture

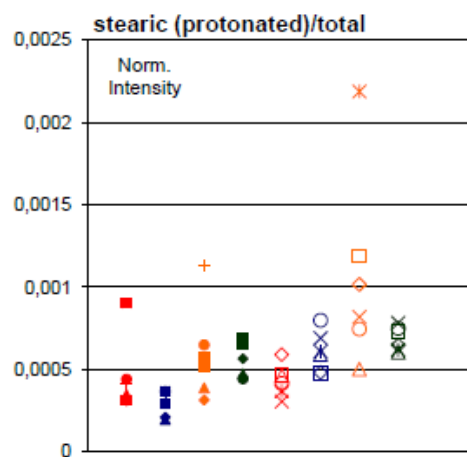


Figure D.12: Positive protonated ions of stearic acid  $C_{18}H_{37}O_2^+$  at  $m/z$  285 in the linseed oil-lead carbonate mixture

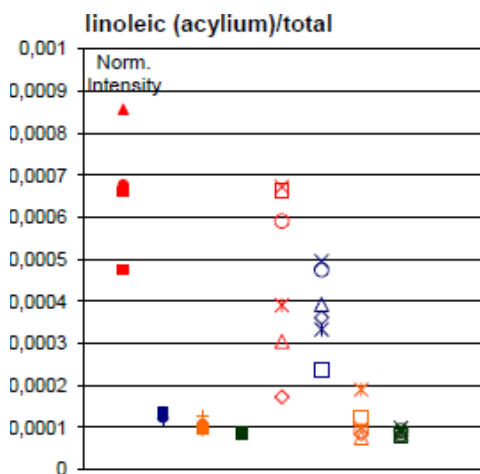


Figure D.13: Positive acylium ions of linoleic acid  $C_{18}H_{31}O^+$  at  $m/z$  263 in the linseed oil-lead carbonate mixture

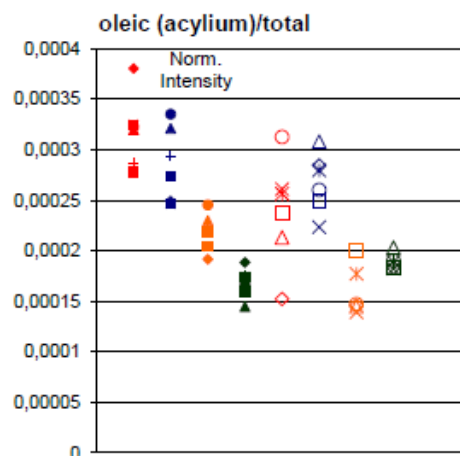
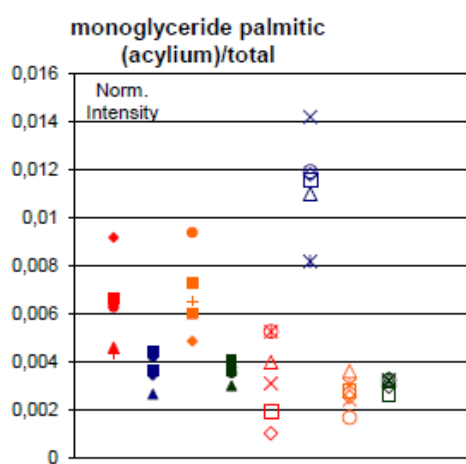


Figure D.14: Positive acylium ions of oleic acid  $C_{18}H_{33}O^+$  at  $m/z$  265 in the linseed oil-lead carbonate mixture





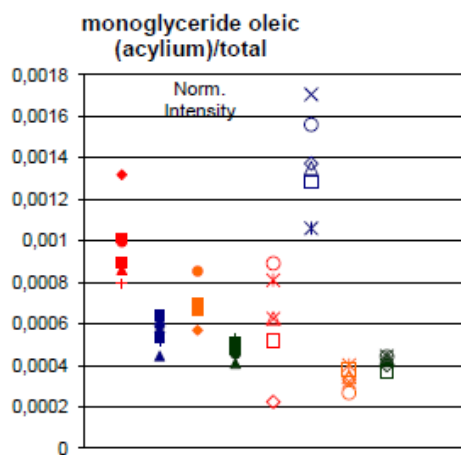


Figure D.21: Positive acylium ions of monoglyceride with oleic acid  $C_{21}H_{39}O_3^+$  at  $m/z$  339 in the linseed oil-lead carbonate mixture

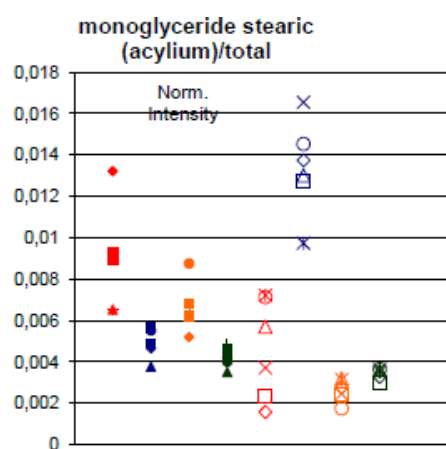


Figure D.22: Positive acylium ions of monoglyceride with stearic acid  $C_{21}H_{41}O_3^+$  at  $m/z$  341 in the linseed oil-lead carbonate mixture

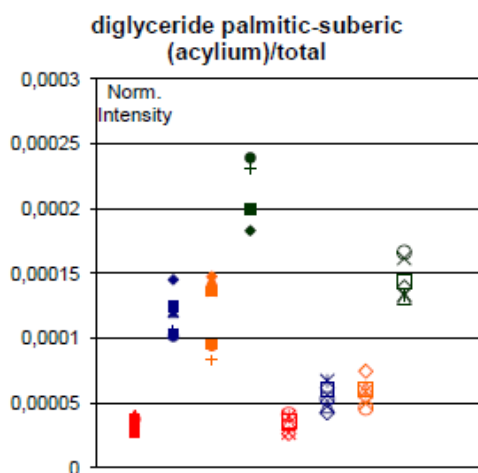


Figure D.23: Positive acylium ions of diglyceride with palmitic/suberic acid  $C_{27}H_{49}O_6^+$  at  $m/z$  469 in the linseed oil-lead carbonate mixture

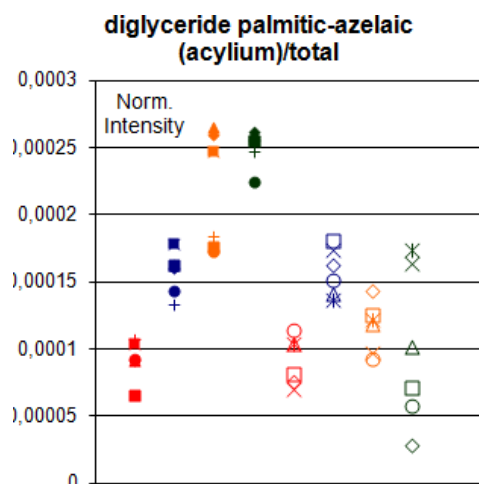


Figure D.24: Positive acylium ions of diglyceride with palmitic/azelaic acid  $C_{28}H_{51}O_6^+$  at  $m/z$  483 in the linseed oil-lead carbonate mixture

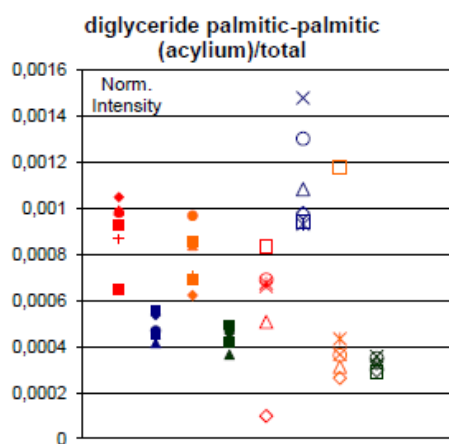


Figure D.25: Positive acylium ions of diglyceride with twice palmitic acid  $C_{35}H_{67}O_4^+$  at  $m/z$  551,5 in the linseed oil-lead carbonate mixture

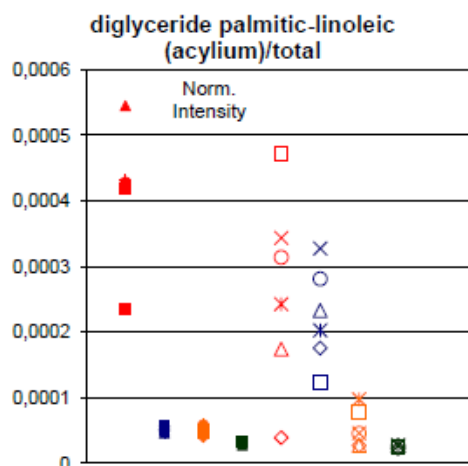


Figure D.26: Positive acylium ions of diglyceride with palmitic/linoleic acid  $C_{37}H_{67}O_4^+$  at  $m/z$  575,5 in the linseed oil-lead carbonate mixture

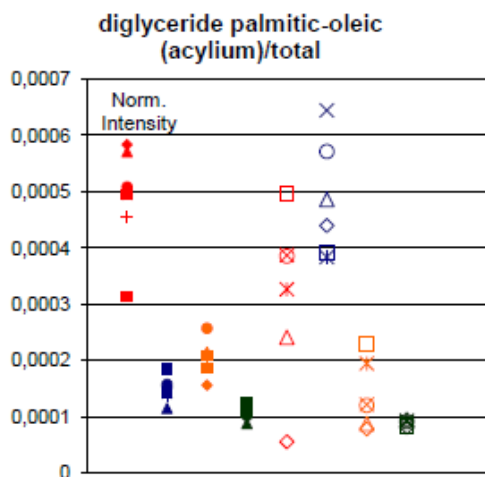


Figure D.27: Positive acylium ions of diglyceride with palmitic/oleic acid  $C_{37}H_{69}O_4^+$  at  $m/z$  577,5 in the linseed oil-lead carbonate mixture

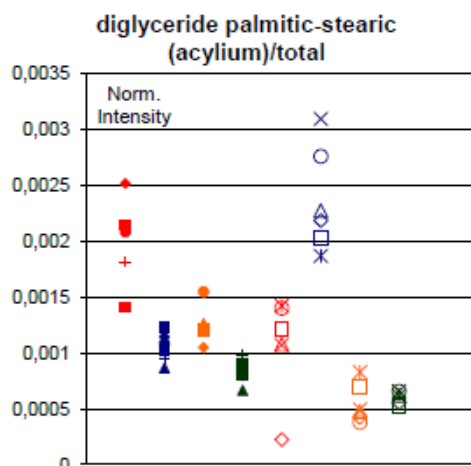


Figure D.28: Positive acylium ions of diglyceride with palmitic/stearic acid  $C_{37}H_{71}O_4^+$  at  $m/z$  579,5 in the linseed oil-lead carbonate mixture

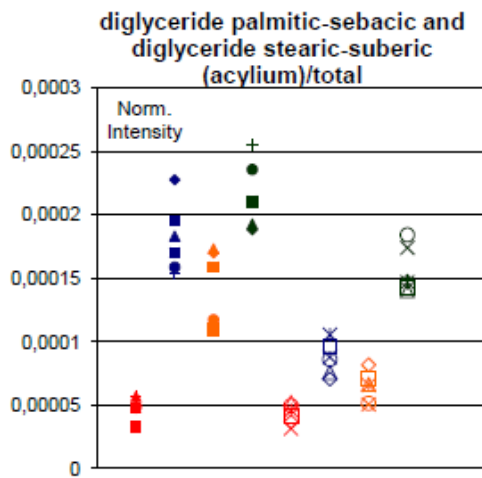


Figure D.29: Positive acylium ions of diglyceride with stearic/suberic acid and of diglyceride with palmitic/sebacic acid  $C_{29}H_{53}O_6^+$  at  $m/z$  497 in the linseed oil-lead carbonate mixture

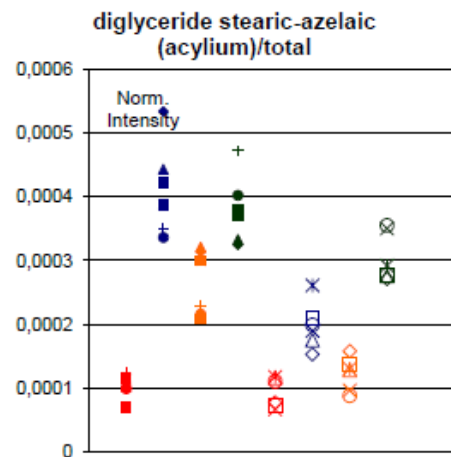


Figure D.30: Positive acylium ions of diglyceride with stearic/azelaic acid  $C_{30}H_{55}O_6^+$  at  $m/z$  511 in the linseed oil-lead carbonate mixture

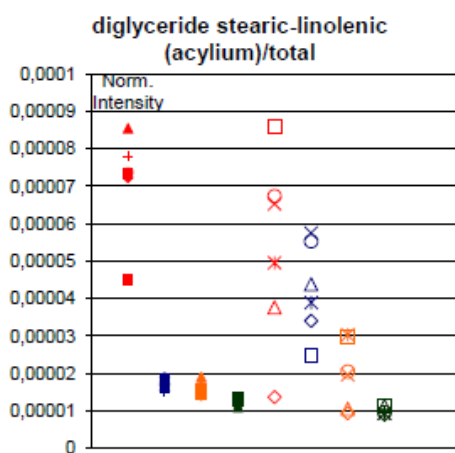


Figure D.31: Positive acylium ions of diglyceride with stearic/linolenic acid  $C_{39}H_{69}O_4^+$  at  $m/z$  601,5 in the linseed oil-lead carbonate mixture

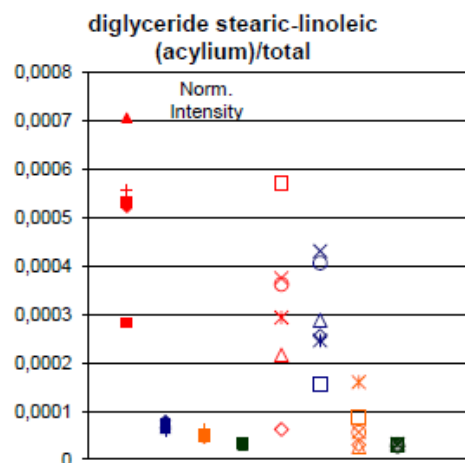


Figure D.32: Positive acylium ions of diglyceride with stearic/linoleic acid  $C_{39}H_{71}O_4^+$  at  $m/z$  603,5 in the linseed oil-lead carbonate mixture

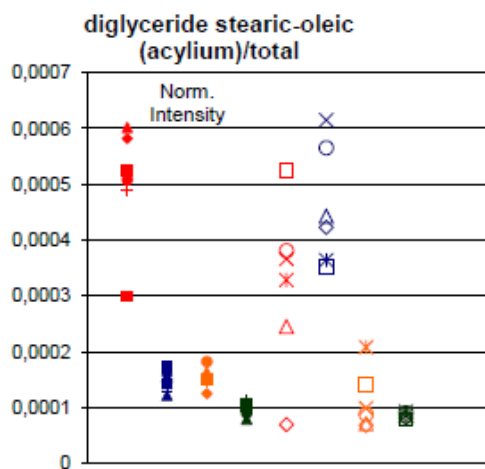


Figure D.33: Positive acylium ions of diglyceride with stearic/oleic acid  $C_{39}H_{73}O_4^+$  at  $m/z$  605,5 in the linseed oil-lead carbonate mixture

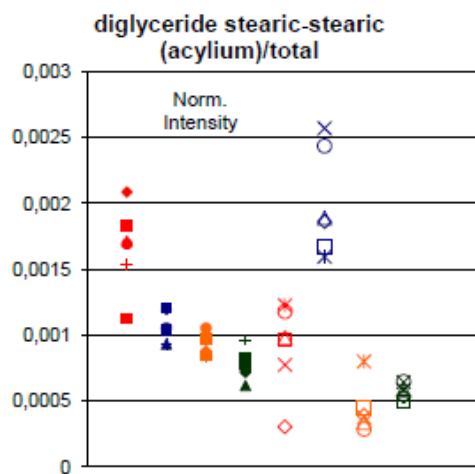


Figure D.34: Positive acylium ions of diglyceride with twice stearic acid  $C_{39}H_{75}O_4^+$  at  $m/z$  607,5 in the linseed oil-lead carbonate mixture

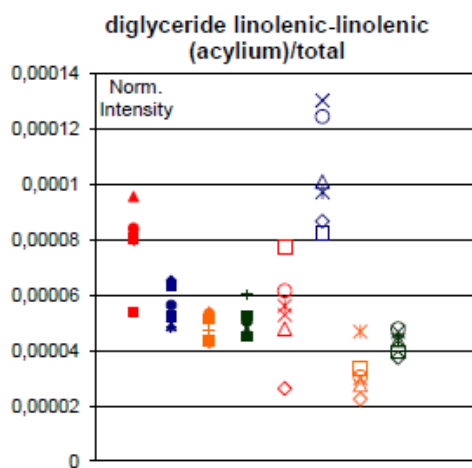


Figure D.35: Positive acylium ions of diglyceride with twice linolenic acid  $C_{39}H_{63}O_4^+$  at  $m/z$  595,5 in the linseed oil-lead carbonate mixture

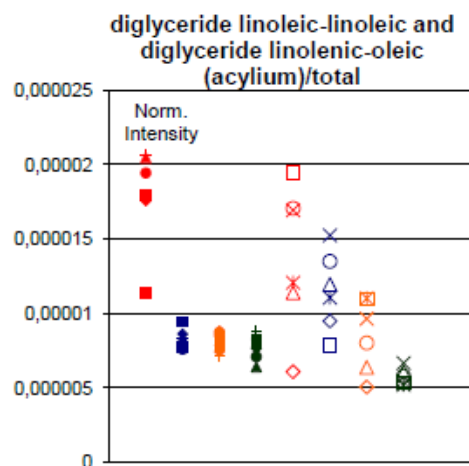


Figure D.36: Positive acylium ions of diglyceride with twice linoleic acid and of diglyceride with linolenic/oleic  $C_{39}H_{67}O_4^+$  at  $m/z$  599,5 in the linseed oil-lead carbonate mixture

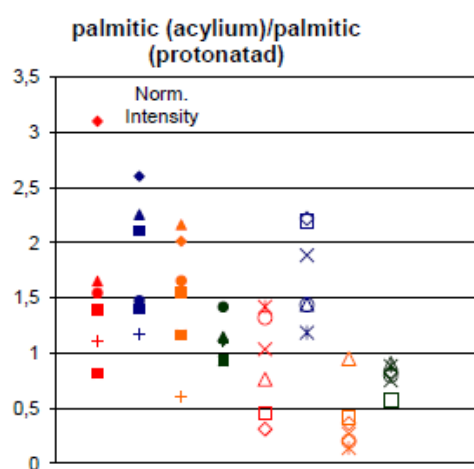


Figure D.37: Ratio of positive acylium and protonated ions of palmitic acid in the linseed oil-lead carbonate mixture

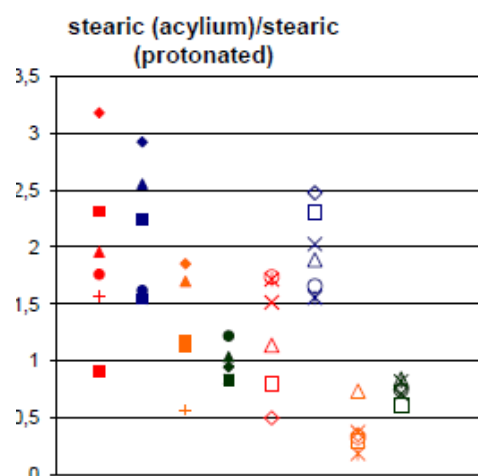


Figure D.38: Ratio of positive acylium and protonated ions of stearic acid in the linseed oil-lead carbonate mixture

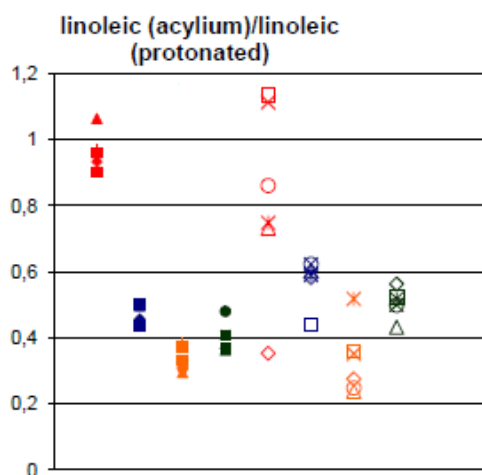


Figure D.39: Ratio of positive acylium and protonated ions of linoleic acid in the linseed oil-lead carbonate mixture

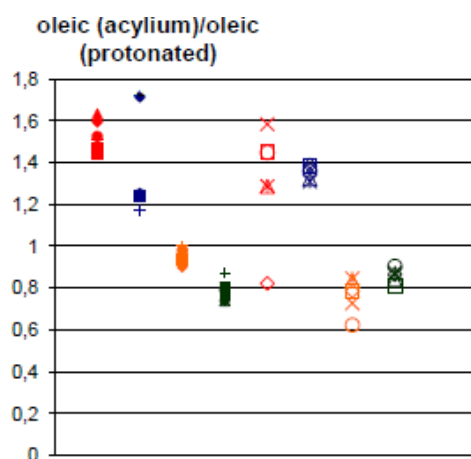


Figure D.40: Ratio of positive acylium and protonated ions of oleic acid in the linseed oil-lead carbonate mixture

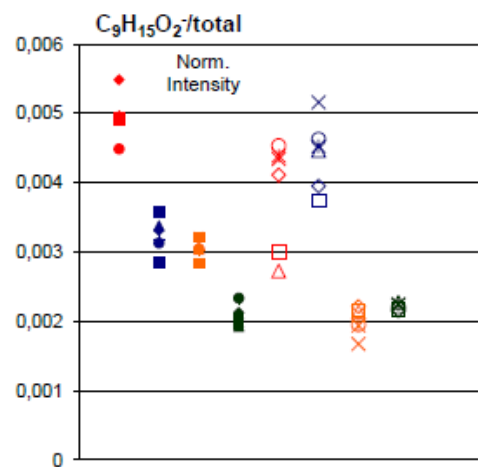


Figure D.41: Negative ions of aliphatic chain fragment with formula  $C_2H_3(CH_2)_6COO^-$  at  $m/z$  155 in the linseed oil-lead carbonate mixture

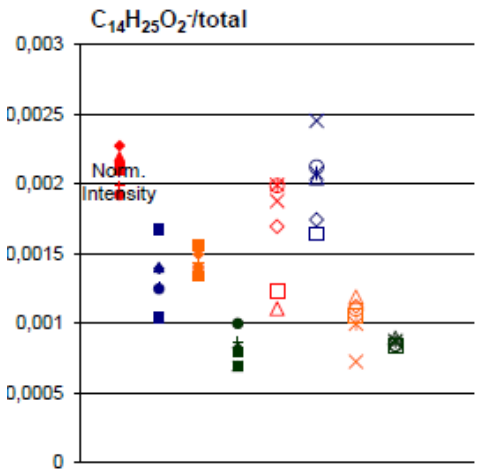


Figure D.42: Negative ions of aliphatic chain fragment with formula  $C_2H_3(CH_2)_{11}COO^-$  at  $m/z$  225 in the linseed oil-lead carbonate mixture

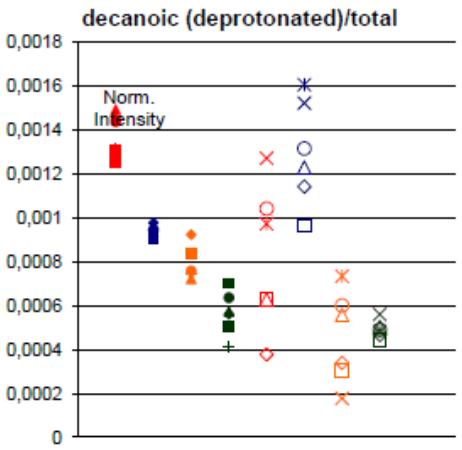


Figure D.43: Negative deprotonated ions of decanoic acid  $C_{10}H_{19}O_2^-$  at  $m/z$  171 in the linseed oil-lead carbonate mixture

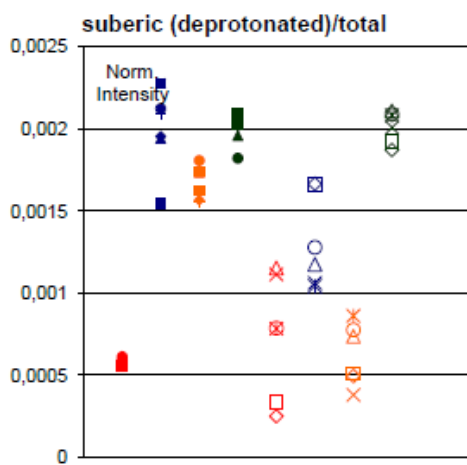


Figure D.44: Negative deprotonated ions of suberic acid  $C_8H_{13}O_4^-$  at  $m/z$  173 in the linseed oil-lead carbonate mixture

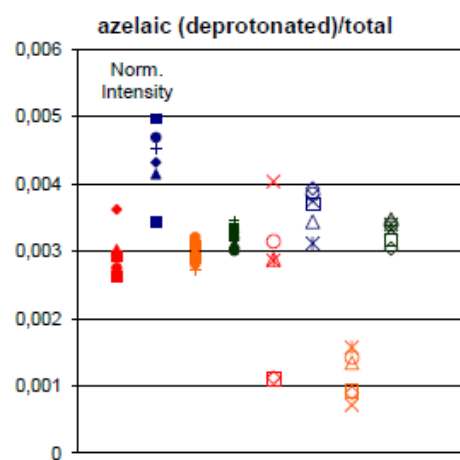


Figure D.45: Negative deprotonated ions of azelaic acid  $C_9H_{15}O_4^-$  at  $m/z$  187 in the linseed oil-lead carbonate mixture

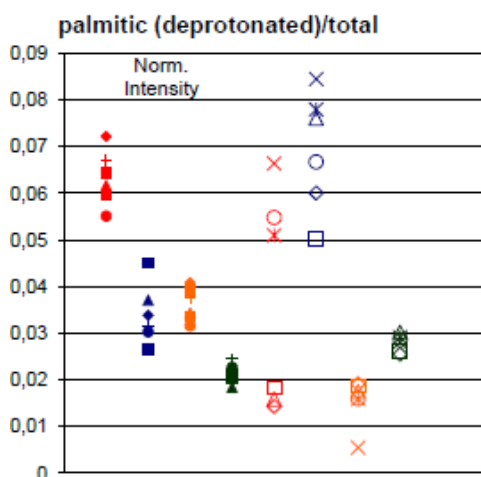


Figure D.46: Negative deprotonated ions of palmitic acid  $C_{16}H_{31}O_2^-$  at  $m/z$  255 in the linseed oil-lead carbonate mixture

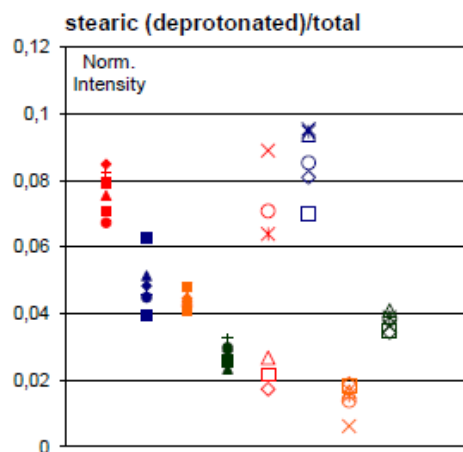


Figure D.47: Negative deprotonated ions of stearic acid  $C_{18}H_{35}O_2^-$  at  $m/z$  283 in the linseed oil-lead carbonate mixture

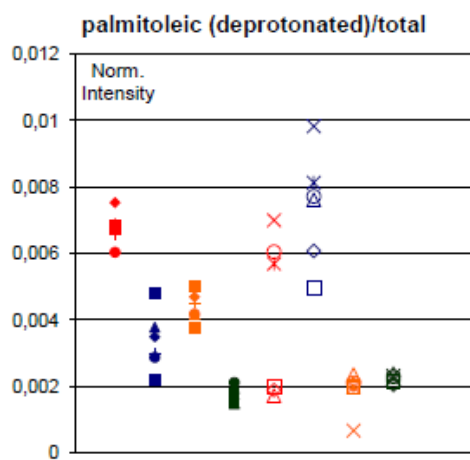


Figure D.48: Negative deprotonated ions of palmitoleic acid  $C_{16}H_{29}O_2^-$  at  $m/z$  253 in the linseed oil-lead carbonate mixture

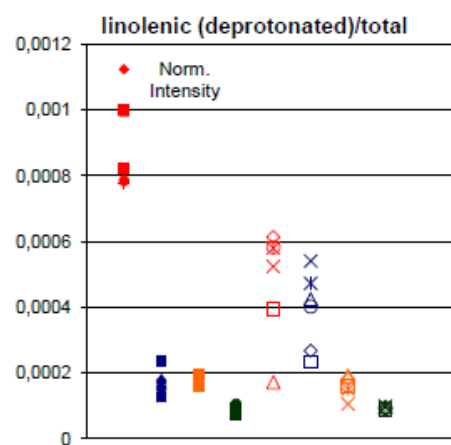


Figure D.49: Negative deprotonated ions of linolenic acid  $C_{18}H_{29}O_2^-$  at  $m/z$  277 in the linseed oil-lead carbonate mixture

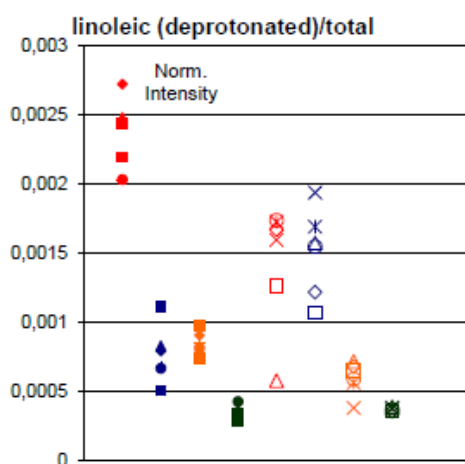


Figure D.50: Negative deprotonated ions of linoleic acid  $C_{18}H_{31}O_2^-$  at  $m/z$  279 in the linseed oil-lead carbonate mixture

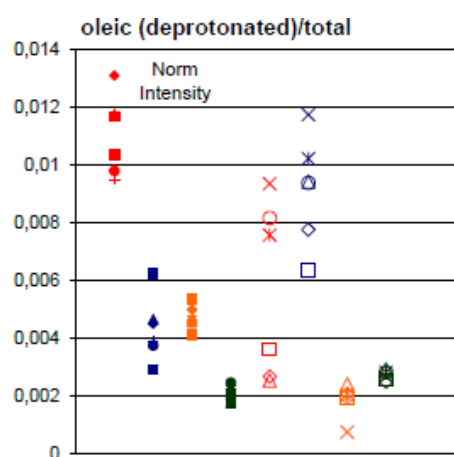


Figure D.51: Negative deprotonated ions of oleic acid  $C_{18}H_{33}O_2^-$  at  $m/z$  281 in the linseed oil-lead carbonate mixture



# Appendix E

## Results of ToF-SIMS measurements of Linseed oil with Lead Chloride

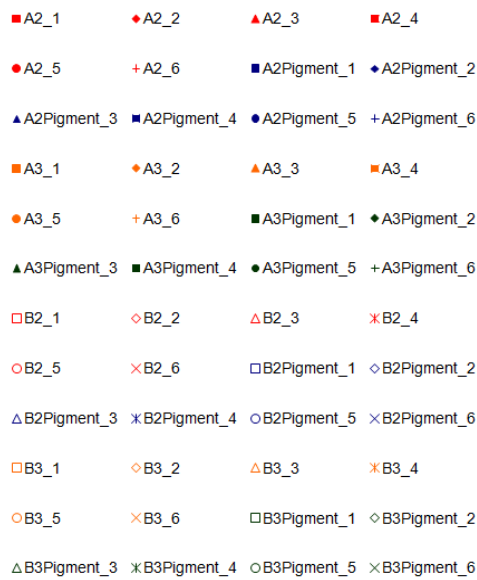


Figure E.1: Legend used for Figures E.2 to E.55

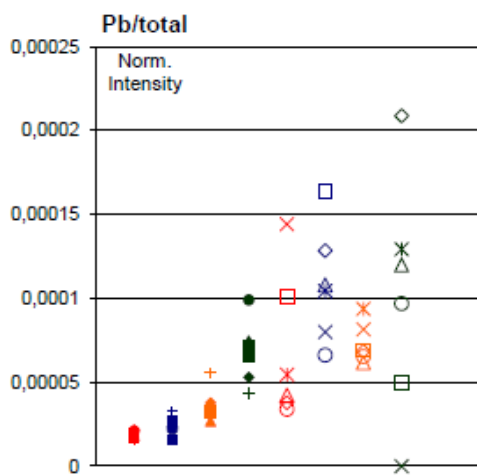


Figure E.2: Positive  $Pb^+$  ions in the linseed oil-lead chloride mixture at  $m/z$  208

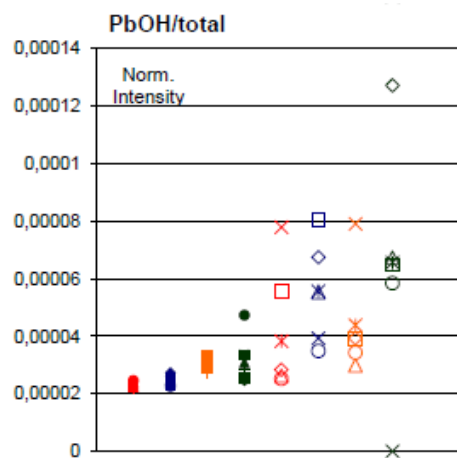


Figure E.3: Positive  $PbOH^+$  ions in the linseed oil-lead chloride mixture at  $m/z$  225

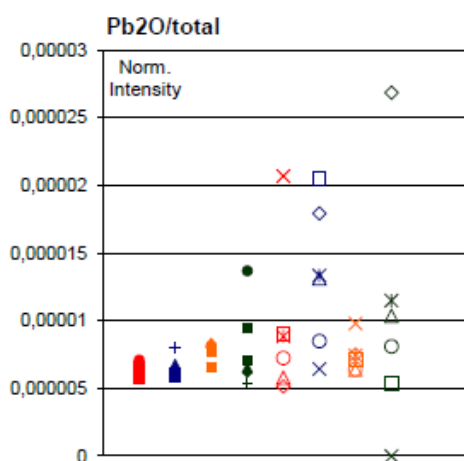


Figure E.4: Positive  $Pb_2O^+$  ions in the linseed oil-lead chloride mixture at  $m/z$  432

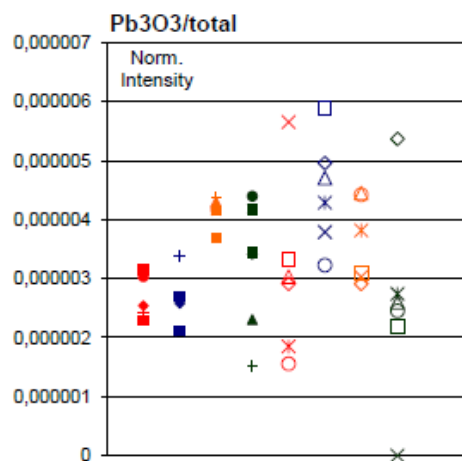


Figure E.5: Positive  $Pb_3O_3^+$  ions in the linseed oil-lead chloride mixture at  $m/z$  672

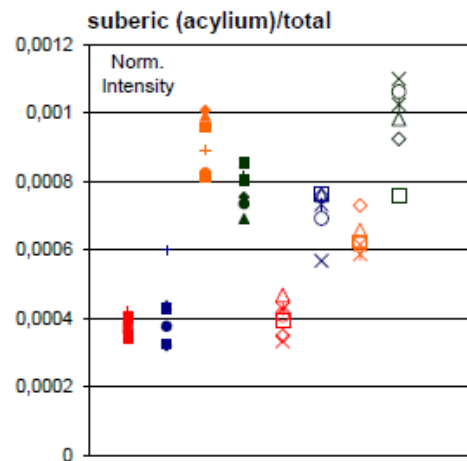


Figure E.6: Positive acylium ions of suberic acid,  $C_8H_{13}O_3^+$  at  $m/z$  157 in the linseed oil-lead chloride mixture

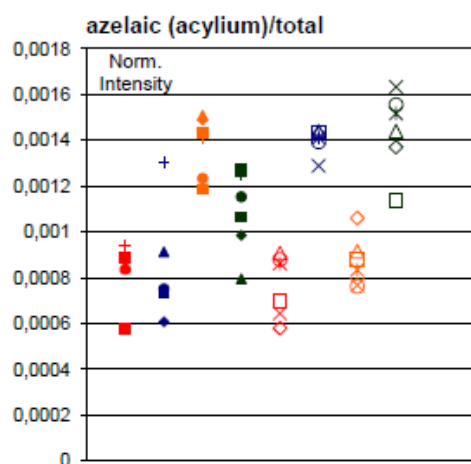


Figure E.7: Positive acylium ions of azelaic acid  $C_9H_{15}O_3^+$  at  $m/z$  171 in the linseed oil-lead chloride mixture

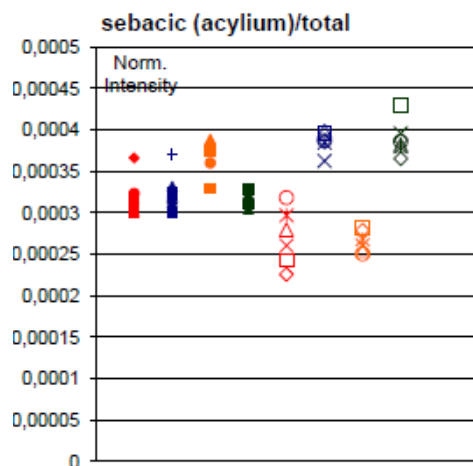


Figure E.8: Positive acylium ions of sebacic acid  $C_{10}H_{17}O_3^+$  at  $m/z$  185 in the linseed oil-lead chloride mixture

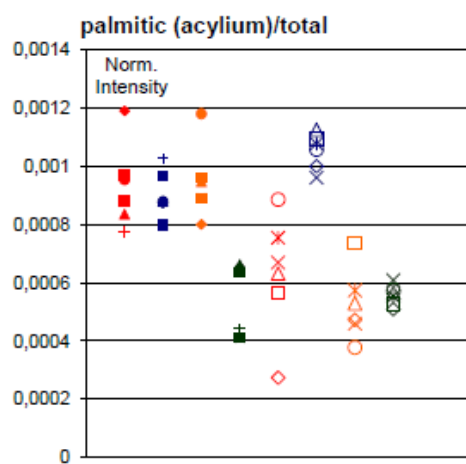


Figure E.9: Positive acylium ions of palmitic acid  $C_{16}H_{31}O^+$  at  $m/z$  239 in the linseed oil-lead chloride mixture

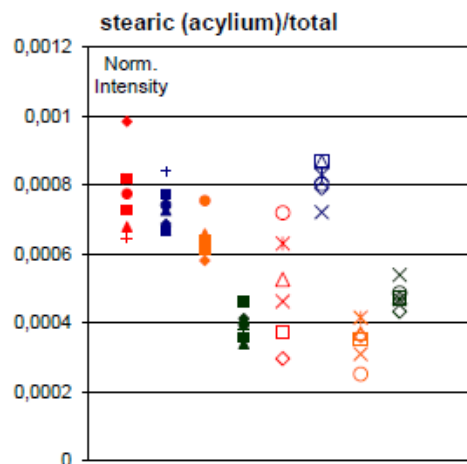


Figure E.10: Positive acylium ions of stearic acid  $C_{18}H_{35}O^+$  at  $m/z$  267 in the linseed oil-lead chloride mixture

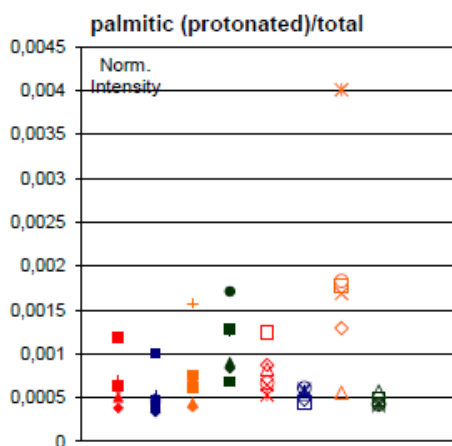


Figure E.11: Positive protonated ions of palmitic acid  $C_{16}H_{33}O_2^+$  at  $m/z$  257 in the linseed oil-lead chloride mixture

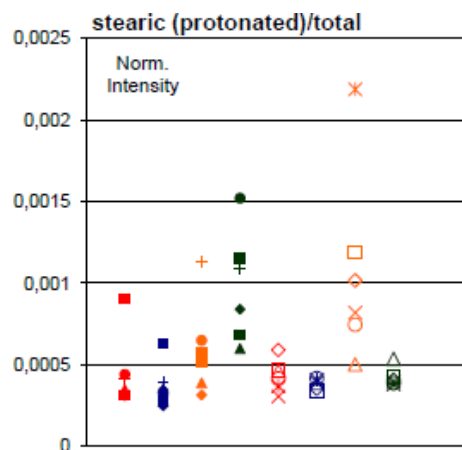


Figure E.12: Positive protonated ions of stearic acid  $C_{18}H_{37}O_2^+$  at  $m/z$  285 in the linseed oil-lead chloride mixture

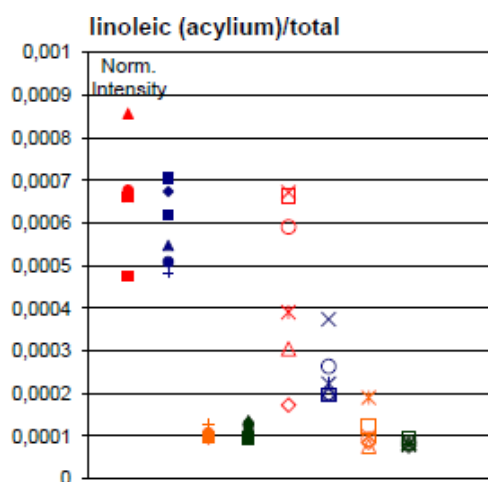


Figure E.13: Positive acylium ions of linoleic acid  $C_{18}H_{31}O^+$  at  $m/z$  263 in the linseed oil-lead chloride mixture

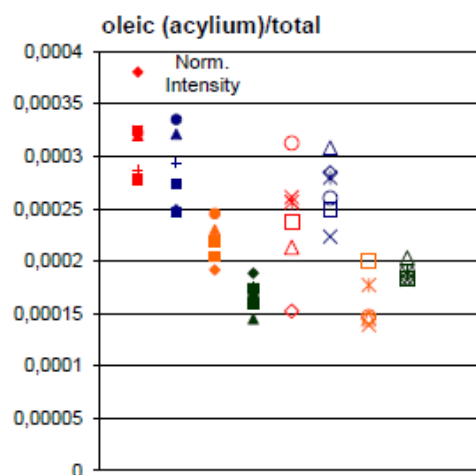


Figure E.14: Positive acylium ions of oleic acid  $C_{18}H_{33}O^+$  at  $m/z$  265 in the linseed oil-lead chloride mixture

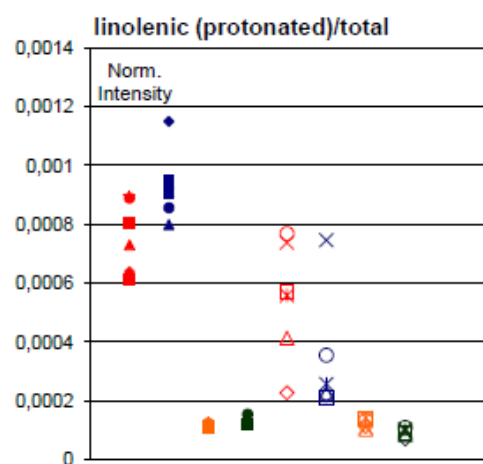


Figure E.15: Positive protonated ions of linolenic acid  $C_{18}H_{31}O_2^+$  at  $m/z$  279 in the linseed oil-lead chloride mixture

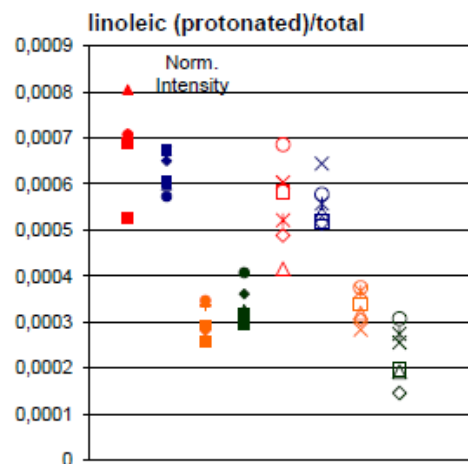


Figure E.16: Positive protonated ions of linoleic acid  $C_{18}H_{33}O_2^+$  at  $m/z$  281 in the linseed oil-lead chloride mixture

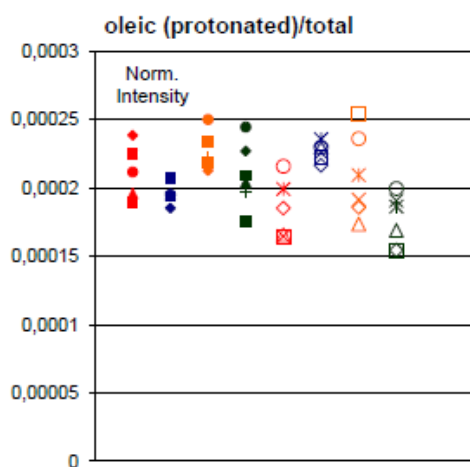


Figure E.17: Positive protonated ions of oleic acid  $C_{18}H_{35}O_2^+$  at  $m/z$  283 in the linseed oil-lead chloride mixture

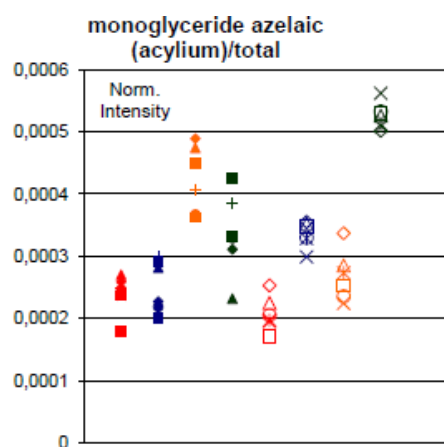


Figure E.18: Positive acylium ions of monoglyceride with azelaic acid  $C_{12}H_{21}O_5^+$  at  $m/z$  245 in the linseed oil-lead chloride mixture

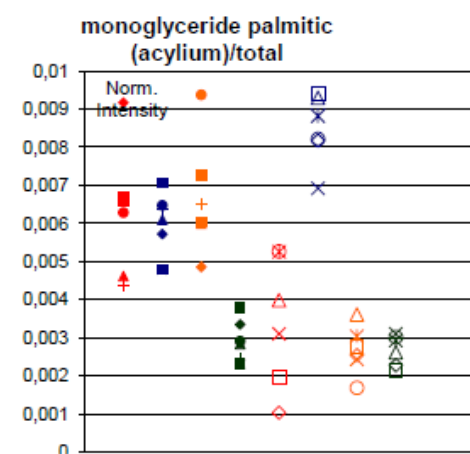


Figure E.19: Positive acylium ions of monoglyceride with palmitic acid  $C_{19}H_{37}O_3^+$  at  $m/z$  313 in the linseed oil-lead chloride mixture

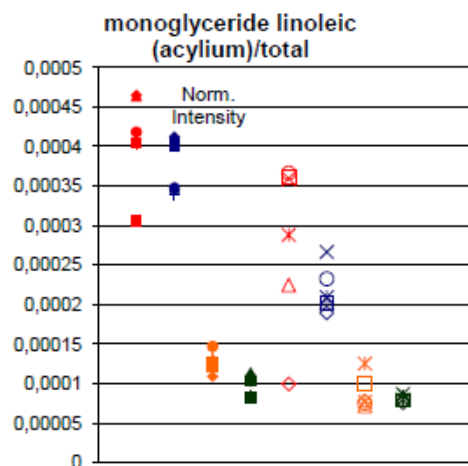


Figure E.20: Positive acylium ions of monoglyceride with linoleic acid  $C_{21}H_{37}O_3^+$  at  $m/z$  337 in the linseed oil-lead chloride mixture

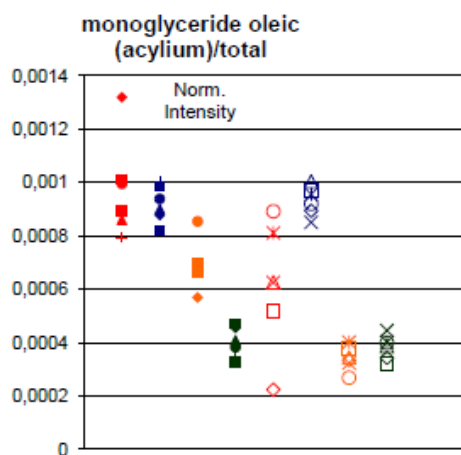


Figure E.21: Positive acylium ions of monoglyceride with oleic acid  $C_{21}H_{39}O_3^+$  at  $m/z$  339 in the linseed oil-lead chloride mixture

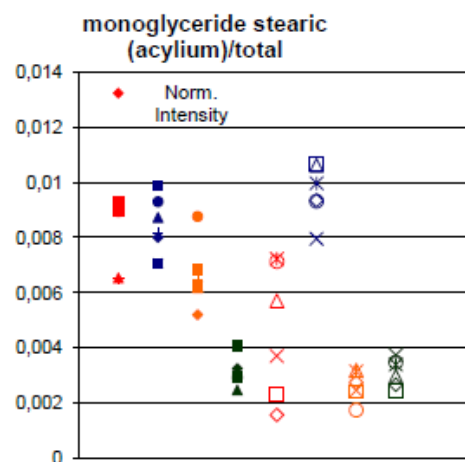


Figure E.22: Positive acylium ions of monoglyceride with stearic acid  $C_{21}H_{41}O_3^+$  at  $m/z$  341 in the linseed oil-lead chloride mixture

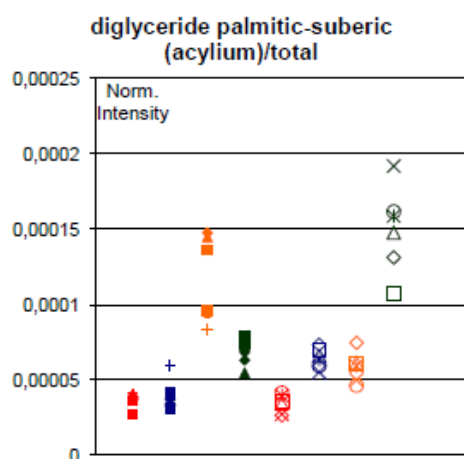


Figure E.23: Positive acylium ions of diglyceride with palmitic/suberic acid  $C_{27}H_{49}O_6^+$  at  $m/z$  469 in the linseed oil-lead chloride mixture

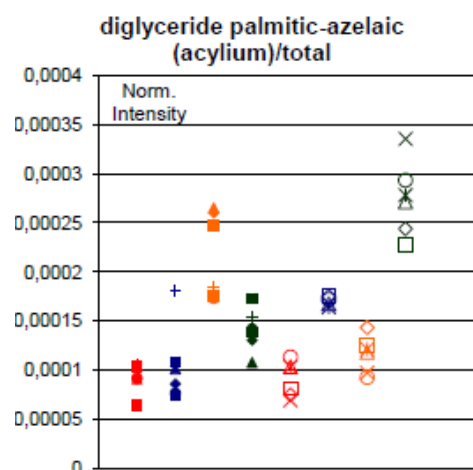


Figure E.24: Positive acylium ions of diglyceride with palmitic/azelaic acid  $C_{28}H_{51}O_6^+$  at  $m/z$  483 in the linseed oil-lead chloride mixture

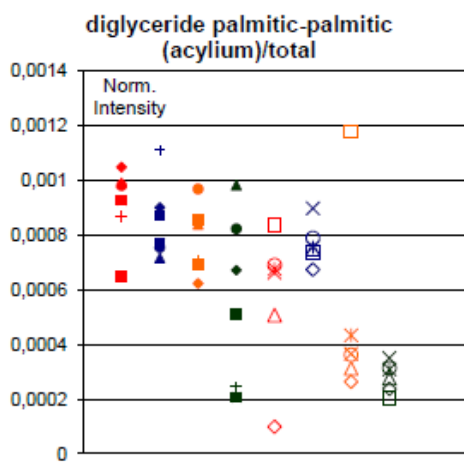


Figure E.25: Positive acylium ions of diglyceride with twice palmitic acid  $C_{35}H_{67}O_4^+$  at  $m/z$  551,5 in the linseed oil-lead chloride mixture

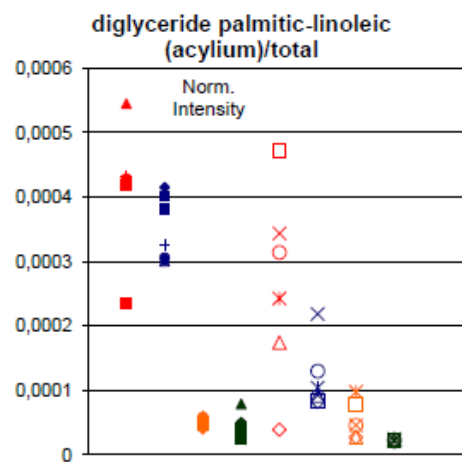


Figure E.26: Positive acylium ions of diglyceride with palmitic/linoleic acid  $C_{37}H_{67}O_4^+$  at  $m/z$  575,5 in the linseed oil-lead chloride mixture

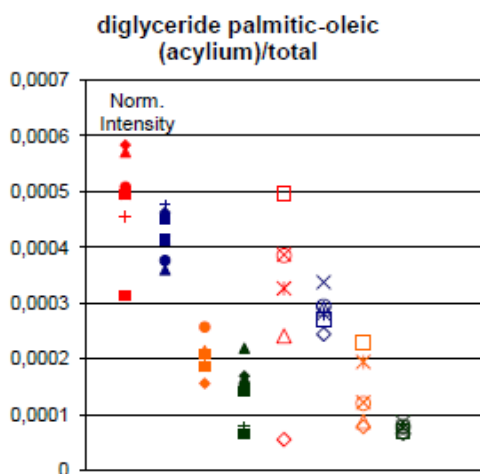


Figure E.27: Positive acylium ions of diglyceride with palmitic/oleic acid  $C_{37}H_{69}O_4^+$  at  $m/z$  577,5 in the linseed oil-lead chloride mixture

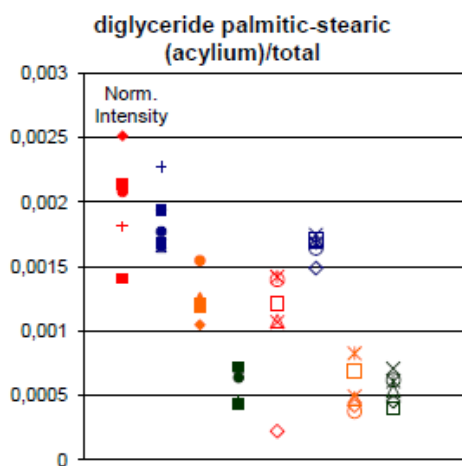


Figure E.28: Positive acylium ions of diglyceride with palmitic/stearic acid  $C_{37}H_{71}O_4^+$  at  $m/z$  579,5 in the linseed oil-lead chloride mixture

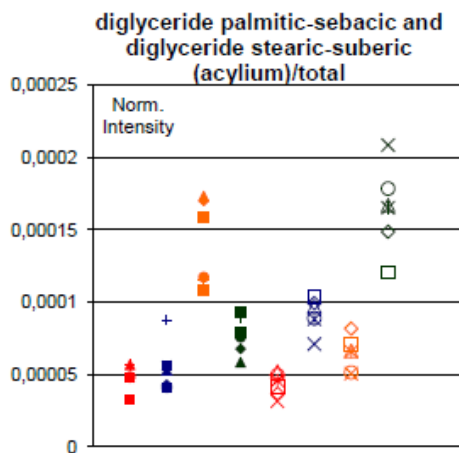


Figure E.29: Positive acylium ions of diglyceride with stearic/suberic acid and of diglyceride with palmitic/sebaric acid  $C_{29}H_{53}O_6^+$  at  $m/z$  497 in the linseed oil-lead chloride mixture

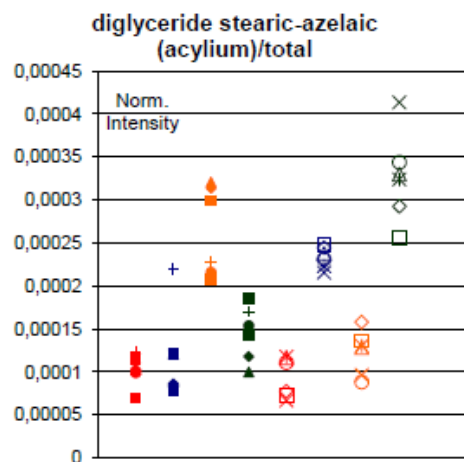


Figure E.30: Positive acylium ions of diglyceride with stearic/azelaic acid  $C_{30}H_{55}O_6^+$  at  $m/z$  511 in the linseed oil-lead chloride mixture

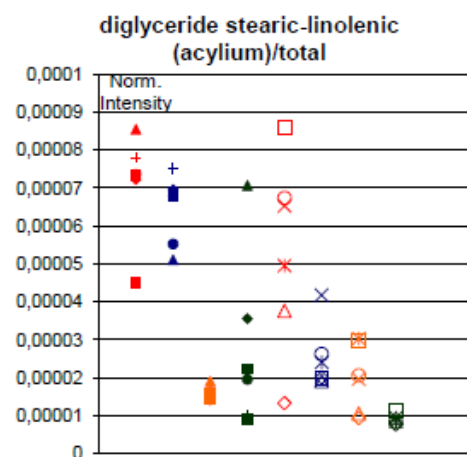


Figure E.31: Positive acylium ions of diglyceride with stearic/linolenic acid  $C_{39}H_{69}O_4^+$  at  $m/z$  601,5 in the linseed oil-lead chloride mixture

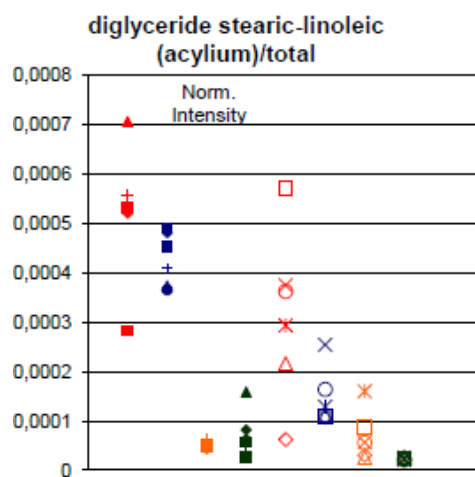


Figure E.32: Positive acylium ions of diglyceride with stearic/linoleic acid  $C_{39}H_{71}O_4^+$  at  $m/z$  603,5 in the linseed oil-lead chloride mixture

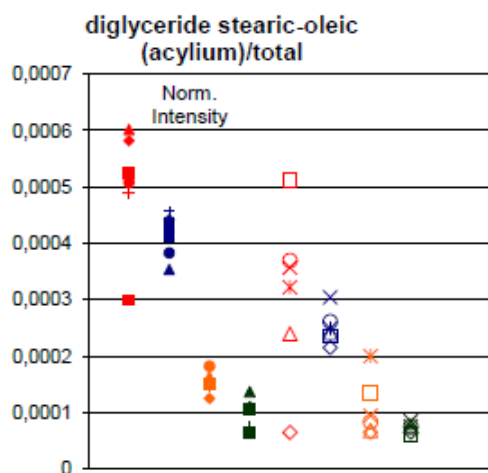


Figure E.33: Positive acylium ions of diglyceride with stearic/oleic acid  $C_{39}H_{73}O_4^+$  at  $m/z$  605,5 in the linseed oil-lead chloride mixture

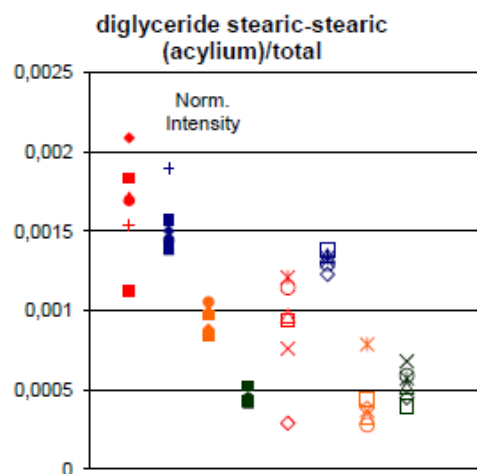


Figure E.34: Positive acylium ions of diglyceride with twice stearic acid  $C_{39}H_{75}O_4^+$  at  $m/z$  607,5 in the linseed oil-lead chloride mixture

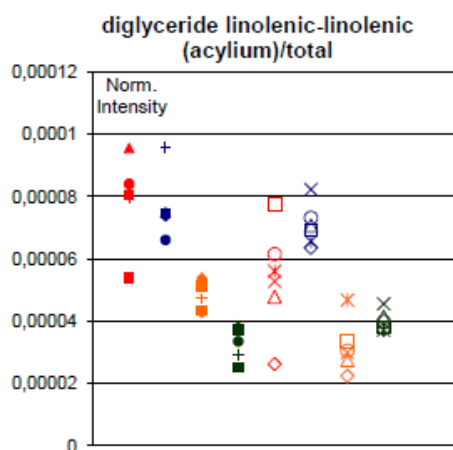


Figure E.35: Positive acylium ions of diglyceride with twice linolenic acid  $C_{39}H_{63}O_4^+$  at  $m/z$  595,5 in the linseed oil-lead chloride mixture

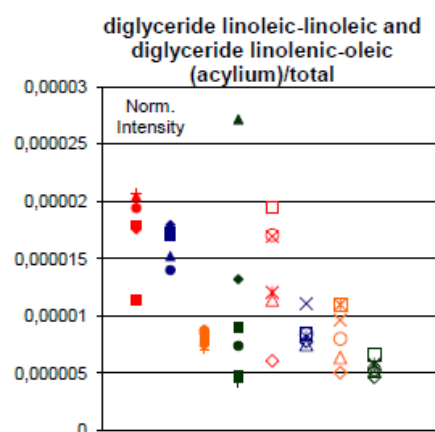


Figure E.36: Positive acylium ions of diglyceride with twice linoleic acid and of diglyceride with linolenic/oleic  $C_{39}H_{67}O_4^+$  at  $m/z$  599,5 in the linseed oil-lead chloride mixture

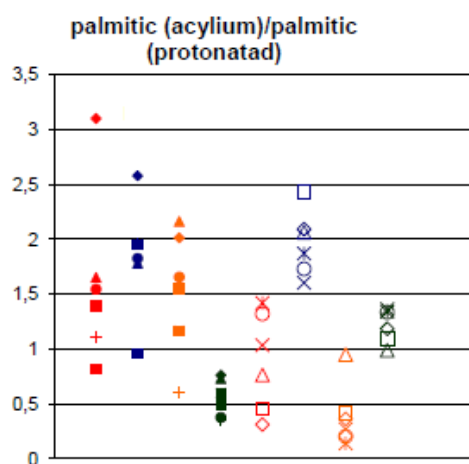


Figure E.37: Ratio of positive acylium and protonated ions of palmitic acid in the linseed oil-lead chloride mixture

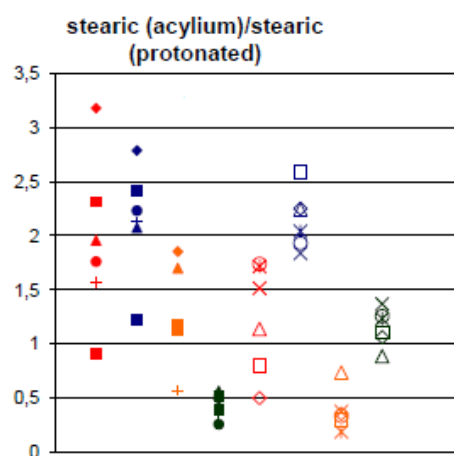


Figure E.38: Ratio of positive acylium and protonated ions of stearic acid in the linseed oil-lead chloride mixture

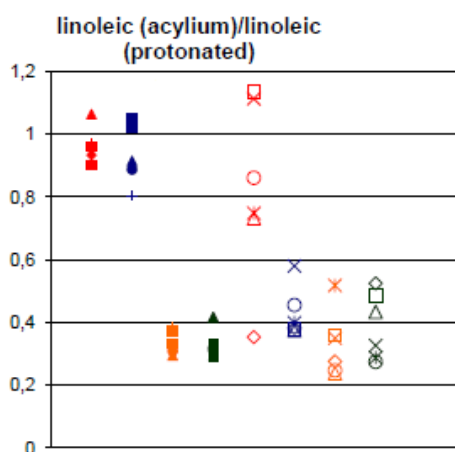


Figure E.39: Ratio of positive acylium and protonated ions of linoleic acid in the linseed oil-lead chloride mixture

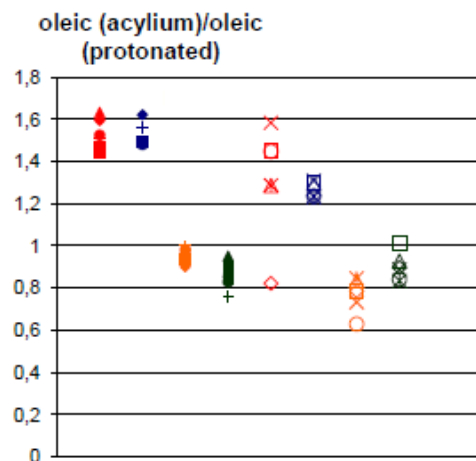


Figure E.40: Ratio of positive acylium and protonated ions of oleic acid in the linseed oil-lead chloride mixture

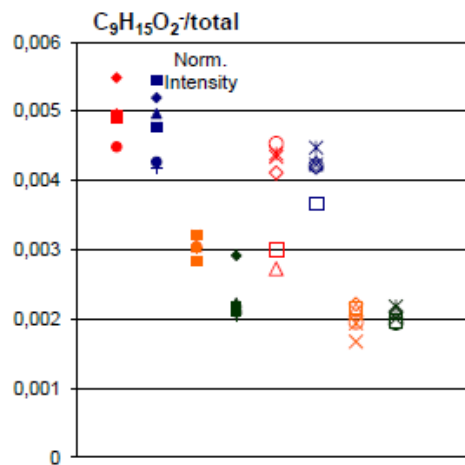


Figure E.41: Negative ions of aliphatic chain fragment with formula  $C_2H_3(CH_2)_6COO^-$  at  $m/z$  155 in the linseed oil-lead chloride mixture

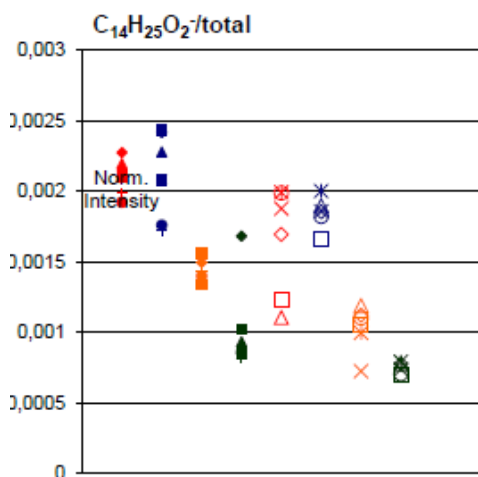


Figure E.42: Negative ions of aliphatic chain fragment with formula  $C_2H_3(CH_2)_{11}COO^-$  at  $m/z$  225 in the linseed oil-lead chloride mixture

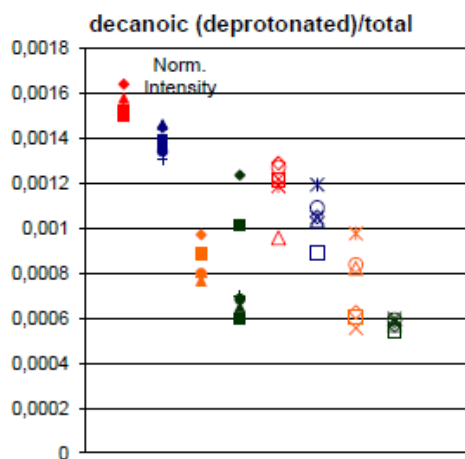


Figure E.43: Negative deprotonated ions of decanoic acid  $C_{10}H_{19}O_2^-$  at  $m/z$  171 in the linseed oil-lead chloride mixture

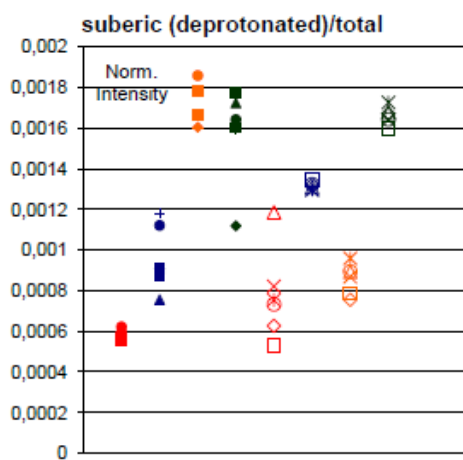


Figure E.44: Negative deprotonated ions of suberic acid  $C_8H_{13}O_4^-$  at  $m/z$  173 in the linseed oil-lead chloride mixture

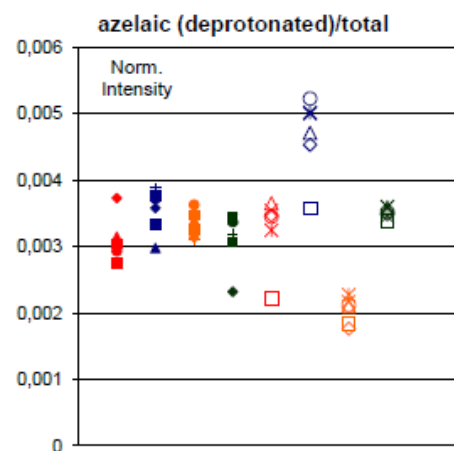


Figure E.45: Negative deprotonated ions of azelaic acid  $C_9H_{15}O_4^-$  at  $m/z$  187 in the linseed oil-lead chloride mixture

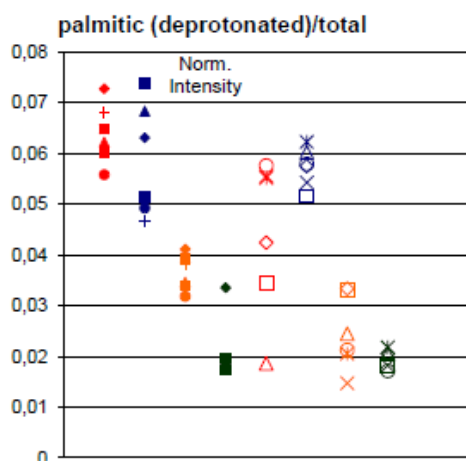


Figure E.46: Negative deprotonated ions of palmitic acid  $C_{16}H_{31}O_2^-$  at  $m/z$  255 in the linseed oil-lead chloride mixture

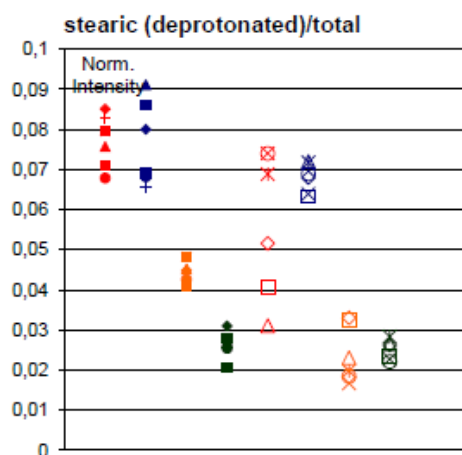


Figure E.47: Negative deprotonated ions of stearic acid  $C_{18}H_{35}O_2^-$  at  $m/z$  283 in the linseed oil-lead chloride mixture



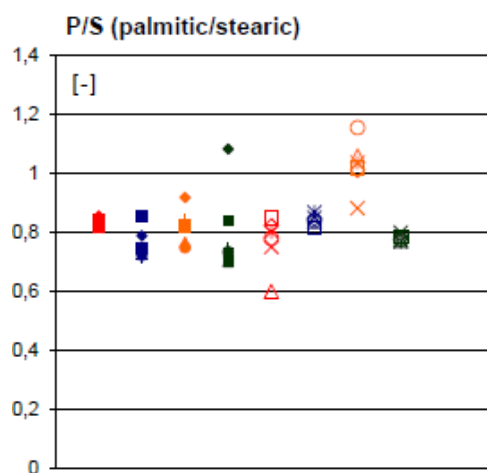


Figure E.52: Ratio of negative deprotonated palmitic and stearic acid ions in the linseed oil-lead chloride mixture

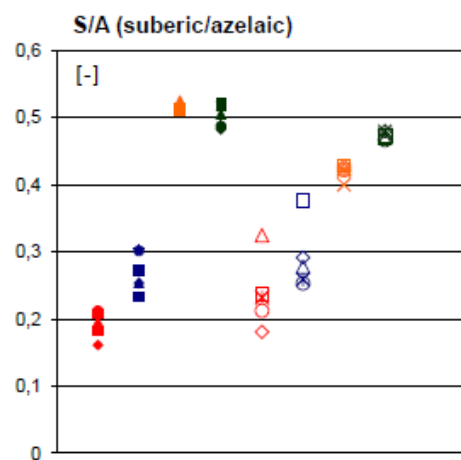


Figure E.53: Ratio of negative deprotonated suberic and azelaic acid ions in the linseed oil-lead chloride mixture

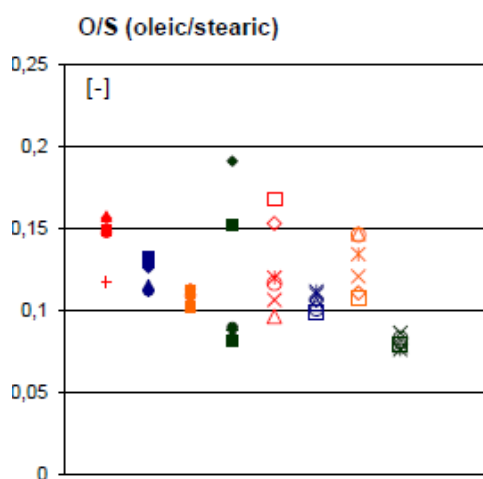


Figure E.54: Ratio of negative deprotonated oleic and stearic acid ions in the linseed oil-lead chloride mixture

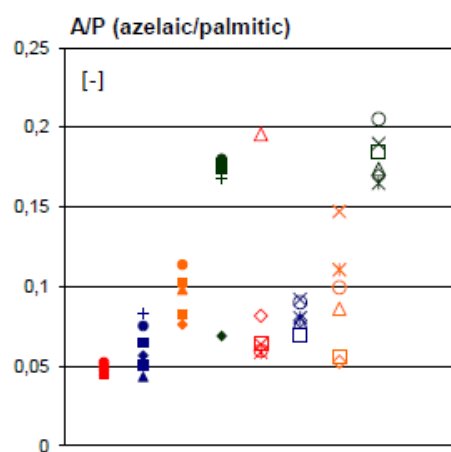


Figure E.55: Ratio of negative deprotonated azelaic and palmitic acid ions in the linseed oil-lead chloride mixture

# Appendix F

## Results of ToF-SIMS measurements of Linseed oil with Minium

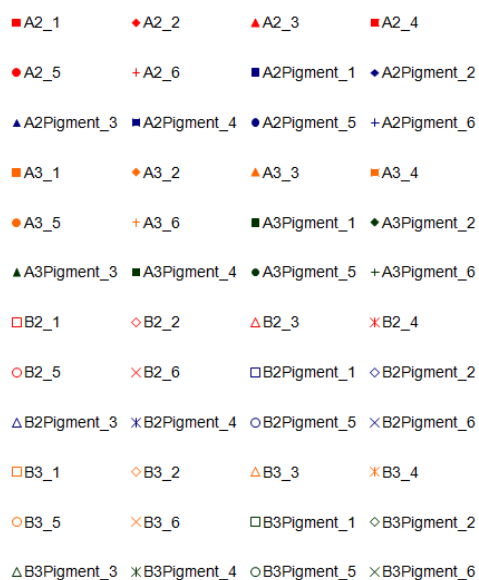


Figure F.1: Legend used for Figures F.2 to F.54

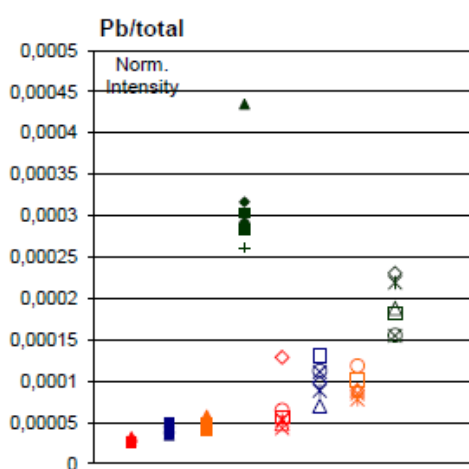


Figure F.2: Positive  $Pb^+$  ions in the linseed oil-minium mixture at  $m/z$  208

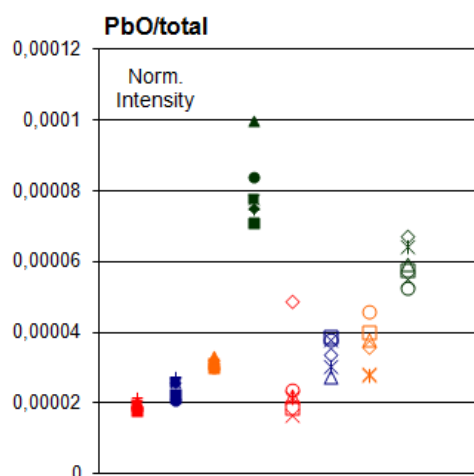


Figure F.3: Positive  $PbO^+$  ions in the linseed oil-minium mixture at  $m/z$  224

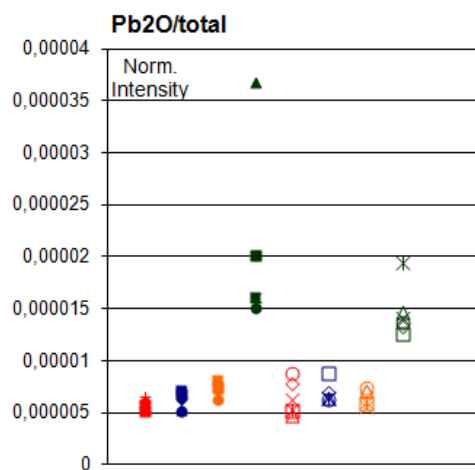


Figure F.4: Positive  $Pb_2O^+$  ions in the linseed oil-minium mixture at  $m/z$  432

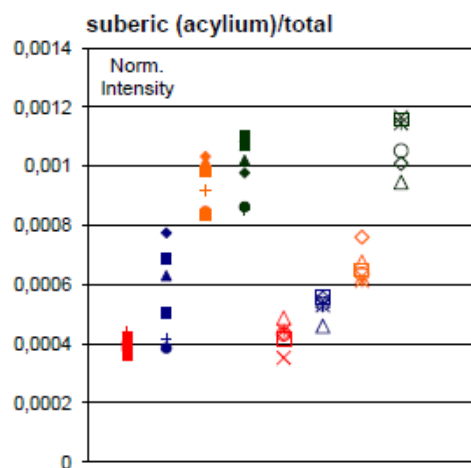


Figure F.5: Positive acylium ions of suberic acid,  $C_8H_{13}O_3^+$  at  $m/z$  157 in the linseed oil-minium mixture

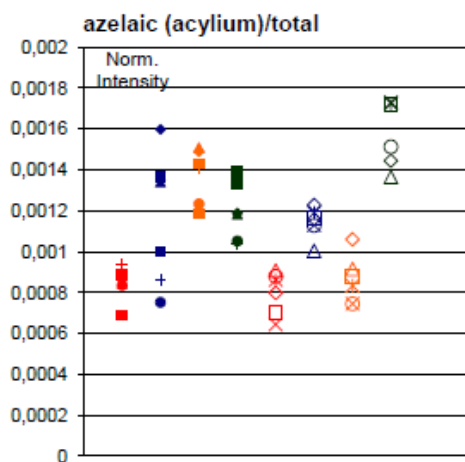


Figure F.6: Positive acylium ions of azelaic acid  $C_9H_{15}O_3^+$  at  $m/z$  171 in the linseed oil-minium mixture

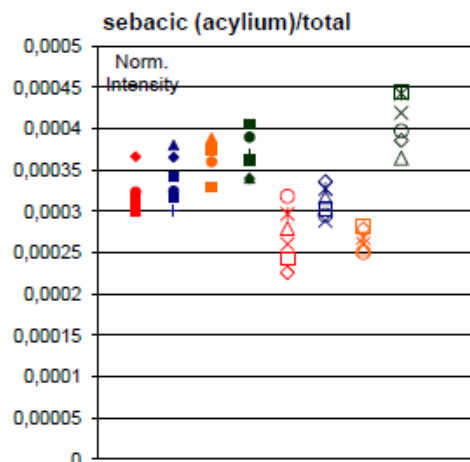


Figure F.7: Positive acylium ions of sebacic acid  $C_{10}H_{17}O_3^+$  at  $m/z$  185 in the linseed oil-minium mixture

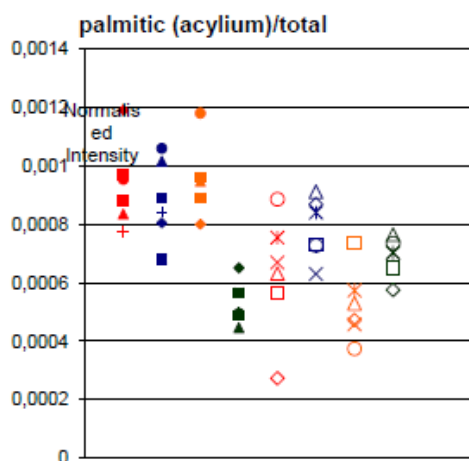


Figure F.8: Positive acylium ions of palmitic acid  $C_{16}H_{31}O^+$  at  $m/z$  239 in the linseed oil-minium mixture

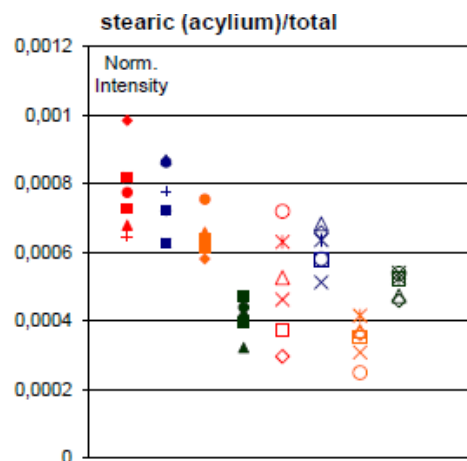


Figure F.9: Positive acylium ions of stearic acid  $C_{18}H_{35}O^+$  at  $m/z$  267 in the linseed oil-minium mixture

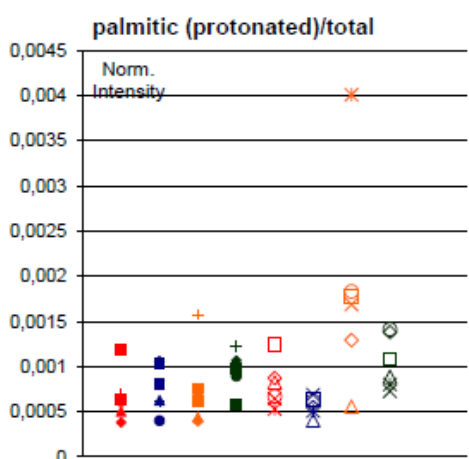


Figure F.10: Positive protonated ions of palmitic acid  $C_{16}H_{33}O_2^+$  at  $m/z$  257 in the linseed oil-minium mixture

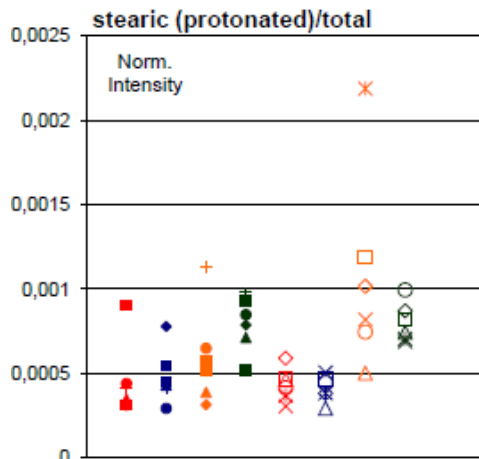


Figure F.11: Positive protonated ions of stearic acid  $C_{18}H_{37}O_2^+$  at  $m/z$  285 in the linseed oil-minium mixture

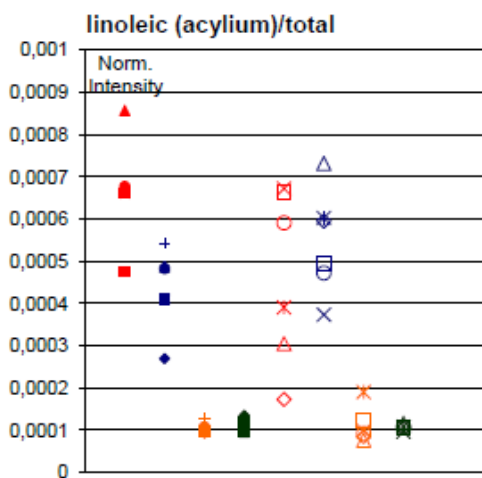


Figure F.12: Positive acylium ions of linoleic acid  $C_{18}H_{31}O^+$  at  $m/z$  263 in the linseed oil-minium mixture

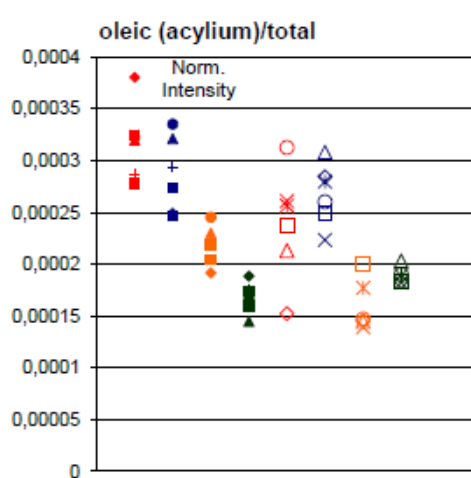


Figure F.13: Positive acylium ions of oleic acid  $C_{18}H_{33}O^+$  at  $m/z$  265 in the linseed oil-minium mixture

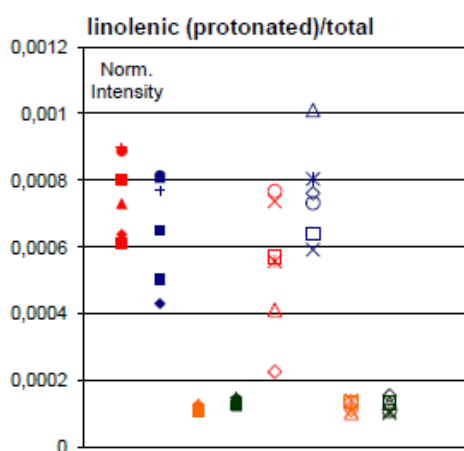


Figure F.14: Positive protonated ions of linolenic acid  $C_{18}H_{31}O_2^+$  at  $m/z$  279 in the linseed oil-minium mixture

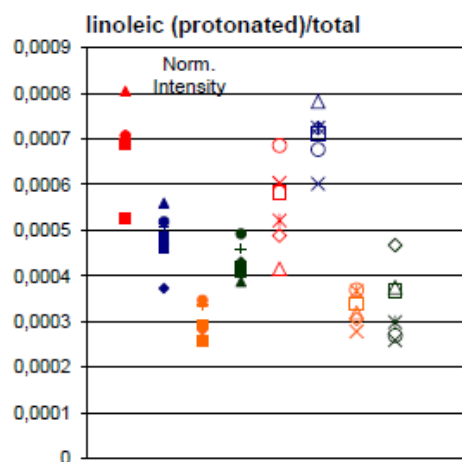


Figure F.15: Positive protonated ions of linoleic acid  $C_{18}H_{33}O_2^+$  at  $m/z$  281 in the linseed oil-minium mixture

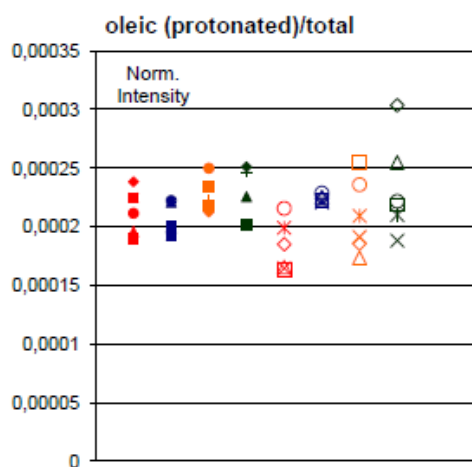


Figure F.16: Positive protonated ions of oleic acid  $C_{18}H_{35}O_2^+$  at  $m/z$  283 in the linseed oil-minium mixture

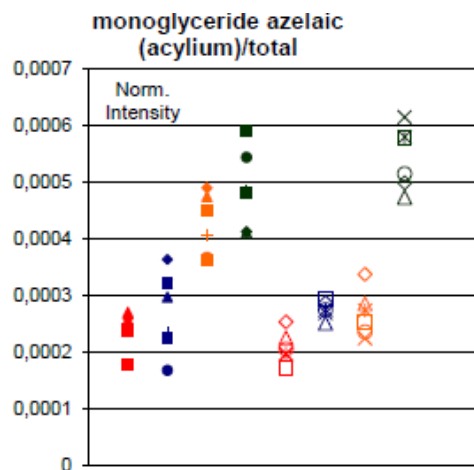


Figure F.17: Positive acylium ions of monoglyceride with azelaic acid  $C_{12}H_{21}O_5^+$  at  $m/z$  245 in the linseed oil-minium mixture

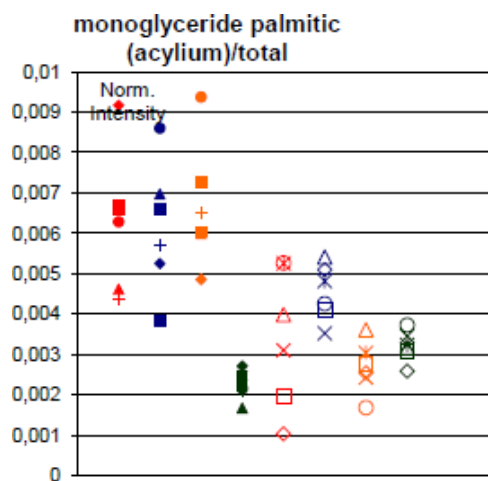


Figure F.18: Positive acylium ions of monoglyceride with palmitic acid  $C_{19}H_{37}O_3^+$  at  $m/z$  313 in the linseed oil-minium mixture

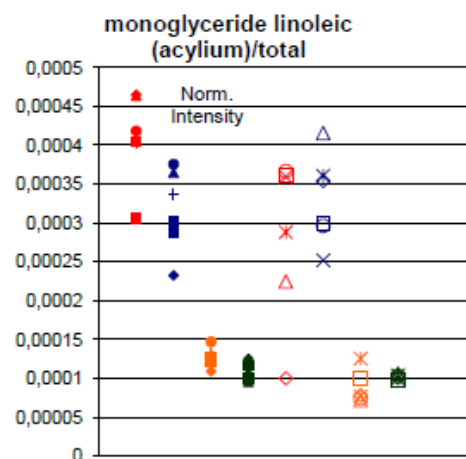


Figure F.19: Positive acylium ions of monoglyceride with linoleic acid  $C_{21}H_{37}O_3^+$  at  $m/z$  337 in the linseed oil-minium mixture

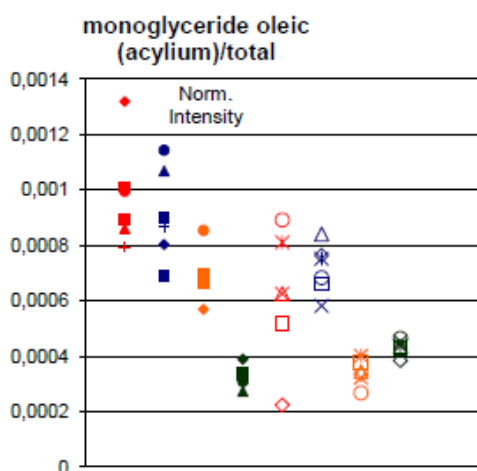


Figure F.20: Positive acylium ions of monoglyceride with oleic acid  $C_{21}H_{39}O_3^+$  at  $m/z$  339 in the linseed oil-minium mixture

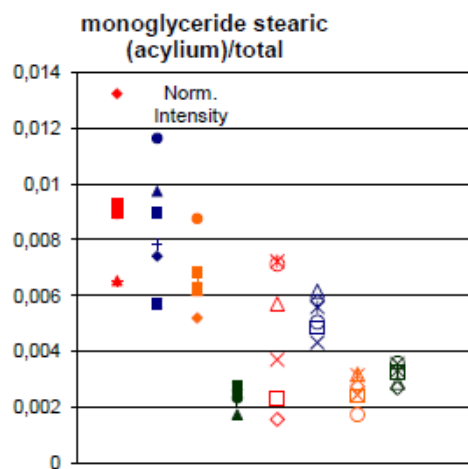


Figure F.21: Positive acylium ions of monoglyceride with stearic acid  $C_{21}H_{41}O_3^+$  at  $m/z$  341 in the linseed oil-minium mixture

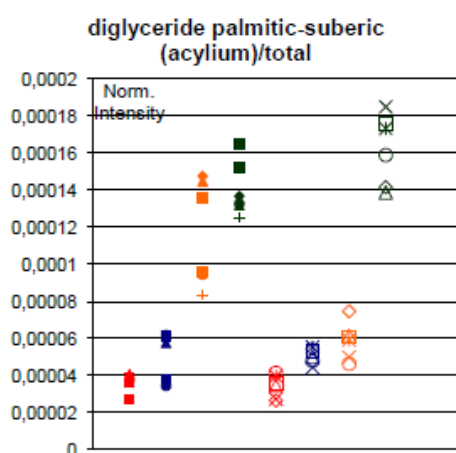


Figure F.22: Positive acylium ions of diglyceride with palmitic/suberic acid  $C_{27}H_{49}O_6^+$  at  $m/z$  469 in the linseed oil-minium mixture

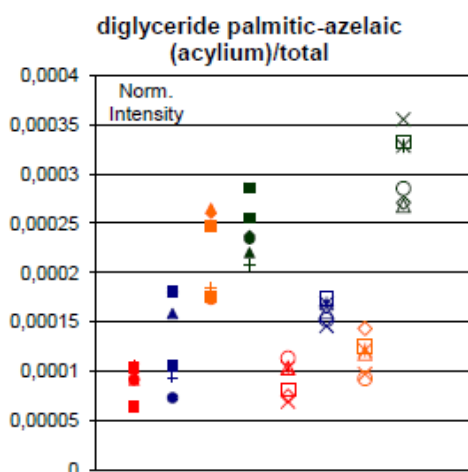


Figure F.23: Positive acylium ions of diglyceride with palmitic/azelaic acid  $C_{28}H_{51}O_6^+$  at  $m/z$  483 in the linseed oil-minium mixture

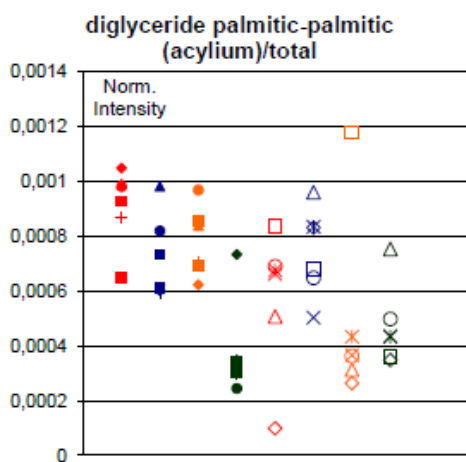


Figure F.24: Positive acylium ions of diglyceride with twice palmitic acid  $C_{35}H_{67}O_4^+$  at  $m/z$  551,5 in the linseed oil-minium mixture

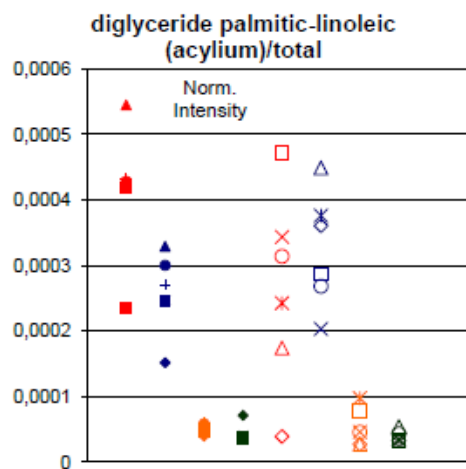


Figure F.25: Positive acylium ions of diglyceride with palmitic/linoleic acid  $C_{37}H_{67}O_4^+$  at  $m/z$  575,5 in the linseed oil-minium mixture

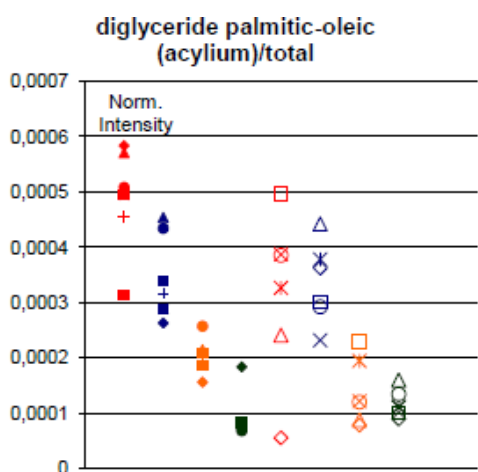


Figure F.26: Positive acylium ions of diglyceride with palmitic/oleic acid  $C_{37}H_{69}O_4^+$  at  $m/z$  577,5 in the linseed oil-minium mixture

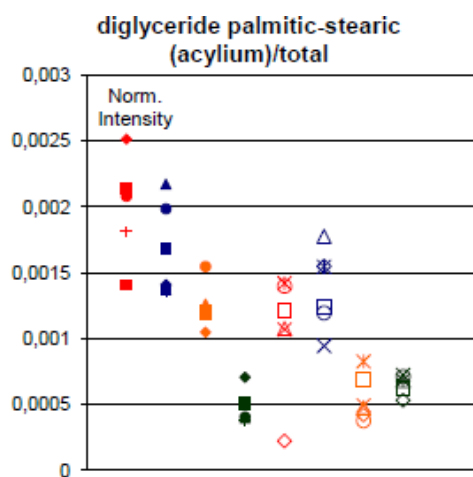


Figure F.27: Positive acylium ions of diglyceride with palmitic/stearic acid  $C_{37}H_{71}O_4^+$  at  $m/z$  579,5 in the linseed oil-minium mixture

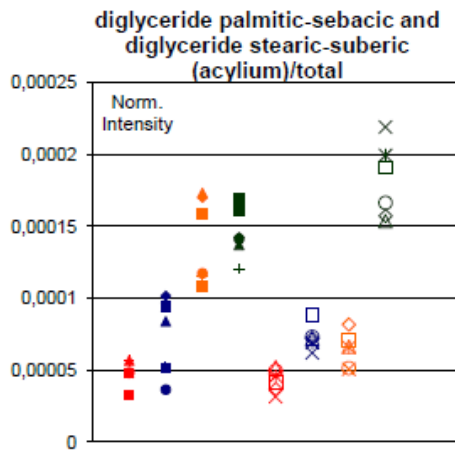


Figure F.28: Positive acylium ions of diglyceride with stearic/suberic acid and of diglyceride with palmitic/sebacic acid  $C_{29}H_{53}O_6^+$  at  $m/z$  497 in the linseed oil-minium mixture

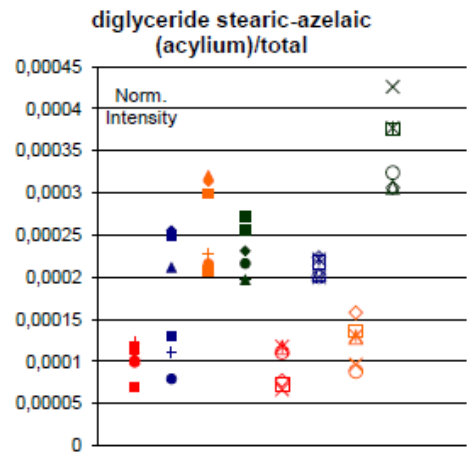


Figure F.29: Positive acylium ions of diglyceride with stearic/azelaic acid  $C_{30}H_{55}O_6^+$  at  $m/z$  511 in the linseed oil-minium mixture

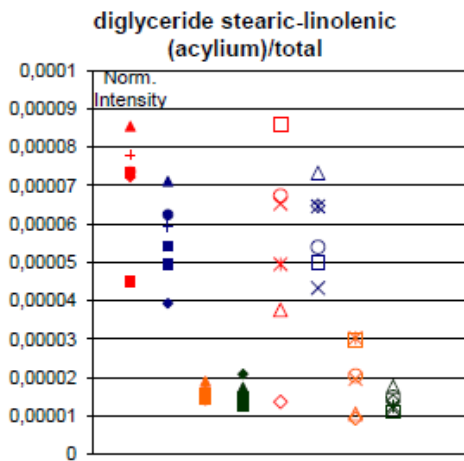


Figure F.30: Positive acylium ions of diglyceride with stearic/linolenic acid  $C_{39}H_{69}O_4^+$  at  $m/z$  601,5 in the linseed oil-minium mixture

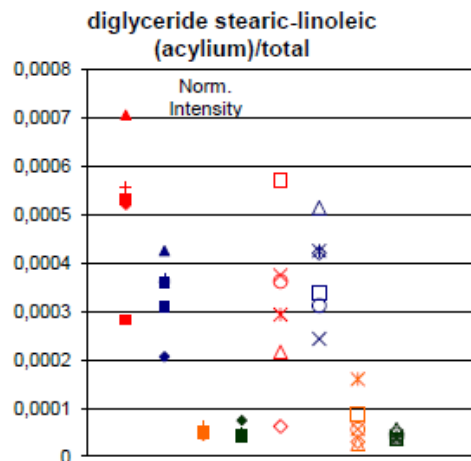


Figure F.31: Positive acylium ions of diglyceride with stearic/linoleic acid  $C_{39}H_{71}O_4^+$  at  $m/z$  603,5 in the linseed oil-minium mixture

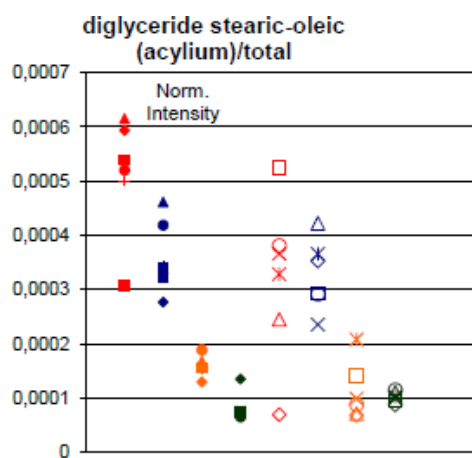


Figure F.32: Positive acylium ions of diglyceride with stearic/oleic acid  $C_{39}H_{73}O_4^+$  at  $m/z$  605,5 in the linseed oil-minium mixture

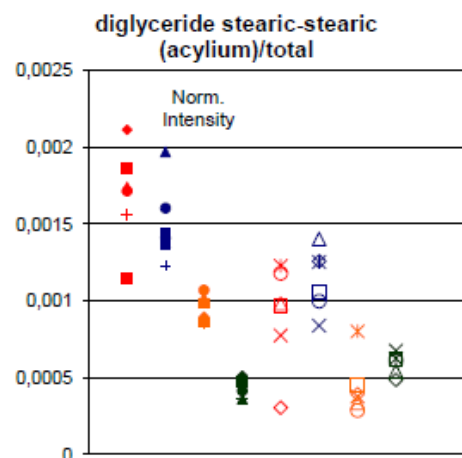


Figure F.33: Positive acylium ions of diglyceride with twice stearic acid  $C_{39}H_{75}O_4^+$  at  $m/z$  607,5 in the linseed oil-minium mixture

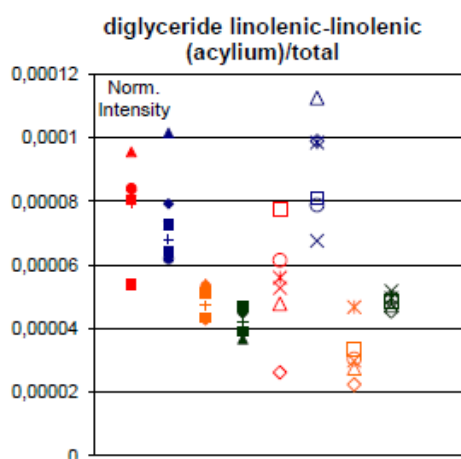


Figure F.34: Positive acylium ions of diglyceride with twice linolenic acid  $C_{39}H_{63}O_4^+$  at  $m/z$  595,5 in the linseed oil-minium mixture

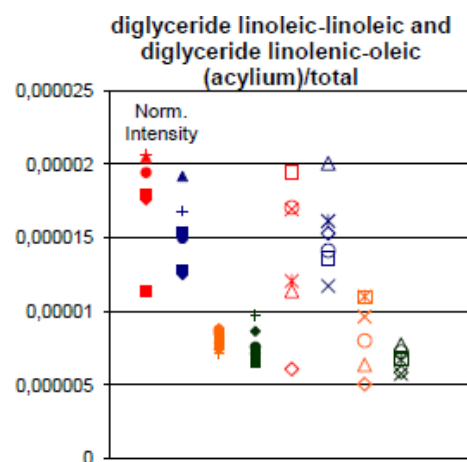


Figure F.35: Positive acylium ions of diglyceride with twice linoleic acid and of diglyceride with linolenic/oleic  $C_{39}H_{67}O_4^+$  at  $m/z$  599,5 in the linseed oil-minium mixture

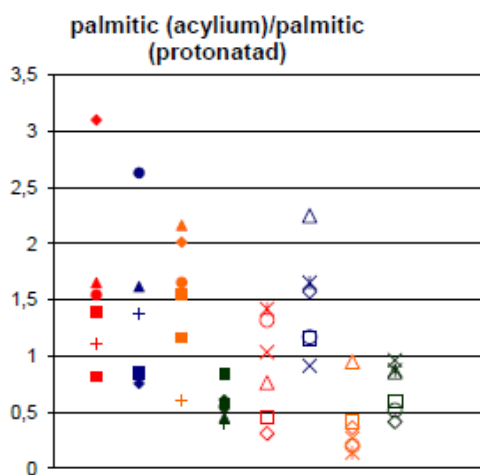


Figure F.36: Ratio of positive acylium and protonated ions of palmitic acid in the linseed oil-minium mixture

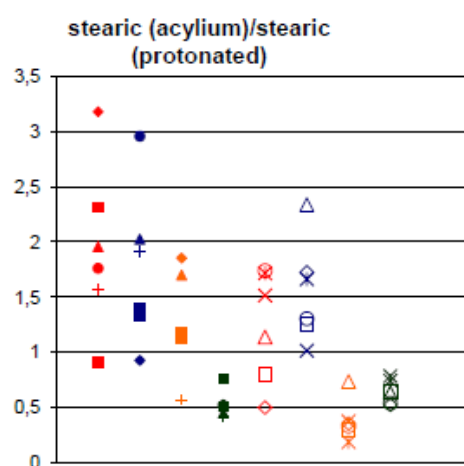


Figure F.37: Ratio of positive acylium and protonated ions of stearic acid in the linseed oil-minium mixture

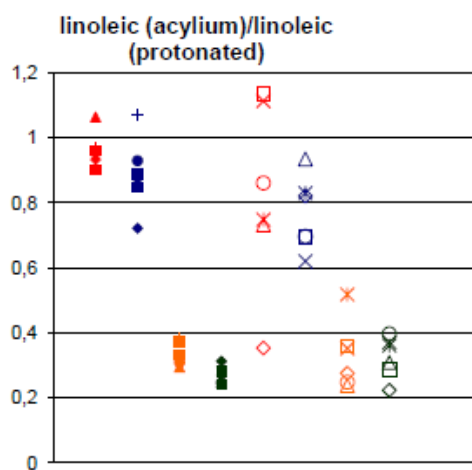


Figure F.38: Ratio of positive acylium and protonated ions of linoleic acid in the linseed oil-minium mixture

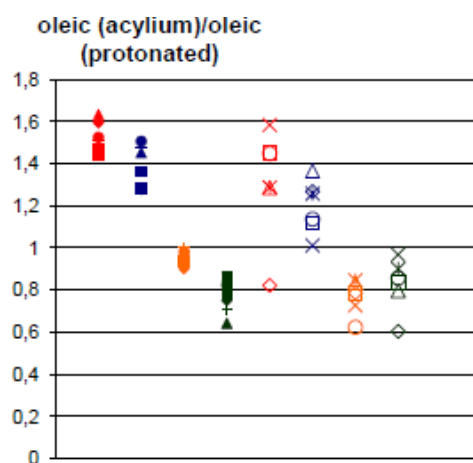


Figure F.39: Ratio of positive acylium and protonated ions of oleic acid in the linseed oil-minium mixture

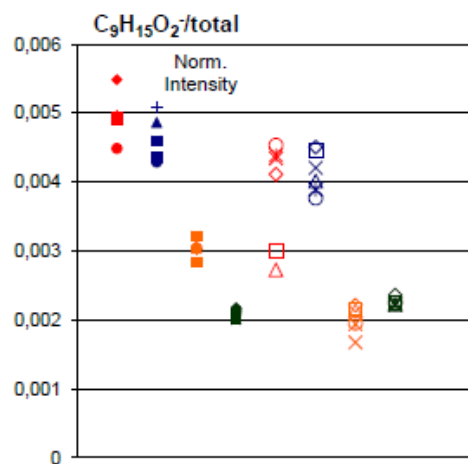


Figure F.40: Negative ions of aliphatic chain fragment with formula  $C_2H_3(CH_2)_6COO^-$  at  $m/z$  155 in the linseed oil-minium mixture

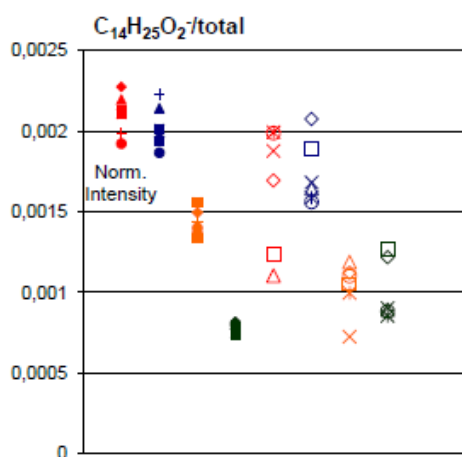


Figure F.41: Negative ions of aliphatic chain fragment with formula  $C_2H_3(CH_2)_{11}COO^-$  at  $m/z$  225 in the linseed oil-minium mixture

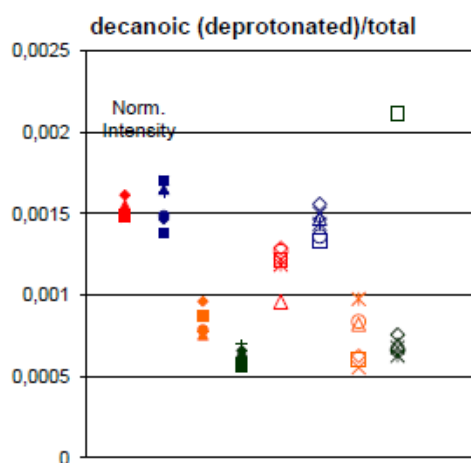


Figure F.42: Negative deprotonated ions of decanoic acid  $C_{10}H_{19}O_2^-$  at  $m/z$  171 in the linseed oil-minium mixture

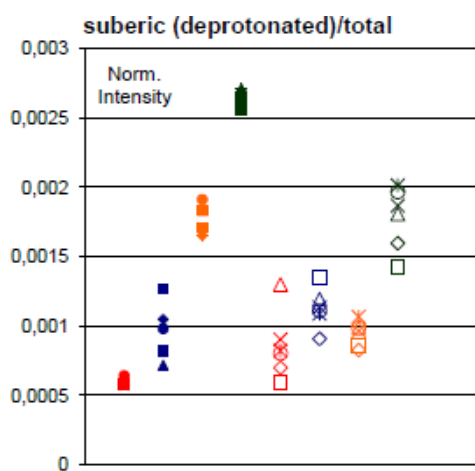


Figure F.43: Negative deprotonated ions of suberic acid  $C_8H_{13}O_4^-$  at  $m/z$  173 in the linseed oil-minium mixture

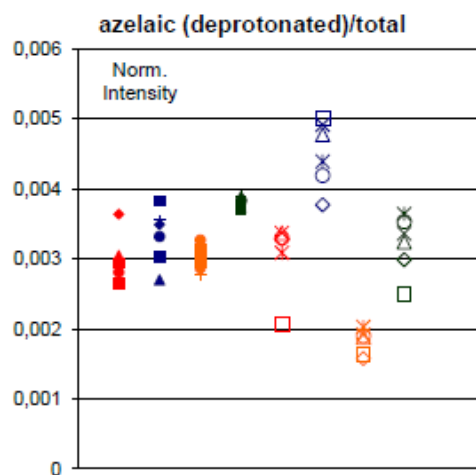


Figure F.44: Negative deprotonated ions of azelaic acid  $C_9H_{15}O_4^-$  at  $m/z$  187 in the linseed oil-minium mixture

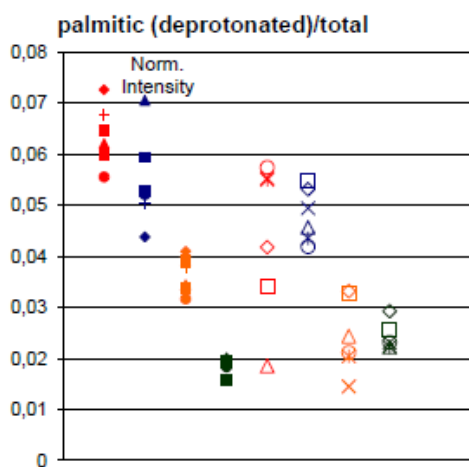


Figure F.45: Negative deprotonated ions of palmitic acid  $C_{16}H_{31}O_2^-$  at  $m/z$  255 in the linseed oil-minium mixture

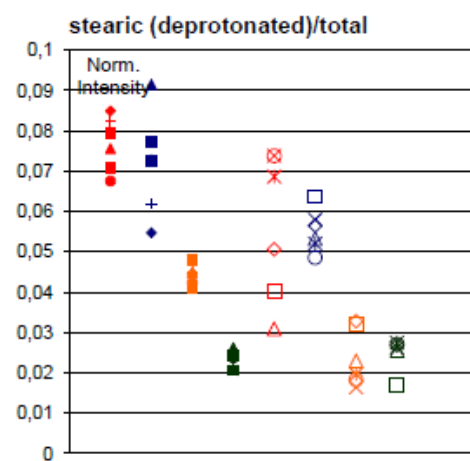


Figure F.46: Negative deprotonated ions of stearic acid  $C_{18}H_{35}O_2^-$  at  $m/z$  283 in the linseed oil-minium mixture

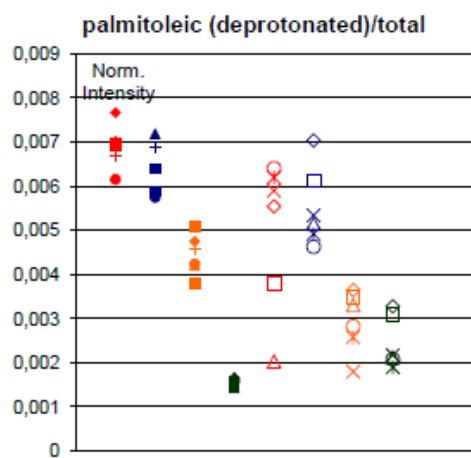


Figure F.47: Negative deprotonated ions of palmitoleic acid  $C_{16}H_{29}O_2^-$  at  $m/z$  253 in the linseed oil-minium mixture

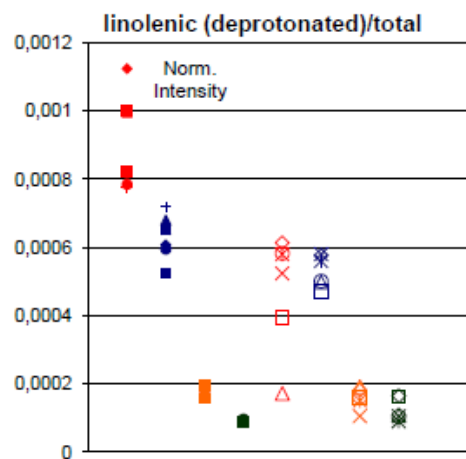


Figure F.48: Negative deprotonated ions of linolenic acid  $C_{18}H_{29}O_2^-$  at  $m/z$  277 in the linseed oil-minium mixture

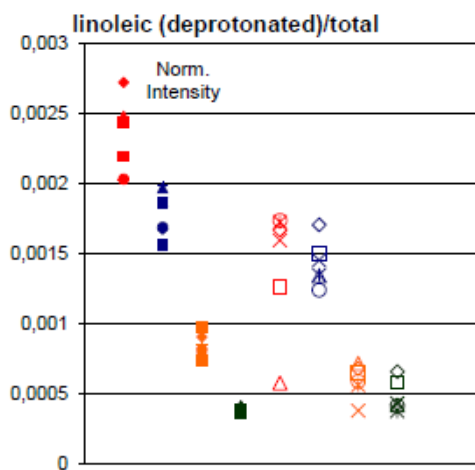


Figure F.49: Negative deprotonated ions of linoleic acid  $C_{18}H_{31}O_2^-$  at  $m/z$  279 in the linseed oil-minium mixture

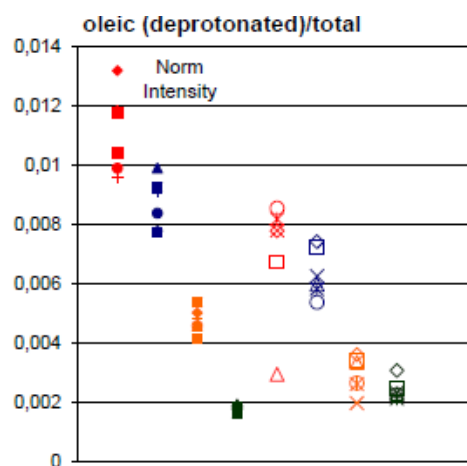


Figure F.50: Negative deprotonated ions of oleic acid  $C_{18}H_{33}O_2^-$  at  $m/z$  281 in the linseed oil-minium mixture

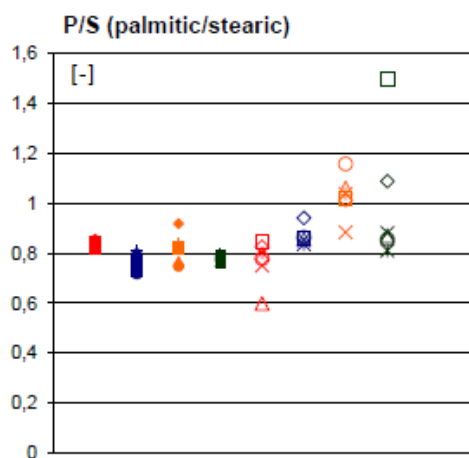


Figure F.51: Ratio of negative deprotonated palmitic and stearic acid ions in the linseed oil-minium mixture

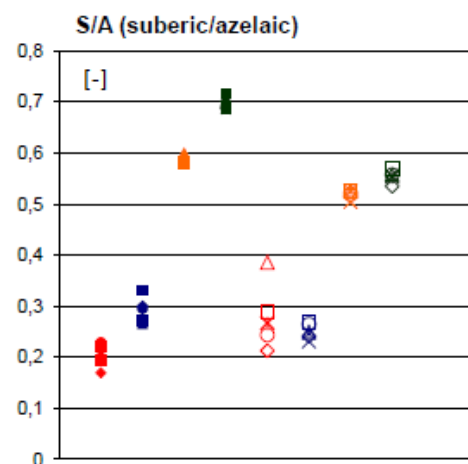


Figure F.52: Ratio of negative deprotonated suberic and azelaic acid ions in the linseed oil-minium mixture

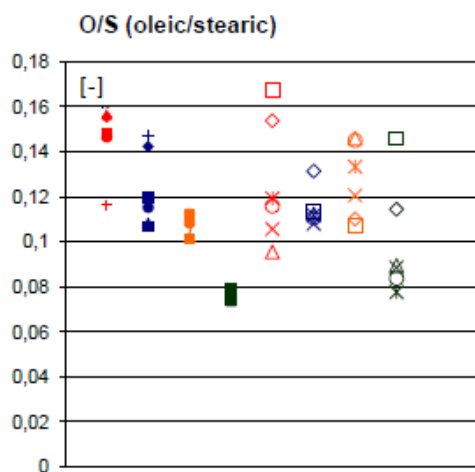


Figure F.53: Ratio of negative deprotonated oleic and stearic acid ions in the linseed oil-minium mixture

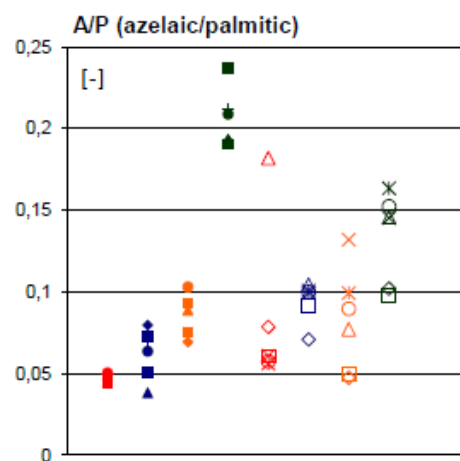


Figure F.54: Ratio of negative deprotonated azelaic and palmitic acid ions in the linseed oil-minium mixture

## Appendix G

# Results of ToF-SIMS measurements of Linseed oil with Azurite

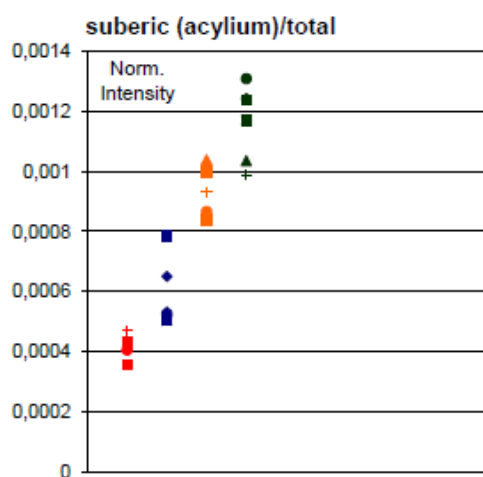


Figure G.1: Positive acylium ions of suberic acid,  $C_8H_{13}O_3^+$  at  $m/z$  157 in the linseed oil-azurite mixture

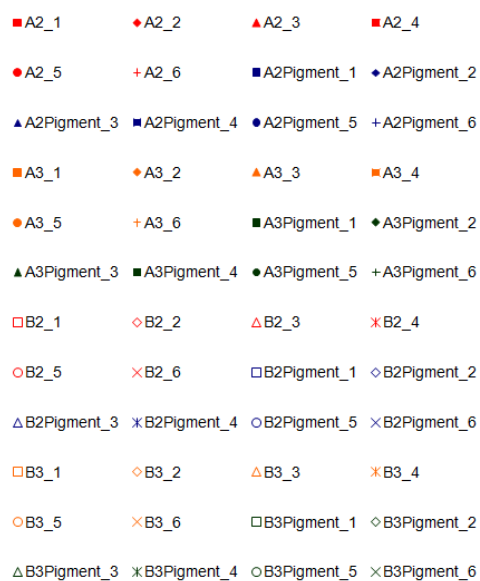


Figure G.2: Legend used for Figures G.3 to G.51

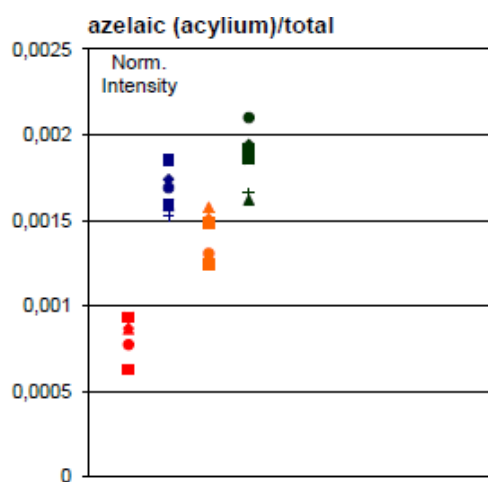


Figure G.3: Positive acylium ions of azelaic acid  $C_9H_{15}O_3^+$  at  $m/z$  171 in the linseed oil-azurite mixture

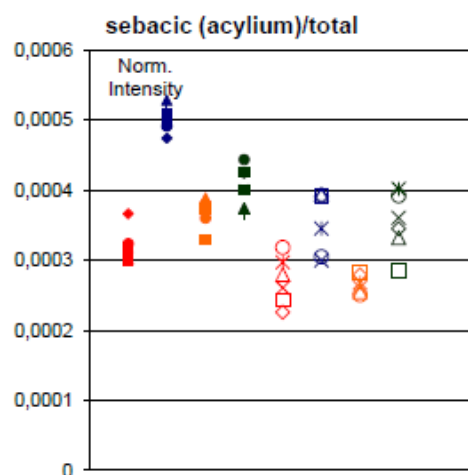


Figure G.4: Positive acylium ions of sebacic acid  $C_{10}H_{17}O_3^+$  at  $m/z$  185 in the linseed oil-azurite mixture

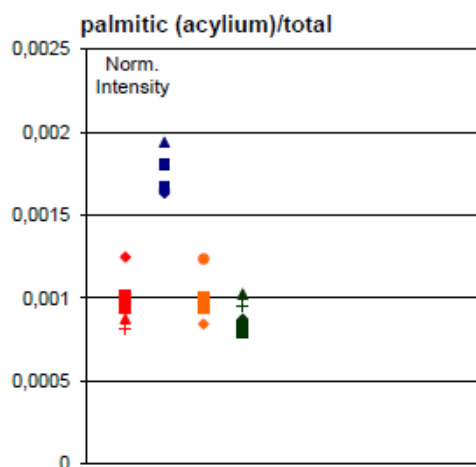


Figure G.5: Positive acylium ions of palmitic acid  $C_{16}H_{31}O^+$  at  $m/z$  239 in the linseed oil-azurite mixture

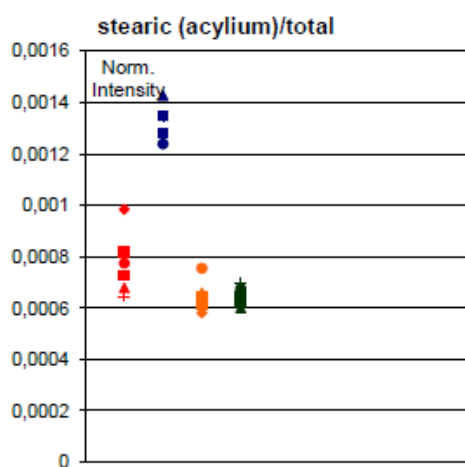


Figure G.6: Positive acylium ions of stearic acid  $C_{18}H_{35}O^+$  at  $m/z$  267 in the linseed oil-azurite mixture

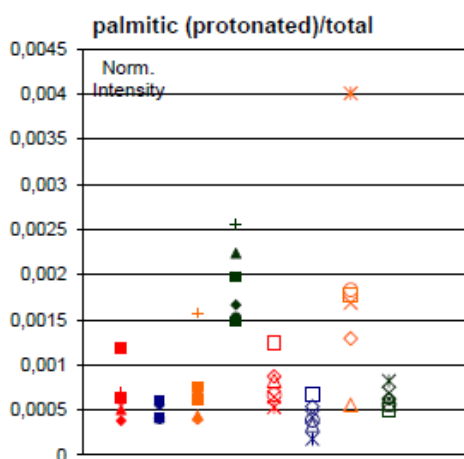


Figure G.7: Positive protonated ions of palmitic acid  $C_{16}H_{33}O_2^+$  at  $m/z$  257 in the linseed oil-azurite mixture

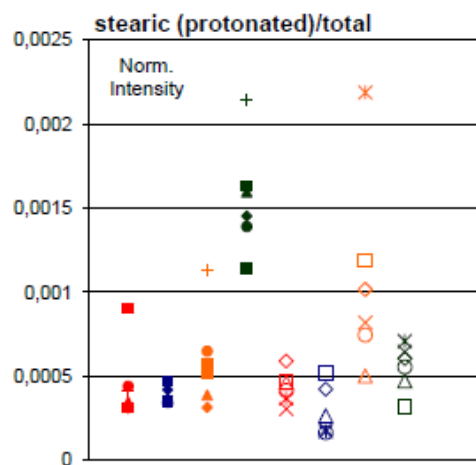


Figure G.8: Positive protonated ions of stearic acid  $C_{18}H_{37}O_2^+$  at  $m/z$  285 in the linseed oil-azurite mixture

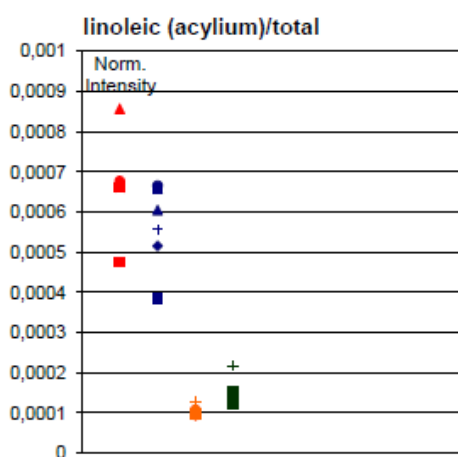


Figure G.9: Positive acylium ions of linoleic acid  $C_{18}H_{31}O^+$  at  $m/z$  263 in the linseed oil-azurite mixture

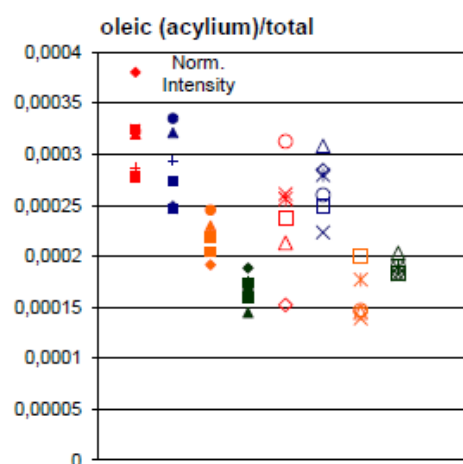


Figure G.10: Positive acylium ions of oleic acid  $C_{18}H_{33}O^+$  at  $m/z$  265 in the linseed oil-azurite mixture

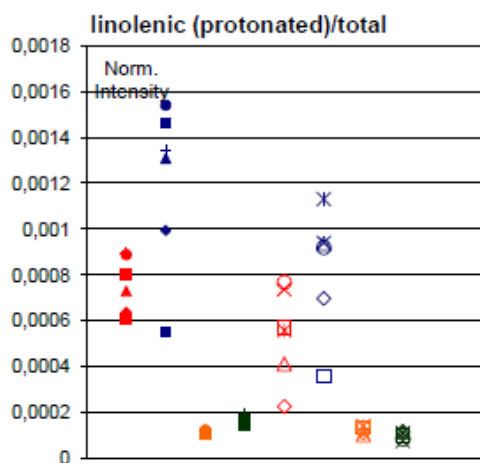


Figure G.11: Positive protonated ions of linolenic acid  $C_{18}H_{31}O_2^+$  at  $m/z$  279 in the linseed oil-azurite mixture

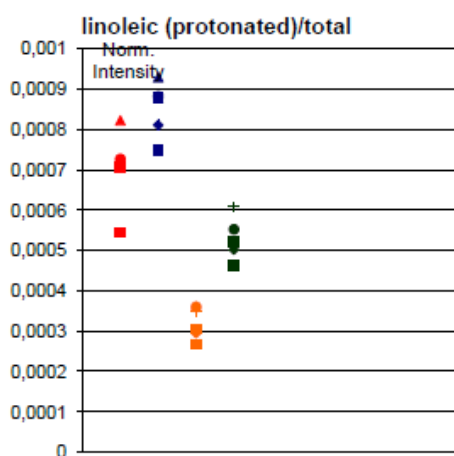


Figure G.12: Positive protonated ions of linoleic acid  $C_{18}H_{33}O_2^+$  at  $m/z$  281 in the linseed oil-azurite mixture

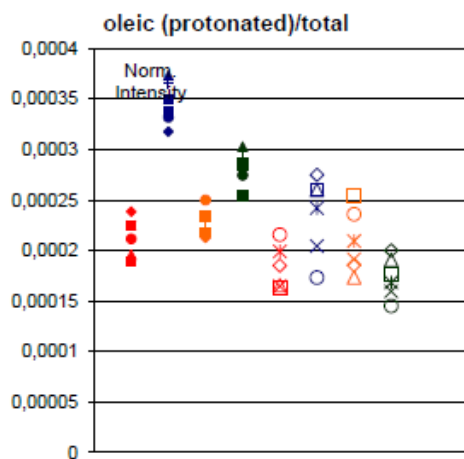


Figure G.13: Positive protonated ions of oleic acid  $C_{18}H_{35}O_2^+$  at  $m/z$  283 in the linseed oil-azurite mixture

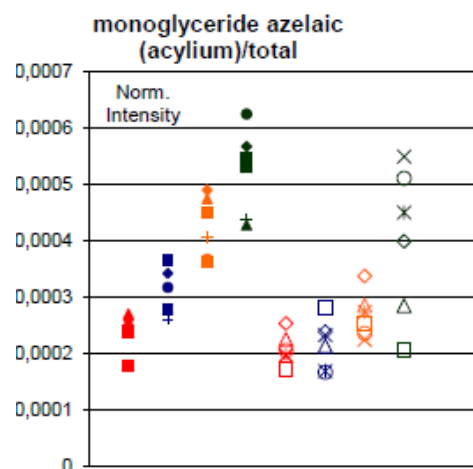


Figure G.14: Positive acylium ions of monoglyceride with azelaic acid  $C_{12}H_{21}O_5^+$  at  $m/z$  245 in the linseed oil-azurite mixture

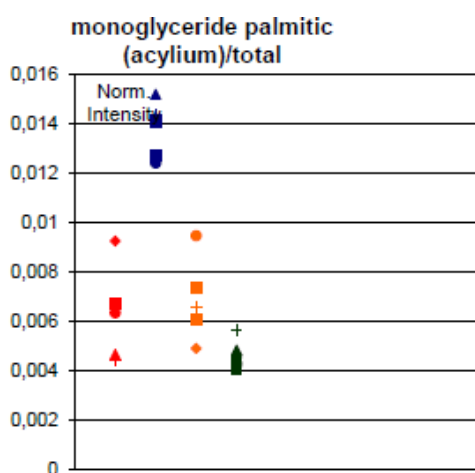


Figure G.15: Positive acylium ions of monoglyceride with palmitic acid  $C_{19}H_{37}O_3^+$  at  $m/z$  313 in the linseed oil-azurite mixture

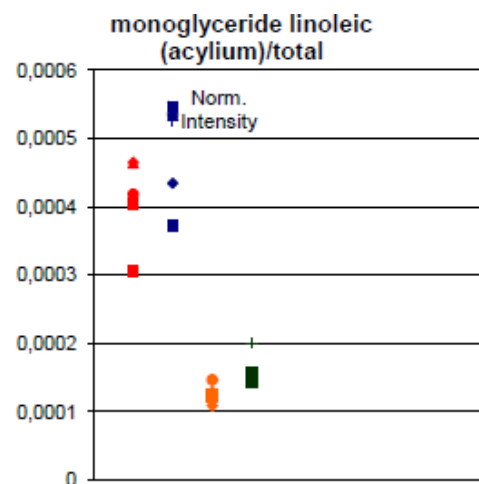


Figure G.16: Positive acylium ions of monoglyceride with linoleic acid  $C_{21}H_{37}O_3^+$  at  $m/z$  337 in the linseed oil-azurite mixture

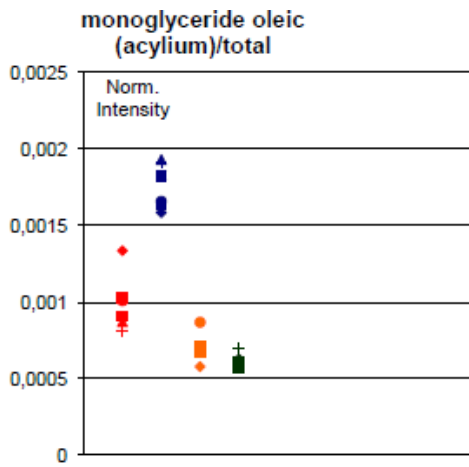


Figure G.17: Positive acylium ions of monoglyceride with oleic acid  $C_{21}H_{39}O_3^+$  at  $m/z$  339 in the linseed oil-azurite mixture

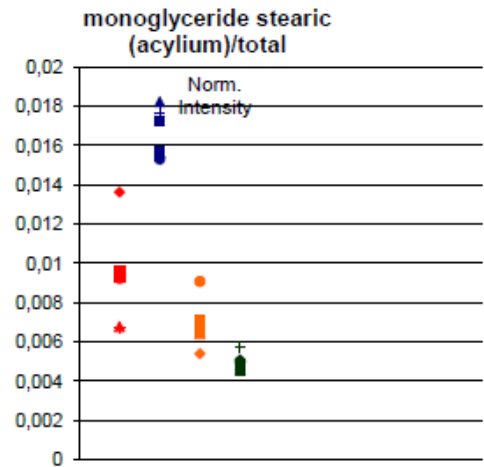


Figure G.18: Positive acylium ions of monoglyceride with stearic acid  $C_{21}H_{41}O_3^+$  at  $m/z$  341 in the linseed oil-azurite mixture

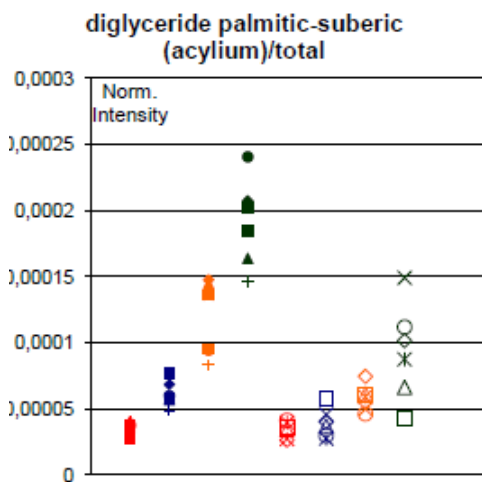


Figure G.19: Positive acylium ions of diglyceride with palmitic/suberic acid  $C_{27}H_{49}O_6^+$  at  $m/z$  469 in the linseed oil-azurite mixture

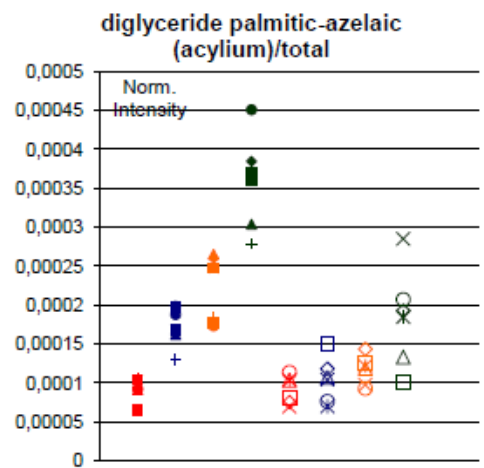


Figure G.20: Positive acylium ions of diglyceride with palmitic/azelaic acid  $C_{28}H_{51}O_6^+$  at  $m/z$  483 in the linseed oil-azurite mixture

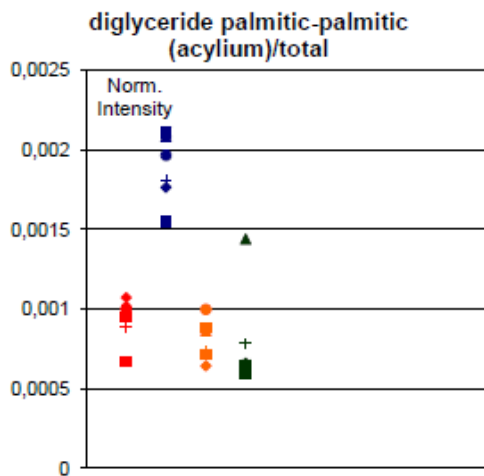


Figure G.21: Positive acylium ions of diglyceride with twice palmitic acid  $C_{35}H_{67}O_4^+$  at  $m/z$  551,5 in the linseed oil-azurite mixture

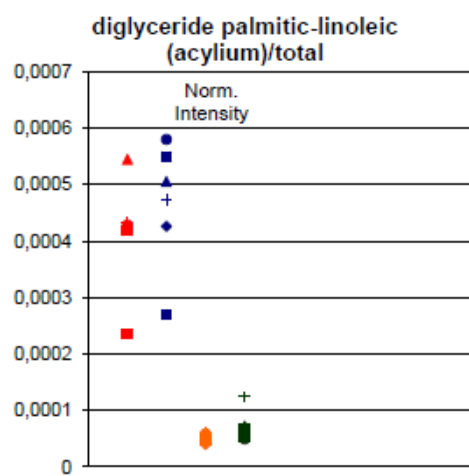


Figure G.22: Positive acylium ions of diglyceride with palmitic/linoleic acid  $C_{37}H_{67}O_4^+$  at  $m/z$  575,5 in the linseed oil-azurite mixture

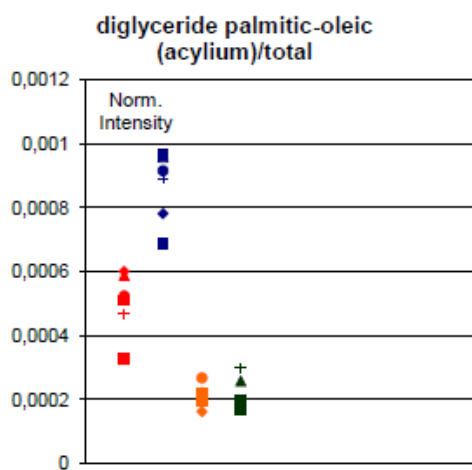


Figure G.23: Positive acylium ions of diglyceride with palmitic/oleic acid  $C_{37}H_{69}O_4^+$  at  $m/z$  577,5 in the linseed oil-azurite mixture

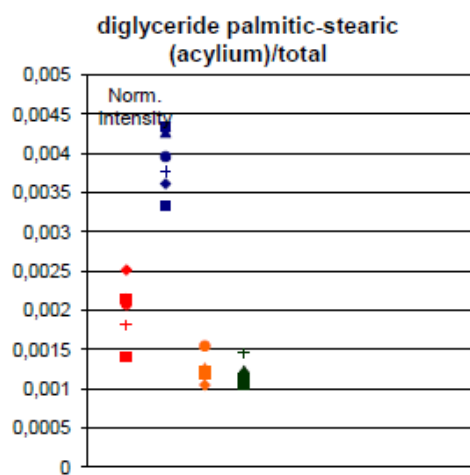


Figure G.24: Positive acylium ions of diglyceride with palmitic/stearic acid  $C_{37}H_{71}O_4^+$  at  $m/z$  579,5 in the linseed oil-azurite mixture

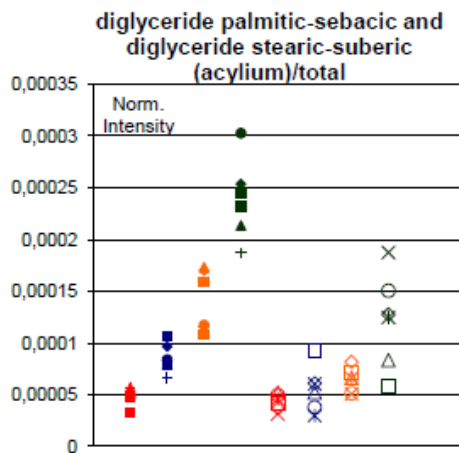


Figure G.25: Positive acylium ions of diglyceride with stearic/suberic acid and of diglyceride with palmitic/sebacic acid  $C_{29}H_{53}O_6^+$  at  $m/z$  497 in the linseed oil-azurite mixture

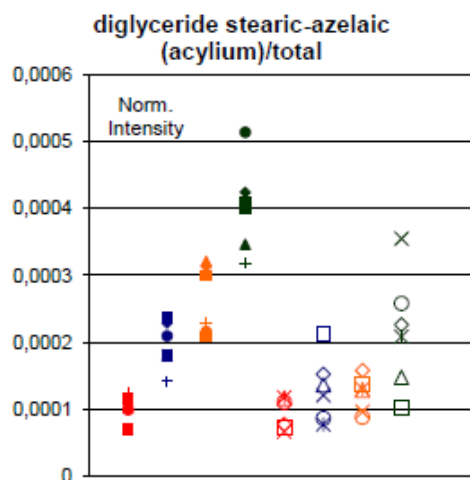


Figure G.26: Positive acylium ions of diglyceride with stearic/azelaic acid  $C_{30}H_{55}O_6^+$  at  $m/z$  511 in the linseed oil-azurite mixture

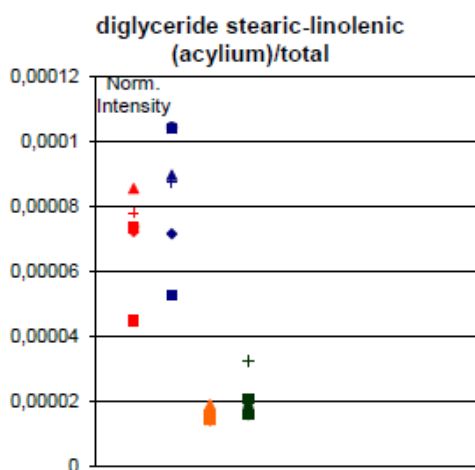


Figure G.27: Positive acylium ions of diglyceride with stearic/linolenic acid  $C_{39}H_{69}O_4^+$  at  $m/z$  601,5 in the linseed oil-azurite mixture

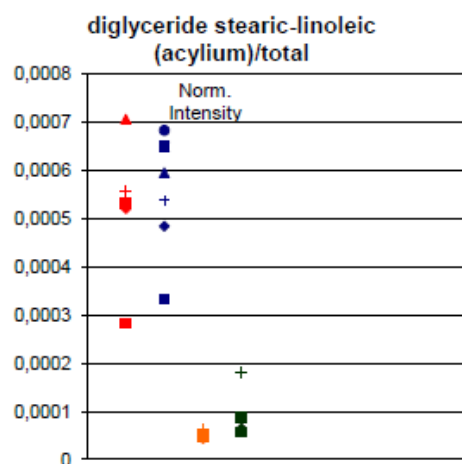


Figure G.28: Positive acylium ions of diglyceride with stearic/linoleic acid  $C_{39}H_{71}O_4^+$  at  $m/z$  603,5 in the linseed oil-azurite mixture

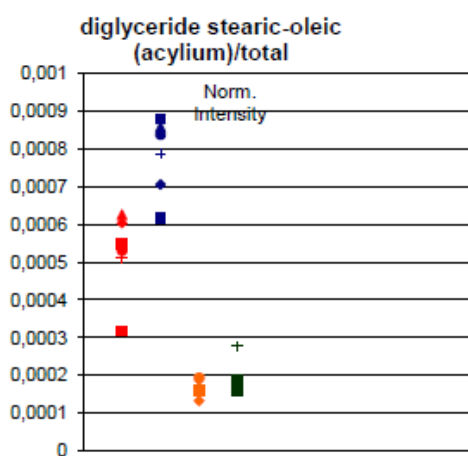


Figure G.29: Positive acylium ions of diglyceride with stearic/oleic acid  $C_{39}H_{73}O_4^+$  at  $m/z$  605,5 in the linseed oil-azurite mixture

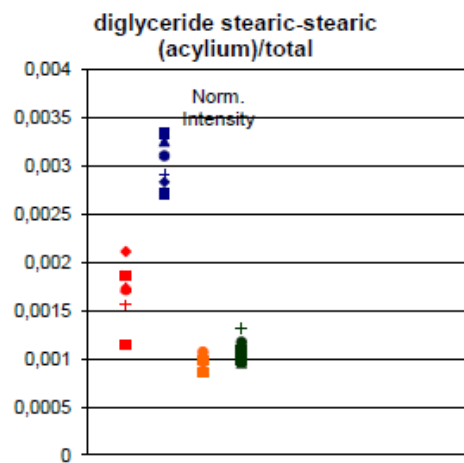


Figure G.30: Positive acylium ions of diglyceride with twice stearic acid  $C_{39}H_{75}O_4^+$  at  $m/z$  607,5 in the linseed oil-azurite mixture

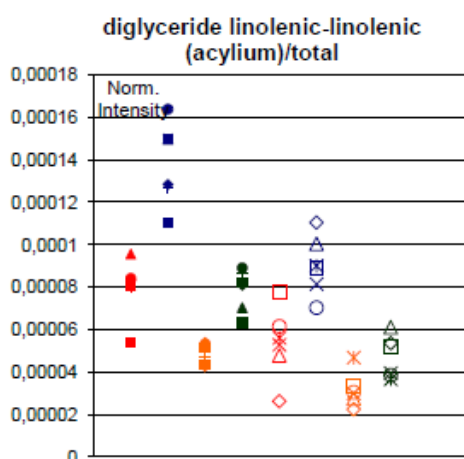


Figure G.31: Positive acylium ions of diglyceride with twice linolenic acid  $C_{39}H_{63}O_4^+$  at  $m/z$  595,5 in the linseed oil-azurite mixture

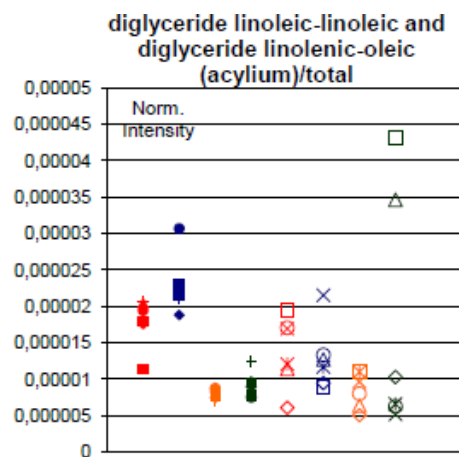


Figure G.32: Positive acylium ions of diglyceride with twice linoleic acid and of diglyceride with linolenic/oleic  $C_{39}H_{67}O_4^+$  at  $m/z$  599,5 in the linseed oil-azurite mixture

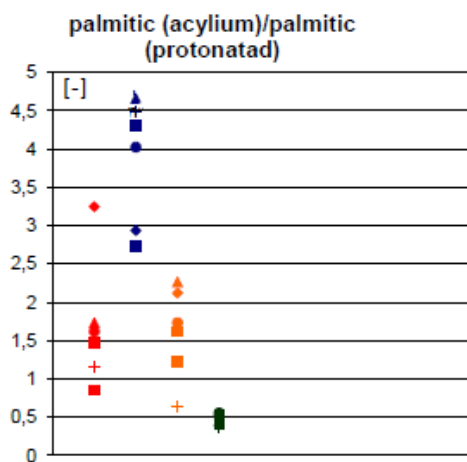


Figure G.33: Ratio of positive acylium and protonated ions of palmitic acid in the linseed oil-azurite mixture

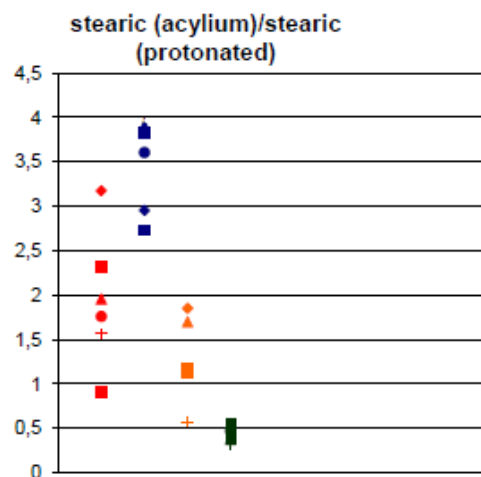


Figure G.34: Ratio of positive acylium and protonated ions of stearic acid in the linseed oil-azurite mixture

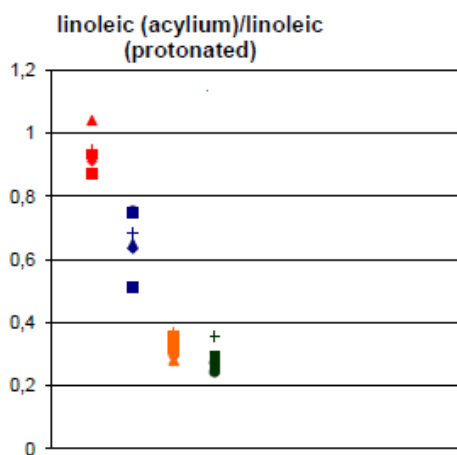


Figure G.35: Ratio of positive acylium and protonated ions of linoleic acid in the linseed oil-azurite mixture

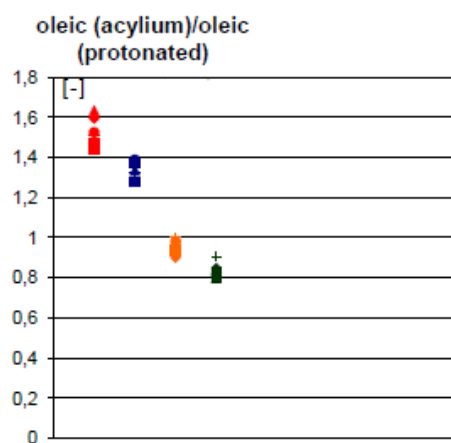


Figure G.36: Ratio of positive acylium and protonated ions of oleic acid in the linseed oil-azurite mixture

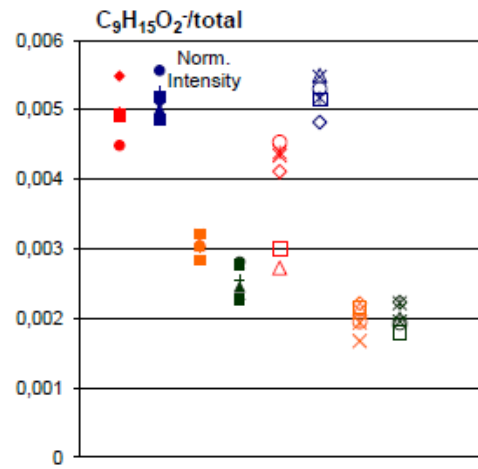


Figure G.37: Negative ions of aliphatic chain fragment with formula  $C_2H_3(CH_2)_6COO^-$  at  $m/z$  155 in the linseed oil-azurite mixture

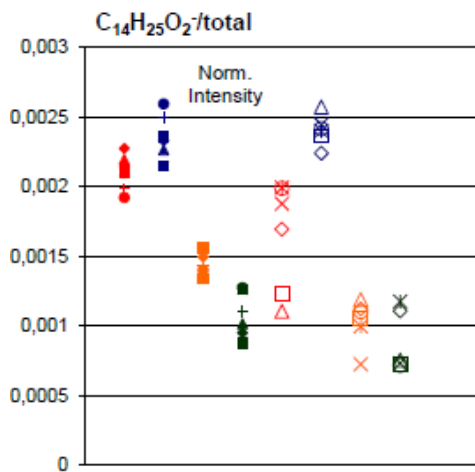


Figure G.38: Negative ions of aliphatic chain fragment with formula  $C_2H_3(CH_2)_{11}COO^-$  at  $m/z$  225 in the linseed oil-azurite mixture

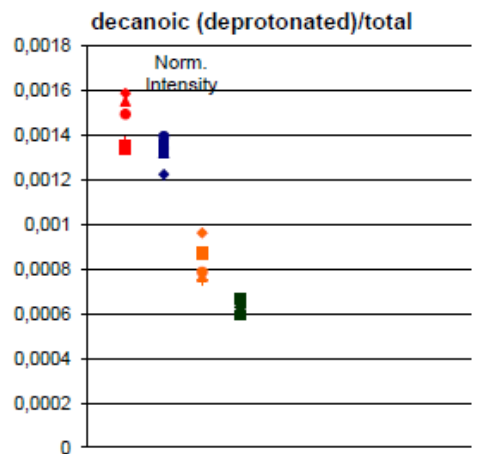


Figure G.39: Negative deprotonated ions of decanoic acid  $C_{10}H_{19}O_2^-$  at  $m/z$  171 in the linseed oil-azurite mixture

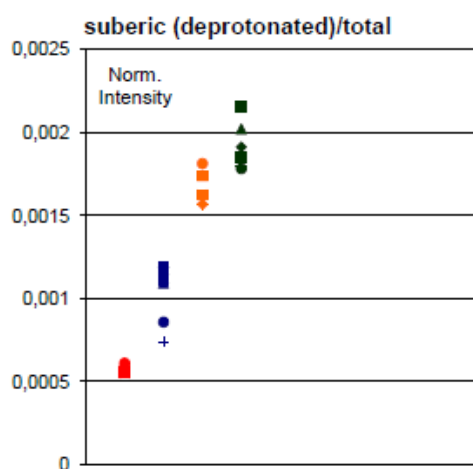


Figure G.40: Negative deprotonated ions of suberic acid  $C_8H_{13}O_4^-$  at  $m/z$  173 in the linseed oil-azurite mixture

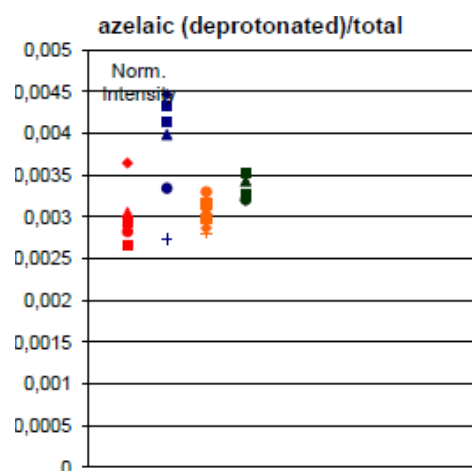


Figure G.41: Negative deprotonated ions of azelaic acid  $C_9H_{15}O_4^-$  at  $m/z$  187 in the linseed oil-azurite mixture

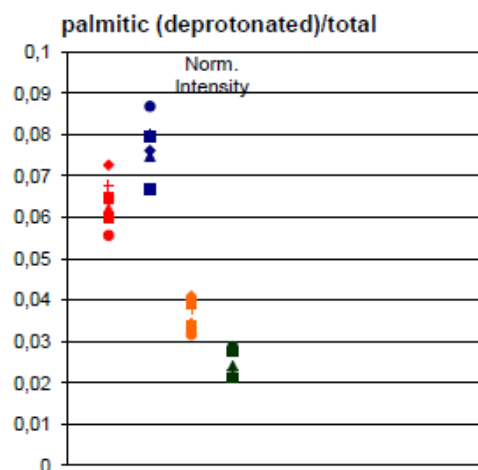


Figure G.42: Negative deprotonated ions of palmitic acid  $C_{16}H_{31}O_2^-$  at  $m/z$  255 in the linseed oil-azurite mixture

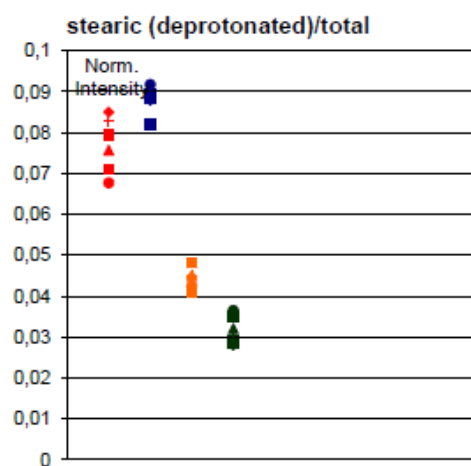


Figure G.43: Negative deprotonated ions of stearic acid  $C_{18}H_{35}O_2^-$  at  $m/z$  283 in the linseed oil-azurite mixture

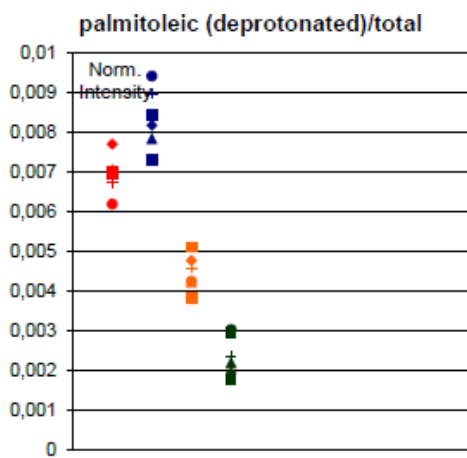


Figure G.44: Negative deprotonated ions of palmitoleic acid  $C_{16}H_{29}O_2^-$  at  $m/z$  253 in the linseed oil-azurite mixture

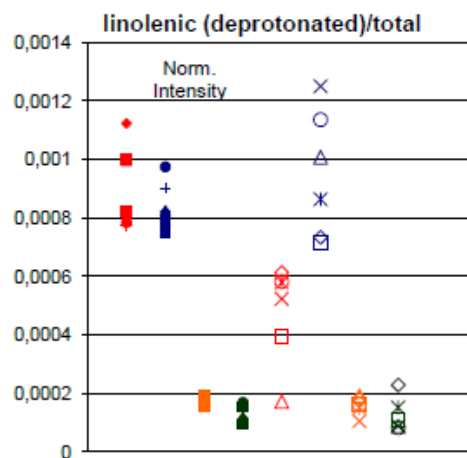


Figure G.45: Negative deprotonated ions of linolenic acid  $C_{18}H_{29}O_2^-$  at  $m/z$  277 in the linseed oil-azurite mixture

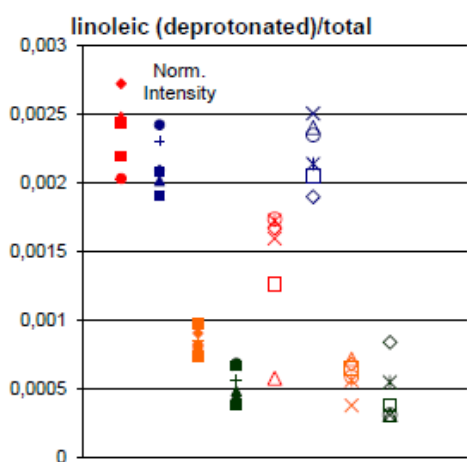


Figure G.46: Negative deprotonated ions of linoleic acid  $C_{18}H_{31}O_2^-$  at  $m/z$  279 in the linseed oil-azurite mixture

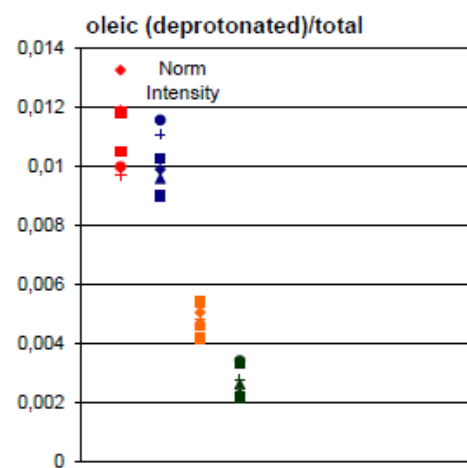


Figure G.47: Negative deprotonated ions of oleic acid  $C_{18}H_{33}O_2^-$  at  $m/z$  281 in the linseed oil-azurite mixture

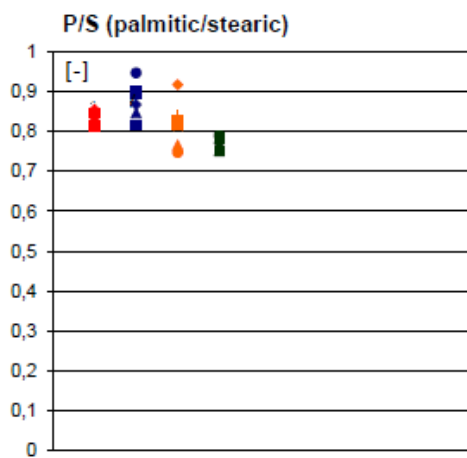


Figure G.48: Ratio of negative deprotonated palmitic and stearic acid ions in the linseed oil-azurite mixture

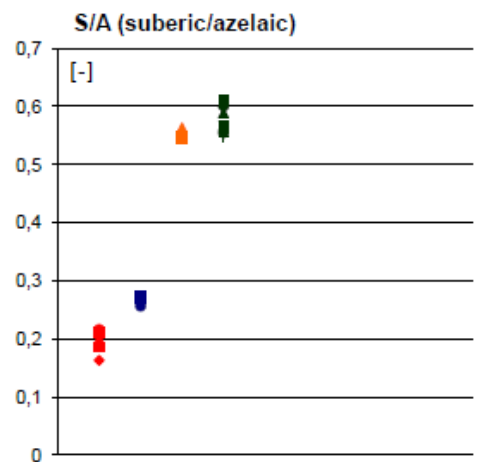


Figure G.49: Ratio of negative deprotonated suberic and azelaic acid ions in the linseed oil-azurite mixture

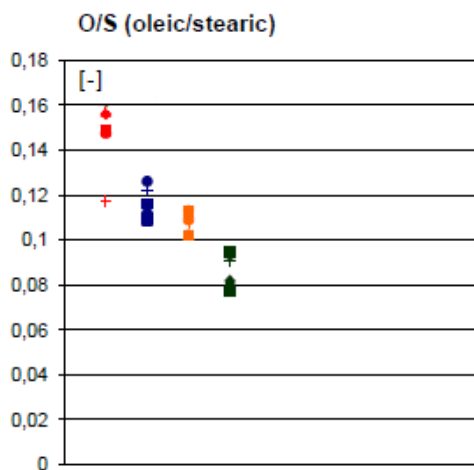


Figure G.50: Ratio of negative deprotonated oleic and stearic acid ions in the linseed oil-azurite mixture

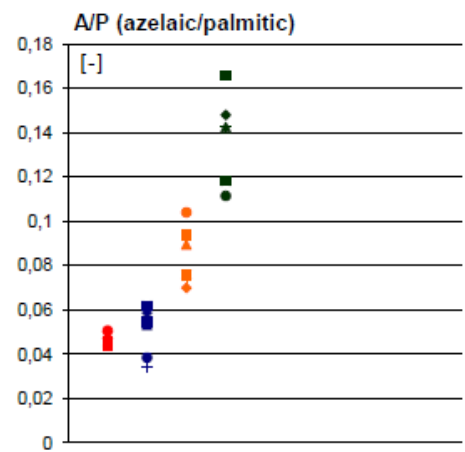


Figure G.51: Ratio of negative deprotonated azelaic and palmitic acid ions in the linseed oil-azurite mixture

## Appendix H

# Results of ToF-SIMS measurements of Lead containing Pigments

- ◆ Lead carbonate\_1
- Lead carbonate\_2
- ▲ Lead carbonate\_3
- ◆ Hydrocerussite\_1
- Hydrocerussite\_2
- ▲ Hydrocerussite\_3
- ◆ Blanc d'argent\_1
- Blanc d'argent\_2
- ▲ Blanc d'argent\_3
- ◆ Flake white\_1
- Flake white\_2
- ▲ Flake white\_3
- ◆ Blanc de saturne\_1
- Blanc de saturne\_2
- ▲ Blanc de saturne\_3
- ◆ Minium\_1
- Minium\_2
- ▲ Minium\_3
- ◇ Lead chloride\_1
- Lead chloride\_2
- △ Lead chloride\_3

Figure H.1: Legend used for Figures H.2 to H.31

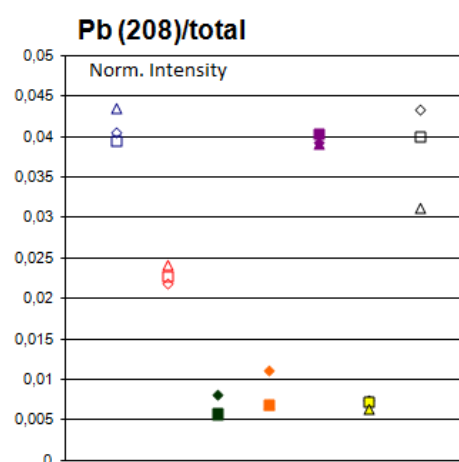


Figure H.2: Positive  $Pb^+$  ions at  $m/z$  208

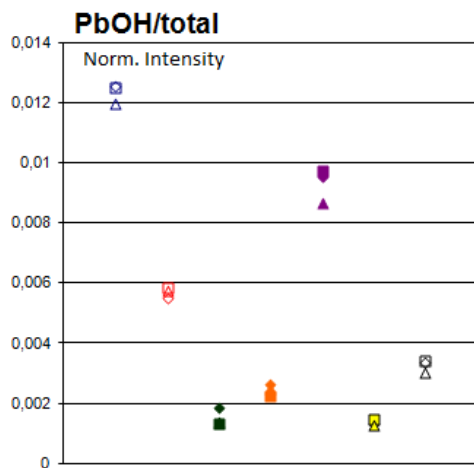


Figure H.3: Positive  $PbOH^+$  ion at  $m/z$  225

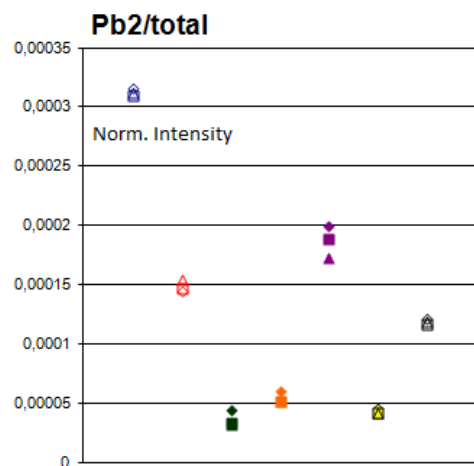


Figure H.5: Positive  $Pb_2^+$  ion at  $m/z$  416

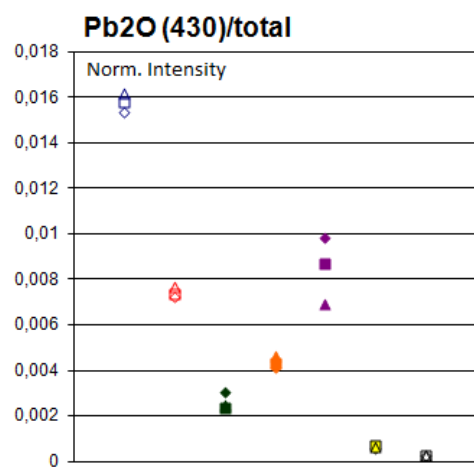


Figure H.7: Positive  $^{207}Pb_2O^+$  ion at  $m/z$  430

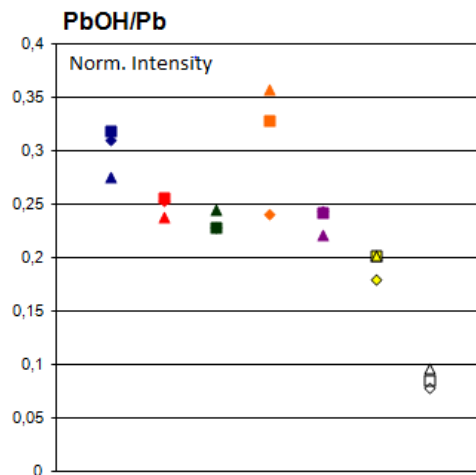


Figure H.4: Positive  $PbOH^+$  ion at  $m/z$  225 relative to the counts of the  $Pb^+$  peak

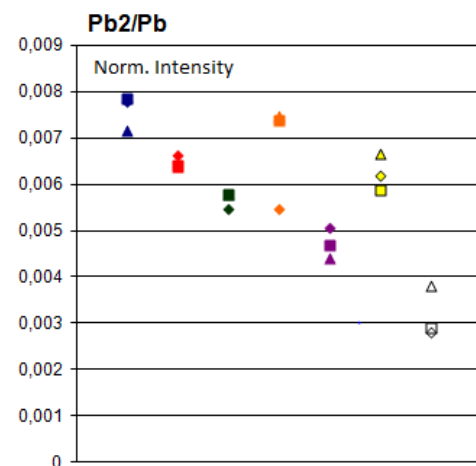


Figure H.6: Positive  $Pb_2^+$  ion at  $m/z$  416 relative to the counts of the  $Pb^+$  peak

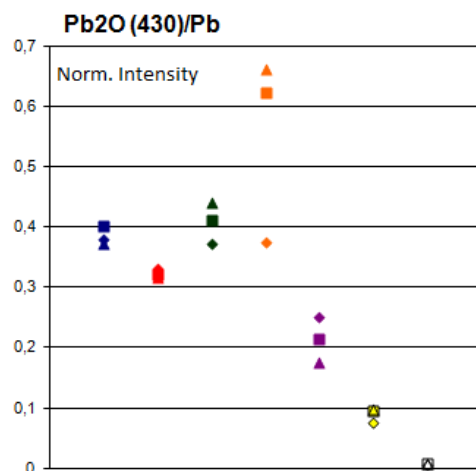


Figure H.8: Positive  $^{207}Pb_2O^+$  ion relative to the counts of the  $Pb^+$  peak at  $m/z$  430

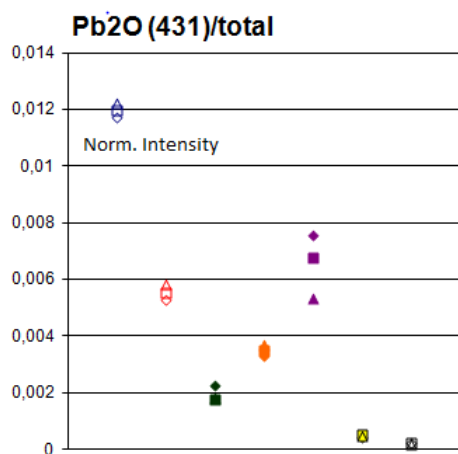


Figure H.9: Positive  $^{207}\text{PbPbO}^+$  ion at  $m/z$  431

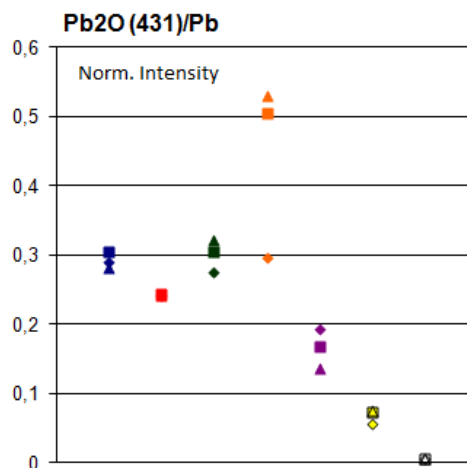


Figure H.10: Positive  $^{207}\text{PbPbO}^+$  ion relative to the counts of the  $\text{Pb}^+$  peak at  $m/z$  431

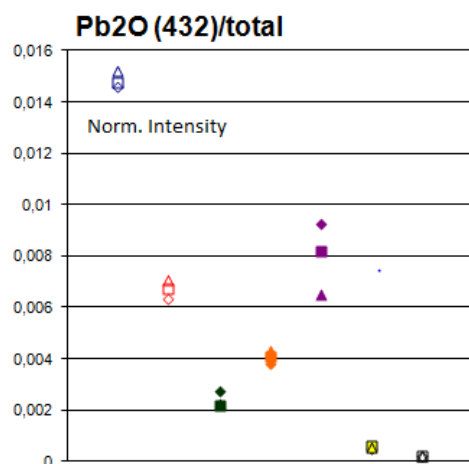


Figure H.11: Positive  $\text{Pb}_2\text{O}^+$  ion at  $m/z$  432

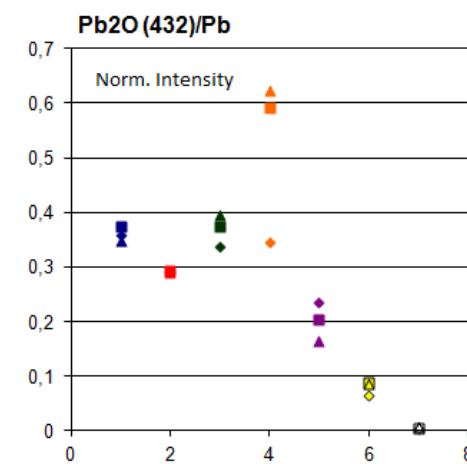


Figure H.12: Positive  $\text{Pb}_2\text{O}^+$  ion relative to the counts of the  $\text{Pb}^+$  peak at  $m/z$  432

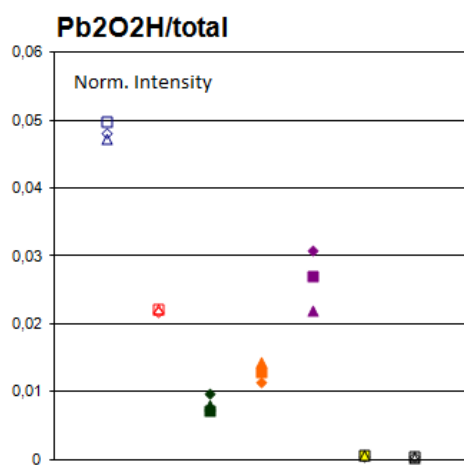


Figure H.13: Positive  $\text{Pb}_2\text{O}_2\text{H}^+$  ion at  $m/z$  447

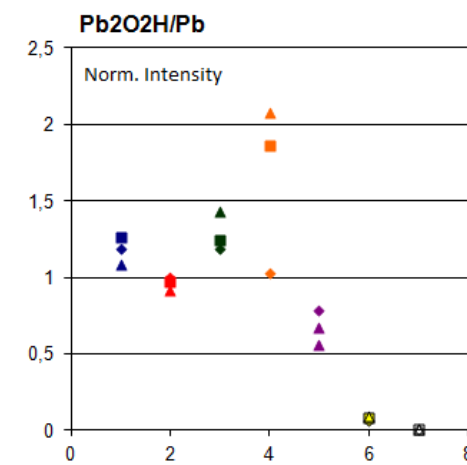


Figure H.14: Positive  $\text{Pb}_2\text{O}_2\text{H}^+$  ion relative to the counts of the  $\text{Pb}^+$  peak at  $m/z$  447

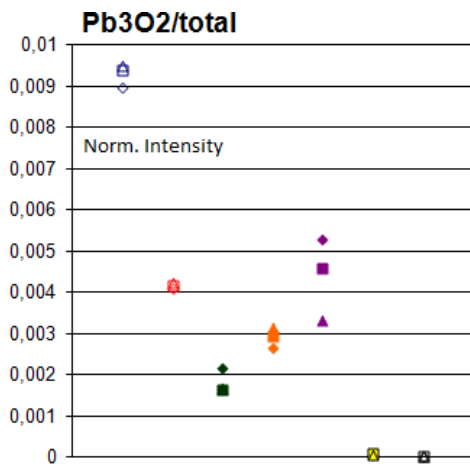


Figure H.15: Positive  $Pb_3O_2^+$  ion at  $m/z$  654

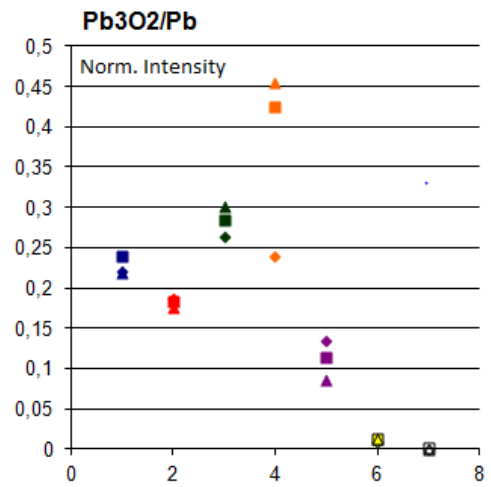


Figure H.16: Positive  $Pb_3O_2^+$  ion at  $m/z$  654 relative to the counts of the  $Pb^+$  peak

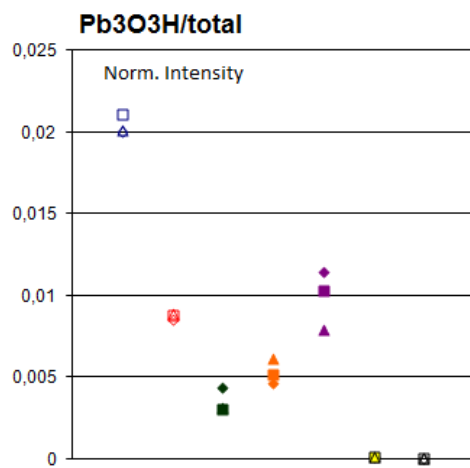


Figure H.17: Positive  $Pb_3O_3H^+$  ion at  $m/z$  671

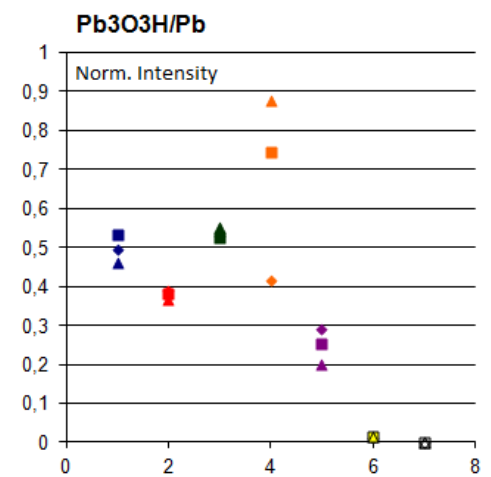


Figure H.18: Positive  $Pb_3O_3H^+$  ion at  $m/z$  671 relative to the counts of the  $Pb^+$  peak

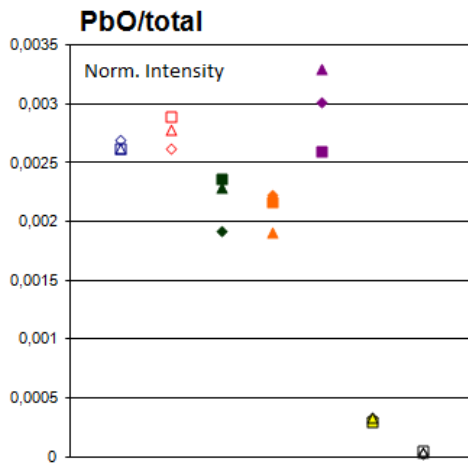


Figure H.19: Negative  $PbO^-$  ion at  $m/z$  224

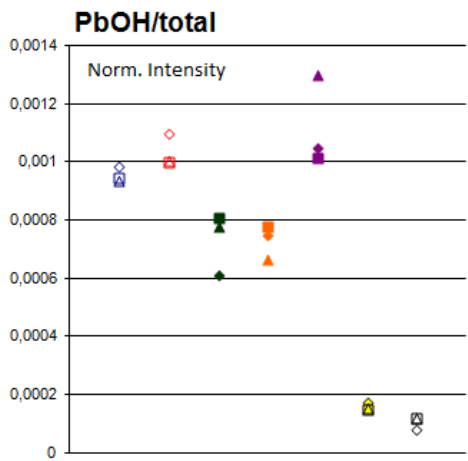


Figure H.20: Negative  $PbOH^-$  ion at  $m/z$  225

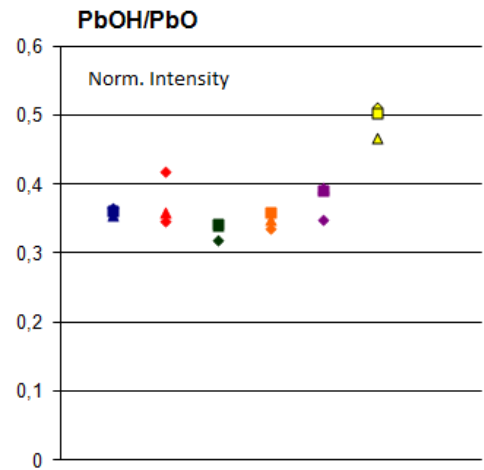


Figure H.21: Negative  $PbOH^-$  ion at  $m/z$  225 relative to the counts of the  $PbO^-$  peak

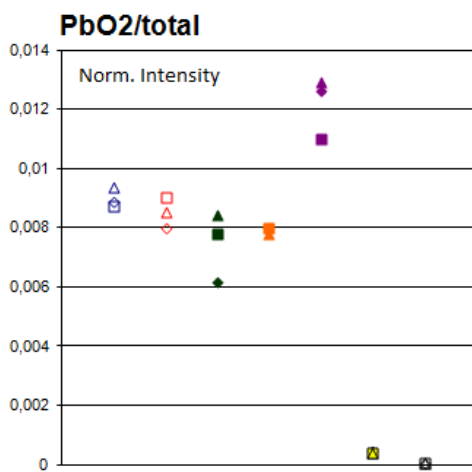


Figure H.22: Negative  $PbO_2^-$  ion at  $m/z$  240

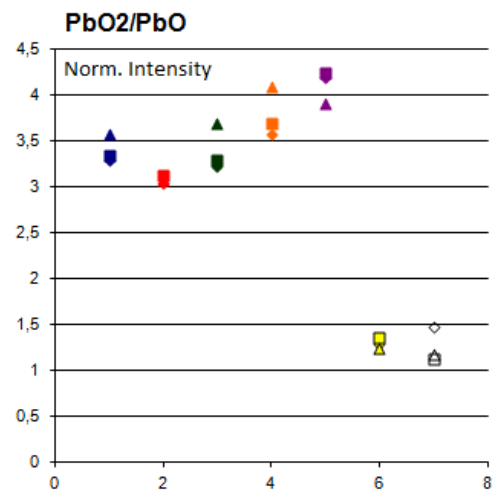


Figure H.23: Negative  $PbO_2^-$  ion at  $m/z$  240 relative to the counts of the  $PbO^-$  peak

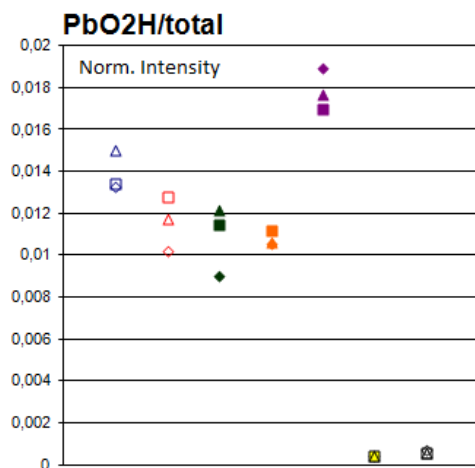


Figure H.24: Negative  $PbO_2H^-$  ion at  $m/z$  241

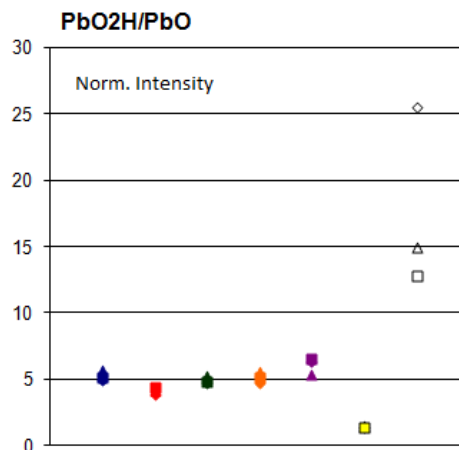


Figure H.25: Negative  $PbO_2H^-$  ion at  $m/z$  241 relative to the counts of the  $PbO^-$  peak

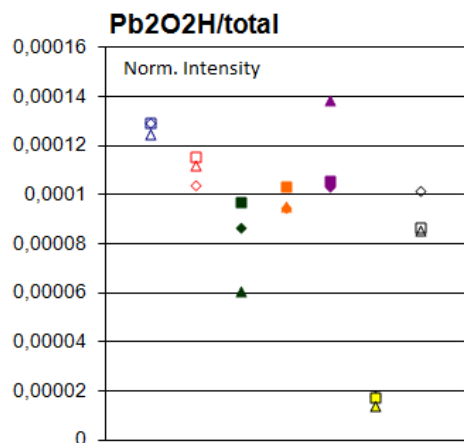


Figure H.26: Negative  $Pb_2O_2H^-$  ion at  $m/z$  449

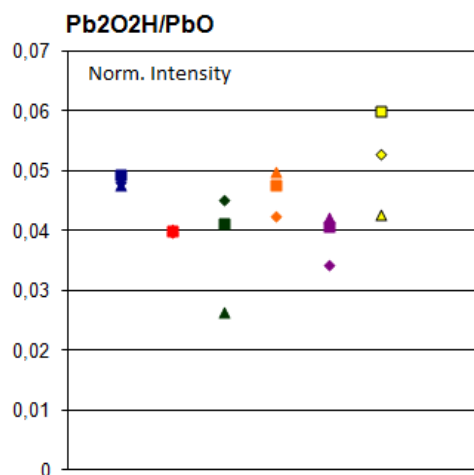


Figure H.27: Negative  $Pb_2O_2H^-$  ion at  $m/z$  449 relative to the counts of the  $PbO^-$  peak

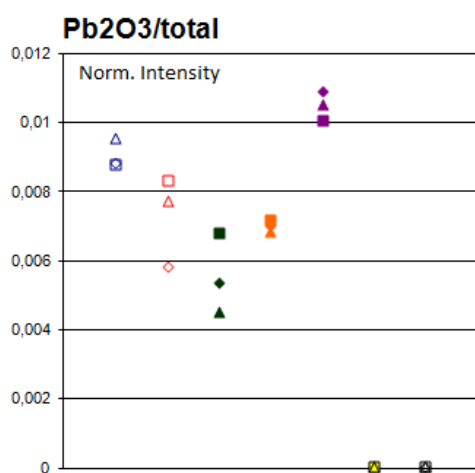


Figure H.28: Negative  $Pb_2O_3^-$  ion at  $m/z$  464

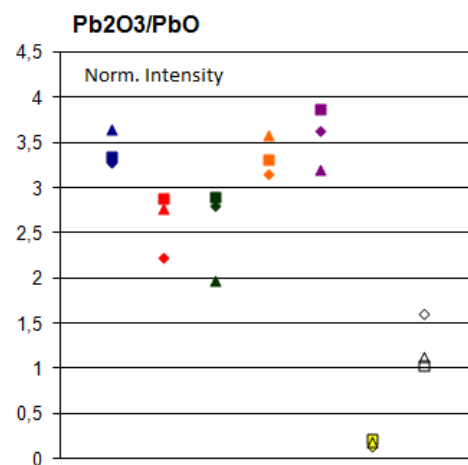


Figure H.29: Negative  $Pb_2O_3^-$  ion at  $m/z$  464 relative to the counts of the  $PbO^-$  peak

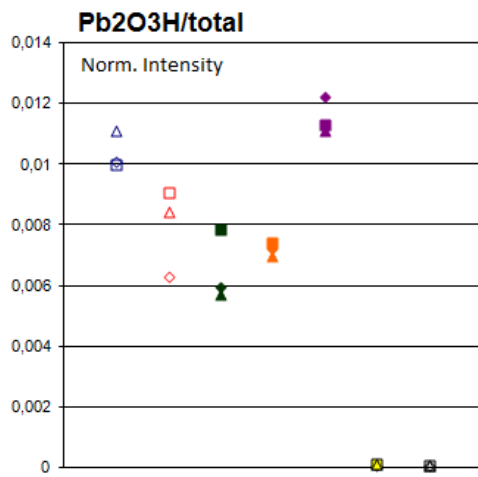


Figure H.30: Negative  $Pb_2O_3H^-$  ion at  $m/z$  465

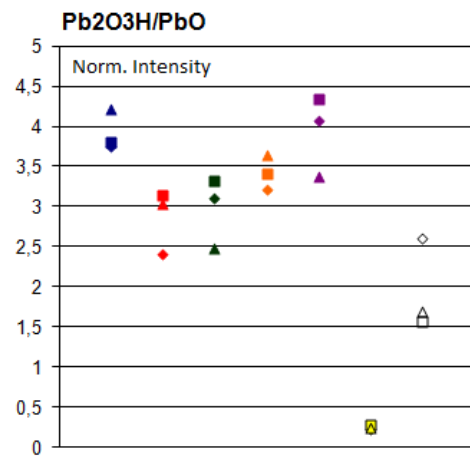


Figure H.31: Negative  $Pb_2O_3H^-$  ion at  $m/z$  465 relative to the counts of the  $PbO^-$  peak

# Bibliography

- [1] Molart reports and phd theses. <http://www.jaap-enterprise.com/art-science/theses/>. Accessed 20/08/2016.
- [2] *Brochure Agneau Mystique*, 2012. accessed via <http://www.kikirpa.be/FR/249/460/Restauration%20de%20l%E2%80%99Agneau%20mystique.htm>.
- [3] Kik-irpa's projects: The ghent altarpiece in the laboratory 60 years after paul coremans: The contribution of new analytical techniques. [http://www.kikirpa.be/uploads/files/projects/display\\_project.php?id=106&lang=en](http://www.kikirpa.be/uploads/files/projects/display_project.php?id=106&lang=en). Accessed 20/08/2016.
- [4] Kik-irpa: Restoration of the ghent altarpiece. <http://www.kikirpa.be/EN/249/0/Restoration+of+the+Ghent+Altarpiece.htm>. Accessed 20/08/2016.
- [5] Katrien Keune. *Binding medium, pigments and metal soaps characterised and localised in paint cross-sections, PhD Thesis*. Institute for Atomic and Molecular Physics Amsterdam, MOLART Report, Amsterdam, Netherlands, 2005.
- [6] Ilaria Bonaduce, Leslie Carlyle, Maria Perla Colombini, Celia Duce, Carlo Ferrari, et al. A multi-analytical approach to studying binding media in oil paintings. *Journal of Thermal Analysis and Calorimetry*, 107(3):1055–1066, march 2012.
- [7] Ilaria Bonaduce, Leslie Carlyle, Maria Perla Colombini, Celia Duce, Carlo Ferrari, et al. New insights into the ageing of linseed oil paint binder: A qualitative and quantitative analytical study. *PLoS ONE*, 7(11):1055–1066, november 2012.
- [8] Annemie Adriaens. Non-destructive analysis and testing of museum objects: An overview of 5 years of research. *Spectrochimica Acta Part B*, 60:1503–1516, 2005.
- [9] Sylvana Barrett and Dusan C. Stulik. An integrated approach for the study of painting techniques. In *Historical Painting Techniques, Materials and Studio Practice*, chapter 2, pages 6–11. The Getty Conservation Institute, Los Angeles, California, USA, 1995.
- [10] Mark Dowsett and Annemie Adriaens. The role of sims in cultural heritage studies. *Nuclear Instruments and Methods in Physics Research B*, 226:38–52, 2004.
- [11] Katrien Keune and Jaap J. Boon. Imaging secondary ion mass spectrometry of a paint cross section taken from an early netherlandish painting by roger van der weyden. *Analytical Chemistry*, 76:1374–1385, 2004.
- [12] Barbara J. Garrison, Arnaud Delcorte, and Kristin D. Krantzman. Molecule liftoff from surfaces. *Accounts of Chemical Research*, 33(2):69–77, february 2000.
- [13] John C. Vickerman. Prologue: Tof-sims - an evolving mass spectrometry of materials. In John C. Vickerman and David Briggs, editors, *ToF-SIMS, Materials Analysis by Mass Spectrometry, 2nd Edition*, chapter 1, pages 1–37. SurfaceSpectra Ltd/IM Publications, Manchester, UK, 2013.

- [14] Arnaud Delcorte. Fundamentals of organic sims: insights from experiments and models. In John C. Vickerman and David Briggs, editors, *ToF-SIMS, Materials Analysis by Mass Spectrometry, 2nd Edition*, chapter 4, pages 87–123. SurfaceSpectra Ltd/IM Publications, Manchester, UK, 2013.
- [15] Thomas Batardy. *Contribution de la spectrométrie ToF-SIMS à l'étude d'une peinture issue de l'atelier de Lambert Lombard (1505-1566), Travail de fin d'études*. Université Catholique de Louvain, Faculté des Sciences Appliquées, Département de Sciences des Matériaux et des Procédés, Unité de Physico-Chimie et de Physique des Matériaux, Louvain-la-Neuve, Belgium, 2006.
- [16] Theophilus. *The Various Arts: De Diversis Artibus. Edited and translated by C.R. Dodwell*. Clarendon Press, Oxford, UK, 1986.
- [17] Susan Jones. *Painting in Oil in the Low Countries and Its Spread to Southern Europe, Heilbrunn Timeline of Art History*. 2002. on the website of the The Metropolitan Museum of Art [http://www.metmuseum.org/toah/hd/optg/hd\\_optg.htm](http://www.metmuseum.org/toah/hd/optg/hd_optg.htm), accessed 18-07-2016.
- [18] Fred S. Kleiner. *Gardner's Art through the Ages, the Western Perspective, Volume II*. Cengage Learning, Boston, Massachusetts, USA, 2015.
- [19] Xavier de Langlais. *La Technique de la Peinture à l'Huile*. Flammarion, Paris, France, 1959.
- [20] Abraham Pincas e.a. *Le Lustre de la main, Esprit, matière et techniques de la peinture*. Ecole nationale supérieure des Beaux-Arts, Paris, France, 1991.
- [21] John Mills and Raymond White. *Organic Chemistry of Museum Objects, Second Edition*. Butterworth-Heinemann, Oxford, UK, 1994.
- [22] Francois Perego. *Le dictionnaire des Matériaux du Peintre*. Belin, Paris, France, 2005.
- [23] Massimo Lazzari and Oscar Chiantore. Drying and oxidative degradation of linseed oil. *Polymer Degradation and Stability*, 65:303–313, 1999.
- [24] Charles S. Tumosa and Marion F. Mecklenburg. Oil paints: The chemistry of drying oils and the potential for solvent disruption. *Smithsonian Contributions to Museum Conservation*, 3:51–58, 2013.
- [25] Maria Perla Colombini and Francesca Modugno. *Organic Mass Spectrometry in Art and Archaeology*. Wiley, Hoboken, New Jersey, USA, 2009.
- [26] Jorrit D.J. van den Berg, Klaas Jan van den Berg, and Jaap J. Boon. Identification of non-cross-linked compounds in methanolic extracts of cured and aged linseed oil-based paint films using gas chromatography-mass spectrometry. *Journal of Chromatography A*, 950:195–211, 2002.
- [27] Cennino D' Andrea Cennini. *The Craftsman's Handbook: The Italian 'Il Libro dell' Arte', Translated by Daniel V. Thompson Jr*. Dover Publications, Inc. by Yale University Press, New York, USA, 1933. accessed via <http://www.noteaccess.com/Texts/Cennini/index.htm>.
- [28] Nicholas Eastaugh, Valentine Walsh, Tracey Chaplin, and Ruth Siddall. *Pigment Compendium, A Dictionary and Optical Microscopy of Historical Pigments*. Butterworth-Heinemann, Oxford, UK, 2008.
- [29] John F. Watts and John Wolstenholme. *An introduction to Surface Analysis by XPS and AES*. Wiley, Chichester, UK, 2003.

- [30] Giuseppino Fortunato, Axel Ritter, and Daniel Fabian. Old masters' lead white pigments: investigations of paintings from the 16th to the 17th century using high precision lead isotope abundance ratios. *The Analyst*, 130:898–906, 2005.
- [31] Zofia Anna Stos-Gale and Noël H. Gale. Metal provenancing using isotopes and the oxford archaeological lead isotope database (OXALID). *Archaeological and Anthropological Sciences*, 1:195–213, september 2009.
- [32] Giuseppino Fortunato and Daniel Fabian. Tracing white: a study of lead white pigments found in seventeenth-century paintings using high precision lead isotope abundance ratios. In Jo Kirby, Susie Nash, and Joanna Cannon, editors, *Trade in artists' materials, markets and commerce in Europe to 1700*, chapter 27, pages 426–443. Archetype Publications, London, UK, 2010.
- [33] P.J. Potts. *A Handbook on Silican Rock Analysis. Chapter 17: Thermal ionization mass spectrometry*. Springer Science and Business Media, New York, USA, 1987.
- [34] Joel Baker, Sophie Stos, and Tod Waight. Lead isotope analysis of archaeological metals by multiple-collector inductively coupled plasma mass spectrometry. *Archaeometry*, 48:45–56, february 2006.
- [35] Adrian A. Ammann. Inductively coupled plasma mass spectrometry (ICPMS): a versatile tool. *Journal of Mass Spectrometry*, 42:419–427, 2007.
- [36] Sims microprobe for isotopic and trace element analysis at high spatial resolution. <http://www.cameca.com/instruments-for-research/nanosims.aspx>. Accessed 15/08/2016.
- [37] Zofia Stos-Gale. Interpretation of lead isotope data of lead white from the painting by Farinati(?). unpublished data, acquired via Dr. Jana Sanyova (KIK-IRPA), 2011.
- [38] Bambang Wiyono, Sanro Tachibana, and Djaban Tinambunan. Chemical compositions of pine resin, rosin and turpentine oil from west java. *Journal of Forestry Research*, 3:7–17, 2006.
- [39] Mario V. Russo and Pasquale Avino. Characterization and identification of natural terpenic resins employed in *Madonna con Bambino e Angeli* by *Antonello da Messina* using gas chromatography-mass spectrometry. *Chemistry Central Journal*, 6(1):1–10, 2012.
- [40] A. Atrei, F. Benetti, E. Gliozzo, G. Perra, and N. Marchettini. Chemical characterization of protein based binders in painting samples by means of tof-sims: Tests on ancient and model samples. *International Journal of Mass Spectrometry*, 369:9–15, 2014.

